GEOLOGICA ULTRAIECTINA

Mededelingen van de
Faculteit Aardwetenschappen der
Rijksuniversiteit te Utrecht

No. 103

THE METAMORPHIC EVOLUTION OF THE BAMBLE SECTOR, SOUTH NORWAY.

A PARAGENETIC AND MINERAL CHEMICAL STUDY OF CORDIERITE-ORTHOAMPHIBOLE-BEARING ROCKS WITH SPECIAL REFERENCE TO BOROSILICATE-BEARING MINERAL ASSEMBLAGES.

D. Visser

GEOLOGICA ULTRAIECTINA

Mededelingen van de
Faculteit Aardwetenschappen der
Rijksuniversiteit te Utrecht

No. 103

THE METAMORPHIC EVOLUTION OF THE BAMBLE SECTOR, SOUTH NORWAY.

A PARAGENETIC AND MINERAL CHEMICAL STUDY OF CORDIERITE-ORTHOAMPHIBOLE-BEARING ROCKS WITH SPECIAL REFERENCE TO BOROSILICATE-BEARING MINERAL ASSEMBLAGES.

CIP-GEGEVENS KONINKLIJKE BIBLIOTHEEK, DEN HAAG

Visser, Diederik

The metamorphic evolution of the Bamble Sector, south Norway: a paragenetic and mineral chemical study of cordierite-orthoamphibole-bearing rocks with special reference to borosilicate-bearing mineral assemblages / Diederik Visser. - Utrecht: Faculteit Aardwetenschappen der Rijksuniversiteit Utrecht. - (Geologica Ultraiectina, ISSN 0072-1026; no. 103)
Proefschrift Rijksuniversiteit Utrecht. - Met lit.opg. - Met samenvatting in het Nederlands.
ISBN 90-71577-59-7
Trefw.:Bamble / Noorwegen; geologie.

THE METAMORPHIC EVOLUTION OF THE BAMBLE SECTOR, SOUTH NORWAY.

A PARAGENETIC AND MINERAL CHEMICAL STUDY OF CORDIERITE-ORTHOAMPHIBOLE-BEARING ROCKS WITH SPECIAL REFERENCE TO BOROSILICATE-BEARING MINERAL ASSEMBLAGES.

DE METAMORFE EVOLUTIE VAN DE BAMBLE SECTOR, ZUID NOORWEGEN.

EEN PARAGENETISCH EN MINERAAL CHEMISCH ONDERZOEK VAN CORDIERIET-ORTHOAMFIBOOL HOUDENDE GESTEENTES MET SPECIALE NADRUK OP BOROSILICAAT HOUDENDE MINERAAL ASSEMBLAGES.

(MET EEN SAMENVATTING IN HET NEDERLANDS)

PROEFSCHRIFT

TER VERKRIJGING VAN DE GRAAD VAN DOCTOR
AAN DE RIJKSUNIVERSITEIT TE UTRECHT OP GEZAG VAN DE
RECTOR MAGNIFICUS, PROF.DR. J.A. VAN GINKEL,
INGEVOLGE HET BESLUIT VAN DEKANEN IN HET OPENBAAR TE
VERDEDIGEN OP DONDERDAG 13 MEI 1993 DES NAMIDDAGS OM 12.45 UUR.

DOOR

DIEDERIK VISSER

GEBOREN OP 10 MAART 1963, TE 's-GRAVENHAGE

PROMOTOR: Prof.Dr. R.D. Schuiling
CO-PROMOTOR: Dr. C. Maijer

Aan Anneke

VOORWOORD

Bij het gereedkomen van dit proefschrift wil ik graag de volgende personen bedanken:

Mijn co-promotor, Dr. C. Maijer, voor zijn voortdurend enthousiasme, deskundige begeleiding en ter beschikking stellen van zijn handstukken en slijpplaten. Zijn zeer goede neus voor de "juiste" monsters is opmerkelijk !!

Mijn promotor, Prof. Dr. R.D. Schuiling voor de constructieve review van de manuscripten en de laatste nuttige suggesties.

Paul Buining, Geert-Jan de Haas, Gé Hermans, Natalie Hulzebos-Sijen, Theo Kloprogge, Andries Krijgsman, Dick Lieftink, Pim van Linschooten, Laurens Nieuwkamp, Timo Nijland, Max Röhrman, Tony Senior, Piet Thijssen, Rob Verschure, en Roland Vogels voor de gezellige tijd, en de vele discussies.

D. Ackermand (Kiel), Paul Anten, Tilly Bouten, Berta Djie-Kwee, Ad van der Eerden, Chiel Eussen, Vian Govers, Ineke Kalt, Pieter Kleingeld, Angelique Lesquillier, Wim Lustenhouwer (Amsterdam), B. Mader (Kiel), Thea van Meerten (Delft), René Poorter, John Schumacher (Freiburg), Nellie Slaats, Christina Strom, tijdschrift-reviewers, Ton Zalm, Theo van Zessen, en alle medewerkers van de gesteente preparatie, de Bibliotheek en de Audio-Visuele dienst voor hun vakkundige inzet, hulp en bijdragen.

Speciaal wil ik, de onlangs overleden, Marius Maarschalkerweerd bedanken voor zijn inzet en enthousiasme bij al het optische werk. Zijn ondersteuning en interesse bij ons gezamenlijke onderzoek naar het intrigerende mineraal kornerupien waren voor mij van grote waarde.

Mijn werkgever, Rijkswaterstaat, dienstkring Huis ter Heide, voor de laserprinter-, plotter- en kopieerfaciliteiten alsmede voor het continue interesse in de voortgang van mijn proefschrift. Alfred, Andre, Arend, Bennie, Dick, Dion, Folkert, Hans, Hetty, Ina, Joke, Meneer de Leeuw, Rob, Ruud en Zwaan en alle andere medewerkers van de dienstkring, bedankt.

Het proefschrift draag ik op aan Anneke, voor de mentale ondersteuning thuis, meestal in de vorm van de van tijd tot tijd hard nodige "stok achter de deur" en natuurlijk voor de geweldige redactionele ondersteuning.

CONTENTS

Chapter 1 has been published in *Journal of Metamorphic Geology,* 8 (1990), 231-246.
Co-author: A. Senior.

Chapter 2 is submitted for publication in *Lithos.*
Co-authors: J.T. Kloprogge and C. Maijer.

Chapter 3 is submitted for publication in *Contributions to Mineralogy and Petrology.*

Chapter 4 has been published in *Mineralogical Magazine,* 55 (1991), 563-577.
Co-author: A. Senior.

Chapter 5 has been published in *Neues Jahbuch für Mineralogie, Monatshefte,* Heft 11 (1992), 513-527.

Chapter 6 has been published in *Mineralogical Magazine,* 56 (1992), 343-351.
Co-authors: P.H.M. Thijssen and J.C. Schumacher.

Chapter 7 has been published in *Norsk Geologisk Tiddskrift,* 72 (1992), 385-388.

INTRODUCTION

The present study is a continuation of a M.Sc. thesis on orthoamphibole-bearing rocks from the Nidelva area, Bamble Sector, south Norway (Visser, 1987), which was carried out within the framework of the Bamble project of the Department of Petrology of the University of Utrecht, the Netherlands. Some of the cordierite-orthoamphibole rocks documented in this pilot study contained a wealth of preserved reaction textures. Furthermore, it was noted that many of the cordierite-orthamphibole rocks contained significant amounts of boron-bearing minerals such as tourmaline, kornerupine and dumortierite.

These observations provided a promising starting point for further investigation aimed at 1) improving the knowledge of the metamorphic evolution of the Proterozoic high-grade Bamble Sector and 2) providing constraints on the behaviour of boron in this lower continental crust. Additionally, the volatile content of several cordierites was studied to provide information on the regional variation in metamorphic fluid compositions.

The Bamble project

The field-research dominated Bamble project was started by Prof. Dr. A.C. Tobi and Dr. C. Maijer in 1983 in response to the new and much shorter student education program. In close cooperation with the Norwegian Geological Survey (N.G.U.) detailed mapping on 1:5000 scale was carried out by M.Sc. students in the summers of 1984-1990. 1:20.000 copies of the mapping activities were supplied to the N.G.U. The mapping area covers the topographical 1:50.000 series M711 map Nelaug (1612 III) and parts of the 1:50.000 maps Mykland (1512 II), Arendal (1611 IV) and Tvedestrand (1612 II) prepared by Norges Geografiske Oppmåling. The map grid of these maps is used as reference grid for location coordinates in this thesis. Besides 23 unpublished mapping-reports the Bamble project has resulted up till now (februari 1993) in some 29 mineralogical, petrological, geochemical, geochronological or ore-related unpublished M.Sc studies (most in dutch), 4 Ph.D. studies (de Haas, 1992; Nijland, 1993; Dam in prep., and this thesis), 34 congres-abstracts, 20 publications in international journals (e.g. Visser & Senior, 1990; Nijland & Senior, 1991; de Haas et al., 1992; Lieftink et al., 1993) and 4 submitted manuscripts.

Organization of this thesis

In Chapter 1 the complex reaction textures and mineral assemblages of three key localities of orthoamphibole-bearing rock in the Froland area, north-west of the Arendal granulite facies terrain are described. The inferred reaction sequence, phase relations and several geothermometers are used to constrain the prograde and part of the retrograde metamorphic P-T path of the area.

Chapter 2 presents and discusses the H_2O, CO_2 and light element (Li, Be, Na) characteristics of cordierites from the Arendal-Tvedestrand amphibolite-granulite facies transition and the Froland and Söndeled amphibolite facies areas.

In Chapter 3 both the prograde formation and retrograde breakdown of the borosilicate kornerupine from Böylefossbru are documented. Implications for early and late metamorphic fluid activity at this kornerupine locality are discussed.

The formation of the borosilicate dumortierite by retrograde breakdown of cordierite, garnet and orthoamphibole is investigated in Chapter 4. Several new substitutions are proposed to explain the observed variations in dumortierite chemistry.

In Chapters 5 and 6 two case studies on mid-amphibolite facies (530-620 °C) retrogradation of high-grade upper-amphibolite to granulite facies assemblages are presented. Chapter 5 discusses a new gedrite-breakdown reaction observed in a gedrite-oligoclase rock from Blengsvatn. Chapter 6 presents the detailed petrography and mineral chemistry of two different polytypes of the Fe-Mg-Zn-Al-Ti oxide högbomite in spinel-sapphirine rocks at Snaresund and Rangleåsen and discusses their petrogenesis.

Chapter 7 presents ammonium (NH_4^+) data for cordierite-orthoamphibole-bearing rocks from Rød and discusses their pre-metamorphic origin.

A summary of the results and the main conclusions are given in Chapter 8.

CHAPTER 1

ALUMINOUS REACTION TEXTURES IN ORTHOAMPHIBOLE-BEARING ROCKS: THE PRESSURE-TEMPERATURE EVOLUTION OF THE HIGH-GRADE PROTEROZOIC OF THE BAMBLE SECTOR, SOUTH NORWAY.

ABSTRACT

Aluminous reaction textures in orthoamphibole-bearing rocks from the Froland area, Bamble, south Norway, record the prograde pressure-temperature path of the high-grade Kongsbergian Orogeny (1600-1500 Ma) and the low-mid amphibolite facies overprint during the Sveconorwegian Orogeny ($\approx$1200-900 Ma). The rocks contain anthophyllite / gedrite, garnet, cordierite, biotite, quartz, andalusite, kyanite, Cr-rich staurolite, tourmaline, ilmenite, rutile and corundum in a variety of parageneses. The P-T path is deduced from petrographic observations, mineral chemistry and zoning, geothermometry and (N)FMASH equilibria. The results indicate the following sequence of metamorphic stages:

- The M_1 phase characterized by the presence of strongly deformed andalusite, gedrite and tourmaline.
- Pressure (4 $\longrightarrow$ 8 kbar) and temperature (500-650 °C) increase with the development of kyanite after andalusite and the growth of staurolite associated with strong Na-Al-Mg zoning in orthoamphibole (M_2 phase).
- Pressure decrease at high P (6-7 kbar) and high T (600-700 °C) during M_{3a} with the production of cordierite $\pm$ corundum between kyanite, staurolite and orthoamphibole and cordierite-growth between corundum and orthoamphibole.
- Temperature increase to 740 $\pm$ 60 °C and 7 kbar; static growth of garnet (M_{3b}), metamorphic climax. The heat supply necessary to explain the temperature increase between the M_{3a} and M_{3b} phases is suggested to be correlated with synkinematic enderbitic-charnockitic and basic intrusions in the Arendal granulite facies terrain.
- M_{3b} metamorphic conditions were followed by an initial isobaric cooling path (early M_4) and late stage pressure decrease (late M_4). Early M_4 conditions of 6-7 kbar and 550-600 °C, assuming $P_{H_2O} < P_{Total}$, are indicated by the retrograde talc-kyanite-quartz assemblage in late quartz-cordierite veins. Late M_4 conditions of 3-4 kbar and 420-530 °C are implied by the kyanite-andalusite-chlorite-quartz assemblage in vein cordierite.

The M_1-M_3 stages are interpreted as being the result of the same metamorphic P-T-path, which was caused by both tectonic and magmatic thickening. A prolonged crustal residence time is proposed for the Bamble Sector before uplift during the later stages of M_4 occurred.

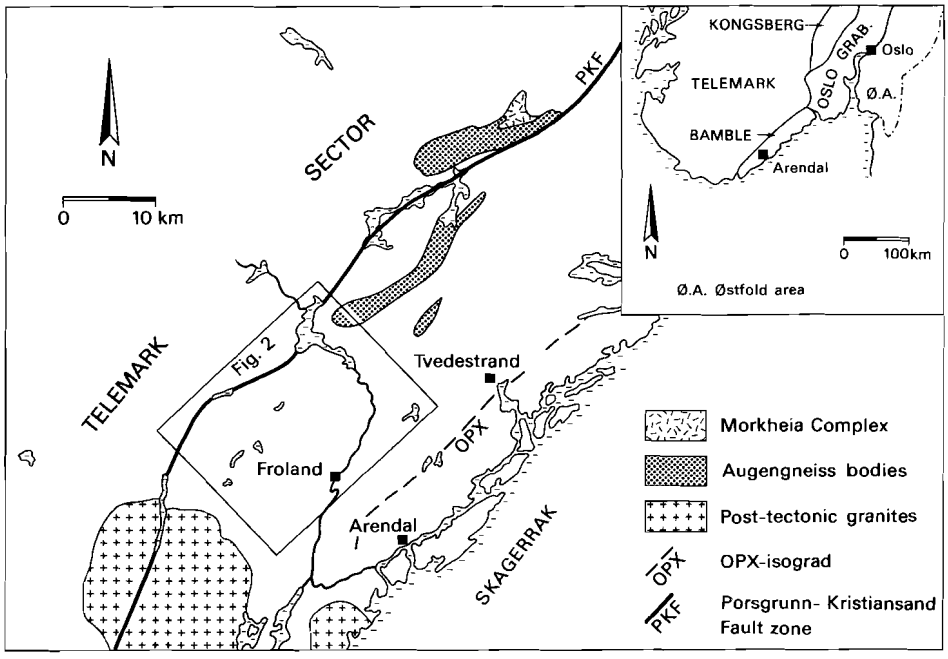

Figure 1.1. Map of the central part of the high-grade Bamble sector. OPX-isograd after Field et al., 1976.

INTRODUCTION

Recent studies (e.g. Baker, Powell, Sandiford & Muhling, 1987; Harley, 1985; Hudson & Harte, 1985) have stressed the importance of orthoamphibole-bearing mineral assemblages as indicators of variations in metamorphic conditions of medium- to high-grade metamorphic terrains.

Corona textures or aluminous enclaves in orthoamphibole-bearing rocks (e.g. Harley, 1985; Robinson & Jaffe, 1969; Schumacher & Robinson, 1987; Sharma & MacRae, 1981) provide information concerning the pressure-temperature (P-T) vectors which are important tools in deducing the P-T-time path and possibly the paleo-tectonic environment of a metamorphic area (e.g. Bohlen, 1987; Ellis, 1987; Thompson & England, 1984). In this paper the petrographic and geochemical aspects of reaction textures involving aluminous minerals (aluminous enclaves) and mineral zoning in orthoamphibole-bearing rocks of the Proterozoic of the Bamble sector, south Norway, are discussed and a possible P-T path documented by these textures is proposed.

GEOLOGICAL SETTING

The high-grade Proterozoic of the Bamble sector, south Norway, records two main periods of metamorphism and deformation. During the Kongsbergian orogeny (1600-1500 Ma) both the Bamble and Kongsberg sectors (Fig. 1.1) were subject to a major gneiss-forming event which reached amphibolite-granulite facies conditions and produced a N.E.- S.W. trending grain (Field & Råheim, 1979, 1981; Field et al., 1985; Smalley & Field, 1985; Starmer, 1972, 1985). In the Bamble sector, granulite facies conditions were reached along the Skagerrak coast between Arendal and Risör (Cooper & Field, 1977; Field et al., 1980; Starmer, 1969, 1972, 1985). P-T estimates for the Arendal granulite facies area range 700-800 °C at 6-8 kbar (Touret, 1971a) and 800 $\pm$ 60 °C at 7.3 $\pm$ 0.5 kbar (Lamb et al., 1986). The Kongsbergian orogeny was accompanied by basic intrusives, concordant to slightly discordant sheets with tholeiitic to calc-alkaline affinities. These intrusives were metamorphosed under the amphibolite-granulite facies conditions (Smalley et al., 1983). The geochemical signature of both charnockitic-enderbitic orthogneisses and basic intrusives has been interpreted as the result of subduction-related processes analogous to the evolution of an 'Andes type' orogenic belt.

Around 1200 Ma numerous concordant to discordant stocks and sheets of olivine gabbros and norites (hyperites) intruded. This basic activity was probably related to an anorogenic period of large-scale tension-related magmatism, which began with the intrusion of the Morkheia layered alkaline complex (Milne & Starmer, 1982), of which the monzonitic suite

is dated at about 1250 Ma (Smalley et al., 1988). This period of continental thinning without rifting ended by the beginning of the Sveconorwegian orogeny.

The metamorphic grade of this orogeny ($\approx$1200-900 Ma) in both the Bamble and Kongsberg sectors has been a matter of debate. Originally the high-grade, upper-amphibolite to granulite facies, metamorphism in southern Norway was considered to be Sveconorwegian in age (e.g. Touret, 1971a, 1971b). During the last decade it has been shown that the high-grade event was Kongsbergian in age (Field & Råheim, 1979, 1981; Smalley et al., 1988; Starmer, 1985). The Sveconorwegian event is now considered by many to have been a period of extensive fluid activity associated with the formation of granites, pegmatites and albitites. The metamorphic grade reached greenschist to mid-amphibolite facies conditions. The intensity of the deformation associated with the Sveconorwegian Orogeny increases towards the Porsgrunn-Kristiansand-Faultzone (PKF) and seems, therefore, cogenetic.

Orthoamphibole-bearing rocks are well known from the Bamble sector (e.g. Beeson, 1976, 1978; Bugge, 1943). The samples described in this study (localities A, B and C, in Fig. 1.2) come from the Froland area N.W. of the Arendal granulite facies terrain. The rocks of the Froland area comprise quartzites, graphite-bearing gneisses, actinolite-hedenbergite gneisses with rare intercalations of marble, nodular sillimanite $\pm$ muscovite gneisses, garnet-amphibolites as well as a possible metavolcanic or meta-greywacke suite of tonalitic to granodioritic biotite-hornblende gneisses. Peak metamorphic conditions in the Froland area reached upper-amphibolite facies, with sillimanite as the stable aluminium silicate. Sheets of gneissified biotite-hornblende granite cut discordantly across the sedimentary-volcanic suite. Gabbroic stocks and sheets intruded the sedimentary-volcanic suite and the granitic rocks during the first stages of the Sveconorwegian orogeny (Theulings et al., 1986; Verdonk et al., 1986; de Haas et al., 1992). The orthoamphibole-bearing rocks in the Froland area occur as thin layers and lenses associated with sillimanite gneisses, quartzites and thin amphibolite layers.

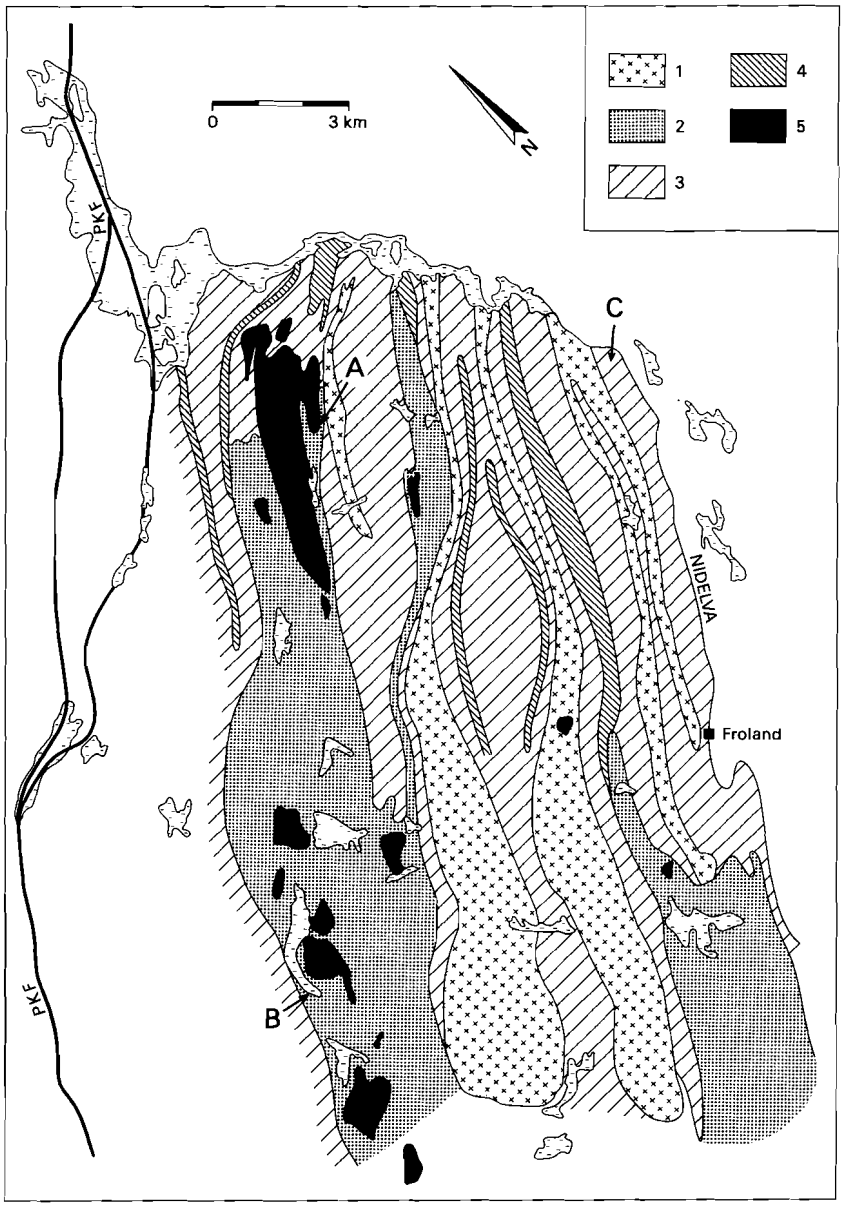

Figure 1.2. Location map of the Froland area showing the positions of sample localities A, B and C. Geology modified after Starmer (1986). 1 = granites, granitic gneisses; 2 = quartzites, calc-silicate rocks, marbles; 3 = tonalitic to granodioritic gneisses; 4 = amphibolites; 5 = metagabbros.

PETROGRAPHY

The mineral assemblages and the modal amounts at the three localities are summarized in Table 1.1.

Locality A (PL055) is a small occurrence in a unit consisting of hedenbergite-actinolite gneiss, thin amphibolites and nodular muscovite-sillimanite gneiss. The initial mineral assemblage consists of coarse (1-5 mm) sub- to anhedral elongate kyanite with a sporadic faint purple-blue colour, elongated, euhedral to subhedral prismatic colourless orthoamphibole, minor amounts of intergranular plagioclase, euhedral to subhedral elongated brown tourmaline, quartz and abundant subhedral rutile. A very thin rim of cordierite is always developed between kyanite and orthoamphibole (Fig. 1.3). Light-brown biotite flakes occur as a common replacement of orthoamphibole. Exsolution lamellae have not been observed in orthoamphibole. Primary kyanite has not previously been reported from the Bamble sector.

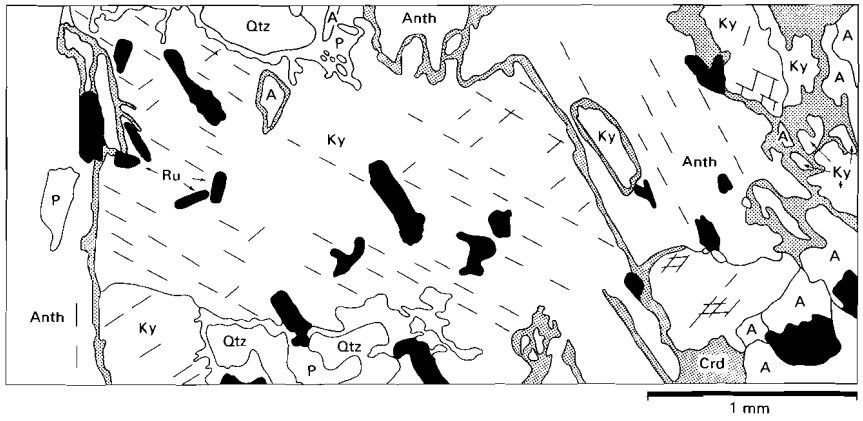

Figure 1.3. Reaction textures in PL055, locality A. Cordierite (Crd, stippled) formed between kyanite (Ky) and anthophyllite (Anth, A). P = Plagioclase, Qtz + Quartz.

Locality B (BD031-033, DV042, DV301) is a lens-shaped body, within a sequence of quartzites and nodular muscovite-sillimanite gneisses. In most thin sections a compositional layering is present consisting of

a Quartz-tourmaline-rich layers with enclaves (0.5-30 mm) of strongly deformed and elongated andalusite, subordinate weakly deformed kyanite and staurolite in a matrix of cordierite. Occasionally, corundum rims large andalusite and kyanite grains. Reddish brown biotite and orthoamphibole occur in small amounts.

Table 1.1.
Mineral assemblages, modal proportions and metamorphic sequences in selected samples

				M1				M2		M3a		M3b	M4						Accessories			
	Qtz	Pl	Bt	And	Tur	Oam	Ky	St	Crn	Crd	Crn	Grt	Crd	Chl	Dum	Grn	Tur	Ky	And	Ilm	Rt	Zrn	Ap
A PL055#	a	O	a		O	XXX	XX			O											O	a	O
B BD031	O		O	O	a	XX	O	O		XXX	a			a						O	a	a	O
BD032	X		XX	a	a	XXX	O	O		XX				O						X	O	a	O
BD033	X		X	O	O	XX	O	O		XXX				a						O	a	a	O
DV042			XX			XXX	a	a		XXX				O						O	O	a	a
DV301	XX		a		X	XXX	a			XXX				a						O	a	a	O
C DV029			O			XXX		O	O	XX				a							O	a	a
DV030	O		X			XX				XXX		XXX		a	a						O	a	a
DV034	XXX												a	XX	a	a	a	X	O				a
DV035	XX		O			XXX				XX		X			a						a	a	a
DV036	XXX		O			X				O		XXX		a	a						a	a	a
DV037	XX		O			XX		a		X		XXX		a	a						O	a	O

Abbreviations after Kretz (1983) except for Dum = Dumortierite; Grn = Grandidierite.
# Average of 5 thin sections
a = 0-1 vol.% ; O = 1-5 vol.% ; X = 5-10 vol.% ; XX = 10-30 vol.% ; XXX > 30 vol.%

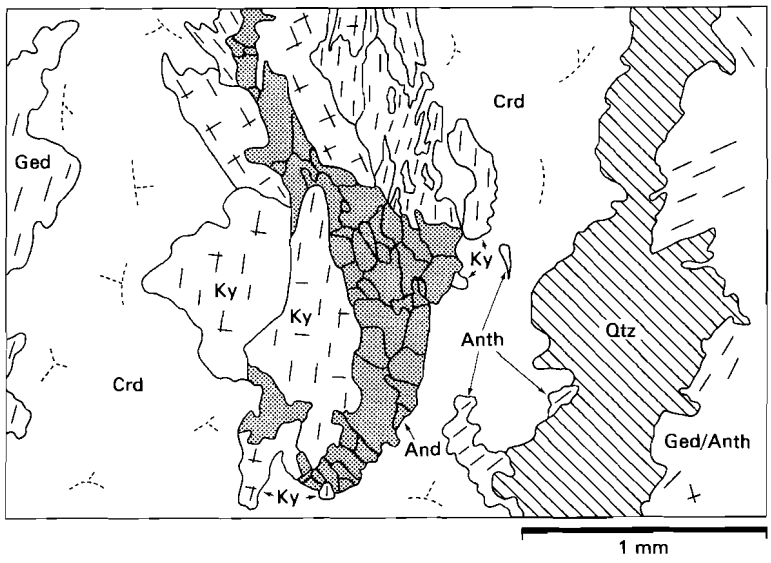

Figure 1.4. Reaction textures in BD031, locality B. Kyanite overgrowth on deformed andalusite (stippled) set in cordierite.

b Biotite-orthoamphibole-rich layers with enclaves (1-20 mm) of staurolite, kyanite, and sometimes andalusite in a matrix of cordierite. Quartz is only present as inclusions in the orthoamphibole.

Both andalusite and yellow-brown tourmaline in the quartz-tourmaline-rich layers show an anhedral strongly elongated subgrain fabric parallel to the compositional layering. Weakly deformed kyanite and staurolite are commonly intergrown, but also occur as solitary grains. Neither one of the minerals show a preferred orientation. Although staurolite is generally intergrown with kyanite, some small crystals are located near andalusite. Kyanite grains have been observed overgrowing the deformed andalusite crystals (Fig. 1.4). Elongate kyanite occurs in the quartz-tourmaline-andalusite layers suggesting a pseudomorphism of the elongated deformed andalusite by kyanite. Usually, however, kyanite and andalusite grains do not occur together. Colourless, irregularly shaped and inclusion-free grains of corundum rim large (> 4 mm) andalusite and kyanite grains. Staurolite has not been observed in the corundum-bearing enclaves.

At least two generations of orthoamphibole were detected:

- strongly deformed crystals, showing an elongated subgrain fabric, which developed in the biotite-rich layers consuming most of the biotite. Some crystals crosscut the andalusite-tourmaline-quartz layers, but most are parallel to the compositional layering.

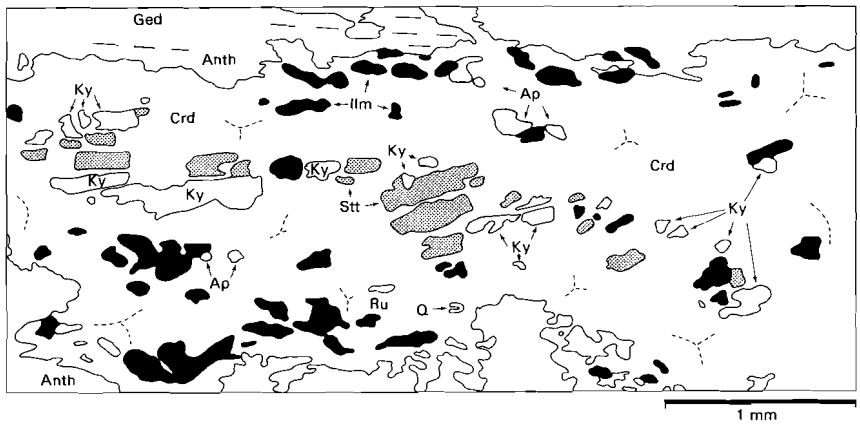

Figure 1.5. Reaction textures in BD031, locality B. Cordierite formed between orthoamphibole and embayed grains of kyanite and less resorbed staurolite (stippled).

- weakly deformed to undeformed grains overgrowing the deformed grains at their margins.

Both orthoamphiboles are colourless, although a light-brown coloration occurs where exsolution lamellae of orthoamphibole are developed parallel to (010) and (001) in the center of the strongly deformed grains. The two directions of exsolution were only observed in separate grains and never in the same single crystal. The deformed orthoamphiboles contain inclusions of quartz in contrast to the weakly deformed orthoamphiboles which are virtually free of inclusions.

Polygonal cordierite aggregates occur between and around both orthoamphibole generations, kyanite, staurolite, andalusite and corundum. Andalusite, kyanite, corundum and orthoamphiboles show resorbed margins adjacent to the cordierite (Fig. 1.5, 1.6). Small staurolite grains tend to show less resorbed or rounded margins in contact with cordierite while large grains have strongly resorbed or ragged margins. Staurolite, andalusite and kyanite have not been observed in contact with orthoamphibole, biotite or quartz. Cordierite is slightly pinitised; aggregates of chlorite replace orthoamphibole and cordierite. No spatial relationship between the chlorite aggregates and the aluminium silicates exists. Accessory minerals are apatite, rutile, zircon and ilmenite. Staurolite has only been reported once before from the Bamble (C.Nnanedu, personal comment, in Ramsay & Morton, 1971).

Locality C (DV029, 030, DV034-037), is a small heterogeneous lens (5x2 m) with quartz-free and quartz-bearing parts. The surrounding rocks consist of an alternation of garnet-amphibolites and biotite-muscovite-sillimanite gneisses. Several coarse-grained cordierite-quartz $\pm$ garnet segregations are present. The petrographic observations show very

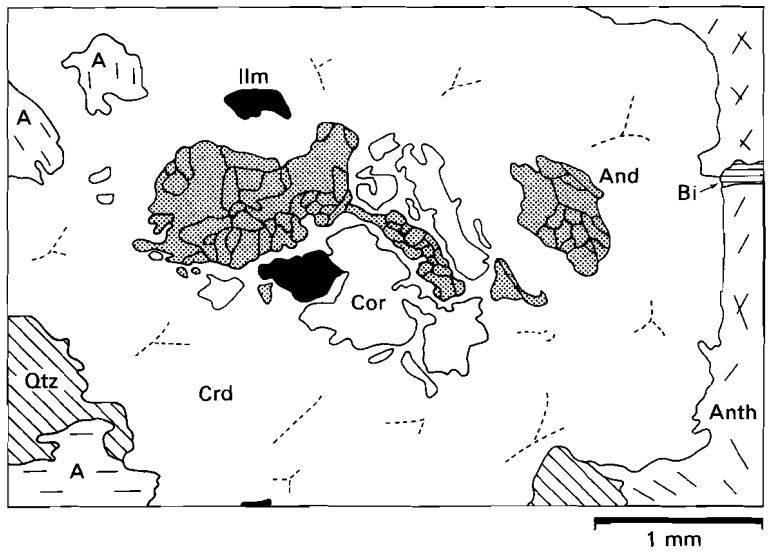

Figure 1.6. Reaction textures in BD031, locality B. Corundum and cordierite formation between orthoamphibole and strong deformed andalusite (stippled). Note the presence of quartz (hatched) near the edge of the enclave.

coarse-grained anhedral poikiloblastic cordierite grains, euhedral to subhedral yellow-brown orthoamphibole, reddish brown biotite and abundant rutile. The biotite, orthoamphibole and rutile grains are deformed and foliated. No new-growth of orthoamphibole has been observed. Anhedral corundum and staurolite grains, with inclusions of rutile, apatite and biotite occur as corroded and foliated relics in the cordierite blasts, in the quartz-free parts of the rock. The corundum and staurolite enclaves usually contain only one or a few large crystals (up to 9 mm) and are not observed together in the same enclave. The orthoamphibole often shows corroded margins when in contact with cordierite. Exsolution lamellae were not detected on microscopic scale. In the quartz-bearing part of the rock subhedral garnet porphyroblasts up to several centimeters in diameter developed, overgrowing the biotite-orthoamphibole foliation. Locally garnet developed between orthoamphibole and cordierite (Fig. 1.7). The garnet is poikiloblastic with inclusions of cordierite, biotite, orthoamphibole, quartz and rutile. Strong retrogradation of the garnet occurred along cracks with formation of white mica, chlorite and rarely dumortierite.

The younger coarse-grained quartz-cordierite $\pm$ garnet segregations cut across the garnet blasts. Cordierite within these segregations is partially to totally replaced by a mixture of quartz, chlorite, kyanite and andalusite crystals. Textural relationships between both aluminium silicates do not resolve the relative ages of both minerals. Small tourmaline, dumortierite and grandidierite crystals occur in the replacement aggregates. Mutual contacts

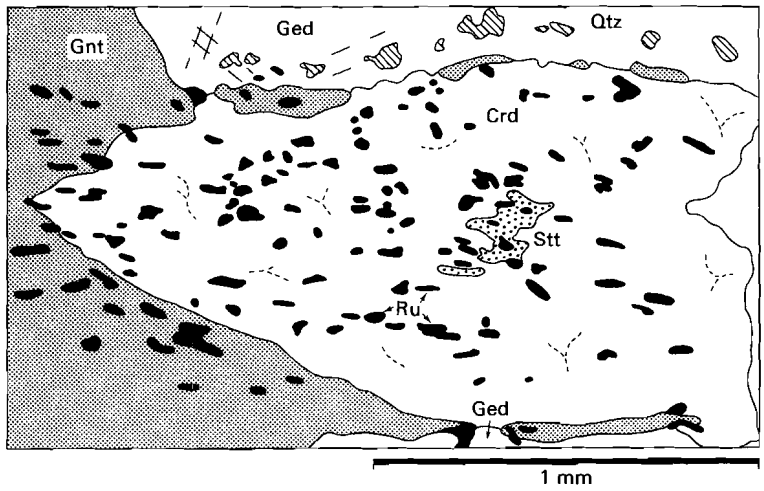

Figure 1.7. Reaction textures in DV037, locality C. Formation of garnet (fine stippled) between cordierite and gedrite. Cr-rich staurolite (stippled) occurs in the centre of the cordierite enclave. Note the numerous quartz inclusions (hatched) in gedrite near cordierite.

between the three borosilicates have, however, not been observed. The quartz-cordierite segregations are probably cogenetic with the abundant quartz-feldspar veins and pegmatites near locality C.

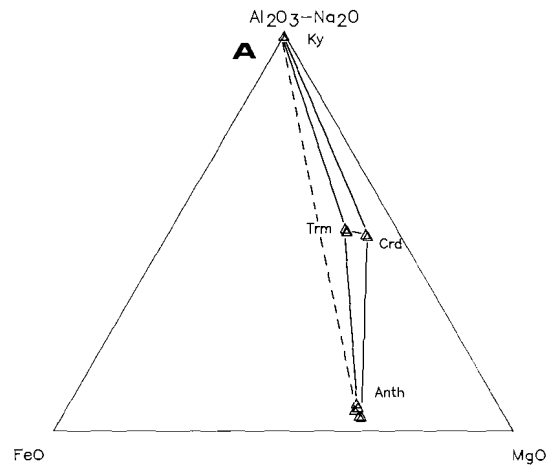

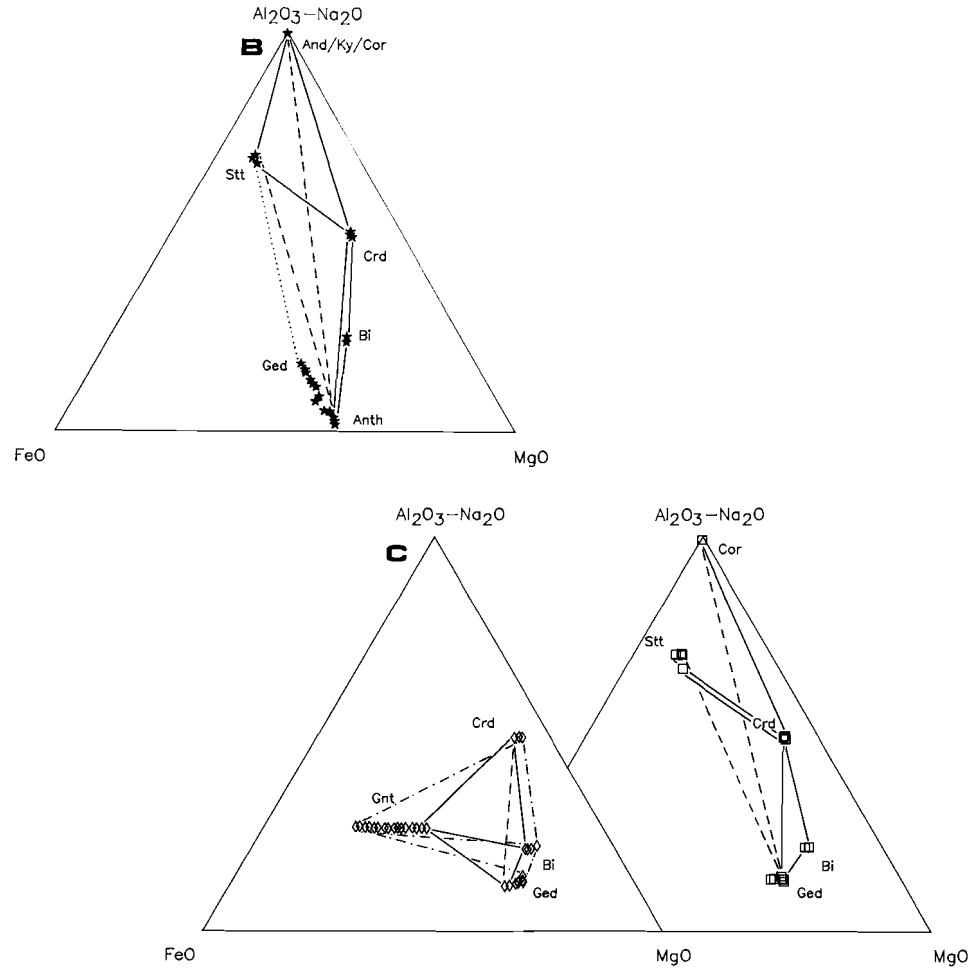

Figure 1.8. (a) (Al_2O_3-Na_2O)-FeO-MgO diagram illustrating compositions of minerals and mineral assemblages from locality A (PL055). Solid lines represent M_3 relations; broken lines represent M_2 relations.
(b) (Al_2O_3-Na_2O)-FeO-MgO diagram illustrating compositions of minerals and mineral assemblages from locality B (BD031). Solid lines represent M_3 relations; broken lines represent M_2 relations; dotted lines represent M_1-early M_2 relations.
(c) (Al_2O_3-Na_2O)-FeO-MgO diagram illustrating compositions of minerals and mineral assemblages from locality C (DV030\036; DV029). Solid lines represent M_3 relations; solid-dashed lines represent M_4 relations; broken lines represent M_2 relations.

MINERAL CHEMISTRY

The analyses have been obtained using a Cambridge Instrument Co. Microscan Mark-9 electron probe operated at an acceleration potential of 20 kV and a sample current of 25 nA

at the Free University of Amsterdam. Raw data were corrected with a ZAF correction computer program. Natural minerals and synthetic compounds were used as standards.

Staurolite compositions were normalized to 23 oxygens consistent with a half unit cell of 22 oxygens and two (OH-) groups (Griffen & Ribbe, 1973). Only minerals in thin sections PL055 (Loc. A), BD031, DV301 (Loc. B), DV029, DV030 and DV036 (Loc. C) were analyzed. In Fig. 1.8a, b, c the compositions of the minerals from localities A, B, C respectively are presented in A'FM diagrams, with projection from H_2O in the system Na_2O-FeO-MgO-Al_2O_3-SiO_2-H_2O (NFMASH). Representative compositions of major and minor constituents are presented in Tables 1.2.1 - 1.2.5.

Table 1.2.1.
Representative mineral analyses from sample no. Pl055, locality A.

Spot	Ath AD	Ath AE	Tur 36a	Pl 21	Pl 46	Ky 9	Crd 19	Crd 41	Rt 17
SiO_2	50.52	51.07	35.14	67.64	65.48	37.16	49.35	49.19	0.00
TiO_2	0.13	0.04	1.27	0.00	0.00	0.00	0.00	0.00	100.20
Al_2O_3	7.79	6.51	32.90	19.65	20.72	62.93	32.92	33.14	0.00
FeO*	17.48	18.24	4.26	0.30	0.11	0.18	3.46	3.35	0.26
MnO	0.05	0.05	0.03	0.00	0.00	0.00	0.00	0.00	
MgO	19.94	20.29	8.40	0.09	0.22	0.03	11.25	11.53	0.00
CaO	0.14	0.10	1.48	0.43	1.90				0.00
Na_2O	0.84	0.71	1.48	11.45	10.83		0.07	0.10	
K_2O	0.00	0.00	0.00	0.00	0.05		0.00	0.00	
Total	96.89	97.01	84.96	99.56	99.31	100.30	97.05	97.31	100.46
O-basis	23	23	49	8	8	5	18	18	2
Si	7.246	7.339	11.518	2.973	2.901	1.000	5.029	5.000	0.000
Ti	0.014	0.004	0.313	0.000	0.000	0.000	0.000	0.000	0.998
Al^{IV}	0.754	0.661	0.482	1.018	1.082	0.000	3.954	3.971	0.000
Al^{VI}	0.564	0.442	12.227			1.996			
Fe	2.096	2.191	1.167	0.011	0.004	0.004	0.295	0.285	0.003
Mn	0.007	0.007	0.007	0.006	0.000		0.000	0.000	0.000
Mg	4.263	4.346	4.102	0.000	0.015	0.001	1.708	1.747	0.000
Ca	0.021	0.015	0.518	0.020	0.090				0.000
Na	0.233	0.197	0.942	0.976	0.931		0.014	0.020	
K	0.000	0.000	0.000	0.000	0.003		0.000	0.000	
Total	15.198	15.202	31.276	5.004	5.026	3.001	11.000	11.023	1.001
XMg**	0.670	0.665	0.779				0.853	0.860	
Na(A)	0.198	0.202							
An %				2.0	9.1				

* total iron as FeO.
** XMg as Mg/(Mg + Fe^{2+}).
Cr, Zn, Nb and Cl not detected.

Table 1.2.2.
Representative mineral analysis from samples no. BD031 and DV301, locality B.

	BD031							Deformed grains →				New grains →		DV301	
Spot	Ky 10	And XB	St DN	Bt 25	Crd 17	Ilm 18	Core Ged AI	Ged 54	Ged OG	Rim Ath OC	Rim Ath OM	Ath 23	Core Ath 52	Core Tur 2-17	Rim Tur 2-25
SiO_2	37.46	36.71	27.18	38.29	49.43	0.00	43.99	45.50	48.72	53.53	53.65	54.92	54.39	35.43	36.14
TiO_2	0.00	0.06	0.38	1.26	0.00	54.15	0.17	0.13	0.15	0.07	0.07	0.00	0.00	1.06	0.80
Al_2O_3	62.27	62.63	54.73	18.07	32.80	0.00	15.71	13.81	9.37	2.55	3.03	1.47	2.06	33.47	32.82
FeO*	0.17	0.24	12.98	12.81	5.25	46.54	20.57	21.26	21.10	21.62	21.04	21.88	21.40	4.29	3.76
MnO	0.00	0.00	0.07	0.04	0.00	0.00	0.17	0.16	0.16	0.13	0.15	0.13	0.19	0.00	0.01
MgO	0.05	0.09	2.66	14.92	10.25	0.07	13.62	14.74	16.53	18.84	18.51	19.28	19.17	8.67	8.86
CaO	0.00	0.00	0.00	0.00	0.00		0.46	0.37	0.35	0.25	0.29	0.19	0.31	1.83	0.93
Na_2O	0.00	0.05	0.00	0.33	0.30		1.58	1.26	0.84	0.14	0.11	0.05	0.13	1.26	2.05
K_2O	0.00	0.00	0.00	8.58	0.00		0.00	0.00	0.00	0.00	0.00	0.00	0.00	0.00	0.00
ZnO			0.19	0.00											
Total	99.95	99.78	98.19	94.30	98.03	100.76	96.28	97.23	97.23	97.13	96.85	97.92	97.65	86.11	85.36
O-basis	5	5	23	22	18	3	23	23	23	23	23	23	23	49	49
Si	1.011	0.994	3.750	5.645	5.031	0.000	6.499	6.661	7.099	7.775	7.786	7.899	7.840	11.453	11.739
Ti	0.000	0.001	0.039	0.139	0.000	1.013	0.019	0.014	0.016	0.008	0.008	0.000	0.000	0.258	0.195
Al^{IV}			0.250	2.355	3.935	0.000	1.501	1.339	0.901	0.225	0.214	0.101	0.160	0.547	0.261
Al^{VI}	1.982	1.999	8.651	0.785			1.235	1.044	0.708	0.212	0.304	0.149	0.190	12.207	12.305
Fe	0.004	0.005	1.498	1.579	0.447	0.968	2.541	2.603	2.571	2.626	2.553	2.631	2.580	1.160	1.021
Mn	0.000	0.000	0.008	0.005	0.000	0.000	0.022	0.020	0.020	0.016	0.018	0.016	0.023	0.000	0.003
Mg	0.002	0.004	0.546	3.279	1.556	0.003	2.998	3.215	3.589	4.078	4.003	4.134	4.118	4.178	4.290
Ca	0.000	0.000	0.000	0.000	0.000		0.072	0.059	0.054	0.039	0.045	0.030	0.047	0.634	0.324
Na	0.000	0.003	0.000	0.095	0.058		0.452	0.359	0.237	0.040	0.030	0.015	0.035	0.790	1.291
K	0.000	0.000	0.000	1.614	0.000		0.000	0.000	0.000	0.000	0.000	0.000	0.000	0.000	0.000
Zn			0.019	0.000											
Total	2.999	3.006	14.761	15.496	11.027	1.984	15.339	15.314	15.195	15.019	14.961	14.975	14.993	31.062	31.429
XMg**			0.267	0.675	0.777		0.541	0.553	0.583	0.608	0.611	0.611	0.615	0.783	0.808
Na(A)							0.339	0.314	0.195	0.019	-	-	-	-	-

* Total iron as FeO.
** XMg as $Mg/(Mg + Fe^{2+})$.

Table 1.2.3.
Representative mineral analyses from sample no. DV029, locality C.

Spot	Core St DM	Rim St DG	St DA	Crn 1	Crd C1	Crd C3	Bt B2	with Crn Ged AB	with St Ged AK	Rt R1
SiO_2	26.33	26.45	26.49	0.00	49.18	48.87	38.51	47.60	47.10	0.00
TiO_2	1.11	1.06	1.11	0.00	0.00	0.00	1.71	0.30	0.38	94.53
Al_2O_3	55.30	54.91	52.86	99.86	32.87	33.01	17.01	13.11	12.52	0.00
Cr_2O_3	0.64	0.72	2.18	0.13			0.07	0.06	0.14	0.49
FeO*	10.67	11.15	10.47	0.18	3.08	3.35	8.70	14.48	14.47	0.56
MnO	0.08	0.05	0.04		0.00	0.00	0.00	0.20	0.20	0.00
MgO	3.37	2.90	3.39	0.00	11.29	11.15	18.64	19.55	19.56	0.00
CaO	0.00	0.00	0.00		0.00	0.00	0.00	0.71	0.73	0.00
Na_2O	0.00	0.00	0.00		0.13	0.22	0.41	1.11	1.15	
K_2O	0.00	0.00	0.00		0.00	0.00	8.67	0.00	0.00	
ZnO	0.33	0.47	0.32				0.00	0.00	0.09	
Nb_2O_5										1.51
Total	97.83	97.71	96.86	100.17	96.55	96.60	93.72	97.12	96.34	97.09
O-basis	23	23	23	3	18	18	22	23	23	2
Si	3.623	3.655	3.697	0.000	5.029	5.005	5.620	6.751	6.751	0.000
Ti	0.115	0.110	0.116	0.000	0.000	0.000	0.188	0.032	0.041	0.981
Al^{IV}	0.377	0.345	0.303	0.000	3.962	3.985	2.380	1.249	1.249	0.000
Al^{VI}	8.594	8.598	8.391	1.996			0.546	0.943	0.867	
Cr	0.070	0.078	0.241	0.002			0.008	0.007	0.016	0.005
Fe	1.228	1.288	1.222	0.003	0.264	0.287	1.062	1.717	1.735	0.006
Mn	0.009	0.006	0.005		0.000	0.000	0.000	0.024	0.025	0.000
Mg	0.691	0.597	0.704	0.000	1.721	1.702	4.055	4.133	4.178	0.000
Ca	0.000	0.000	0.000		0.000	0.000	0.000	0.109	0.112	0.000
Na	0.000	0.000	0.000		0.026	0.043	0.116	0.305	0.318	
K	0.000	0.000	0.000				1.614	0.000	0.000	
Zn	0.034	0.048	0.033				0.000	0.000	0.009	
Nb										0.009
Total	14.741	14.725	14.712	2.010	11.002	11.022	15.590	15.301	15.301	1.001
XMg**	0.360	0.317	0.366		0.867	0.856	0.792	0.706	0.707	
Na(A)								0.301	0.301	

* total iron as FeO.
** XMg as $Mg/(Mg + Fe^{2+})$.
Cl not detected

Table 1.2.4.
Representative mineral analyses from sample no. DV030, locality C.

	Core →		Rim	with garnet			with garnet		with garnet	
	Grt	Grt	Grt	Ged	Ged	Crd	Crd	Bt	Bt	Rt
Spot	30	36	54	OB	OF	17	28	8	3	25
SiO_2	40.36	39.50	38.90	46.97	47.04	48.76	48.69	38.32	37.82	0.00
TiO_2	0.00	0.04	0.00	0.38	0.38	0.00	0.00	2.41	1.29	95.43
Al_2O_3	22.24	22.20	21.72	14.18	13.25	32.86	32.99	16.39	17.42	0.00
Cr_2O_3	0.00	0.00	0.00	0.14	0.12	0.00	0.00	0.00	0.00	1.28
FeO*	23.52	26.40	30.27	13.54	14.99	3.53	3.01	9.98	8.97	0.19
MnO	0.47	0.58	0.74	0.13	0.13	0.00	0.00	0.00	0.00	
MgO	11.64	10.12	7.06	19.89	18.44	11.16	11.51	17.27	18.70	0.00
CaO	2.32	1.86	2.23	0.72	0.67	0.00	0.00	0.00	0.00	0.00
Na_2O				1.21	1.15	0.09	0.06	0.29	0.27	
K_2O				0.00	0.00			8.83	8.71	
Nb_2O_5										1.06
Total	100.55	100.70	100.92	97.16	96.17	96.40	96.26	93.49	93.18	97.96
O-basis	12	12	12	23	23	18	18	22	22	2
Si	3.028	3.001	3.010	6.637	6.754	5.006	4.995	5.649	5.563	0.000
Ti	0.000	0.002	0.000	0.040	0.041	0.000	0.000	0.268	0.142	0.980
Al^{IV}	0.000	0.000	0.000	1.363	1.246	3.977	3.990	2.351	2.437	0.000
Al^{VI}	1.967	1.988	1.981	0.999	0.996			0.496	0.583	
Cr	0.000	0.000	0.000	0.016	0.014	0.000	0.000	0.000	0.000	0.014
Fe	1.476	1.677	1.959	1.600	1.801	0.303	0.258	1.230	1.103	0.002
Mn	0.030	0.038	0.048	0.016	0.016	0.000	0.000	0.000	0.000	
Mg	1.301	1.146	0.814	4.188	3.945	1.708	1.759	3.795	4.099	0.000
Ca	0.186	0.151	0.185	0.108	0.103	0.000	0.000	0.000	0.000	0.000
Na				0.331	0.321	0.017	0.011	0.083	0.077	
K				0.000	0.000			1.660	1.635	
Nb										0.007
Total	7.988	8.003	7.997	15.298	15.237	11.011	11.013	15.532	15.639	1.003
XMg**	0.468	0.406	0.294	0.724	0.687	0.849	0.872	0.755	0.788	
Na(A)				0.298	0.237					

* Total iron as FeO.
** XMg as $Mg/(Mg + Fe^{2+})$.
Cl and Zn not detected.

Table 1.2.5.
Representative mineral analyses from sample no. DV036, locality C.

	Core →		Rim			with garnet		with garnet
	Grt	Grt	Grt	Ged	Crd	Crd	Bt	Bt
Spot	61	13	74	24	75	80	2	10
SiO_2	39.85	39.45	38.56	47.16	48.17	49.23	37.85	37.81
TiO_2	0.00	0.00	0.00	0.45	0.00	0.00	2.28	1.44
Al_2O_3	22.33	21.99	21.53	12.56	32.76	32.85	16.36	16.78
Cr_2O_3	0.00	0.00	0.00		0.00	0.00		
FeO*	24.13	27.69	30.35	15.89	3.51	2.77	10.06	9.60
MnO	0.56	0.78	0.92	0.12	0.00	0.00	0.00	0.00
MgO	11.45	9.33	6.78	18.63	11.19	11.55	17.02	17.78
CaO	2.43	2.03	2.09	0.74	0.00	0.00	0.00	0.00
Na_2O				1.09	0.10	0.11	0.41	0.29
K_2O				0.00	0.00	0.00	8.55	8.78
Total	100.75	101.27	100.23	96.64	95.73	96.51	92.53	92.48
O-basis	12	12	12	23	18	18	22	22
Si	2.998	3.002	3.010	6.770	4.984	5.029	5.636	5.621
Ti	0.000	0.000	0.000	0.049	0.000	0.000	0.255	0.161
Al^{IV}	0.002	0.000	0.000	1.230	3.995	3.956	2.364	2.379
Al^{VI}	1.978	1.972	1.982	0.896			0.417	0.562
Cr					0.000	0.000		
Fe	1.518	1.762	1.982	1.908	0.304	0.237	1.253	1.193
Mn	0.036	0.050	0.061	0.015	0.000	0.000	0.000	0.000
Mg	1.283	1.058	0.789	3.985	1.726	1.758	3.778	3.941
Ca	0.196	0.165	0.175	0.114	0.000	0.000	0.000	0.000
Na				0.305	0.020	0.023	0.117	0.084
K				0.000	0.000	0.000	1.625	1.666
Total	8.011	8.009	7.999	15.272	11.029	11.003	15.445	15.607
XMg**	0.458	0.375	0.285	0.676	0.850	0.881	0.751	0.768
Na(A)				0.272				

* Total iron as FeO.
** XMg as $Mg/(Mg + Fe^{2+})$.
Zn, Nb and Cl not detected.

The analyzed **garnets** in DV030 and 036 are pyrope-rich almandines with an average X_{Mg}, defined as $Mg/(Mg+Fe^{2+})$, for the core of 0.470. Due to later retrogradation the garnet is fractured along cracks. Small fragments of garnet show a continuous decrease of Mg and increase of Fe and Mn towards their margins. Large fragments, with homogeneous pyrope-rich cores, exhibit only a small retrograde rim. X_{Mg} varies from 0.481 to 0.323.

Grossular mole proportions range from 0.050 to 0.071 but show no relationship with the retrograde zoning pattern. Spessartine mole proportions range from 0.010 in the core to 0.020 in the edge of the garnet.

Cordierite is the most magnesian mineral at all localities. The cordierites are homogeneous at localities A and B and the quartz-free part of locality C (DV029) with X_{Mg} values ranging 0.77-0.78 (Loc. B) and 0.85-0.86 (Loc. A, C). In the garnet and quartz bearing parts of locality C cordierite is zoned from X_{Mg} = 0.85 in the matrix to X_{Mg} = 0.88 adjacent to the garnet. Na is the only trace element to be detected and ranges 0.05-0.07 (Loc. B), 0.07-0.14 (Loc. A) and 0.06-0.41 wt.% (Loc. C).

Staurolite has X_{Mg} values which range 0.24-0.30 (BD031) and 0.35-0.37 (DV029). Despite the range in X_{Mg} each individual staurolite grain in BD031 is chemically homogeneous. Large grains always display higher X_{Mg} than the smaller grains. The large staurolites from DV029 are slightly zoned with Mg-rich cores and Fe-enriched rims. Average Si-content per formula unit is 3.63 for DV029 and 3.83 for BD031. These low Si-contents are characteristic for Mg-rich staurolites in silica-deficient rocks (Grew & Sandiford, 1984). The zinc content is low, 0.003-0.033 (BD031) and 0.023-0.050 (DV029) wt.% ZnO, and is, therefore, not considered important in stabilizing the staurolites. Chromium was not detected in BD031 but occurs in considerable amounts in the staurolites of DV029. The chromium content of the large grains, 0.58-0.72 wt.% Cr_2O_3, does not correlate with the observed Mg-zoning. In a small grain values up to 2.18 wt.% Cr_2O_3 were obtained. Moderate to high Cr_2O_3 contents in staurolites are known from several places (e.g. Enami & Zang, 1988; Sharma & MacRae, 1981); however, the analyses indicate that this is one of the Cr-richest staurolite ever reported (e.g. Nicollet, 1986 (2.2 wt.%) and Ward, 1984a (2.01 wt.%)). The unusual pleochroic scheme of the Cr-rich staurolite described by Ward (X clear, slightly bluish green, Y yellowish green and Z muddy greenish yellow) was not detected in the small grain (X light-yellow, Y yellow and Z yellow), probably the very high Ti-content (1.13 wt.% TiO_2, see Table 1.2.3) of the small grain stabilizes the normal yellow pleochroism with higher Cr-contents (Ward, 1984b).

The compositions of BD031 and DV029 staurolites plot with a large scatter (0-0.7 atom per formula unit) around the "maximum likelihood line", (Al+Si-8)= 20.5 - 0.80 (Fe + Mg + Zn), of Griffen et al. (1982). This scatter is significantly reduced if Ti and especially Cr (DV029) are added to Al'(= Al+ Si - 8) and Mn to (Fe + Mg + Zn) as recommended by Grew & Sandiford (1984) and Nicollet (1986).

The analyzed **orthorhombic amphiboles** at locality A are anthophyllites, (nomenclature according to Leake, 1978), Al^{IV} ranging 0.43-0.84 while the orthoamphiboles from both quartz-free and quartz-bearing parts at locality C are gedrites (Al^{IV} ranging 1.19-1.36). At locality B the deformed orthoamphiboles are zoned from gedrite in the core to anthophyllite

adjacent to the enclaves. The new-grown orthoamphibole is unzoned and has a anthophyllite composition. Al^{IV} range 0.12-0.26 for the new-grown orthoamphiboles and 0.10-1.50 for the zoned species with a small gap from 0.38-0.68. The orthoamphiboles contain low to negligible amounts of CaO, TiO_2, and MnO. X_{Mg} values range 0.54-0.62 (Loc. B), 0.66-0.68 (Loc. A) to 0.68-0.72 (Loc. C). The amphiboles at locality C contain 0.014-0.019 wt.% Cr_2O_3. The compositional variation of orthoamphiboles can be described by the edenite-($\square Si = NaAl^{IV}$), tschermakite- ($Mg^{VI}Si^{IV} = Al^{VI}Al^{IV}$) and $FeMg_{-1}$ substitutions (Robinson et al., 1971, 1982). As pointed out by Baker et al. (1987) and Beeson (1978) the ratio of edenite to tschermakite substitution varies due to local variations in Na content. A plot of Na(A) versus Al^{IV} (Fig. 1.9), indicates a ratio of edenite to tschermakite substitution for the anthophyllites of location A of about 1 : 3.6, for the orthoamphiboles of location B 1 : 4.0 and for the gedrites of location C 1 : 4.4. The presence of exsolution lamellae parallel to (010) indicates that the orthoamphiboles formed or equilibrated at temperatures above the crest of the orthoamphibole solvus (Robinson et al., 1971; Spear, 1980). The pressure, the combined edenite and tschermakite components and X(Fe-Mg) dependence of this critical temperature, T decreasing with increase in Mg/Fe ratio and decrease of pressure (Crowley & Spear, 1981), suggests the lamellae formed below 600 °C.

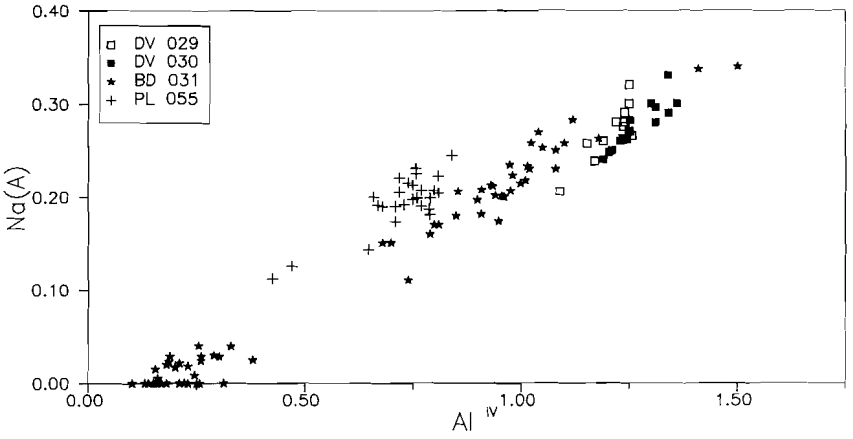

Figure 1.9. Plot of Na(A) versus Al^{IV} for the orthoamphiboles from localities A (PL055), B (BD031) and C (DV030 and DV029). The difference in the slope between the three localities, indicates a different ratio of edenite to tschermak substitution. The difference between DV030 and DV029, both from locality C, is attributed to the later Mg-Fe exchange of gedrite in DV030 with garnet.

Orthoamphibole zoning

The gedrites from the corundum- and staurolite-bearing enclaves of locality C are unzoned with X_{Mg} ranging 0.70-0.71, Al^{IV} 1.19-1.25, Na(A) 0.26-0.32. No differences between the gedrites near corundum- or staurolite-bearing enclaves have been detected. The gedrites adjacent to the garnet show minor zoning. The X_{Mg} (0.687-0.724), Al^{IV} (1.21-1.36) and Na(A) (0.23-0.29) increase towards the garnet. This zoning is believed to be related to the late retrograde conditions affecting locality C. The rapid decrease of Na(A), Al^{IV} in the deformed orthoamphiboles at locality B is accompanied by a decrease of Ti, Ca (0.17-0.00 wt.% TiO_2; 0.46-0.21 wt.% CaO) and increase of X_{Mg} (0.54-0.62). Total Fe content, however, remains nearly constant. Analyses of newly-grown anthophyllites and the rims of deformed orthoamphiboles are very similar. This suggests that the overgrowths were formed under conditions at which the rims of the deformed grains became sufficiently low in Na and Al and rich in Mg. Similar overgrowths of anthophyllite on highly zoned gedrite have been reported by Schumacher (1980) and Robinson et al. (1982) in a gedrite-staurolite-cordierite assemblage.

Biotite occurs as a minor phase at locality B and as a major phase at locality C. The biotites have low to moderate TiO_2 content (1.3-2.4 wt.%). X_{Mg} does not show any variation at locality B (0.67-0.68) but varies in the quartz-bearing parts of locality C from 0.75-0.76 for the matrix biotite to 0.78-0.79 for biotite adjacent to the garnet. Biotite in DV029 has a X_{Mg} of 0.79.

Ilmenite and **rutile** are the most abundant accessory minerals of the cordierite-orthoamphibole bearing rocks. Both ilmenite (Loc. B) and rutile (Loc. A) are pure phases. Rutile from locality C contains some Cr (0.49-1.28 wt.%) and Nb (0.20-1.51 wt.%). Mineral analyses show 0.1-0.4 (BD031) and 0.2-0.6 (PL055) wt.% Fe_2O_3 and trace amounts of MgO and Cr_2O_3.

Kyanite is homogeneous at both localities. Mineral analyses of the strongly deformed **andalusite** in BD031 show low amounts of Fe_2O_3 (0.2 wt.%) and trace amounts of TiO_2, MgO and Cr_2O_3. **Corundum** in DV029 is pure with traces of Cr_2O_3 and Fe_2O_3. MgO was not detected. Corundum in BD031 was not analyzed. **Tourmaline** at locality A is an unzoned dravite-rich variety (X_{Mg} = 0.77-0.78) with moderate amounts of TiO_2 (1.1-1.3 wt.%) and CaO (1.4-1.5 wt.%). The tourmalines in sample DV301 (locality B) display a discontinuous zoning with Fe- and Ca-rich cores (Ca/(Ca+Na)= 0.40-0.45; X_{Mg} = 0.75-0.78) and Mg-, Na-enriched and Ca-depleted rims (Ca/(Ca+Na)= 0.20-0.25; X_{Mg} = 0.79-0.83). TiO_2 varies 0.80-1.13 wt.%. The **plagioclase** from locality A shows relatively minor compositional variation (An_{02-10}), with Or_{0-01}.

Mg/Fe Partitioning

The Mg/Fe partitioning trend for locality A follows: anthophyllite < tourmaline < cordierite; for locality B: ilmenite < staurolite < gedrite < anthophyllite < biotite < cordierite ≤ tourmaline; and for locality C: garnet < gedrite ≤ biotite < cordierite (DV030, DV036) and staurolite < gedrite < biotite < cordierite (DV029).

PHASE PETROLOGY

The earliest recognizable assemblage (M_1) is characterized by biotite, tourmaline, deformed andalusite and orthoamphibole at locality B (Table 1.1). The presence of orthoamphibole is restricted to the biotite-rich layers indicating:

biotite + (chlorite ??) ⟶
gedrite + Mg-richer biotite + quartz. (1)

Chlorite, although not present anymore as primary phase, could have been present in this orthoamphibole producing reaction. In the andalusite-tourmaline-quartz layers kyanite occasionally developed from andalusite. In the gedrite-(biotite) layers kyanite and staurolite formed after the deformation of andalusite. The large staurolites at localities B and C most probably have developed from gedrite, biotite and possibly chlorite. The generalized staurolite forming reaction will be:

gedrite + biotite + chlorite (??) ⟶
staurolite + Mg-richer biotite + Mg-richer gedrite. (2)

There are no textural indications for the prograde staurolite forming reaction Grt + Chl (± Bt) = St + Ged + Vap. The development of the newly-grown anthophyllite occurred mainly in the biotite-gedrite-rich and staurolite-kyanite-bearing layers. Although zoning from gedrite-rich cores to anthophyllite-rich rims usually are attributed to retrograde effects (Robinson et al., 1982), the zoning in the deformed orthoamphiboles and the new-growth of anthophyllite must have occurred before the growth of cordierite because the newly-grown anthophyllite is consumed by cordierite. The presence of a small compositional gap in the orthoamphibole-zoning indicates that the zoning developed at temperatures below the orthoamphibole solvus.

The increase of Mg in the gedrites rimwards can not be explained by cordierite-growth, which would cause gedrites to zone from Mg-rich cores to Fe-rich rims (e.g. Harley, 1985) and cordierites would show Mg-enrichment adjacent to the orthoamphibole instead of the

observed absence of Mg-zoning. The zoning might be explained by the simplified reaction 2-equivalent:

gedrite + quartz (+ biotite + chlorite ?) ⟶
staurolite + anthophyllite + vapour. (3)

The absence of staurolite in PL055 is attributed to the higher MgO/(MgO+FeO) ratios of the bulk composition (Hudson & Harte, 1985) at locality A. In the schematic configuration of isopleths of Al^{VI} in orthoamphibole developed by Harley (1985) in the system $MgO-Al_2O_3-SiO_2$ it is shown that Al-isopleths for gedrite in the assemblage Ged-Ky-Qtz have steep negative slopes with XAl^{VI} increasing to lower T. The X_{Mg} isopleths for gedrite will have much shallower slopes with X_{Mg} increasing to higher P. Although only qualitative conclusions can be drawn from these configurations for Mg-rich and quartz-bearing assemblages, the slightly negative V of reaction 3, calculated from the mineral data and the observed Al-Mg zoning suggest a similar configuration for Fe-richer and SiO_2-poorer staurolite-bearing assemblage of BD031. As experimental data are lacking for reaction 3 it can only be concluded that the development of staurolite and Al-Mg zoning in the orthoamphibole points to an increase of temperature and or pressure. Some of the Na released by the breakdown of gedrite is probably incorporated in tourmaline as it shows a rimward increase of Na.

The intergrowth of staurolite with kyanite in the gedrite-(biotite) layers at locality B is indicative for the staurolite-kyanite-gedrite-quartz assemblage. This suggests that the prograde development of kyanite on staurolite according to

staurolite + biotite (+ chlorite ??) ⟶
kyanite + gedrite + vapour (4)

may have occurred. The textural relationships and mineral chemistry in PL055 and BD031 suggest a development of cordierite (M_{3a}-phase) by

kyanite + anthophyllite + quartz ⟶
cordierite + vapour (5)

describing the movement of the Ky-Ath-Crd divariant field to Fe-richer compositions. In BD031 cordierite also developed around the large deformed andalusite grains. The metastable persistence of andalusite during M_2 and up to the M_{3a} phase is surprising.

The absence of staurolite-cordierite symplectitic textures around kyanite (Loc. B), the absence of quartz in the cordierite-coronas around foliated (Loc. C) and resorbed staurolite

and the observed zoning in large staurolite grains (Loc. C) indicate the staurolite-consuming reaction:

staurolite + orthoamphibole + (quartz) ⟶
cordierite + Fe-richer staurolite + Fe-richer orthoamphibole + vapour. (6)

Reaction 6 describes the movement of the staurolite-orthoamphibole-cordierite field to Fe-richer compositions. There are no indications for the following staurolite-forming reaction:

orthoamphibole + kyanite + vapour ⟶
staurolite + cordierite + quartz. (7)

The absence of quartz and possibly the Cr-content stabilized staurolite in DV029 to higher metamorphic grade. In the case of BD031 staurolite locally appears to have occurred next to quartz. The thin rim (minimal 0.1 mm) of cordierite which separates staurolite and quartz and the remarkable absence of garnet in BD031 suggests that reaction 6 was also the mechanism to remove staurolite in these parts of the rock. The subhedral rounded to euhedral shape of small staurolite grains and the anhedral ragged shape of large staurolite grains (BD031 and DV029) suggests a limited recrystallisation (M_{3b} ?) which is possibly connected with the development of a polygonal fabric in the cordierite. The absence of zoning and the observed size-dependent difference for X_{Mg} in the small staurolite grains of BD031 is considered to be the result of homogenization connected with the recrystallisation. The existence of strongly resorbed kyanite grains next to the less resorbed staurolite grains suggests that cordierite in BD031 predominantly developed due to reaction 5 rather than to reaction 6 during the M_{3a} phase.

The corundum-bearing enclave in BD031 suggests a corundum-cordierite development (M_{3a}) in the quartz-free parts of the rock due to reaction 8

gedrite + kyanite/andalusite ⟶
cordierite + corundum + vapour (8)

as described by previous studies (e.g. Robinson & Jaffe, 1969; Schumacher & Robinson, 1987). Locally, corundum and quartz occur close together separated only by a small rim of cordierite. Probably the mobility of SiO_2 was not large during the formation of cordierite (short-range diffusion). The lowered $aSiO_2$ might also have stabilized staurolite next to quartz to higher temperatures before encountering reaction 6.

The textures in the corundum-bearing enclave at locality C (DV029), however, show

large foliated and resorbed corundum crystals with inclusions of biotite, rutile and apatite. It indicates that corundum in DV029 was an early phase. The formation of cordierite and, therefore, consumption of corundum can be described by reaction 9

$$\text{corundum} + \text{gedrite} \longrightarrow$$
$$\text{cordierite} + \text{(Al-richer) gedrite.} \quad (9)$$

Reaction 9 describes the movement of the corundum-gedrite-cordierite field to Fe-richer compositions. The embayed corundum grains around the aluminium silicates in BD031 indicate that reaction 9 overtakes reaction 8. Corundum-bearing enclaves containing sapphirine in rock-types with a similar whole rock chemistry and X_{Mg} as locality C have been reported from the granulite facies area around Arendal in the Bamble sector (Lamb, 1981). Sapphirine and cordierite in these enclaves are produced due to the reaction of gedrite with corundum. This reaction has a relatively steep and positive dP/dT slope (Windley et al., 1984). The absence of sapphirine in the corundum-bearing enclaves of DV029 is compatible with somewhat lower metamorphic temperatures (or higher P) compared with the Arendal locality described.

The garnet at locality C clearly developed at the expense of cordierite, orthoamphibole and biotite. The quartz and large rutile inclusions in the garnet indicate that silica and titanium were concentrated by the growth of the garnet. The generalized garnet-forming reaction (M_{3b}-phase) will, therefore, be

$$\text{cordierite} + \text{gedrite} + \text{biotite} \longrightarrow$$
$$\text{garnet} + \text{quartz} + \text{rutile} + \text{Mg-richer biotite} + \text{vapour.} \quad (10)$$

The increase of Mg in biotite and cordierite and Mg, Al, Na in gedrite next to garnet at locality C is clearly related to the development of the M_4-assemblage of white mica, chlorite and possibly dumortierite along the cracks in the garnet. The retrogressive alteration of the cordierite in the quartz-cordierite segregations (M_4) by quartz, chlorite and aluminium silicate Reaction 11 has locally been observed in the Bamble sector (Ramsay & Morton, 1971; Maijer & Padget, 1987).

$$\text{cordierite} + \text{vapour} \longrightarrow$$
$$\text{chlorite} + \text{quartz} + \text{kyanite/andalusite.} \quad (11)$$

Table 1.3.
Summary of T estimates for locality C (DV030, DV036) based on biotite-garnet and cordierite-garnet thermometry. Calibrations used: (FS), Ferry & Spear, 1978; (P), Perchuk, 1981; (IM), Indares & Martignole, 1985: (a) model A, (b) model B; (H), Hoinkes, 1986; (T), Thompson, 1977; (HL), Holdaway & Lee, 1977; (PL), Perchuk & Lavrent'eva, 1983.

Sample	Garnet			Biotite			Crd	Kd(Fe-Mg) values		Garnet-biotite T (°C)					Garnet-cordierite T (°C)		
	X_{Mg}	X_{Ca}	X_{Mn}	X_{Mg}	X_{Al}	X_{Ti}	X_{Mg}	grt-bt	grt-crd	FS	P	IM (a)	IM (b)	H	T	HL	PL
DV030 Core/ matrix*	0.435	0.071	0.010				0.85		6.31						760	729	690
	0.431	0.069	0.011	0.671	0.083	0.044		0.273		764	665	713	711	861			
Rim**	0.270	0.058	0.017				0.87		15.76						490	495	487
	0.275	0.062	0.018	0.701	0.082	0.030		0.113		444	489	437	432	485			
DV036 Core/ matrix*	0.448	0.053	0.010				0.85		6.26						765	731	706
	0.448	0.053	0.010	0.662	0.087	0.042		0.289		793	679	736	728	873			
Rim**	0.290	0.056	0.017				0.88		13.91						517	518	512
	0.255	0.067	0.020	0.680	0.086	0.022		0.121		462	503	455	455	509			

* Pressure estimates of 7 kbar for core/matrix are based on P-T data from Touret (1971a) and Lamb et al. (1986);

** Pressure estimates of 4 kbar for rim compositions are based on the andalusite-kyanite association in the vein cordierites (DV034)

METAMORPHIC CONDITIONS

Geothermometry

Temperature estimates for the formation of garnet (M_{3b}-phase) at locality C (Table 1.3) are based on the garnet-biotite Fe-Mg exchange reaction (Ferry & Spear, 1978; Hoinkes, 1986; Indares & Martignole, 1985; Perchuk, 1981) and the garnet-cordierite Fe-Mg exchange reaction (Holdaway & Lee, 1977; Perchuk & Lavrent'eva, 1983; Thompson, 1976). Garnet-core T-estimates are based on the combination of the Mg-rich garnet core and Fe-rich "matrix" biotite and cordierite. A pressure estimate of 7 kbar was used for the upper-amphibolite facies metamorphism of the Froland area. Garnet-rim T-estimates are based on the combination of the Fe-rich garnet-rim and the adjacent cordierite and biotite grains. The Perchuk thermometers all yield temperatures of about 680-700 °C for the garnet-cores. Other thermometers yield 710-760 °C (Holdaway & Lee, 1977; Thompson, 1976 and Indares & Martignole, 1985) to 790 °C (Ferry & Spear, 1978). Very high temperatures (830-880 °C) were found using the Hoinkes calibration. These high T-estimates are due to over compensation of the effect of Ca in these low-grossular garnets. The mean of all T-estimates except the Hoinkes (1986) calibration is 740 °C ($\pm$ 60 °C). The T-estimates for the rim of the garnet give low to very low temperatures ranging 420-510 °C for the garnet-biotite thermometers and 460-530 °C for the cordierite-garnet thermometers, all assuming P = 4 kbar (based on the kyanite-andalusite assemblage in DV034). These temperatures are consistent with the retrograde development of the M_4-assemblage of white mica, chlorite and pinite at locality C.

P-T-t evolution

The reaction relations of the M_1-M_3 assemblages of which absolute P-T conditions can not be estimated using empirical or experimentally calibrated thermometers or barometers are presented in Fig. 1.10. The schematic P-T grid presented is based on the (F)MASH nets developed by Grieve & Fawcett (1974), Harley (1985) and Hudson & Harte (1985). The M_1 phase characterized by the presence of andalusite and absence of cordierite is placed at a pressure maximum of 4 kbar at 500 °C when based on the Al_2SiO_5 polymorph transition of Holdaway (1971). The development of gedrite, due to reaction 1, took place when andalusite was the stable aluminium silicate. Increase of both pressure and temperature resulted in the development of the M_2 phase assemblages. In the andalusite-tourmaline-quartz layers kyanite developed from andalusite. In the gedrite-biotite layers staurolite developed from gedrite, biotite, chlorite (?) and quartz producing rimward increase of X_{Mg} and decrease of Al-Na in gedrite and new-growth of anthophyllite Reaction 2 and 3. The P-T vector of the

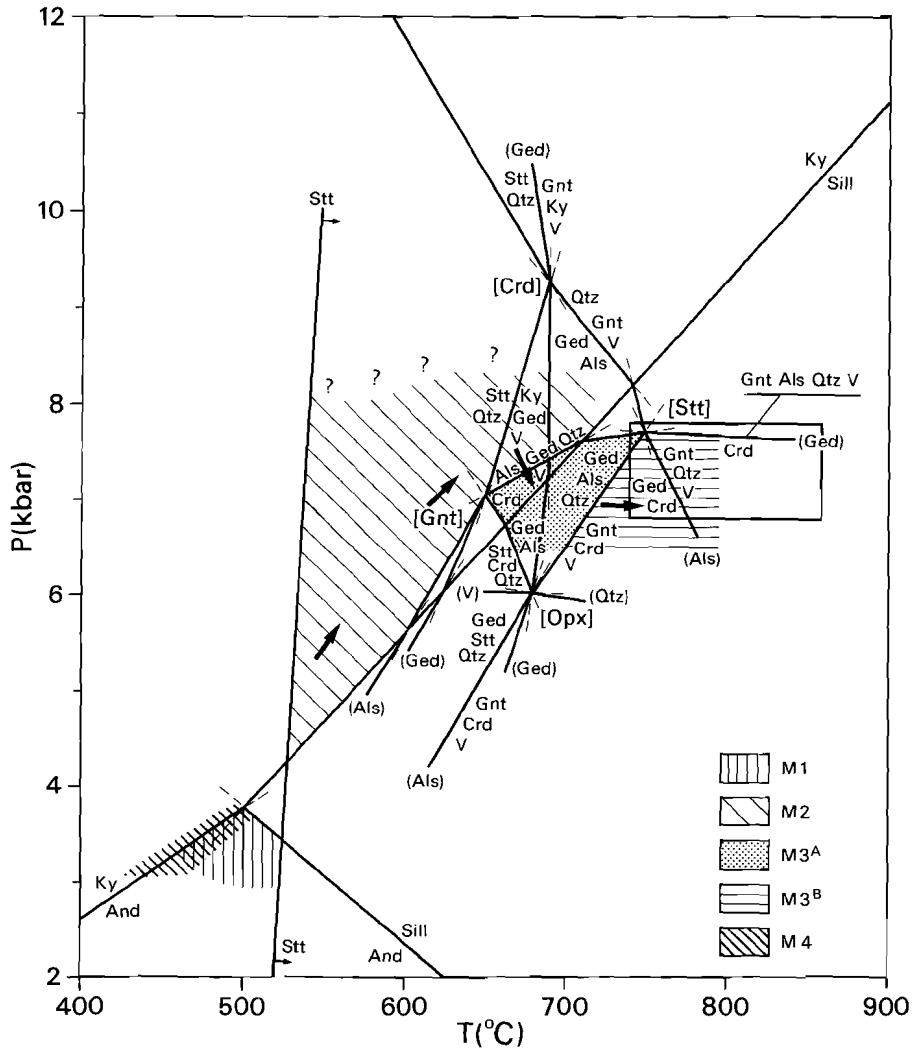

Figure 1.10. P-T diagram for FMASH equilibria after Harley (1985) and Hudson & Harte (1985) for $P_{H_2O} = P_{total}$. Aluminium silicate relations are from Holdaway (1971). The succesive metamorphic stages (shaded) are shown using the best estimated conditions as deduced from textural ans chemical data. P-T box at 7.3 ± 0.5 kbar and 800 ± 60 °C is based on P-T data from Lamb et al. (1986).

compositional zoning in the orthoamphiboles points to a temperature and a possible pressure increase. The compositional gap in the zoning poses a upper-temperature limit on the temperature range of about 600 °C (Spear & Rumble, 1986). Kyanite growth in the

gedrite- (biotite) layers implies the formation of the St-Ky-Ged-Qtz-Bt assemblage from the St-Ged-Qtz-Bt assemblage with increasing temperature.

The M_{3a} phase, the development of cordierite, is placed in the high-pressure (6-8 kbar), high-temperature (600-700 °C) part of the FMASH-grid. The cordierite-forming reactions 5 (Green & Vernon, 1974; Lee & Holdaway, 1976), 6, 8 (Schreyer & Seifert, 1969; Windley et al., 1984) and 9 all have a larger volume on the cordierite side of the reaction, so the M_{3a} phase reactions will be favoured by decreasing pressure. The [st] and [grt] are connected through reaction 5. The textures in BD031 and PL055 indicate that the development of cordierite at these localities took place when kyanite was the stable aluminium silicate or when prevailing P-T conditions were close to the sillimanite-kyanite divariant field. The development of cordierite from a sillimanite-gedrite assemblage reported from the Arendal granulite facies terrain (Lamb, 1981; Visser, unpublished data) indicates that reaction 5 has to cross the kyanite-sillimanite boundary.

The effect of the lower mobility of quartz at locality B will be the movement of [opx] to higher temperatures (Baker et al., 1987) along the quartz-absent univariant to stabilize staurolite to higher temperatures.

The M_{3b} phase, the static growth of garnet replacing cordierite and gedrite at locality C due to (opx, st, als), the FMASH equivalent of reaction 10, is proposed to have taken place at a pressure of about 7 kbar, assuming no large pressure gradient between the Arendal and Froland areas, and with temperatures increasing to 740 $\pm$ 60 °C. Compared with the data from the adjacent Arendal granulite facies terrain (Lamb et al., 1986), 800 $\pm$ 60 °C at pressures of 7.3 $\pm$ 0.3 kbar, these P-T estimates and the absence of sapphirine in the corundum-bearing enclaves of locality C point to lower peak-metamorphic temperatures in the upper-amphibolite facies terrain. This temperature gradient will probably be very smooth as Lamb et al. (1986) found no significant gradient along their sample traverse within the granulite-facies area.

During the initial stages of the M_4 phase, locality C was affected by formation of quartz-cordierite segregations. The later formation of andalusite, kyanite, chlorite and quartz from the vein cordierite and the total absence of sillimanite may indicate that the early stages of M_4 represented a decrease in temperature from M_{3b} conditions with, initially, little change in pressure and later proceeded with a sharp decrease in pressure to cross the divariant andalusite-kyanite field.

Whilst there is no proof for this initial M_4 isobaric cooling path in the samples studied, it is supported by the occurrence of kyanite-talc-quartz assemblages replacing cordierite from the Bjordammen area, northeastern Bamble, (Maijer & Padget, 1987; Visser et al., 1990). The replacement of cordierite by the talc-kyanite-quartz assemblage for $P_T = P_{H_2O}$ takes place at pressures over 8.5 kbar at 700 °C (Newton, 1972). However, at reduced P_{H_2O}

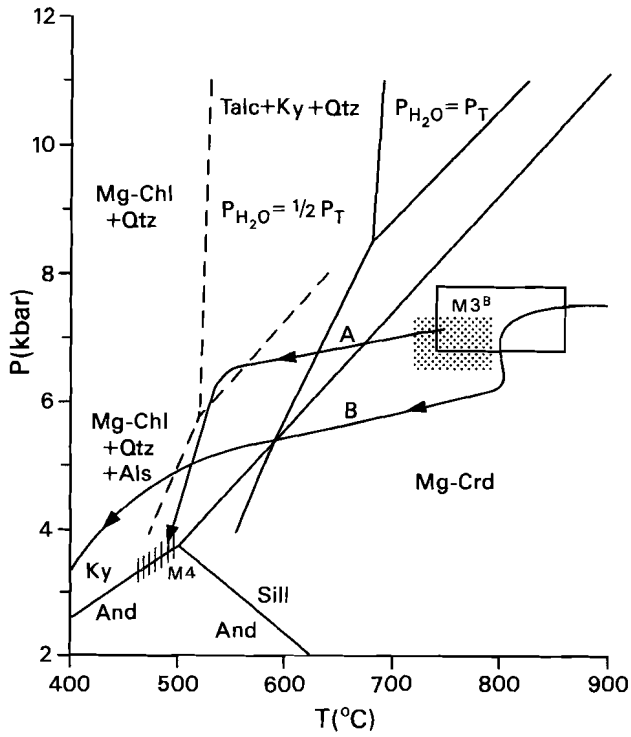

Figure 1.11. P-T diagram showing the fields of stability for Mg-cordierite bulk composition of the assemblage talc + kyanite + quartz for $P_{H_2O} = P_{total}$ (solid lines) and $P_{H_2O} = 0.5\ P_{total}$ (broken lines) according to Newton & Wood (1979). Chlorite-aluminium silicate-quartz relations are from Seifert & Schreyer (1970). The post-metamorphic isobaric cooling path A is deduced from M_{3b}, peak metamorphic data, early M_4 (talc-kyanite-quartz assemblage) and late M_4 (kyanite-andalusite-chlorite-quartz assemblage) mineral data (see text). P-T trajectory B is from Touret & Olson (1985).

the stability field of the talc-kyanite-quartz assemblage is shifted to lower pressures (Newton & Wood, 1979) (Fig. 1.11). Reduced P_{H_2O} in the quartz-cordierite veins can be inferred from the occurrence of borosilicates (B_2O_3) and CO_2 in the cordierites. Early M_4 conditions, assuming $P_{H_2O} = 0.5P_T$, are set at pressures of 6-7 kbar and temperatures of 550-650 °C.

Maximum pressure for the later stages of M_4 based on the stability fields of andalusite (Holdaway, 1971) and Mg-cordierite (Seifert & Schreyer, 1970) at temperatures of 420-530 °C will be about 3-4 kbar. The development of a chlorite-muscovite assemblage and the associated borosilicates suggests an influx of silica-, boron- and alkali-rich fluids. As dumortierite is associated with the M_4-assemblage in the garnet (Visser & Senior, 1991) and is present in the segregations, it is suggested that the T-estimates for the rim of the garnet represent the upper-temperature limit of the later stages of M_4.

DISCUSSION

The textures and mineral chemistry of the three localities investigated suggest that the M_1-M_3 phases may be the result of a single metamorphic cycle. The P-T-t path (Fig. 1.10) of this cycle has a clockwise sense which proceeded in the kyanite-stability field and which culminated after a M_{3a}-phase of pressure decrease and cordierite growth with the formation of garnet at peak P-T conditions (M_{3b}-phase) of about 740 $\pm$ 60 °C at 7 kbar. For the formation of garnet a temperature increase between the M_{3a}- and M_{3b}-phase at pressures of 6-7 kbar will be necessary. The strongly deformed M_1 assemblage at locality B and the weaker to nearly undeformed M_2, M_{3a} and M_{3b} assemblages point out that the main phase of deformation at the three localities occurred before the metamorphic peak. This main phase of deformation was probably related to the tectonic event which gave rise to burial and subsequent heating (Thompson & Ridley, 1987). P-T-t paths with a clockwise sense are suggested to match with the conditions experienced by deep crustal rocks during a continent-continent collisional event (England & Thompson, 1984). Such P-T-t paths usually display a pressure maximum before the thermal maximum. The simple continent-continent collision scenario for Bamble is complicated by the temperature increase between the M_{3a}- and M_{3b}-phases. The synkinematic emplacement of the metabasic and charnockitic-enderbitic suites could have produced the necessary heat to produce this temperature increase. The heat supply is supported by the observed smooth temperature gradient between the peak metamorphic conditions of the Arendal granulite facies and the Froland upper-amphibolite facies areas.

The M_{3b} phase coincides with the granulite facies metamorphism during the Kongsbergian orogeny 1600-1500 Ma ago. The M_1-M_{3a} phases (D1-MD1 event of Starmer, 1985) are proposed to have taken place during the first phases of the Kongsbergian orogeny. The continent-continent collision probably followed the subduction of oceanic crust which caused the generation of the basic and the charnockitic-enderbitic suites (Smalley & Field, 1985; Smalley et al., 1983). Obliteration of the associated (high-pressure ?) assemblages caused by the overprint of the amphibolite-granulite facies metamorphose makes it as yet impossible to prove this tectonic scenario.

The staurolite-kyanite phase may be linked to the metamorphism associated with the F1 folding phase in the Østfold area (Graversen, 1984) of which major structural and metamorphic trends are parallel with those of the Bamble and Kongsberg sectors. This phase, which appears to have taken place pre-1500 Ma, reached medium-high amphibolite facies grade with the development of kyanite, staurolite (Broch, 1926) and ultimately sillimanite (equivalent to the M_{3a} or M_{3b} phase ?).

An initial isobaric cooling path (A) after the metamorphic climax for the Bamble sector is constrained by the observed retrograde kyanite-talc-quartz and kyanite-andalusite-

chlorite-quartz assemblages in the late quartz-cordierite segregations (Fig. 1.11).

The proposed isobaric cooling path (A) is similar in configuration as the isobaric cooling path (B) proposed by Touret & Olsen (1985). The main differences between both P-T paths are the new P-T constraints of the observed retrograde assemblages and the P-T estimates of the peak metamorphic conditions. The new path (A) is consistent with most of the fluid inclusion data (Touret & Olsen, 1985). The later stages of the M_4 phase locality, constrained by the kyanite-andalusite association, require a pressure decrease of 2-3 kbar at temperatures around 500-550 °C. The local influx of hydrous fluids associated with quartz-feldspar veins pegmatites, buffered in case of the cordierite-quartz segregations by the Mg, Al-rich whole-rock chemistry of locality C suggests the M_4 phase to be Sveconorwegian in age. This, at the same time, implies a very long (300 Ma) residence time near the base of the crust to explain the near isobaric cooling path. Prolonged residence time at deep crustal levels before uplift and exposure seem to fit the tectonic model with crust thickened by magmatic addition and slow erosion rates (Ellis, 1987; England & Richardson, 1977).

The P-T path documented by the M_1-M_3 phases can be regarded as a collision scenario with magmatic addition, which, at low erosion rates, also shows a near isobaric cooling path (Thompson & Ridley, 1987). The M_4 phase is interpreted as a major metamorphic and tectonic event, which caused the uplift of the Bamble area after a long period of isobaric cooling. The M_4 phase is considered to be equivalent to the M6-D6 event of Starmer (1985).

ACKNOWLEDGEMENTS

The authors wish to thank Cees Maijer, Theo Kloprogge, Timo Nijland, Paul Buining and Natalie Hulzebos-Sijen for their critical review on earlier drafts of the manuscript. Simon Harley, John Schumacher and editor Michael Brown contributed considerably to this manuscript with their critical review and helpful comments. Electron microprobe analyses were performed at the Institute of Earth Sciences, Free University of Amsterdam, with financial and personnel support by WACOM, a research group for analytical chemistry of minerals and rocks subsidized by the Netherlands Organization for the Advancement of Pure Research (NWO). Financial support for field-work and research for one of us (D.V.) from the Dr. Schürmann and the Molengraaff foundations is gratefully acknowledged.

CHAPTER 2

AN INFRARED SPECTROSCOPIC (IR) STUDY OF CORDIERITES FROM THE BAMBLE SECTOR, SOUTH NORWAY.

ABSTRACT

Infrared absorption spectra of several natural cordierites across the Arendal amphibolite-granulite facies transition, Bamble Sector, south Norway are presented. The infrared spectra essentially record H_2O and CO_2 as fluid constituents in the channels, CO and hydrocarbons were not detected. Type-II water and (Ca+Na+K) are correlated and show a insert molar 2:1 ratio. The infrared and other analytical data indicate a decrease of Na, type-II H_2O, CO_2 and Li with metamorphic grade, type-I H_2O is variable. The decrease of these volatiles and alkalies and the low total volatile contents of the granulite facies cordierites are best explained by progressive dehydration and decarbonation processes, possibly related to partial melting. A progressive change of the X_{H_2O} = $H_2O/(H_2O+CO_2)$ ratio in the cordierites across the transition, as suggested by previous studies, is not observed. Greenschist to low-amphibolite facies re-equilibrated cordierites show a significant increase in either CO_2, or H_2O+CO_2. Na is introduced at some localities. The retrograde fluid phase is calculated to be CO_2-rich.

INTRODUCTION

Cordierite, $(Na, K, Fe^{2+}, Fe^{3+})_{0-1}^{ch}$ $(Mg, Fe^{2+}, Mn, Li)_2^{[VI]}$ $[Si, Al, Be, Fe^{3+})_9^{[IV]}O_{18}$. $x(H_2O, CO_2, Ar, CO, N_2...)^{ch}$ (Schreyer, 1985), is a common metamorphic mineral in upper amphibolite and granulite facies metamorphosed aluminous rock types. Several studies of cordierite-bearing rocks have indicated that molecular H_2O, CO_2 and other gas species are present in appreciable amounts in the ring-shaped structural channels (e.g. Hörmann et al., 1980; Zimmermann, 1981; Armbruster et al., 1982; Scheurs, 1985; Vry et al., 1990; Schenk et al., 1992; Swamy et al., 1992). Johannes & Schreyer (1981) experimentally examined the partitioning of H_2O and CO_2 between Mg-cordierite and a coexisting fluid phase at 1-7 kbar and 210-1000 °C. Lonker (1981), Martignole & Sisi (1981), Bhattacharya & Sen (1985) and Swamy et al. (1992) attempted to calibrate cordierite as a potential water-fugacity indicator by thermodynamic modelling of the available experimental data.

The use of cordierite as a potential monitor of the preserved fluid composition is of

especially great importance in granulite terrains. Granulites, which are characterised by low water activities, are generally suggested to have formed either through fluid-absent conditions achieved by processes of partial-melting (e.g. Lamb et al., 1987) or by infiltration of pervasive CO_2-rich fluids derived from an external source (e.g. Newton, 1992).

In the present study the channel volatile contents of cordierites from the amphibolite-granulite transition of the Mid-Proterozoic Bamble Sector in southern Norway are reported. The results are discussed in comparison with previous studies, which advocate either an origin for the Bamble granulites consistent with the CO_2-flushing or so-called "carbonic" model alone (Touret, 1971; Lamb et al., 1986) or a combination of both the "carbonic" and fluid-absent partial melting models (Touret & Dietvorst, 1983; Touret, 1988). The effect of eminent greenschist to low amphibolite facies retrograde re-equilibration on some of the analysed cordierites is incorporated in the discussion. The study of the Bamble cordierites was further motivated by the experimental results of Mirwald et al. (1979) which show equilibrium isopleths of H_2O in cordierite to run parallel to the retrograde P-T path of the Bamble Sector (Touret & Olsen, 1985). This indicates that retrograde volatile-loss will be minimal.

The infrared (IR) spectroscopy method has been used to characterise quantitatively the channel volatiles. IR spectroscopy provides an extremely sensitive method for detecting H_2O, CO_2 and other possible gas-species (CO and hydrocarbons) in cordierites (see e.g. Le Breton, 1989 and Vry et al., 1990 for detailed descriptions). The IR technique is more appropriate and satisfactory than most other analytical methods, since it is relatively unaffected by impurities such as graphite, carbonate and sulphides, which occur in many of the Bamble cordierites. Furthermore, only a small amount of sample (a few milligrams) is needed for routine analysis.

GEOLOGICAL SETTING

The Bamble Sector, south Norway, is one of the classical examples of intermediate pressure amphibolite to granulite facies transition. The transition itself is located in the Arendal-Tvedestrand-Risör area and is divided into four zones, labelled A through D (Fig. 2.1; Smalley et al., 1983). The amphibolite facies area (zone A) and granulite facies area (zone B) are delineated by an orthopyroxene-in isograd in metabasites (Field & Clough, 1976). A second orthopyroxene-in isograd marks the appearance of orthopyroxene in acidic rocks (zone C). Zone D is situated on the isles of Tromöy and Hisöy and is characterised by a strong LILE- and LREE-depletion in both the enderbitic and metabasic rocks. Recently, Nijland & Maijer (1993) redefined both orthopyroxene-in

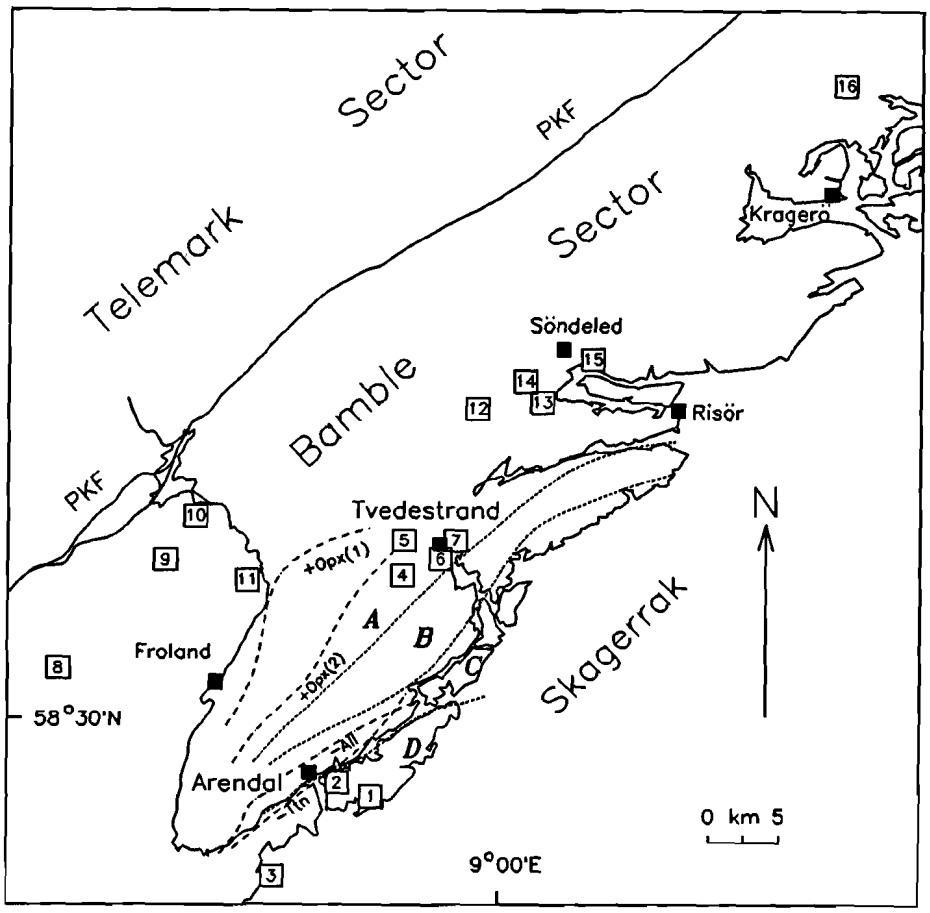

Figure 2.1. Location map showing the central part of the Bamble Sector, south Norway (see Table 2.1). Metamorphic regions A through D are from Smalley et al. (1983) (see text for explanation). Mineral isograds +Opx (1), +Opx (2), -All and -Ttn are from Nijland & Maijer (1993). PKF = Porsgrunn-Kristiansand-Fault.

isograds on the basis of a much larger set of samples and also presented evidence for allanite- and titanite-out isograds in amphibolites, gneisses and metapelites (Fig. 2.1). The same authors further suggested that the allanite-out isograd could represent the true C-D boundary, as allanite is a LREE-carrier.

Fluid inclusion studies by Touret (1971, 1974, 1985) indicated the dominance of high density CO_2-rich inclusions in the granulite facies gneisses and of H_2O and mixed H_2O and CO_2 inclusions in the amphibolite facies area north of the orthopyroxene isograd. Based on the presence of these CO_2-rich fluid inclusions Touret (1971) proposed a large-

scale CO_2 transfer connected to synmetamorphic mantle derived basic intrusives to account for the formation of granulites in the Arendal area. Recent studies by Touret & Dietvorst (1983), Touret & Olsen (1985) and Touret (1988) considered the double mechanism of H_2O extraction by anatectic melting *and* CO_2 introduction to be a more attractive model.

Lamb et al. (1986) found no apparent P-T variation between zones B, C and D, and suggested, on the basis of Touret's data, the amphibolite facies to granulite facies transition to be the result of a progressive change in fluid composition from H_2O-rich to CO_2-rich. Lamb et al. (1986) estimated the average metamorphic conditions of the granulite facies metamorphism at 800 $\pm$ 60 °C and 7.3 $\pm$ 0.5 kbar. The conclusions of the study by Lamb et al. (1986) are in conflict with the data presented in Nijland & Maijer (1993), which show a gradual increase in temperature and possible in pressure from the amphibolite facies area towards the Skagerrak coast. Average P-T conditions are 752 $\pm$ 34 °C and 7.1 $\pm$ 0.4 kbar for the amphibolite facies area and 836 $\pm$ 49 °C and 7.7 $\pm$ 0.3 kbar for the granulite facies area (Nijland & Maijer, 1993).

The retrograde P-T path (Touret & Olsen, 1985; Visser & Senior, 1990; Nijland et al., 1993) of the Bamble Sector starts with prolonged near-isobaric cooling (early M_4 after Visser & Senior, 1990) and is followed by a near-isothermal decompression phase (late M_4) at 500 $\pm$ 50 °C and 3-6 kbar. Late M_4 conditions are marked by a significant retrogradation in a local fluid-rich environment of the peak-metamorphic (M_{3b}) assemblages.

CORDIERITE SAMPLES

The studied cordierites are distributed regionally over the Bamble Sector, south Norway (Fig. 2.1). The samples cover the Arendal-Tromöy granulite facies area (localities 1-3), the Tvedestand amphibolite-granulite facies transition zone (localities 4-7) and the amphibolite facies areas around Froland (localities 8-11), Akland-Söndeled (localities 12-15) and Bjordammen (locality 16). The appearance of orthopyroxene in the cordierite-orthoamphibole rocks and the cordierite-bearing metapelites matches more closely with the Opx-in isograd, A-B boundary, after Field & Clough (1976) than the Opx(1) isograd of Nijland & Maijer (1993). The original A-B boundary has, therefore, been used as reference line for the division granulite facies versus amphibolite facies cordierites. Mineral assemblages of the cordierite bearing rocks are presented in Table 2.1.

Most samples are cordierite-orthoamphibole-(orthopyroxene) rocks with a Mg-, Fe-, Al-rich and occasionally Si-poor bulk chemistry. Rocks from localities 1 and 2 probably

belong to a meta-evaporitic sequence as they are very Na-rich (up to 8.47 wt.% Na_2O, Visser et al., 1991), exemplified by abundant albite, and may contain the relatively rare borosilicate kornerupine. Sillimanite-bearing metapelites with minor amounts of orthoamphibole were sampled at localities 4, 6, 7, 8 and 12.

Cordierite occurs as conspicuous lilac blue to colourless rounded grains with diameters of 100 μm-2 cm and occasionally up to 10 cm in diameter (samples DV064 and CM175) in the quartz- and plagioclase-rich parts of the samples. Elongated grains occur parallel to biotite or orthoamphibole cleavages. Elongated grains often show a polygonal subgrain texture. Polysynthetic twinning is very common, whereas sector twinning is

Table 2.1.
Location and mineral assemblage of selected cordierite-bearing gneisses

	Locality	sample	coordinates	assemblage (> 0.5 vol.%)
1	Hove	CM092	4909-64786	Qtz Ab Crd Opx Ilm Krn Ath
		CM093		Qtz Ab Crd Opx Ilm Krn Ath Trm
		DV148		Qtz Ab Crd Grt Opx Krn Oam Ilm
		DV149		Qtz Ab Crd Grt Opx Oam Ilm
		DV286		Qtz Ab Crd Grt Opx Oam
		DV288		Qtz Ab Crd Grt Opx Oam Ilm Rt
2	Faervik	TN260	4885-64797	Qtz Ab Crd Opx Ged Bt Krn Rt Spl
3	Hasleholmen	PT138	4849-64723	Crd Opx Oam Bt Sil Spl Spr Rt
4	Holt	EJ041	4931-64959	Qtz Pl Crd Opx Bt Sil Ky
5	Gliddi	CM175	4932-64987	Qtz Crd Oam Bt Rt Ap
6	Gladstad	DV084	4958-64973	Qtz Crd Oam Bt Sil Gr
		DV085		Qtz Crd Oam Bt Rt
		DV261		Qtz Crd Grt Bt Opq
		DV263		Qtz Crd
7	Tvedestrand	MA995	4969-64987	Qtz Crd Bt Sil Opq, Gr
8	Blengsvatn	BD033	4686-64886	Qtz Crd Ged Ath Bt Ky Stt Ilm Trm
9	Bilitt	DV080	4762-64971	Qtz Crd Oam Ilm Bt Stt Rt Ap Trm
10	Öyras	DV064	4783-65006	Qtz Pl Crd Oam Bt Ilm Rt (Ky Chl Qtz)
11	Böylefossbru	DV029	4820-64956	Crd Ged Bt Crn St Rt Ap (Chl Pin Crb)
		DV037		Qtz Crd Grt Ged Bt Stt Rt Ap (Chl Pin Crb)
12	Vieli	DV153	4984-65091	Qtz Crd Bt Sil
13	Röd	DV122	5030-65096	Qtz Crd Grt Oam Bt Rt
		MA780		Qtz Crd Grt Ath Bt Gr Ilm Krn Trm Dum Ap
14	Moland	DV114	5018-65112	Qtz Crd Bt Act Ap Opq
15	Ronsdalen	DV159	5066-65129	Qtz Crd Ath Bt Ilm Rt Opq (Chl)
		DV165		Qtz Crd Trm (Ky And Chl Qtz Scp Crb)
		DV330		Crd
16	Bjordammen	MA822	5245-65342	Qtz Crd Trm Mag (Ky And Dum Chl Qtz)
		MA998		Qtz Crd Trm Opq (Chl)

Mineral abbreviations after Kretz (1983) except for Dum = dumortierite, Opq = opaque, Crb = carbonate and Pin = pinite. Brackets indicate secondary assemblage after cordierite. Minor phases (< 0.5 vol.%) are not shown. Ged and Ath are used were microprobe data are available for orthoamphibole, otherwise Oam is used.

rare. Cordierites from localities 8, 9 and 11 contain relics of a prograde reaction sequence (M_1-M_{3a}) consisting of strongly deformed andalusite, kyanite+staurolite and corundum (Visser & Senior, 1990). Inclusions of quartz, plagioclase, sillimanite, biotite, rutile, ilmenite, apatite and tourmaline are common, especially in the amphibolite facies area. Rarely kornerupine (loc. 1 and 2), spinel and sapphirine (loc. 2 and 3) are included in cordierite. Most cordierite samples were selected on the basis of two textural criteria. Firstly, cordierites (and other primary phases) are visibly unaltered or contain only traces (< 0.5 vol.%) of secondary minerals such as pinite and chlorite. Secondly, cordierites should contain only trace amounts of mineral inclusions. This is especially important in the amphibolite facies cordierites, which usually contain numerous very small opaque inclusions. Cordierites from localities 10, 11, 15 and 16 were selected because these localities show extensive retrograde exchange with externally derived fluids (Visser & Senior, 1991; Chapter 3). This exchange is, however, limited to distinct pathways or trails. Along these pathways cordierite breaks down to form the late M_4 assemblages Ky-Chl-Qtz, And-Chl-Qtz and Dum-Chl-Qtz (Visser & Senior, 1990, 1991). Cl-rich scapolite (D. Visser, in Lieftink et al., 1993), carbonates and trace amounts of pyrite may accompany these retrograde assemblages. Outside the pathways, exchange with the fluid phase is less intense (or nil, sample DV330) presumably due to a lower fluid/mineral ratio and consequently only minor secondary phases are present. The relatively "fresh" and optically unzoned cordierites may have re-equilibrated either partly or fully with the retrograde fluid and are, therefore, suitable examples to study the retrograde exchange of cordierite with a fluid phase.

PREVIOUS WORK ON BAMBLE CORDIERITES

Zimmermann (1981) investigated the volatile contents of cordierites from Hove (locality 1) and Dypväg in the granulite facies area, and from Tvedestrand (near localities 6 and 7) and Akland (near localities 13 and 14) in the amphibolite facies area. The volatiles were extracted by means of step heating, linear heating and analysed by mass spectrometry. The results show a high aqueous volatile content in the amphibolite facies cordierites (71-91 mol.% H_2O) with low amounts of CO_2 (1-8 mol.%). The granulite facies samples are shown to have lower amounts of H_2O (54-67 mol.%) and higher CO_2 (11-21 mol.%). CO and organic compounds are very high at the Hove and Tvedestrand localities ranging 23-29 and 8-27 mol.% respectively. Kihle (1990) argued on the basis of his study of regionally distributed cordierites that CO_2-enriched fluids were not confined to the Arendal-Tromöy-Tvedestrand area as indicated by Zimmermann (1981) and Touret (1985). Optical analysis of cordierites from locality 3 (Kihle, 1990; Kihle & Bucher-

Nurminen, 1992) indicates the presence of high temperature fluid gradients or disequilibrium on thin section scale. Vry et al. (1990) analysed the channel H_2O, CO_2 and alkali content of four cordierites from the Arendal, Risör and Kragerö areas (no location data given). Total H_2O and CO_2 contents in cordierites from Arendal and Risör range respectively 0.87-1.04 wt.% and 1.04-1.61 wt.%. The amphibolite facies sample from Kragerö yielded high total H_2O (1.75 wt.%) and low CO_2 (0.20 and 0.40 wt.% CO_2).

ANALYTICAL TECHNIQUES

Cordierites were concentrated to about 95-97 % purity from 125-250 μm and 250-500 μm sieve fractions by heavy liquids and a Franz isodynamic magnetic separator. The fractions were handpicked (removal of chlorite and pinitised cordierites) to about 99.5 % purity.

Major elements were determined with a JEOL JXA-8600 superprobe at 15 kV and 10 nA at the University of Utrecht with minerals and synthetic compounds as standards. Raw count data were corrected with a Tracor Northern PROZA correction program. Five to ten grains per thin section were analysed, with a total of 5 to 7 spots per analysed grain.

Be and Li contents were determined by Inductively Coupled Plasma Atomic Emission Spectroscopy (ICPAES) on an ARL 34000. For Be analysis, the sample decomposition procedure of Voncken et al. (1986) was used.

The total volatile content in 21 cordierite fractions was estimated from the weight-loss during ThermoGravimetric Analysis (TGA). The TGA's were performed on 40-50 mgr cordierite using a Dupont 1090 thermal analyzer at a heating rate of 5 and 10 °C/min and nitrogen-flow of 50 ml N_2/min. TGA values were corrected for weight-loss of absorbed H_2O up to 120 °C.

IR absorption spectra were recorded with a double-beam Perkin Elmer 580 IR spectrophotometer. The IR-spectrum of one sample (TN260) was recorded with a Perkin Elmer 1700 spectrophotometer. The samples were prepared using the pressed KBr disk technique. Two mg of cordierite was grounded together with 200 mg spectroscopic grade KBr in an achate mortar and/or in a tungsten carbide ball mill, pressed under vacuum and subsequently dried overnight at 120 °C before recording the spectra. A KBr blank was used as reference. Sample thickness was measured with an optical microscope and proved to be uniform (0.058 $\pm$ 0.002 cm). Duplicate analyses were made for all samples from separate batches. Results are reproducible within 0-6 % of the peak height absorbance. H_2O and CO_2 peak height absorbances determined by IR spectroscopy were used to calculate the H_2O and CO_2 concentrations in cordierite (see results).

The distortion index Δ, an average of 3-5 measurements of the 131, 511 and 421

Table 2.2. Average electron microprobe analyses (wt.% oxides), Be and Li analysis (ppm), distortion index (Δ) (Miyashiro, 1957), type I and II H_2O and CO_2 contents (wt.%) determined from infrared absorbances, and TGA (volatile loss in wt.%) results of selected cordierite samples.

		SiO_2	TiO_2	Al_2O_3	FeO	MnO	MgO	CaO	Na_2O	K_2O	Be	Li	Δ	TGA	Total H_2O+CO_2	H_2O I	H_2O II	CO_2	XH_2O
1	CM092	49.96	0.00	33.33	4.26	0.01	11.14	0.01	0.13	0.00					0.85	0.23	0.13	0.49	0.64
	CM093	49.44	0.00	33.41	4.18	0.04	11.02	0.00	0.17	0.00	9	27	0.258	1.35	1.22	0.37	0.10	0.75	0.61
	DV148	49.47	0.01	33.40	4.40	0.03	11.18	0.00	0.12	0.02	9	27	0.260	0.97	1.17	0.34	0.11	0.72	0.60
	DV149	49.53	0.00	33.42	4.22	0.01	11.29	0.02	0.12	0.01	27	30	0.259	1.33	1.25	0.44	0.12	0.69	0.66
	DV286	49.01	0.01	32.90	5.64	0.05	10.27	0.02	0.14	0.00	7	17	0.257	1.69	1.67	0.52	0.14	1.01	0.61
	DV288	49.30	0.00	33.54	4.22	0.04	11.26	0.02	0.10	0.02	8	28	0.260	1.41	1.32	0.41	0.12	0.79	0.62
2	TN260	49.72	0.00	33.45	3.69	0.04	11.44	0.00	0.12	0.00					1.06	0.21	0.16	0.69	0.57
3	PT138	49.08	0.04	33.82	2.96	0.04	11.93	0.00	0.22	0.00	<2	38	0.260	1.51	1.35	0.45	0.31	0.59	0.76
4	EJ041	49.25	0.02	33.31	3.00	0.12	11.54	0.03	0.13	0.01	18	66	0.257	1.68	1.62	0.64	0.22	0.80	0.72
5	CM175														1.99	0.42	0.16	1.45	0.49
6	DV084	49.05	0.03	33.18	4.03	0.06	11.02	0.00	0.21	0.01	94	74	0.252	2.09	2.20	0.47	0.26	1.47	0.55
	DV085	49.98	0.00	33.45	3.09	0.01	12.31	0.06	0.13	0.02	8	23	0.274	1.30	1.07	0.47	0.11	0.49	0.74
	DV261	49.32	0.01	33.48	4.31	0.03	11.27	0.00	0.19	0.00	9	33	0.250	1.25	1.16	0.45	0.25	0.46	0.79
	DV263	49.20	0.01	33.44	5.44	0.10	10.26	0.00	0.10	0.00	79	33	0.278	1.05	1.04	0.31	0.10	0.63	0.61
7	MA995														1.14	0.35	0.22	0.57	0.71
8	BD033	49.36	0.00	32.81	5.31	0.00	10.19	0.00	0.31	0.00					2.14	0.71	0.45	0.98	0.74
9	DV080										7	115	0.259	1.90	1.80	0.36	0.17	1.27	0.50
10	DV064	49.50	0.01	33.51	3.64	0.07	11.55	0.00	0.11	0.00	40	54	0.261	2.10	2.34	0.37	0.11	1.86	0.39
11	DV029	49.03	0.00	32.94	3.22	0.00	11.22	0.00	0.23	0.00	<2	61	0.256	2.96	3.03	0.65	0.34	2.04	0.54
	DV037	49.21	0.07	32.46	4.19	0.04	10.90	0.00	0.25	0.00	5	67	0.264	2.22	2.43	0.47	0.29	1.67	0.53
12	DV153	49.23	0.03	33.16	3.09	0.19	11.56	0.01	0.21	0.02	257	73	0.249	2.00	2.11	0.40	0.22	1.49	0.50
13	DV122	49.21	0.00	33.38	4.09	0.00	11.03	0.00	0.18	0.02					1.99	0.45	0.20	1.34	0.54
	MA780	49.46	0.02	33.58	3.30	0.01	11.36	0.01	0.22	0.00	8	82	0.238	2.09	1.79	0.30	0.17	1.05	0.52
14	DV114														2.42	0.72	0.43	1.27	0.69
15	DV159	49.78	0.02	33.50	1.63	0.01	12.69	0.01	0.20	0.00	<2	82		2.44	2.38	1.01	0.45	0.92	0.80
	DV165	49.72	0.00	33.34	1.29	0.00	12.72	0.00	0.26	0.00				2.77	3.17	0.73	0.38	2.16	0.56
	DV330	49.70	0.01	33.86	1.61	0.03	13.00	0.10	0.14	0.03	33	121	0.261	1.15	1.08	0.36	0.12	0.60	0.66
16	MA822	49.43	0.00	33.42	1.18	0.00	12.66	0.00	0.36	0.00	53	20	0.239	3.00	3.12	0.95	0.51	1.66	0.68
	MA998														2.93	0.84	0.52	1.57	0.68

peaks, $\Delta = 2\ \Theta_{131}-(2\Theta_{511}-2\Theta_{421})/2$, in the 28° to 30° CuK$\alpha_1$ range (Miyashiro, 1957), of several cordierite fractions was investigated with a Philips PW 1050 Diffractometer, connected to a PW 1710 controlling device, and an Enraf Nonius FR 552 Guinier Camera. Analytical data are presented in Table 2.2.

RESULTS

Cordierite composition, structural state and TGA

The majority of the cordierites are homogeneous Mg-rich with $Mg/(Mg+Fe_{tot})$ ratios (X_{Mg}) between 0.76 and 0.88. Cordierites from localities 15 and 16 are much closer to the Mg-endmember with X_{Mg} between 0.93 and 0.95. Cordierites in samples DV037 (Loc. 11) and MA780 (Loc. 13) appear to be zoned to slightly Mg-richer compositions adjacent to garnet. The Mn-endmember is low in all samples (<0.80 mol.%). Ca and K are generally below detection limit or negligible. The Na-content ranges 0.10-0.36 wt.% Na_2O (0.020-0.071 atoms/formula unit, a.f.u.) and tends to be lower in the granulite facies area (Fig. 2.2).

Be contents in the Bamble cordierites are low, except for DV153 (loc. 12), DV084 and DV263 (loc. 6), which show 257 ppm (0.07 wt.% BeO) and 79-94 ppm Be (0.02-0.03 wt.% BeO) respectively. Li contents range 20-121 ppm Li (0.004-0.027 wt.% Li_2O) with the higher values obtained in amphibolite facies cordierites (Fig. 2.2). Wet-chemical analyses of cordierites from locality 1 and locality 6 were presented by Beeson (1978; samples 635 and 616). The major elements of these samples are comparable in range, except for slightly higher sodium contents at both localities and significantly higher Ca and K contents at locality 6.

On the basis of their high distortion indexes (Δ ranges 0.239-0.278), all measured cordierite fractions can be regarded as 'low cordierites' (Schreyer & Schairer, 1961) or orthorhombic phases (Putnis, 1980). The distortion index, a measure for the magnitude of long-range ordering, is suggested to correlate positively with water (Selkregg & Bloss, 1980) and negatively with Be and/or Na contents (Schreyer et al., 1979; Armbruster & Irouschek, 1983). Our data show no clear correlation of either H_2O, Be or Na with the distortion index. Be concentrations are probably too low to achieve a significant decrease of long-range order. The effects of H_2O on the lattice metrics may well have been neutralized by the influence of Na.

TGA of the cordierite fractions shows a continuous weight loss beginning at about 350-400 °C and ending at 950-1050 °C. The temperatures are in agreement with those obtained in previous studies. A.B. Hunter (personal communication in Vry et al., 1990)

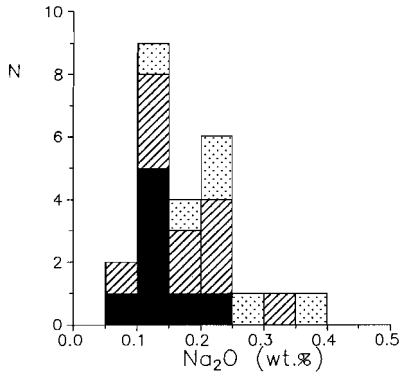

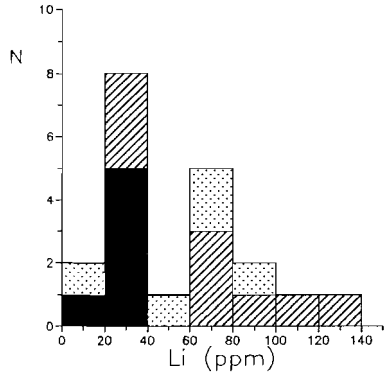

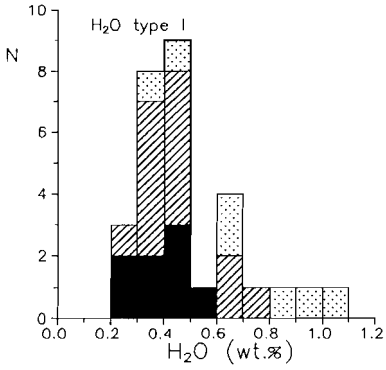

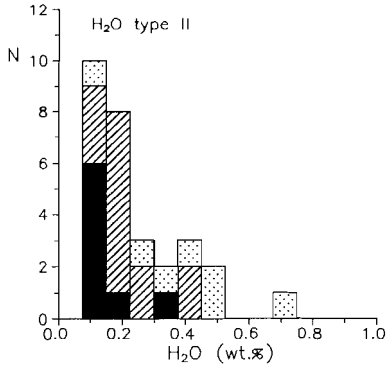

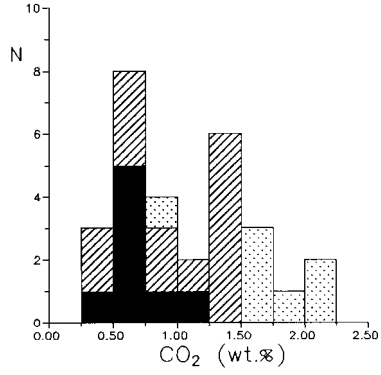

Fig. 2.2. Frequency histograms of Na_2O, Li, type-I H_2O, type-II H_2O and CO_2 in cordierites of the granulite- (black) and amphibolite facies domains (hatched) and in samples showing significant late M_4 retrogradation (stippled).

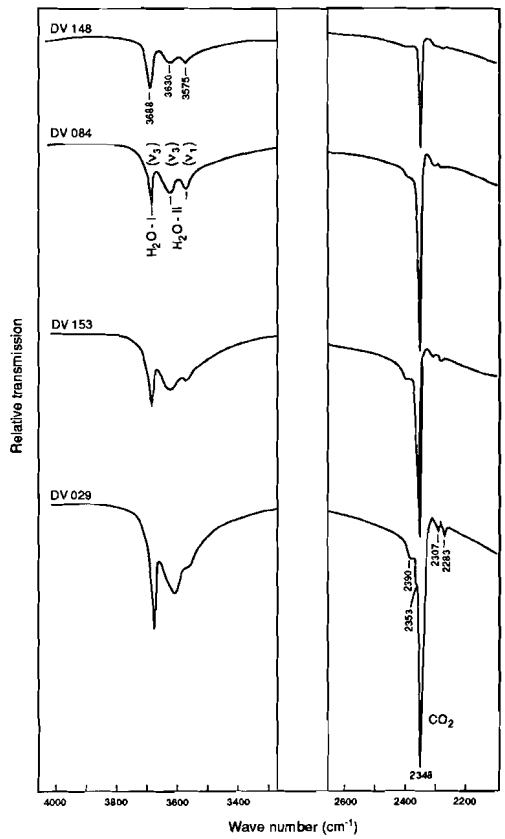

Figure 2.3. Infrared absorbtion spectra of cordierite from regional granulite- (DV148), transitonal- (DV084) and amphibolite facies (DV153) rocks and of a cordierite (DV029) re-equilibrated under retrograde greenschist to low-amphibolite facies conditions, Bamble Sector, south Norway.

reported the volatile loss to begin near 450 °C and to finish near 900 °C. Zimmermann (1981) established a slightly wider temperature range of 250-1000 °C for expulsion of the volatiles. The total TGA weight loss (0.97-3.00 wt.%) corresponds very closely to the total volatile (H_2O and CO_2) content of the cordierites as determined by IR (see below).

IR spectroscopy

Figure 2.3 shows the IR spectra of cordierite from the granulite facies area (DV148, Loc. 1), the transition zone at Tvedestrand (DV084, Loc. 6), the amphibolite facies area (DV153, Loc. 12) and the retrograde sample DV029 (Loc. 11). Absorption spectra

recorded in the 1200-400 cm^{-1} range (not shown) all correspond closely to the 'low cordierite' spectra reported by Langer & Schreyer (1969), thus confirming the XRD results.

H_2O and CO_2 absorption bands can be determined very easily from the IR spectra. The IR spectra show two distinct types of H_2O molecules. The orientations are denoted as type-I, with the H-H vector parallel to the *c*-axis, and type-II, with the H-H vector parallel to the *b*-axis (Aines & Rossman, 1984). The type-II orientation is favoured by the presence of Na and other channel cations. Studies by Goldman et al. (1977) and Vry et al. (1990) show that this essentially involves the coordination of two type-II H_2O molecules to each channel cation.

Asymmetric stretching occurs at 3688 cm^{-1} (ν_3) for type-I H_2O and at 3630 cm^{-1} for type-II H_2O. Symmetric bending of type-II H_2O (ν_1) produces a peak near 3575 cm^{-1} (Fig. 2.3). CO_2 produces five bands at 2390, 2353, 2348, 2307 and 2283 cm^{-1} (Werding & Mirwald, 1982). The two strongest bands, which occur at 2353 cm^{-1} and 2348 cm^{-1} are interpreted by Werding & Mirwald (1982) to belong to respectively an orientation of the CO_2 molecule with the O-C-O vector parallel to the *c*-axis (c-position) and one parallel to the *a*-axis (a-position). In the present study, all five CO_2 absorption bands are detected (Fig. 2.3) in nearly all samples at a large expanded frequency and absorption scale.

Zimmermann (1981) claimed the presence of significant quantities of methane, CO and other organic compounds in his analysed Bamble cordierites. Vibrations of hydrocarbons such as methane, which are resolved in the 3200-2900 cm^{-1} region, and of carbon monoxide, resolved at 2143 cm^{-1} (Werding, unpublished data in Schreyer, 1985), however, were not detected in any of our samples. The discrepancy probably emerges from the possibility, suggested by Zimmermann himself (1981, pp. 329,330), that chemical reactions occur between graphite (present as inclusions?) and the gas phase during the heating experiments which produce CO and the hydrocarbons.

The absolute H_2O and CO_2 contents are determined from the absorbance intensities of the 3688 cm^{-1} (type-I H_2O), the 3630 cm^{-1} (type-II H_2O) and of the 2348 cm^{-1} (CO_2) peak on the basis of Beer's law, $A = \epsilon bc$ (Absorbance = extinction coefficient·sample thickness·concentration) using the integral molar extinction coefficients $\epsilon CO_2 \approx 630$ $L.mol^{-1}.cm^{-1}$ and $\epsilon H_2O \approx 77$ $L.mol^{-1}.cm^{-1}$ as determined by Vry et al. (1990). Following Vry et al. (1990), it is assumed that ϵH_2O is equal for both types of H_2O. The validity for using the extinction coefficients of Vry et al. (1990) is confirmed by the very close correspondence of the TGA weight loss values recorded in nitrogen atmosphere with the IR determined H_2O+CO_2 concentrations.

As evident from the spectra (Fig. 2.3) and Table 2.2, both type-I and type-II water are present in all the samples. The total amount of type-I water ranges 0.23-1.01 wt.% and is similar for both granulite facies and amphibolite facies samples (Fig. 2.2). Most

cordierites from retrograde samples are enriched in type-I H_2O (Fig. 2.2).

Type-II water is present in the range 0.10-0.52 wt.%. Samples from the Arendal-Tromöy granulite facies area are clearly depleted in this type of H_2O, relative to the samples from the amphibolite facies area (Fig. 2.2) and most retrograde samples. A 2:1 correlation is observed between type-II water and the (Na+K+Ca) content (Fig. 2.4) as predicted by Goldman et al. (1977) and likewise observed by Vry et al. (1990).

The CO_2 contents display a total range of 0.46-2.16 wt.%. Compared with the majority of the amphibolite facies cordierites, the CO_2 contents in granulite-facies cordierites are lower (Fig. 2.2). Most higher CO_2 values are found in the cordierites from retrograde and graphite-bearing samples.

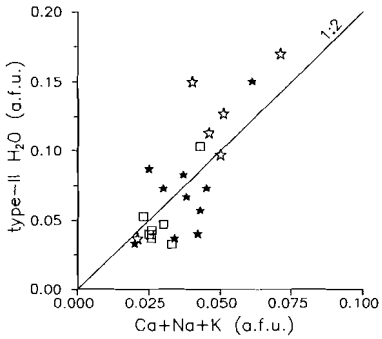

Fig. 2.4. Plot of Ca+Na+K versus type-II H_2O in cordierites of the granulite- (squares), amphibolite facies domains (black stars) and in samples showing significant late M_4 retrogradation (open stars). Line shows 1:2 ratio.

Cordierites from the granulite facies area, the transition zone and some of the amphibolite facies samples are characterised by low total volatile contents and variable X_{H_2O} (with X_{H_2O} = molar $H_2O/(H_2O+CO_2)$ ratio) of 0.57-0.79. Most amphibolite facies samples are volatile-richer and display a larger variation in X_{H_2O} (0.49-0.0.80). The cordierites of retrograde samples have very high total volatile contents and generally show low X_{H_2O} values (0.39-0.68; except for sample DV159: 0.80). The volatile composition on outcrop scale is rather uniform in the cordierites from localities 1, 11, 13 and 16, but heterogeneous at localities 6 and 15.

DISCUSSION

Regional variation

The IR, TGA and analytical data presented in this study give rise to the following major findings:

1. IR observations show only type-I, type II H_2O and CO_2 present as volatile species, hydrocarbons and CO are not detected in the spectra of the 'low cordierites'.

2. The total volatile contents are low in cordierites from the granulite facies area and rather variable in cordierites from the transition zone and the amphibolite facies area.

3. A decrease of Na, type-II H_2O, CO_2 and possibly Li is observed with increasing metamorphic grade. X_{H_2O} and the amount of type-I H_2O is variable but does not show a similar correlation.

High temperature spectroscopic observations by Aines & Rossman (1984) showed that above 400 °C both type-I and II water bound in the channels gradually begin to partition into an unbound state. This enables channel cations like Na to move to the channel walls or diffuse out of the channel. Aines & Rossman (1984) further argued that dehydration occurred after most H_2O is unbounded and that it was facilitated by removal of Na from the channels. The preferential loss of type-II H_2O and Na in the Bamble cordierites with increasing metamorphic grade points to a similar dehydration mechanism. The uncorrelated and variable amount of type-I H_2O indicates that the dehydration was only partial and that some of the type-II H_2O previously present in the channels probably is preserved as type-I H_2O in the cordierites after cooling.

The volatile loss apparently also affected some of the CO_2 present in the channels. In comparison with the channel occupancy data for H_2O+CO_2-bearing cordierites of Vry et al. (1990), the consistently low total volatile content of the granulite facies cordierites (and several of the amphibolite facies ones too) likewise points to volatile-undersaturated conditions.

An experimental pilot study of Mirwald (1986) in the model systems Mg-cordierite-albite-NaOH-H_2O and Mg-cordierite-NaOH-H_2O showed a negative temperature dependance of the Na-content of cordierite. The Na-contents reported in this study and the temperatures as reported by Nijland & Maijer (1993) compare reasonably well with these preliminary experimental data. A similar decrease in Na was observed by Scheurs (1985) in cordierites from the thermally induced amphibolite-granulite facies transition zone of

the West Uusimaa, south Finland (Westra & Scheurs, 1985).

The observed Li values in the Bamble cordierites are much lower than generally encountered in (mid-)amphibolite facies cordierites (0.02-0.74 wt.% Li_2O) (Armbruster & Irouschek, 1983; Dutrow et al., 1986; Ginzburg & Stavrov, 1961; Robinson & Jaffe, 1969) and cordierites associated with lithium pegmatites (0.24-0.64 wt.% Li_2O) (Ginzburg & Stavrov, 1961). Grew et al. (1990) reported similar low values (0.002-0.02) for upper amphibolite to granulite facies cordierites associated with kornerupine. The data presented in this study and the literature data essentially show a decrease of Li in cordierites with the metamorphic grade. Analogous to the behaviour of Na with increasing temperatures, it is suggested that, despite the close crystal chemical relations of Li with Mg, some Li is present in the channels and that it is also released from the channels upon heating. Experimental and IR studies on Li-incorporation in Mg-cordierites by Kirchener et al. (1984) are supportive as they show that Li can be incorporated in both the octahedral- and channel-sites.

The low absolute CO_2 content of the granulite facies cordierites is not consistent with the large-scale CO_2 transfer model of Touret (1971, 1974), which requires high CO_2 activities. Nor do the data support the progressive change in fluid composition from H_2O-rich to CO_2-rich as proposed by Lamb et al. (1986). Taking the suggested temperature increase (Nijland & Maijer, 1993) into account, the cordierite data are best explained by a mechanism of progressive dehydration and some loss of CO_2. The process of lowering P_{fluid} is facilitated by the formation of anatectic melts, which have a widespread occurrence in the area and which provide a perfect sink for the released water and Na. The released CO_2 may explain at least a part of the observed CO_2 inclusions. Fluid absent or fluid-deficient conditions are also suggested as an explanation for the high temperature dis-equilibrium textures documented at locality 3 (Kihle & Bucher-Nurminen, 1992).

The present data are compatible with Touret's (1986; 1988) later combined dehydration and carbonic model. Available isotope data and traces of carbonate-like melts led Touret (1985) to propose an introduction of CO_2 through carbonate melts associated with the synmetamorphic enderbitic and metabasic intrusions on Tromöy. The CO_2-introduction is, however, confined to the close proximity of the intrusives and not considered pervasive (Touret, 1986). The granulite genesis by CO_2 introduction is, therefore, likely to have predominated on a very local scale rather than on a regional one. The "synmetamorphic" intrusive rocks, however, may have been the principal heat source for the temperature increase and the resulting dehydrations. Possible evidence for this scenario is provided by the shape of the prograde P-T path of the Froland area (Visser & Senior, 1990). The P-T path starts as a clockwise continental collision scenario (M_1-M_{3a}). At high temperatures (650-700 °C), however, this scenario is truncated by a phase (M_{3b}) of near-isobaric temperature increase (50-100 °C). The necessary heat to explain the

temperature increase has to involve a significant large magmatic source of which the enderbitic and metabasic rocks, assuming that these rocks intruded under high-grade conditions (Smalley et al., 1983; Touret, 1985), provide the best candidates.

Retrograde re-equilibration

Cordierites from retrograde samples (localities 10, 11, 15 and 16) all show significant higher total volatile contents when compared with other amphibolite facies samples (e.g. DV330 of locality 15).

Based on the IR results the retrograde volatile gains essentially involve CO_2 at localities 10 and 11, and mixed H_2O-CO_2 at localities 15 and 16. The results are compatible with preliminary microthermometric observations (D. Visser, unpublished data), which show only late trail-bound CO_2-bearing fluid inclusions in DV064 (Loc. 10) and DV037 (Loc. 11) and both H_2O- and CO_2-bearing trail-bound fluid inclusions in DV159, DV165 (Loc. 15) and MA822 (Loc. 16). The introduction of Na by the fluid, which may account for the higher Na-contents at localities 15 and 16, is exemplified by the presence of retrograde scapolite (sample DV165) and the presence of NaCl cubes in some of the aqueous inclusions in DV159, DV165 and MA822.

Experimental data reported by Johannes & Schreyer (1981) indicate that X_{H_2O} in cordierite reflects the ratio of these species in the coexisting fluid. Using their 600 °C, 5 kbar data and the obtained X_{H_2O} data (Table 2.2) this would correspond to X_{H_2O} in the retrograde fluid of about 0.05-0.30. This is consistent with the observed cordierite breakdown assemblage Ky-And-Chl-Qtz, which requires $X_{H_2O} < 0.3$, assuming hydrous Mg-cordierite and clinochlore compositions (Berman 1988; see also chapter 3).

One may conclude from the foregoing that the unaltered parts of partially altered Bamble cordierites re-equilibrated completely with the retrograde fluid and that no high-grade fluid composition is preserved. This is in accordance with the absence of any optical zoning or variations in the analysed cordierites.

ACKNOWLEDGEMENTS

We thank Nelly Slaats for assistance during sample separation, Tilly Bouten and René Poorter for assistance with the microprobe analyses, Angelique Lesquillier for the Be and Li analyses, Vian Govers for providing the X-ray diffractograms and T. Zalm for the TGA curves. T.G. Nijland and R.D. Schuiling reviewed a preliminary draft of the manuscript. This work has been supported by grants from the Dr. Schürmann (grant 91-05) and Molengraaff Foundations.

CHAPTER 3

KORNERUPINE IN A BIOTITE-SPINEL-GARNET SCHIST NEAR BÖYLEFOSSBRU, BAMBLE SECTOR, SOUTH NORWAY: IMPLICATIONS FOR EARLY AND LATE METAMORPHIC FLUID ACTIVITY.

ABSTRACT

Kornerupine occurs in a biotite-spinel-garnet schist zone in a small heterogeneous cordierite-orthoamphibole lens-shaped outcrop near Böylefossbru, Bamble Sector, south Norway. Field relations, major, trace and rare earth element geochemistry of the kornerupine-bearing schist and cordierite-orthoamphibole rocks of the same lens suggest that the protolith possibly consisted of mafic rocks that have been altered into illite-chlorite-quartz mixtures due to low-grade hydrothermal interaction with heated seawater at high water/rock ratios.

The Fe-Al-rich kornerupine formed as a coronas between Zn-rich spinel, corundum, ilmenite, rutile and biotite during or shortly after a decompression (M_{3a}) phase in the prograde part of the P-T path (M_1-M_3). Estimated P-T conditions for formation of kornerupine are 6-8 kbar and 630-720 °C. Boron and H_2O for the kornerupine formation were most likely generated by dehydration of possibly boron-bearing muscovite in adjacent polyphase migmatitic metapelites. Large euhedral pyrope-rich almandines developed at peak metamorphic conditions (M_{3b}, 7 kbar and 698-753 °C).

During retrogradation (late M_4), partial breakdown of kornerupine resulted in fine-grained intergrowths of tourmaline-andalusite-chlorite, tourmaline-chlorite-corundum ± hematite and dumortierite-chlorite. Chloritisation of adjacent F-bearing biotite regulated the silica and F-content of the fluid-phase on the micron scale. P-T conditions are estimated at 3-4 kbar and 411-500 °C. The retrograde fluid is calculated to be CO_2-rich with $X_{CO_2} = CO_2/(H_2O+CO_2)$ of 0.7-0.8. A possible source of the CO_2-rich fluids are the residual fluids derived from solidified leucosomes. Retrogradation is interpreted to have been triggered by the late, regional deformation phase (D6).

INTRODUCTION

Kornerupine, a Mg-Fe-Al silicate which contains variable amounts of water and boron, is an uncommon constituent of Mg-Al-rich and generally Si-poor rock types metamorphosed under amphibolite- to granulite facies grade conditions (e.g. Waters & Moore, 1985; Grew et al., 1987a; Lonker, 1988). Experimental stability relations of boron-free kornerupine have been studied in the system MgO-Al_2O_3-SiO_2-H_2O by Seifert (1975) and show kornerupine to be stable at water pressures above 4.5 kbar, and temperatures above 735 °C. Experimental studies on the B-incorporation in kornerupine concentrated on the mechanisms of the boron substitution, and on the effect on the physical properties of kornerupine (Werding & Schreyer, 1978). Preliminary data on the high pressure (>20 kbar) stability of boron-bearing kornerupine were presented by Krosse et al. (1992). Experimental data regarding the effect of Fe-substitution on kornerupine stability are still lacking. Most natural kornerupine-bearing assemblages, however, cannot be described by the MASH system as significant amounts of Fe, B, K, F (biotite), Na and Ca (tourmaline) are present. Furthermore, the coexisting fluid often contains components other than H_2O ($P_{H_2O} < P_{Total}$). Consequently, the documented natural assemblages and reaction textures may deviate markedly from the experimentally determined ones.

This paper reports the detailed petrographic and analytical data of an occurrence of kornerupine near Böylefossbru, situated in the Proterozoic Bamble Sector, south Norway. The data are used to constrain the P-T conditions, the composition and possible origin of the fluid phase during the prograde formation, as well as the low temperature (<500 °C) retrograde breakdown of the kornerupine in this occurrence. Some consideration will be given to the possible protolith of the kornerupine-bearing rock.

The Böylefossbru locality is the sixth reported occurrence of kornerupine from Norway. Four of the five other known occurrences are likewise located within the Bamble Sector (van der Wel, 1973; Hulzebos-Sijen et al., 1990; Visser et al., 1991). A fifth report is from the geologically contiguous Kongsberg Sector (Munz, 1990).

GEOLOGICAL SETTING AND FIELD RELATIONS

The kornerupine-bearing specimen (DV250) was collected from a quartz-free biotite-garnet-rich domain in the centre of a small heterogeneous lens (5x2 m). This lens consists of biotite-gedrite-cordierite-quartz ± garnet rock with quartz-free enclaves of corundum, staurolite and spinel mantled by cordierite. Several late coarse-grained discordant quartz-cordierite ± garnet segregations are present. The surrounding rocks consist of alternating

garnet-amphibolites, polyphase migmatitic biotite-sillimanite-K-feldspar-plagioclase-(muscovite) ± garnet-bearing metapelites, graphite-bearing gneisses and biotite-(muscovite)-bearing quartzites. Primary muscovite has not been observed in the metapelites at the locality. This is consistent with the location of the prograde muscovite-out isograd (Touret, 1971), which is situated just north-west of the investigated area (Fig. 3.1). A few thin schistose concordant zones within the gneisses are impregnated with sulphide minerals, mainly pyrite and pyrrhotite.

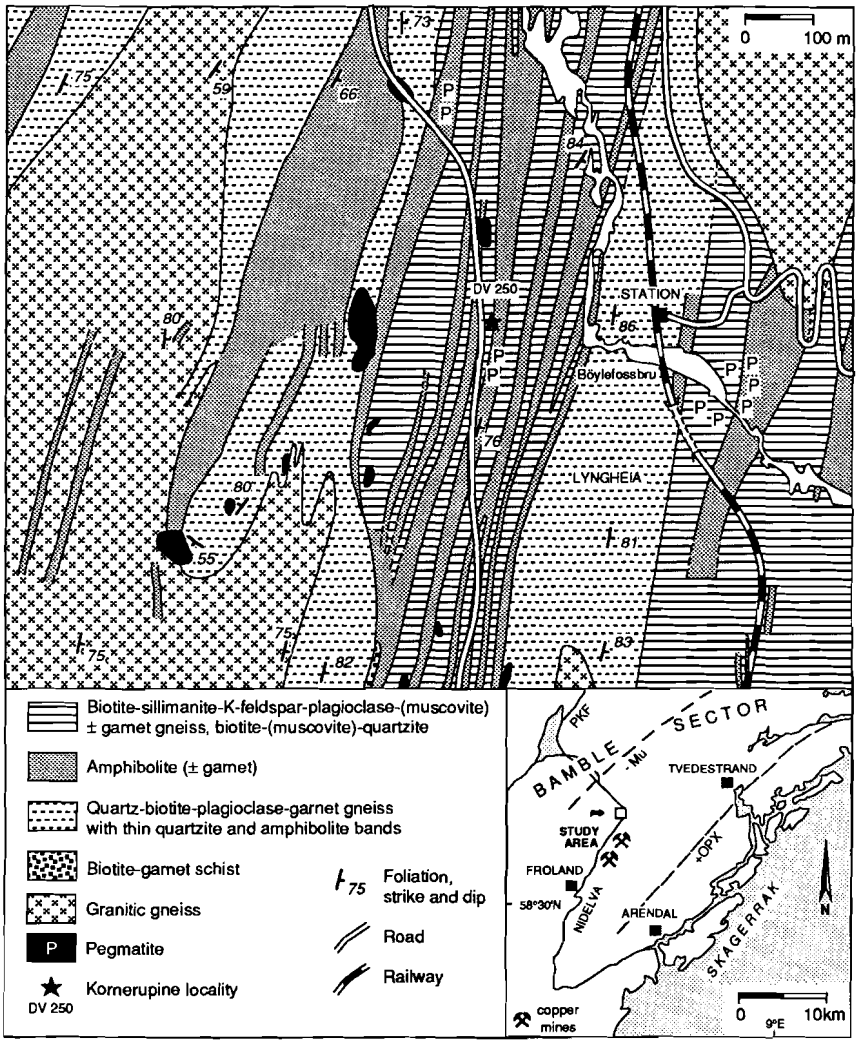

Figure 3.1. Geological map of the Böylefossbru area, showing the kornerupine locality (DV250). The inset is a map of the central part of the Bamble Sector, south Norway showing the location of the study area. The orthopyroxene-in isograd is after Field and Clough (1976), the muscovite-out isograd is after Touret (1971).

The outcrop is situated about 250 meters west of the railwaybridge Böylefossbru, Froland area, and approximately 20 km NNW of Arendal, south Norway (Fig. 3.1; 4831-64956, map reference from Series M711 topographical maps, sheet 1612 III Nelaug). The Froland area is part of the Bamble Sector, a Proterozoic NE-SW trending high-grade belt along the Skagerrak coast. Deformation and metamorphism occurred during the Kongsbergian (1.6-1.5 Ga) and Sveconorwegian (ca. 1.2-0.9 Ga) orogenies (Starmer, 1985, 1991; Verschure, 1985). Based on corona textures in orthoamphibole-bearing rocks from Böylefossbru and other localities in the Froland area, Visser & Senior (1990) proposed a continental collision scenario with magmatic addition (M_1-M_3) during the Kongsbergian orogeny. An early M_1-phase characterised by the presence of andalusite was followed by a very strong deformation phase which correlates very well with the D_1 event of Starmer (1985). The area proceeded through the kyanite-staurolite zone during the M_2-phase indicating an increase of both pressure (4 $\longrightarrow$ 8 kbar) and temperature (500 $\longrightarrow$ 650 °C). Cordierite-corundum coronas between kyanite-orthoamphibole and staurolite-orthoamphibole document a decompression phase (M_{3a}) at about 600-700 °C. The M_{3a} minerals were subsequently deformed during the second deformation phase D2 (Starmer, 1985; Nijland & Senior, 1991), that seems to have been relatively weak in the Böylefossbru area, before the static growth of large garnet porphyroblasts at peak-metamorphic conditions (M_{3b}). Peak-metamorphic conditions at the Böylefossbru locality have been estimated to be 740 $\pm$ 60 °C and 7 kbar.

The D2 phase and the temperature increase between M_{3a} and M_{3b} probably relate to the emplacement of synkinematic charnockites and enderbites in the Arendal area (Smalley & Field, 1985). An alternative hypothesis was presented recently by Nijland & Maijer (1992, 1993) suggesting the formation of a thermal dome presumably caused by mafic underplating (de Haas, 1992).

A prolonged period of near-isobaric cooling (ca. 300 Ma) occurred between the Kongsbergian and Sveconorwegian orogenies (Visser & Senior, 1990). Uplift of the area occurred during the Sveconorwegian orogeny (M_4), which manifested itself as a retrograde greenschist- to amphibolite-facies event with extensive fluid activity. P-T conditions for the onset and completion of this uplift and rehydration event are constrained at 625-700 °C and 6-7 kbar (early M_4) and 420-530°C at 3-4 kbar (late M_4) respectively (Nijland et al., in press; Visser & Senior, 1990).

The metamorphic effects of the Sveconorwegian orogeny (late M_4, retrogradation of peak metamorphic mineral assemblages) are very pronounced in the Böylefossbru area. M_4 involved the development of kyanite-andalusite-chlorite-quartz $\pm$ tourmaline and dumortierite-chlorite-quartz assemblages after cordierite and chlorite-quartz-dumortierite assemblage after garnet and indicate temperatures of 420-530 °C at 3-4 kbar (Visser & Senior, 1990, 1991). Retrogradation in the surrounding gneisses and amphibolites

concentrated along shear- or thrustzones of variable thickness (200 μm up to several meters) which run sub-parallel to the original layering. In the garnet-amphibolites, the assemblage actinolite-cummingtonite-chlorite-albite developed in these zones. In the biotite-sillimanite-K-feldspar$\pm$garnet gneisses, fine-grained secondary muscovite and minor chlorite developed in the neosomes. Small- to meso-scale open folds and the layer-parallel shear or thrust zones near the locality are considered to be late-mid Sveconorwegian D5 (sequence of events according to Nijland & Senior, 1991) or D6 (sequence of events according to Starmer, 1985) structures. Structures related to the deformation phases D3 through D5 (Starmer, 1985) are not developed at the locality.

Figure 3.2. Sketch of a thin section of sample DV250, showing the compositional banding defined by numerous fine-grained ilmenite, rutile and apatite grains and coarse-grained spinel (*black*) in a foliated biotite matrix (*blank with lineations defining the foliation trend*). Elongated kornerupine (*cross-hatching*) partly replaces spinel. Large euhedral garnets (*fine stipple*) overgrow the compositional banding and the biotite foliation and enclose some of the spinel-kornerupine aggregates.

PETROGRAPHY

Sample DV250 consists of a quartz-free foliated red-brown subhedral to euhedral biotite matrix containing large (100-1000 μm) anhedral green spinel, numerous smaller apatite and rutile grains, and occasionally large anhedral ilmenite and colourless corundum. The spinel grains define a compositional layering (Fig. 3.2), thought to be a former S_0, parallel to the biotite foliation and parallel to the macroscopic banding in the

surrounding gneiss-amphibolite sequence. Colourless to light blue-green kornerupine (1-5 vol.%) occurs as euhedral medium-sized (100-400 μm) grains rimming spinel (Fig. 3.3) and locally large anhedral ilmenite, corundum and rutile. The kornerupine coronas around spinel, ilmenite and corundum may occur in the same band. The kornerupine grains are elongated parallel to the biotite foliation. A few coarse-grained (1-5 mm) subhedral poikiloblastic kornerupines occur devoid of spinel and corundum but with numerous apatite, rutile and ilmenite inclusions in the biotite matrix. Spinel-biotite and spinel-corundum contacts are not observed.

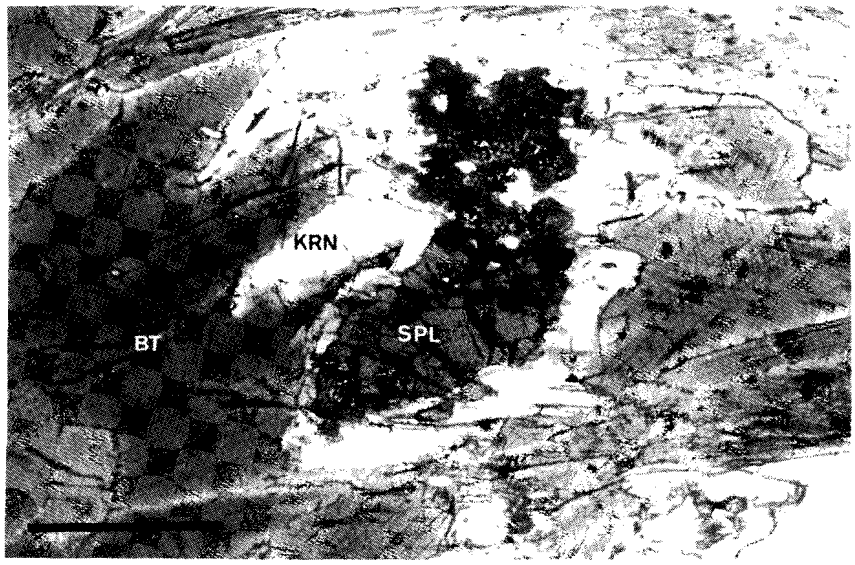

Figure 3.3. Photomicrograph, plane polarized light, showing a kornerupine (KRN) corona between biotite (BT) and Zn-rich spinel (SPL). Note the carbonate lenses intergrown with the biotite cleavage in the upper-left corner of the micro-photograph. Scale bar = 1 mm.

Garnet forms large (up to 5 cm diameter) sub- to euhedral porphyroblasts, which overgrow the biotite foliation and the compositional layering interpreted as S_o and enclose some of the spinel-kornerupine aggregates and large kornerupines. Within these garnets a compositional layering parallel to the biotite foliation and the spinel-kornerupine aggregates is defined by numerous fine-grained bands of ilmenite, apatite and minor rutile (Fig. 3.2). Traces of small-scale folds are retained by the S_o bands. The S_o bands are truncated at the contacts of biotite grains with the garnet-porphyroblasts. In these biotites the S_o bands are less obvious but can be traced by means of isolated rutile and apatite streaks.

Retrogradation of the biotite-(spinel)-kornerupine-garnet aggregates preferentially occurred along fractures and mineral cleavages. Biotite and garnet are replaced by chlorite, white mica and quartz. Less affected biotite grains are sagenitised and show numerous lensoid carbonate intergrowths along their cleavage. Quartz blebs occur intergrown with these carbonate lensoids. The spinel relicts contained in kornerupine are only partly replaced by chlorite and purple-blue corundum. Corundum has a dusty appearance. Minor amounts of chalcopyrite, pyrite and carbonate occur intergrown with chlorite and corundum. Along previous spinel-rutile contacts, a retrograde ilmenite reaction rim developed (Fig. 3.4).

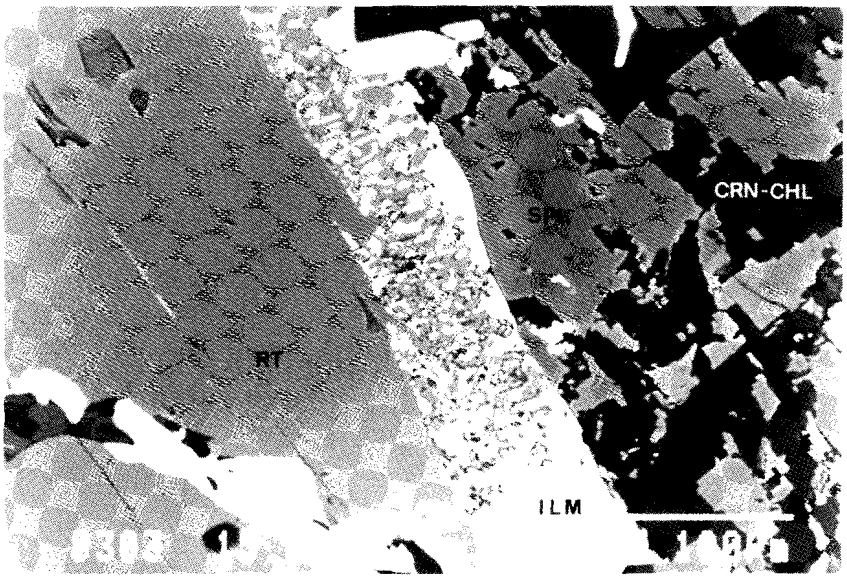

Figure 3.4. Backscattered electron image of ilmenite (ILM) between spinel (SPL) and rutile (RT). Black areas in spinel consists of corundum and minor amounts of chlorite (CRN-CHL).

Large kornerupine grains are partially replaced along their cleavages by fine-grained chlorite, and along fractures and grain boundaries by chlorite, colourless corundum, andalusite and medium-grained euhedral yellow-green tourmaline (Fig. 3.5). Along margins adjacent to altered biotite and upon entering the fractures in the large kornerupine grains the breakdown assemblage is constituted by tourmaline-chlorite-andalusite. In contrast, the tourmaline-chlorite-corundum assemblage developed in the centre of the kornerupine grains, adjacent to garnet and along the cleavage planes of kornerupine. This assemblage itself is zoned, with tourmaline-corundum in the centre of the fracture

bordered by chlorite adjacent to kornerupine. Corundum is locally intergrown with fine-grained hematite. Kornerupine and spinel partially reacted along their contacts to irregular intergrowths of corundum, tourmaline and chlorite (Fig. 3.6). Corundum grains associated with tourmaline and chlorite are clear, whereas corundum grains after spinel are dusty. Both types may occur adjacent to one another. Symmetric zoning of the replacing phases such as observed in the large kornerupine grains has not been observed. Hematite has not been found in these intergrowths. Neither quartz nor carbonate were detected in the replacements after kornerupine. In only one sample, a single grain of reddish-coloured dumortierite was found intergrown with chlorite in the kornerupine margin adjacent to altered biotite (Fig. 3.7).

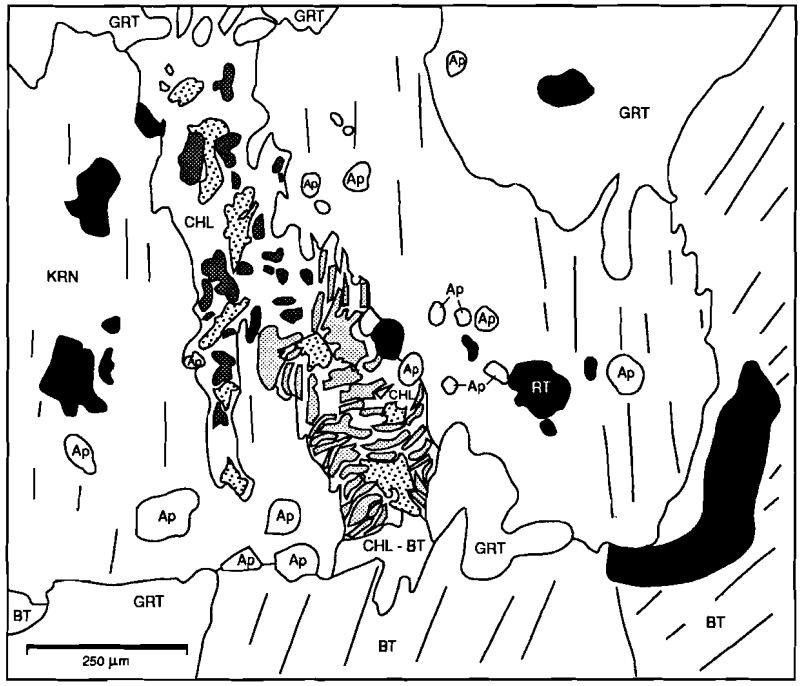

Figure 3.5. Replacement zone in kornerupine drawn from a photomicrograph. Large kornerupine (KRN) is replaced by the assemblage andalusite **(fine stipple)** + tourmaline **(dotted ornament)** + chlorite (CHL) adjacent to biotite (BT) and by the assemblage corundum **(cross-hatching)** + tourmaline + chlorite in the centre of the grain and adjacent to garnet (GRT). Biotite is altered to chlorite, while garnet is brecciated and replaced by chlorite + white mica along this zone. Small cracks in garnet are omitted for clarity.

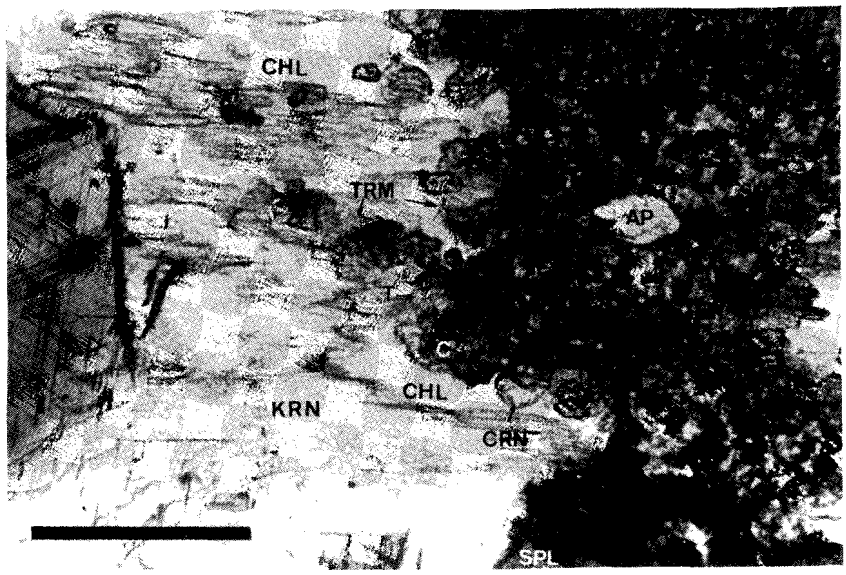

Figure 3.6. Photomicrograph, enlargement of Figure 3.3, plane polarized light, showing the development of chlorite (CHL), tourmaline (TRM,T) and clear corundum (CRN) between kornerupine (KRN) and spinel (SPL). Spinel decomposes to a chlorite-corundum-carbonate mixture. Corundum after spinel (C) has a much darker or dusty appearance. Scale bar = 250 μm.

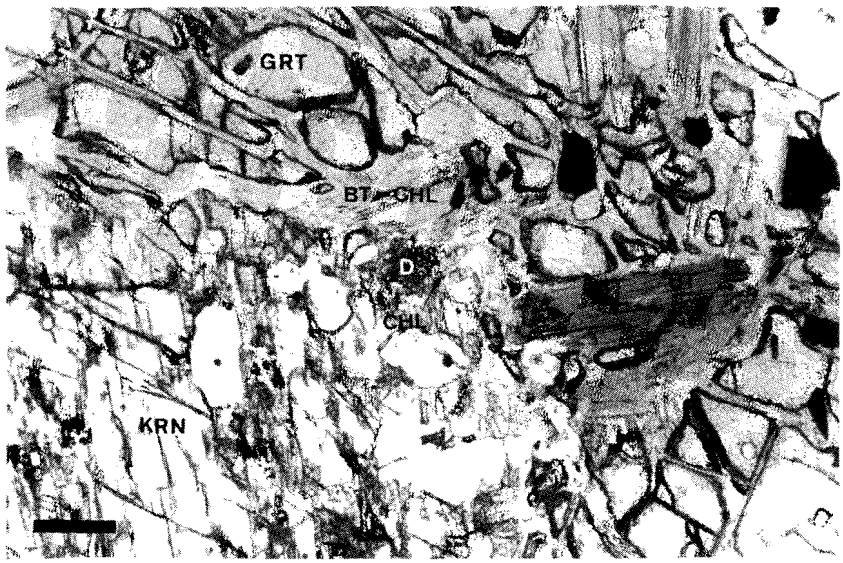

Figure 3.7. Photomicrograph, plane polarized light, showing the intergrowth of dumortierite (D) with chlorite (CHL, see arrows) in the kornerupine (KRN) margin adjacent to altered biotite (BT-CHL). The kornerupine blast is enclosed by garnet (GRT). Scale bar = 125 μm.

Table 3.1. Whole-rock analyses

Sample	DV029	DV037	DV250	amphibolites TN142	amphibolites TN143	range# n=20
SiO_2	46.03	46.58	33.43	46.75	48.68	45.98 - 50.23
TiO_2	0.49	2.51	4.03	2.86	2.25	0.68 - 3.28
Al_2O_3	19.43	17.30	18.83	19.01	20.45	14.13 - 21.28
Fe_2O_3	1.99	3.42	3.61	12.80	9.43	8.82 - 16.36
FeO	9.89	11.39	15.09	-	-	-
MnO	0.20	0.29	0.11	0.21	0.11	0.10 - 0.32
MgO	16.34	12.06	13.87	4.23	3.14	2.77 - 9.78
CaO	0.53	1.48	1.97	8.05	7.78	7.08 - 11.92
Na_2O	0.85	0.35	0.26	3.85	4.62	1.22 - 4.62
K_2O	0.96	0.89	3.02	0.82	1.35	0.19 - 1.40
P_2O_5	0.12	0.47	0.55	0.45	0.57	0.13 - 0.73
LOI	1.96	1.48	3.05	0.05	1.07	-
Total	98.79	98.22	97.82	99.08	99.45	-
Cl	302	320	171	-	-	28 - 192
F	1515	1015	2641	-	-	148 - 1154
B	<20	<20	190	-	-	-
Cr	280	135	142	12	52	12 - 167
Li	57	36	14	-	-	3 - 40
S	26	<25	257	-	-	d.l. - 973
Ba	90	85	316	360	490	163 - 490
Co	61	92	138	78	61	44 - 78
Cu	7	8	40	-	-	d.l. - 33
Ga	19	15	32	-	-	d.l. - 24
Nb	6	16	15	-	-	2 - 8
Ni	334	181	86	57	d.l.	26 - 201
Pb	7	<6	13	-	-	4 - 19
Rb	48	40	118	15	58	5 - 58
Sr	16	15	17	500	910	128 - 910
V	164	273	399	-	-	146 - 333
Y	11	85	124	-	-	8 - 48
Zn	132	110	287	123	86	57 - 181
Zr	97	304	476	190	d.l.	18 - 260
Cs	4.8	4.1	10.7	0.70	1.10	0.70 - 6.0
Hf	2.70	8.1	12.7	4.98	4.50	1.13 - 8.50
Sc	18.0	39.9	58.6	21.2	17.6	17.6 - 45.8
Th	2.21	2.49	2.18	0.70	0.55	0.55 - 1.77
U	1.1	1.6	<1.8	d.l.	d.l.	d.l. - 1.80
La	6.1	12.1	13.0	17.0	18.2	5.8 - 24.0
Ce	14.8	29.7	32.9	43.0	47.9	19.0 - 61.0
Nd	<30.0	<40.0	<28.0	d.l.	29.0	29.0 - 38.0
Sm	1.79	5.7	7.84	5.6	6.4	3.30 - 9.70
Eu	0.21	0.90	1.62	2.26	2.49	1.11 - 2.88
Tb	0.21	2.00	2.35	0.78	0.78	0.62 - 1.69
Yb	1.00	7.85	10.1	2.28	1.39	1.39 - 6.47
Lu	0.17	1.32	1.57	0.38	0.21	0.21 - 1.06
ΣREE	24.28	59.57	69.38	71.30	106.37	

- the range for Cl, F, Li, S and V is based on 12 amphibolite analyses,
the range for Cs, Hf, Sc, Th, U and REE is based on 6 analyses.
d.l. - below detection limit

Mineralogy
DV 029: Crd, Ged, Bt, Stt, Crn, Rt, Ap
DV 037: Grt, Qtz, Ged, Crd, Bt, Stt, Rt, Ap
DV 250: Bt, Grt, Sp, Krn, Ilm, Rt, Ap (And, Chl, Tur, Dum, Crb)
TN 142: Pl, Hbl, Grt, Bt, Zrn, Ap, Ilm, Mag, (Ms, Act, Chl)
TN 143: Pl, Hbl, Grt, Bt, Qtz, Opq, Ap, (Prh, Ep, Cc, Chl)

ANALYTICAL PROCEDURES

Whole rock analyses (Table 3.1) were carried out at the University of Utrecht using gravimetry (LOI), colorimetric titration (FeO), ion selective electrodes (Cl and F), standard X-ray fluorescence techniques with an automated Philips PW1400 Spectrometer (see Bol, 1990, for analytical procedures and accuracies) and Inductively Coupled Plasma Emission Spectroscopy (ICP-ES) on an ARL 34000 spectrometer (for the elements B, S, Li and Cr). REE (La, Ce, Nd, Sm, Eu, Tb, Yb, Lu) and Th, U, Cs, Sc and Hf contents were determined at IRI, Delft by INAA using established techniques (de Bruin, 1983). Mineral analyses were obtained with a Jeol JXA-8600 Superprobe at the University of Utrecht which operated at an accelerating voltage of 15 kV and a sample current of 10 nA. Raw data were corrected with a Tracor Northern PROZA computer program. Natural minerals and synthetic compounds were used as standards. Representative analyses are listed in Tables 3.2-3.4. A X-ray powder diffraction pattern of kornerupine was recorded with a Philips PW 1050/25 diffractometer using CuKα radiation. Unit-cell parameters were calculated with the least-squares refinement computer program Unitcellc (Strom, 1976).

WHOLE ROCK CHEMISTRY

The analysed samples include the kornerupine-bearing sample DV250, a corundum-staurolite-gedrite-cordierite-biotite rock (DV029) and a garnet-cordierite-quartz-gedrite-biotite $\pm$ staurolite rock (DV037) from the Böylefossbru locality. The bulk analyses show that these rocks have low to very low concentrations of SiO_2, high Al_2O_3, very high $FeO_{tot}+MgO$, intermediate MgO/FeO ratios and low CaO and Na_2O contents. The abundances of Nb, V, Y and TiO_2 - F, Ba, Rb and Cs - Cu and Zn, and Zr respectively correlate with the modal abundances of rutile and ilmenite, biotite, spinel and zircon in the samples. K/Rb ratios of 212-389 are comparable to most upper-amphibolite facies amphibolites (Field & Clough, 1976) from the Bamble Sector.

REE patterns are normalised to the average chondritic values given by Taylor & McLennan (1985) and are shown in Fig. 3.8. The REE patterns in samples DV037 and DV250 are rather flat with $(La/Yb)_N$-ratios of respectively 0.98 and 0.87. Both samples have REE concentrations of about 30-40 times chondritic values. LREE are slightly enriched in sample DV029 $(La/Yb)_N$ = 4.12, while the REE concentration of 2(Tb) to 17(La) times chondritic values is somewhat lower than in DV037 and DV250. The lower

HREE abundances are consistent with the absence of garnet in DV029, which is a major constituent of DV037 and DV250. All three samples are characterised by a strong negative Eu anomaly.

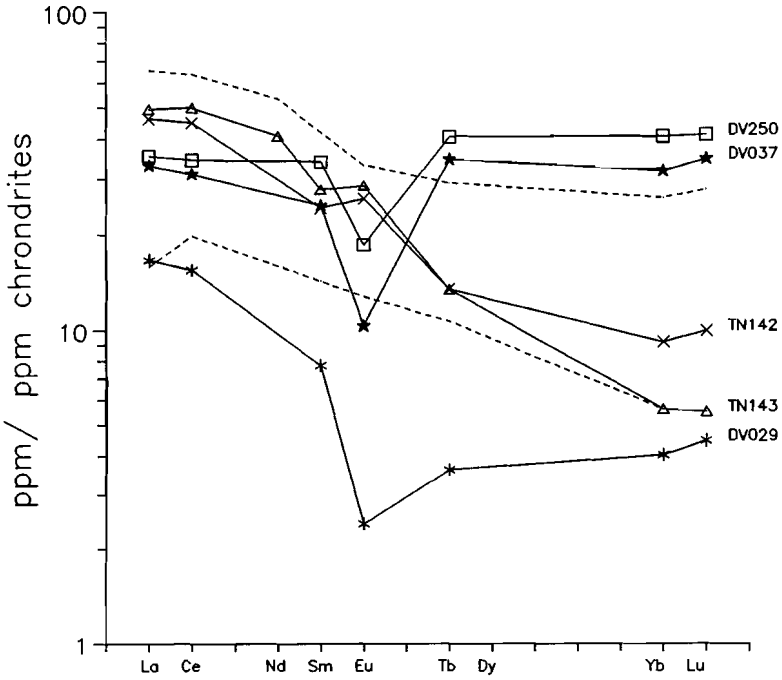

Figure 3.8. Chondrite-normalized REE patterns of the Bøylefossbru samples compared with the range of Bamble amphibolites (broken lines; Nijland and Visser in prep.) and amphibolite samples TN142 and TN143.

MINERAL CHEMISTRY

Primary phases (Table 3.2)

Kornerupine is calculated on the basis of 21.5 oxygens, consistent with a unit cell of 21 oxygens and one (OH,F) group (Moore & Araki, 1979). Cell parameters a_0 and c_0 are used to provide a rough estimate of the boron content in the kornerupine (see Fig. 7a, curve 3 for Al-rich kornerupines, and Fig. 7b in Waters & Moore, 1985; Fig. 3 in Grew et al., 1990). The unit-cell parameters of the kornerupine, a_0 = 16.057(4) Å, b_0 = 13.679(5) Å, c_0 = 6.727(3) Å and V = 1477.5(5) Å^3 are consistent with approximately 1.3 wt.% B_2O_3 ($\approx$ 0.3 B per formula). The presence of OH in the DV250 kornerupine is confirmed by IR analysis, which shows the characteristic absorption bands of OH and

Table 3.2.
Representative analyses of the primary phases in sample DV250.

	Krn		Grt		Bt	Spl	Ap	Ilm
spot	1/4	1/10	2/118 Core	2/116 Rim	1/28	4/10	2/113	3/55
SiO_2	28.76	28.87	39.54	38.02	38.19	0.00	0.00	0.00
TiO_2	0.08	0.19	0.00	0.03	1.74	0.00	0.02	52.64
B_2O_3	1.3	1.3	-	-	-	-	-	-
Al_2O_3	44.68	46.16	22.43	21.79	17.57	59.65	0.00	0.00
Cr_2O_3	0.00	0.00	0.00	0.00	0.00	1.15	0.00	0.00
FeO	7.58	8.69	26.00	32.42	10.72	21.27	0.19	45.71
ZnO	0.00	0.00	0.00	0.00	0.00	10.90	0.00	0.00
MnO	0.00	0.09	0.41	1.02	0.00	0.05	0.00	3.86
MgO	15.51	13.79	11.59	5.77	17.83	7.20	0.00	0.13
CaO	0.00	0.00	1.64	1.62	0.13	0.00	55.85	0.00
Na_2O	0.04	0.00	0.01	0.00	0.52	0.00	0.00	0.00
K_2O	0.00	0.00	0.00	0.00	8.99	0.00	0.00	0.00
P_2O_5	0.00	0.00	0.00	0.00	0.00	0.00	42.17	0.00
Cl	0.00	0.02	0.00	0.00	0.00	0.00	0.03	0.00
F	0.00	0.06	0.00	0.00	0.33	0.00	3.55	0.00
H_2O#	1.18	1.16	-	-	-	-	-	-
Total	100.13	100.30	101.62	100.67	95.88	100.22	100.31	102.34
oxygen	21.5		12		22	4	25	3
Si	3.648	3.629	2.968	2.985	5.509	0.000	0.000	0.000
Ti	0.008	0.018	0.000	0.002	0.189	0.000	0.003	0.974
B	0.285	0.282	-	-	-	-	-	-
Al^{IV}	1.067	1.089	0.032	0.015	2.491	-	-	-
Al^{VI}	5.614	5.752	1.953	1.997	0.497	1.956	0.000	0.000
Cr	0.000	0.000	0.000	0.000	0.000	0.025	0.000	0.000
Fe^{3+}	-	-	-	-	-	0.019	-	0.052
Fe^{2+}	0.804	0.914	1.632	2.129	1.293	0.476	0.027	0.889
Zn	0.000	0.000	0.000	0.000	0.000	0.224	0.000	0.000
Mn	0.000	0.010	0.026	0.068	0.000	0.001	0.000	0.080
Mg	2.932	2.584	1.296	0.675	3.833	0.299	0.000	0.005
Ca	0.000	0.000	0.132	0.136	0.020	0.000	10.021	0.000
Na	0.010	0.000	0.001	0.000	0.145	0.000	0.000	0.000
K	0.000	0.000	0.000	0.000	1.655	0.000	0.000	0.000
P	0.000	0.000	0.000	0.000	0.000	0.000	5.979	0.000
Cl	0.000	0.004	0.000	0.000	0.000	0.000	0.009	0.000
F	0.000	0.024	0.000	0.000	0.151	0.000	1.880	0.000
OH	1.000	0.972	-	-	-	-	-	-
Total	14.368	14.306	8.040	8.007	15.783	3.000	17.919	2.000
X_{Mg}	0.785	0.739	0.443	0.241	0.748	0.377	-	-

SO_3 below detection limit. Oxide-totals corrected for O≡Cl,F.
X_{Mg} = $Mg/(Mg+Fe_{Tot})$. Mineral abbreviations are after Kretz (1983).
Fe^{3+} in spinel and ilmenite calculated assuming perfect stochiometry.
H_2O calculated assuming 1 (OH,Cl,F) per formula unit for kornerupine.

H_2O in the 1600-1700 cm^{-1} and 3300-3700 cm^{-1} ranges (Visser, unpublished data). Recalculated oxide totals are close to 100 %, compatible with the estimated boron and calculated H_2O contents.

The homogeneous kornerupine, with a wide range in X_{Mg} = (Mg/(Mg+Fe_{Tot}) and Al of respectively 0.74-0.81 and 6.72-6.99, plots between 11:10:11 and 1:1:1 in terms of (Mg,Fe,Mn)O:Al_2O_3:SiO_2. There is no compositional difference between coarse and medium-grained kornerupines. Compositional variations between the analysed grains can be related by the tschermak substitution (Mg,Fe) + Si = Al^{VI} + Al^{IV} and possibly by the substitution B = Al^{IV}, or their combination i.e. (Mg,Fe) + Si = Al^{VI} + $(B,Al)^{IV}$ (Grew, 1988). Sodium and fluorine content are low but variable ($\leq$0.06 wt.% Na_2O, $\leq$0.15 wt.% F). The relatively high Ti content (0.08-0.19 wt.% TiO_2) is comparable to those in kornerupine occurrences reported in the literature (e.g. Grew et al., 1987a) in which the mineral occurs in close association associated with Ti-bearing phases.

Biotites have intermediate Al contents between 2.9 and 3.2 atoms per formula unit. TiO_2 contents (1.13-1.74 wt.%) are moderate to low. X_{Mg} varies between 0.75 and 0.78. Fluorine values are moderate (0.33-0.76 wt.% F), while Cl is below detection limit.

Garnet porphyroblasts are homogeneous except for a thin rim (100-150 μm) along their margins and along cracks. Core compositions have an average composition of $Prp_{42-43}Alm_{51-52}Grs_4Sps_1$ and X_{Mg} ranging 0.42-0.44. Rim compositions, typically $Prp_{22-23}Alm_{70-71}Grs_4Sps_3$, show an enrichment of Fe and Mn at the expense of Mg. The grossular component, 4-5 mol%, remains constant from core to rim. Cr was not detected.

The green **spinel** is an unzoned Zn-rich variety. Individual grains fall in the range $Ghn_{12-34}Hc_{44-58}Spl_{19-33}Mag_{1-3}$. Cr contents range 0.00-1.45 wt.% Cr_2O_3, with Cr_2O_3 typically between 1.0-1.3 wt.% in most analysed grains. Very high Cr_2O_3 contents (3.67-17.98 wt.%) were found in strongly resorbed blebs in the altered parts of the spinel. High Cr contents are accompanied by lower Mg-, higher Fe- and variable Zn contents. The presence of Cr-bearing spinel is in accordance with the presence of Cr-rich staurolite and Cr-bearing rutile in other samples of the locality (Visser & Senior, 1990). Minor amounts of Cu ($\leq$0.68 wt.% CuO) are detected in grains which contain chalcopyrite as a retrograde phase. The zincian spinels plot in the compositional field of spinels from aluminous metasediments (Fig. 3.9).

Apatite inclusions in garnet, biotite and within the kornerupine breakdown aggregates are essentially fluorapatites (2.82-4.14 wt.% F). Chlorine ($\leq$0.15 wt.%) and sulphur contents ($\leq$0.20 wt.% SO_3) are at the detection limit. **Ilmenites** enclosed in garnet cores and rims contain 3.74-3.87 wt.% MnO and $\leq$0.23 wt.% MgO. Calculated hematite component ranges 2.6-3.6 mol.%. Large **corundum** mantled by kornerupine contains $\leq$0.30 wt.% Fe_2O_3.

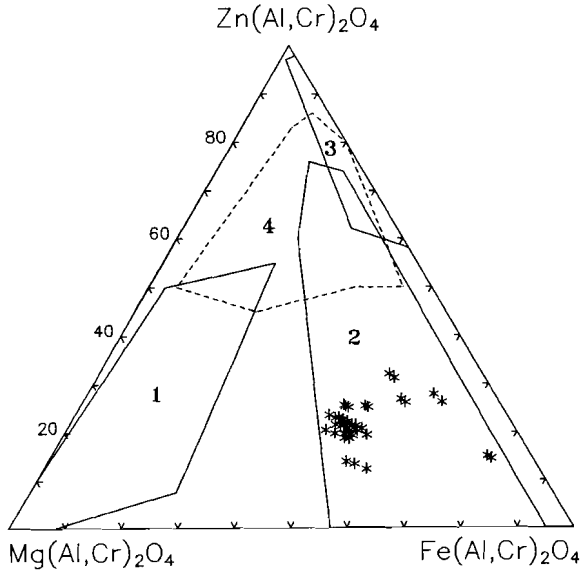

Figure 3.9. Ternary plot of spinel compositions (*) in sample DV250 shown relative to the compositional fields 1-4 of Spry and Scott (1986) representing Zn-bearing spinel from marbles (1), aluminous metasediments (2) and pegmatites (3) and metamorphosed massive sulphide deposits (4).

Secondary assemblages after kornerupine (Table 3.3)

Chlorites after kornerupine are clinochlores ($d_{001} \approx 14.0$ Å) with Al^{IV} and X_{Mg} ranging 2.66-2.99 and 0.76-0.80 respectively. Both Al^{IV} and Al^{VI} are higher in chlorites adjacent to corundum (2.86-2.99 and 2.78-2.99 respectively) than in those adjacent to andalusite (2.66-2.87 and 2.55-2.74). X_{Mg} does not vary systematically with the mineral association. Fluorine is high (0.15-0.37 wt.% F) in chlorites that are situated along previous kornerupine-biotite contacts. The F-content is below detection limit in chlorites located in the centre of the kornerupine grains or along former kornerupine-garnet and kornerupine-spinel contacts.

Electron microprobe analyses of **tourmaline** were calculated on the basis of 24.5 oxygens consistent, with the general formula $XY_3Z_6(BO_3)_3Si_6O_{18}(OH,O,F,Cl)_4$, the assumption of 3 atoms B per formula, and full occupancy of the OH-O-F-Cl site by OH and measured F, Cl.

The tourmalines are unzoned aluminous dravites with X_{Mg} of 0.83-0.87 and Na/(Na+Ca) of 0.60-0.70. The Na-content is fairly constant in all analysed grains (1.51-1.78 wt.% Na_2O), whereas Ca (1.16-1.90 wt.% CaO) varies from grain to grain. Ti-contents are moderate to high (0.27-1.44 wt.% TiO_2), with the higher values obtained

Table 3.3.
Representative analyses of the kornerupine breakdown products in sample DV250.

	Trm		Chl		Crn	And
spot	2/139 with Crn	2/144 with And	2/154 with And	2/152 with Crn	2/134	2/129
SiO_2	36.05	35.77	27.04	25.35	0.00	36.20
TiO_2	0.37	0.53	0.07	0.03	0.07	0.03
Al_2O_3	33.92	34.03	23.24	25.49	99.69	62.90
Fe_2O_3	-	-	-	-	0.18	0.56
FeO	3.14	3.13	12.02	11.76	-	-
MnO	0.00	0.00	0.00	0.01	0.00	0.00
MgO	9.38	9.30	24.37	23.71	0.00	0.00
CaO	1.50	1.83	0.00	0.00	0.00	0.00
Na_2O	1.59	1.51	0.03	0.00	0.00	0.00
K_2O	0.00	0.00	0.00	0.17	0.00	0.00
SO_3	0.17	0.00	0.00	0.00	0.00	0.00
Cl	0.00	0.00	0.04	0.03	0.00	0.00
F	0.00	0.46	0.15	0.00	0.00	0.00
Total	86.12	86.56	87.25	86.54	99.92	99.63
O-basis	24.5		28		3	5
Si	5.781	5.724	5.333	5.030	0.000	0.983
Ti	0.044	0.063	0.010	0.006	0.001	0.001
Al^{IV}	0.219	0.276	2.667	2.970	-	-
Al^{VI}	6.191	6.138	2.736	2.990	1.997	2.014
Fe^{3+}	-	-	-	-	0.002	0.011
Fe^{2+}	0.420	0.423	1.983	1.955	-	-
Mn	0.000	0.000	0.000	0.000	0.000	0.000
Mg	2.245	2.221	7.166	7.009	0.000	0.000
Ca	0.260	0.317	0.000	0.000	0.000	0.000
Na	0.501	0.462	0.011	0.000	0.000	0.000
K	0.000	0.000	0.000	0.048	0.000	0.000
S	0.039	0.000	0.000	0.000	0.000	0.000
Cl	0.000	0.000	0.013	0.012	0.000	0.000
F	0.000	0.231	0.094	0.000	0.000	0.000
Total	15.700	15.855	20.013	20.020	2.001	3.009
X_{Mg}	0.841	0.840	0.783	0.782	-	-

Cr_2O_3, ZnO, and P_2O_5 below detection limit.
Oxide totals corrected for O≡Cl,F.

in tourmalines occurring adjacent to ilmenite and rutile. Si and Al are highly variable but show no correlation with the presence of corundum or andalusite in the intergrowths. The fluorine-content has the same textural control as with chlorite. Higher fluorine contents (0.17-0.50 wt.% F) are recorded near biotites, whereas lower values ($\leq$0.10 wt.%) are recorded in the centre of the kornerupine grains and near spinel or garnet.

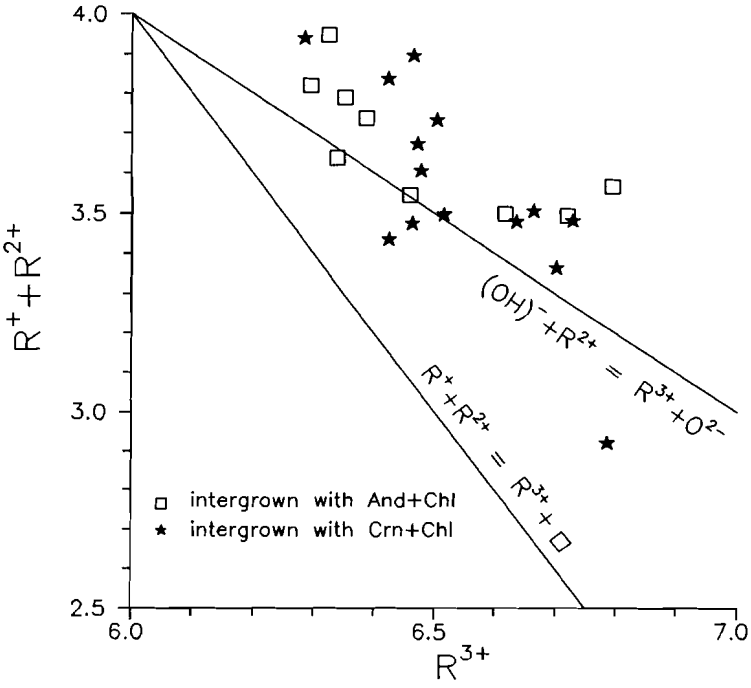

Figure 3.10. Alkali-defect versus proton-loss substitution in the Böylefossbru tourmalines, with R^{3+} = $(Al^{3+} + 4/3Ti^{4+})$ and $(R^+ + R^{2+})$ = $(Na^+ + 2Ca^{2+} + K^+ + Fe^{2+} + Mg^{2+} + Mn^{2+})$.

The calculated formulae show that there is a deficiency in the X and Y sites. Al_{Tot} shows a good negative correlation with Mg and Fe. Substitution of Al for Mg and Fe at the Y site requires a compensation of the charge imbalance. This may involve both the proton-loss or dehydroxylation and the alkali-defect coupled substitutions (Foit & Rosenberg, 1977)

$$OH^- + Y^{2+} = O^{2-} + Y^{3+} \text{ and } X^+ + Y^{2+} = \square + Y^{3+}.$$

Low whole rock Li content (Li = 14 ppm) and Li-partitioning data from the literature (Li/Fe ratio follows Krn>>Bt>Tur,Grt; Grew et al., 1990) indicate that substitutions involving Li are of minor significance. In Fig. 3.10, the effect of the proton-loss and alkali-defect coupled substitutions is illustrated. It can be seen that the Böylefossbru

tourmalines are dominated by the proton-loss substitution. This indicates that tourmaline probably formed in an environment which was more buffered with respect to alkalies than H_2O. Tourmalines plot in the fields of metapelites and metapsammites with an Al-saturating phase and low-Ca metaultramafics and Cr, V-rich metasediments (Henry & Guidotti, 1985).

The presence of **andalusite** as an alteration product of kornerupine was verified by XRD analysis. The analyses show 0.34-1.04 wt.% Fe_2O_3 and trace amounts of MgO and TiO_2. **Corundum** contains $\leq$0.74 wt.% Fe_2O_3 and trace amounts of MnO and Cr_2O_3. **Hematite** is Fe_2O_3 with only trace amounts of Mg and Mn.

Other secondary phases (Table 3.4)

Carbonate lensoids intergrown with biotite and rutile are pure calcite (e.g. $Ca_{0.99}Mg_{0.01}CO_3$), whereas those intergrown with gahnite are variably calcite, dolomite/ankerite ($Ca_{0.48\text{-}0.51}Mg_{0.32\text{-}0.44}Fe_{0.08\text{-}0.17}$ CO_3) or siderite ($Ca_{0.01}Mg_{0.02\text{-}0.04}Fe_{0.94\text{-}0.99}CO_3$). Only traces of Mn were detected. Minor amounts of **chalcopyrite** and **pyrite** are intergrown with carbonate, chlorite and corundum in the altered parts of the Cu-bearing spinels. Chalcopyrite may show traces of Mg and Zn, while pyrite contains traces of Zn and Cu **Chlorites** after spinel contain up to 0.65 wt.% ZnO. X_{Mg} (0.77-0.78), Al^{IV} (2.70-2.84) and Al^{VI} (2.70-2.74) are similar to chlorites associated with tourmaline and andalusite. Chlorite after garnet is relatively magnesian (X_{Mg} = 0.79-0.80) with low total Al (5.15-5.18). Fluorine is below detection limit. **Corundum** after spinel contains $\leq$0.55 wt.% ZnO and $\leq$0.67 wt.% Fe_2O_3 as the only significant impurities. Cr_2O_3 was not detected. One analysis of **ilmenite** which developed between rutile and spinel shows lower Mn (1.07 wt.% MnO) and hematite component (1.2 mol.%) compared to the primary ilmenites enclosed in garnet.

Table 3.4.
Representative analyses of other retrograde phases

spot	Chl 3/49 after Grt	Chl 4/17 after Spl	Spl# 4/36	Ilm* 3/46
SiO_2	27.24	25.89	0.00	0.00
TiO_2	0.07	0.00	0.00	52.61
Al_2O_3	22.23	24.19	40.13	0.00
Cr_2O_3	0.00	0.00	17.98	0.00
FeO	12.19	11.89	31.03	46.76
ZnO	0.00	0.22	6.50	0.00
MnO	0.00	0.00	0.09	1.07
MgO	25.49	24.26	1.64	0.32
CuO	0.00	0.00	0.45	0.00
CaO	0.00	0.10	0.00	0.00
Total	87.23	87.24	97.82	100.76
O-basis	28	28	4	3
Si	5.368	5.144	0.000	0.000
Ti	0.000	0.000	0.000	0.988
Al	5.164	5.665	1.492	0.000
Cr	0.000	0.000	0.448	0.000
Fe^{3+}	-	-	0.060	0.023
Fe^{2+}	2.009	1.976	0.758	0.954
Zn	0.000	0.032	0.151	0.000
Mn	0.000	0.000	0.002	0.023
Mg	7.488	7.185	0.077	0.012
Cu	0.000	0.000	0.011	0.000
Ca	0.000	0.021	0.000	0.000
Total	20.040	20.024	3.000	2.000
X_{Mg}	0.788	0.784	-	-

Na_2O, K_2O, SO_3, P_2O_5, F and Cl not detected
- most Cr-rich strongly resorbed spinel bleb
* - reaction rim between spinel and rutile

DISCUSSION

Protolith composition

The three analysed samples have whole rock compositions compatible with an original protolith composed of quartz + chlorite + illite (muscovite) mixtures (Fig. 3.11). The intermediate MgO/FeO ratios, the close association with garnet-amphibolites and the heterogeneous nature of the lens strongly favour a chloritic protolith formed through hydrothermal alteration or weathering of rocks of volcanogenic origin (Moine et al., 1981; Reinhardt, 1987). The low SiO_2 and relatively high Cr, Ni and Sc contents may point to a mafic precursor.

Comparison with the major oxides, trace and REE elements of two amphibolite samples taken a few kilometers south along the strike (Table 3.1, samples TN142 and TN143, Nijland & Visser, in prep.) and other amphibolites in the Froland-Arendal area (Nijland & Visser, in prep) shows that SiO_2 (DV250 only), CaO, Sr and Na_2O are strongly depleted, while MgO is strongly enriched in the three Böylefossbru rocks. Sample DV250 also shows a relative enrichment of total iron, K_2O, TiO_2, Co, Zn, Cu and Zr. SiO_2, TiO_2, total iron, K_2O in samples DV029 and DV037, and Al_2O_3, P_2O_5, MnO and most trace elements in all three samples are comparable. Compared with the REE data of samples TN142 and TN143 (Fig. 3.8), samples DV037 and DV250 show a mild depletion of LREE and a strong enrichment of HREE. The REE pattern of DV029 deviates significantly in that both LREE and HREE are strongly to mildly depleted.

Depletion of LREE, Eu (negative Europium anomaly), Na, Ca and Sr together with a strong enrichment of Mg and variable behaviour of SiO_2 are considered to be characteristic for a low-grade hydrothermal alteration of either felsic or mafic volcanic rocks by heated seawater at high water/rock ratios (e.g. Lamb, 1981; Baker & de Groot, 1983; Windrim et al., 1984 and Dymek & Smith, 1990). The enrichment of HREE in DV037 and DV250 is suggested to reflect the high model chlorite content in these samples (Fig. 3.11), consistent with the trace element data presented for hydrothermal chlorite (Baker & de Groot, 1983), which show that relative to the whole rock chlorite is enriched in Cr, Zn and HREEs. However, the large HREE depletion and the low Zr content in DV029, which has a higher model chlorite content than DV037, indicate that control of the HREE abundances by the HREE-carrier zircon is also important.

The relative enrichment of FeO_{tot}, Zn, Co and Cu in DV250, exemplified by the presence of spinel-rich and ilmenite-apatite-rich bands, and the small sulphidic fahlbands (see Gammon, 1966 for full definition) in the surrounding gneisses indicate that the hydrothermal fluids were potentially ore forming. Though barren at the Böylefossbru locality, two nearby small abandoned copper mines situated in a large fahlband at

Böylestad and Skyttemyr (Bugge, 1978; Fig. 3.1) indicate that ore formation was effective on a small scale in this part of the Bamble Sector.

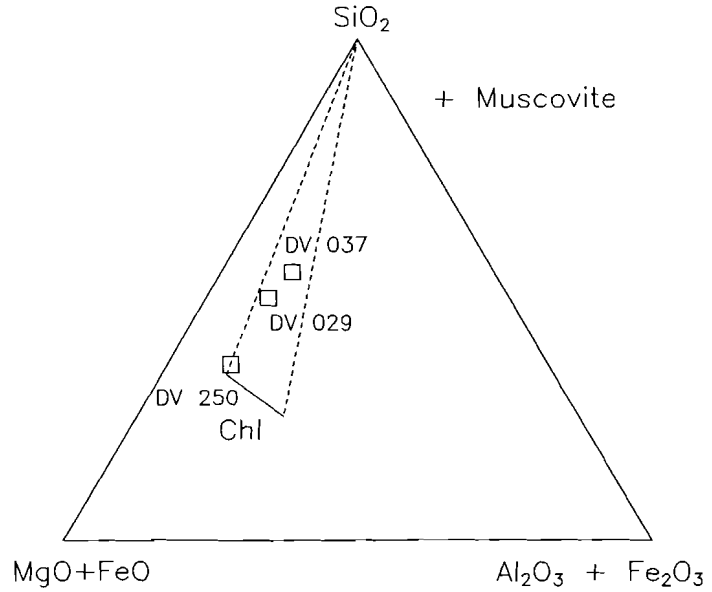

Figure 3.11. Bulk compositions projected from muscovite (illite) into the (MgO+FeO)-(Al_2O_3+Fe_2O_3)-SiO_2 triangle. Note that the analyses project in the field chlorite+quartz, suggesting that the compositions can be resolved into chlorite, quartz and illite.

Formation of kornerupine

The textural relations suggest an early stable assemblage consisting of biotite-spinel-ilmenite-rutile-apatite±corundum, in a banded appearance with spinel-rich and ilmenite-apatite-rich layers. Kornerupine reaction rims developed mainly around spinel but also around large corundum, ilmenite and rutile grains. The reaction between spinel and biotite may be written as a hydration reaction and involves the introduction of large amounts of silica:

$$\underset{\text{biotite}}{0.03\ K_{1.7}Na_{0.1}(Mg,Fe)_{5.2}Ti_{0.2}Al_{3.0}Si_{5.5}O_{20}(OH)_4} + \underset{\text{spinel}}{3.35\ (Mg,Fe)Al_2O_4} +$$
$$0.15\ B_2O_3 + 0.44\ H_2O + 3.54\ SiO_{2(aq)} \longrightarrow$$

$$\underset{\text{kornerupine}}{(Mg,Fe)_{3.5}Ti_{0.01}Al_{6.8}Si_{3.7}B_{0.3}O_{21}(OH)} + 0.03\ K_2O_{aq}. \quad (1)$$

The reaction involving corundum which may occur within the same band as reaction 1, however, can be written as a dehydration reaction with no addition of silica:

$$0.67\ \underset{\text{biotite}}{K_{1.7}Na_{0.1}(Mg,Fe)_{5.2}Ti_{0.2}Al_{3.0}Si_{5.5}O_{20}(OH)_4} + 2.40\ \underset{\text{corundum}}{Al_2O_3} + 0.15\ B_2O_3 \longrightarrow$$

$$\underset{\text{kornerupine}}{(Mg,Fe)_{3.5}Ti_{0.01}Al_{6.8}Si_{3.7}B_{0.3}O_{21}(OH)} + 0.02\ SiO_{2(aq)} + 0.84\ H_2O +$$

$$0.57\ K_2O_{aq} + 0.03\ Na_2O_{aq}. \quad (2)$$

Both reactions, however, raise more questions than they solve. Firstly, there is a contradicting behaviour of silica and H_2O within the same band. Secondly, both reactions do not explain the large kornerupine grains devoid of spinel and corundum and the kornerupine growth around ilmenite and rutile.

An alternative possibility is the contribution of the shift in biotite composition along the tschermak vector, $Al_2Mg_{-1}Si_{-1}$, (Thompson, 1982), as proposed by Waters (1986), to account for sapphirine rims on spinel in similar rocks from Namaqualand, South Africa. For sample DV250 this can be written as:

$$\text{(spinel, corundum, ilmenite, rutile)} + \text{biotite} + Al_2Mg_{-1}Si_{-1}\ \text{(in biotite)} + B_2O_3 \longrightarrow$$

$$\text{kornerupine} + K_2O_{aq} + H_2O \quad (3)$$

with biotite becoming less Al-rich. The reaction reduces the silica requirement in reaction 1 and gives a good explanation for the kornerupine growth around ilmenite and rutile. Both ilmenite and rutile grains must have acted as seeds for kornerupine to develop on. A change of about 0.02-0.08 atoms per mole in the Al content of biotite, assuming a volume of biotite of about 80 vol.% of the rock prior to the development of kornerupine, would already generate the observed amount of kornerupine (1-5 vol.%). Reaction 3 is a dehydration and should involve an increase in temperature to proceed.

Comparison of the textures in DV250 with other samples (DV029, DV030, DV036 and DV037) in the outcrop indicates a similar sequence of mineral-growth and deformation:

1) Reactions involving the formation of cordierite (M_{3a}) demonstrate a decompression phase, accompanied by a possible increase temperature, during the prograde P-T trajectory at 6-8 kbar and 630-720 °C (Fig. 3.12), before the maximum temperature was reached.

2) Orthoamphibole, biotite and M_{3a}-cordierite are deformed during a second deformation phase (D2 event of Starmer, 1985 and Nijland & Senior, 1991) and subsequently overgrown during M_{3b} by large euhedral non-foliated garnet porphyroblasts (Fig. 3.2). Biotite, spinel and kornerupine in DV250 are likewise deformed and overgrown by large euhedral non-foliated garnet porphyroblasts.

3) M_{3b} peak-metamorphic conditions are estimated from the Fe-Mg partitioning between garnet-biotite and garnet-cordierite in the samples DV030 and DV036 at 740 ± 60 °C at 7 kbar (Visser & Senior, 1990). Temperature estimates for the formation or equilibration of garnet in sample DV250, based on the garnet-biotite Fe-Mg exchange reaction (Ferry & Spear, 1978) are very similar. Biotite(matrix)-garnet(core) and biotite(inclusion)-garnet(core) pairs fall in the range 698-753 °C at 7 kbar.

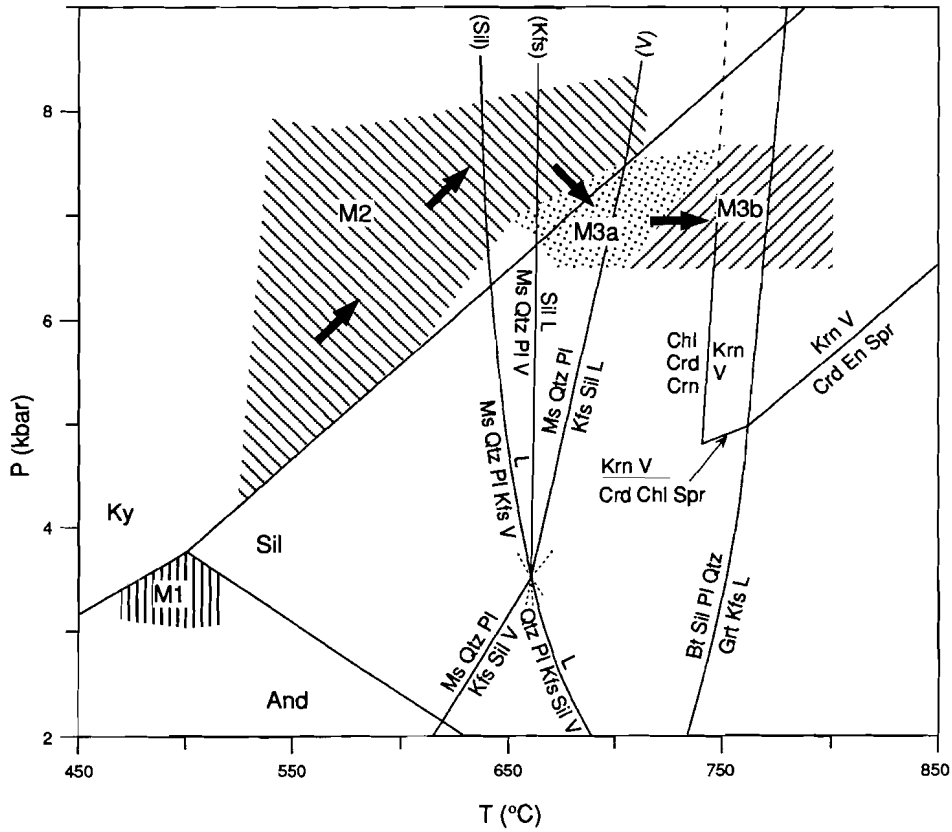

Figure 3.12. P-T diagram illustrating the conditions of the successive metamorphic stages M_1, M_2, M_{3a} and M_{3b} and the inferred prograde P-T path (Visser and Senior 1990) in relation with the dehydration (melting) reactions of muscovite (Thompson, 1982) and biotite. The dehydration melting curve for biotite, Bt + Sil + Pl + Qtz = Grt + Kfs + L, is given for biotite with X_{Mg} = 0.56 (Le Breton and Thompson 1988). The grid for boron-free kornerupine in the MASH system (Seifert 1975) is given for comparison. Aluminium silicate relations are from Holdaway (1971).

The dehydration reaction 3 and the sequence given above situate the formation of kornerupine during or shortly after M_{3a} and before peak metamorphic conditions are reached. The inferred P-T conditions lie on the low temperature side of the stability field of boron-free Mg-kornerupine as determined by Seifert (1975) (Fig. 3.12). Incorporation of boron and iron, however, is expected to extend the range of kornerupine stability significantly to lower temperatures. In view of this it is worthwhile to note the previously reported association andalusite-kornerupine from Canada (Girault, 1952) and Madagascar (Grew et al., 1990).

Boron source

The kornerupine-forming reaction 3 requires significant amounts of boron, originating either from within or outside the immediate rock volume. The model chlorite-illite precursor composition of DV250 (Fig. 3.11) indicates that boron, which shows a strong association with illite (Harder, 1959), could have been present in the system prior to metamorphism. The main reactants, biotite and spinel, generally contain only trace amounts of boron (e.g. 0.4-6 ppm B, Shaw et al., 1988; 0-0.009 wt.% B_2O_3, Grew et al., 1990) and are not regarded possible sources of B. Furthermore, there is no evidence for other possible boron-bearing precursor minerals (e.g. tourmaline, plagioclase and muscovite) within sample DV250 and in other samples from the outcrop. This suggests either that original boron-levels were low or that boron was lost upon breakdown of illite during the earlier stages of metamorphism. It is, therefore, suggested that kornerupine crystallised due to introduction of boron-bearing fluids from outside the lens.

The surrounding polyphase migmatitic biotite-sillimanite-K-feldspar-plagioclase-(muscovite)±garnet metapelites (Fig. 3.1), are a very likely source for these boron-bearing fluids. The garnet-amphibolites are thought to have played no major role. Fluids released by the metapelites have to involve the breakdown of a boron-bearing hydrous phase like muscovite or tourmaline. Muscovite is reported to contain boron usually in the 1-100 ppm range in granites, marbles and schists and higher values of up to 480 ppm B in pegmatites (e.g. Harder, 1959; Sauerer & Troll, 1990; Bebout et al., 1990; Sisson & Pu, 1991). The alternative source, tourmaline, is not observed in the migmatites. Furthermore, breakdown of tourmaline occurs at much higher temperatures (>800 °C; e.g. Werding & Schreyer, 1984; Manning & Pichavant, 1983) than encountered at the Böylefossbru locality.

The migmatitic gneisses give evidence for at least two periods of deformation and migmatisation. The sequence of events is similar to that recorded for the Kongsbergian MIG 1 and MIG 2 migmatisation events from Krossvatnet, 8km NNE of the Böylefossbru locality (Nijland & Senior, 1991; Nijland, personal communication, 1992). MIG 1

stromatic leucosomes, containing quartz, plagioclase and K-feldspar (micro- to mesoperthitic) and large muscovite, interpreted to result from partial melting, have formed *in situ* between the D1 and D2 deformation phases. MIG 2 leucosomes are considered to have formed synkinematically during the D2 deformation phase. Gupta & Johannes (1982) performed melting experiments at P_{H_2O} = 5 kbar on the leucosomes and adjacent mesosomes of two stromatic migmatite samples from Krossvatnet yielding solidus temperatures of 640 $\pm$ 7 °C for both leucosomes and mesosomes. Johannes (1988) interpreted this to be the result of a small pre-migmatitic compositional difference between layers in the parent rock, now represented by the leucosome (neosome) and mesosome layers, and selective mineralogically controlled access of water.

The relatively small amount of generated melt (20-25 vol.%) in the biotite-sillimanite-K-feldspar-plagioclase-(muscovite) gneisses of the Böylefossbru area, indicates that melting was controlled by the dehydration of minerals such as muscovite and biotite. The absence of prograde muscovite in gneisses with suitable composition, and the proximity of the muscovite-out isograd (Fig. 3.1) suggests that initial melting started with the dehydration of muscovite. Depending on the composition of the different layers dehydration melting of muscovite starts at the end of M_2 and continues during M_{3a} (see Fig. 3.12 for possible muscovite dehydration melting curves). The sparse appearance of garnet in the leucosomes suggests that, at the Böylefossbru locality, the amount of melt contributed to the leucosomes by dehydration melting of biotite was minimal. In the adjacent quartz-biotite-plagioclase gneiss-units garnet is an abundant phase in the leucosomes. Considering the minimum temperature conditions for dehydration of biotite with intermediate X_{Mg}, which lie at about 760 °C at 7 kbar (Le Breton & Thompson, 1988; Fig. 3.12), the development of garnet in these leucosomes probably took place at peak-metamorphic M_{3b}-conditions.

The development of kornerupine, during or shortly after M_{3a}, has to involve a migration of the B-bearing fluids from adjacent or nearby layers. The involvement of a melt is considered unlikely since most melts developed *in situ*. Obviously, the fluids released by the breakdown of B-bearing muscovite must have formed in layers of inappropriate composition to start dehydration melting at these conditions (e.g. only plagioclase and quartz), as melts provide a prefect sink for H_2O and boron. The relatively permeable biotite-spinel schist may have acted as a pathway for the fluids. Interaction of the fluid with biotite and spinel, corundum, ilmenite and rutile subsequently fixed the boron in kornerupine.

Retrogradation of kornerupine

Kornerupine was retrograded along fractures and cleavages and produced a wide variety of breakdown assemblages (Fig. 3.13). The assemblage tourmaline-chlorite-corundum developed between kornerupine and spinel and can be explained by the reaction:

$$\underset{\text{kornerupine}}{(Mg,Fe)_{3.5}Al_{6.8}Si_{3.7}B_{0.3}O_{21}(OH)} + 2.34\ \underset{\text{spinel}}{(Mg,Fe)Al_2O_4} + 0.05\ Na_2O_{aq} + 0.03\ CaO_{aq} + 4.66\ H_2O \longrightarrow$$

$$0.1\ \underset{\text{tourmaline}}{Na_{0.5}Ca_{0.3}(Mg,Fe)_{2.55}Al_{6.6}Si_{5.75}B_3O_{27}(OH)_4} + 0.62\ \underset{\text{chlorite}}{(Mg,Fe)_{9.0}Al_{2.99}[Al_{2.97}Si_{5.03}]O_{20}(OH)_{16}} + 3.56\ \underset{\text{corundum}}{Al_2O_3}. \quad (4)$$

The succession of phases along the fractures in the large kornerupines, tourmaline + chlorite + andalusite close to the margin and adjacent to altered biotite, and tourmaline + chlorite + corundum ± hematite occupying the centre, suggests that kornerupine first reacted with the infiltrating fluid according to the reaction:

$$\underset{\text{kornerupine}}{(Mg,Fe)_{3.5}Al_{6.8}Si_{3.7}B_{0.3}O_{21}(OH)} + 0.86\ SiO_{2(aq)} + 0.05\ Na_2O_{aq} + 0.03\ CaO_{aq} + 2.5\ H_2O \longrightarrow$$

$$0.1\ \underset{\text{tourmaline}}{Na_{0.5}Ca_{0.3}(Mg,Fe)_{2.55}Al_{6.6}Si_{5.75}B_3O_{27}(OH)_4} + 0.35\ \underset{\text{chlorite}}{(Mg,Fe)_{9.2}Al_{2.75}[Al_{2.67}Si_{5.33}]O_{20}(OH)_{16}} + 2.12\ \underset{\text{andalusite}}{Al_2SiO_5}. \quad (5)$$

The removal of silica from the fluid phase in this reaction with kornerupine lowered the silica activity, $aSiO_2$, of the remaining fluid, thus leading to the formation of corundum and an observed increase of Al^{IV} and Al^{VI} in chlorite in the centre of the kornerupine. The calculated corundum-forming reaction (excluding trace amounts of hematite),

$$(Mg,Fe)_{3.5}Al_{6.8}Si_{3.7}B_{0.3}O_{21}(OH) + 0.45\ B_2O_3 +$$
kornerupine
$$2.50\ H_2O + 0.2\ Na_2O_{aq} + 0.12\ CaO_{aq} \longrightarrow$$

$$0.40\ Na_{0.5}Ca_{0.3}(Mg,Fe)_{2.55}Al_{6.6}Si_{5.75}B_3O_{27}(OH)_4 +$$
tourmaline
$$0.275\ (Mg,Fe)_{9.0}Al_{2.99}[Al_{2.97}Si_{5.03}]O_{20}(OH)_{16} + 1.26\ Al_2O_3 \quad (6)$$
chlorite corundum

is balanced on the components (FeO+MgO), Al_2O_3 and SiO_2, and seems to require the introduction of boron. However, this boron may well have originated from the non-isochemical chlorite replacements along the kornerupine cleavage planes.

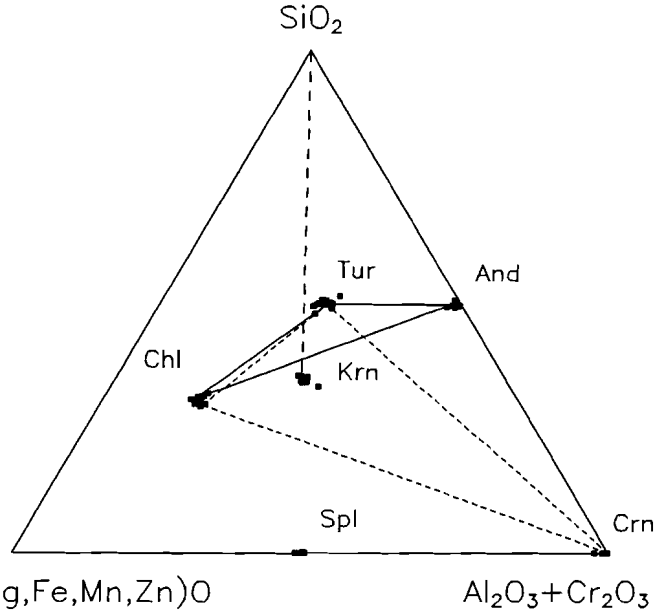

Figure 3.13. (Mg,Fe,Mn,Zn)O-Al_2O_3-SiO_2 diagram illustrating the relations between kornerupine and its breakdown products.

Reactions 4-6 are considered open to Na and Ca, species which are present in tourmaline. Possible sources for Ca are the release of Ca upon the breakdown of garnet to chlorite and muscovite and the numerous late carbonate intergrowths with biotite and spinel.

The relatively constant Na content of the tourmaline and the dominance of the proton-loss substitution may suggest that Na was buffered on the scale of a thin section. However, evidence for local variation in alkali content of the fluid is provided by the

development of dumortierite and chlorite after kornerupine due to

$$\text{kornerupine} + \text{quartz} \longrightarrow \text{dumortierite} + \text{chlorite}. \quad (7)$$

Dumortierite is stabilised relative to tourmaline at lower Na^+ and Ca^{2+} concentrations in the fluid (Visser & Senior, 1991). Trace amounts of Na are released by the kornerupine itself, while the bulk of the Na is supplied by the release of the Na-component in biotite. Retrogradation of biotite to chlorite suggests the generalised reaction:

$$\text{biotite} + \text{water} \longrightarrow \text{chlorite} + \text{quartz} + K_2O_{aq} + Na_2O_{aq}. \quad (8)$$

The fluorine levels in tourmaline and chlorite show a clear textural relation with F-bearing biotite suggesting that quartz released by reaction 8 in adjacent biotite is used in reaction 5. The combined net generalised reaction can be written as:

$$\text{kornerupine} + \text{biotite} + H_2O + CaO_{aq} \longrightarrow$$
$$\text{chlorite} + \text{tourmaline} + \text{andalusite} + K_2O_{aq}. \quad (9)$$

P-T conditions of retrogradation and fluid composition

The presence of andalusite places an important pressure constraint of $P \leq 4$ kbar (Holdaway, 1971) on the P-T conditions of reactions 4-9. Temperatures are best estimated with the garnet-chlorite-quartz Fe-Mg exchange geothermometer (Grambling, 1990). Six garnet(rim)-chlorite pairs yield temperatures of 411-440 °C at 4 kbar. Temperatures calculated for twelve pairs of garnet-rim and adjacent biotite, using the Ferry & Spear (1978) calibration, range 432-522 °C at a fixed pressure of 4 kbar. The temperature estimates above 500 °C obtained with the Ferry & Spear calibration are inconsistent with the kyanite-andalusite assemblage in other samples (see below) and probably reflect a partial "peak-metamorphic memory".

The retrograde fluid clearly is composed of an H_2O-CO_2 mixture, as exemplified by the hydrous nature of the alteration aggregates and the presence of the numerous carbonate intergrowths with biotite and spinel. The late M_4 cordierite breakdown assemblage kyanite-andalusite-chlorite-quartz in other samples from the outcrop likewise suggest $P_{H_2O} < P_{Total}$. Theoretical calculations with this reaction,

$$\text{cordierite} + H_2O \longrightarrow \text{kyanite/andalusite} + \text{chlorite} + \text{quartz} \quad (10),$$

indicate low partial water pressures in the fluid with $X_{H_2O} < 0.3$, assuming hydrous Mg-cordierite and clinochlore compositions (Fig. 3.14; Berman, 1988). The breakdown of the hercynite component in spinel:

$$\text{hercynite } (a_{hc} = 0.49) + CO_2 \longrightarrow \text{siderite} + \text{corundum} \quad (11)$$

in sample DV250 (see petrography section) indicates similar low X_{H_2O} and high X_{CO_2} (Fig. 3.14; Holland & Powell, 1990). The hercynite activity is calculated from the mineral data. Reactions 10 and 11 intersect with another spinel-breakdown reaction in DV250 (Figs. 3.4 and 3.14; Holland & Powell, 1990):

$$\text{hercynite } (a_{hc} = 0.49) + \text{rutile} \longrightarrow \text{ilmenite} + \text{corundum} \quad (12)$$

at about 450 °C, 3400 bar and complementary X_{H_2O} and X_{CO_2} (respectively 0.2 and 0.8). This could suggest that X_{H_2O} of the retrograde fluid does not vary within the outcrop. The activity of H_2O in the fluid is also calculated with the absolute chlorite-garnet water barometer (Grambling, 1990), but due to its sensitivity to errors in pressure, calculated X_{H_2O} should be handled with caution. Nevertheless, the calculated X_{H_2O}, 0.19-0.24 at 4 kbar and 0.31-0.39 at 3 kbar, are in good agreement to the value calculated from spinel equilibria.

The trace amounts of pyrite and chalcopyrite associated with spinel indicate that the retrograde fluid locally was sulphur-bearing. The kornerupine breakdown reactions suggest a closed system for boron in DV250, although the occurrence of tourmaline and dumortierite in cordierite-breakdown aggregates in other samples (Visser & Senior, 1991) indicates that some of the boron may have been introduced with the retrograde fluids.

Reactions 4 and 6 have previously been described from Fiskenæsset, West Greenland (reaction 6 only; Ackermand et al., 1984) and southern Madagascar (Ackermand et al., 1991). Both studies considered the chlorite-tourmaline-corundum breakdown assemblage produced by reaction 4 and 6 to be analogous to the isobaric low-temperature breakdown reactions Krn + Spr = Chl + Crn and Krn = Chl + Crd + Crn in the alkali and boron-free MASH system (Seifert, 1975). Ackermand et al. (1991) further suggested that both reactions proceed with either a decrease in temperature, or an increase in water- and Na_2O activities, or both. The present study indicates that all three causes may have operated simultaneously for these reactions. Tourmaline compositions in all three studies also indicate a concurrent increase of the Ca-activity in the fluid.

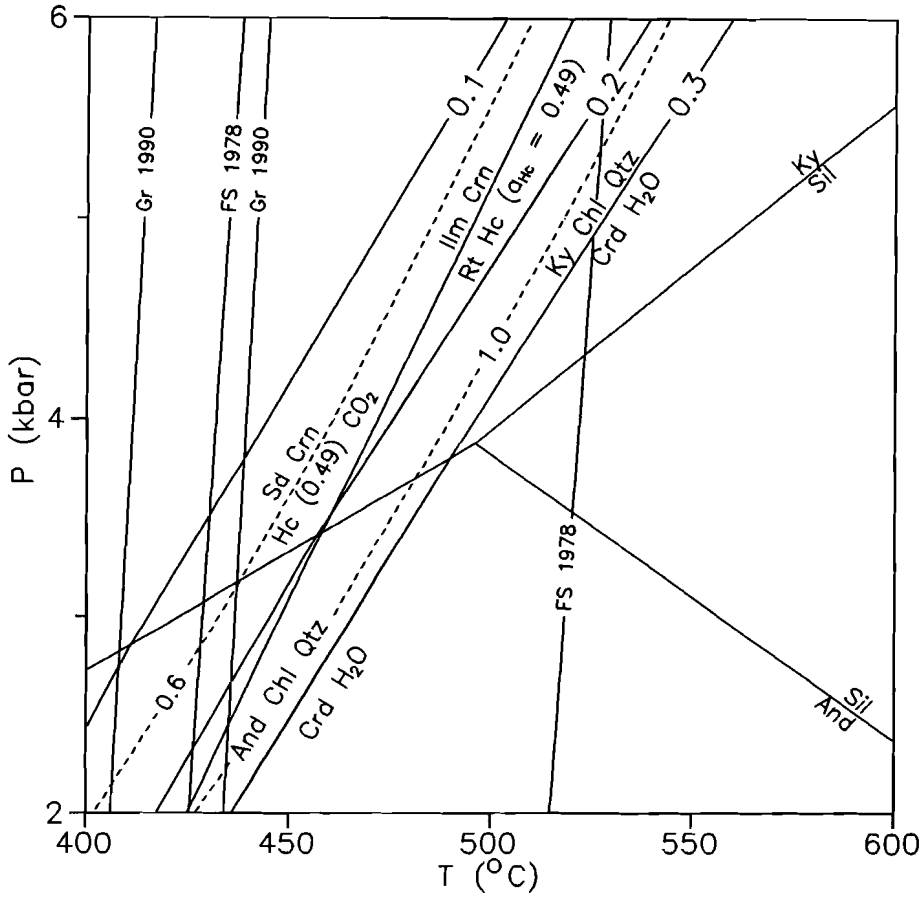

Figure 3.14. P-T diagram illustrating the conditions of retrogradation at the Böylefossbru area. Aluminium silicate relations are from Holdaway (1971). The cordierite breakdown reactions Crd + V = Ky + Chl + Qtz and Crd + V = And + Chl + Qtz (solid lines) are calculated at aH_2O of 0.1-0.3, using the thermodynamic dataset of Berman (1988). Reactions involving the breakdown of the hercynite component in spinel ($a_{hercynite}$ = 0.49) are calculated using the thermodynamic dataset of Holland and Powell (1990). The reaction Rt + Hc = Ilm + Crn (reaction 13; Figure 3.4) is shown as a solid line. The reaction Hc + CO_2 = Sid + Crn (reaction 12) is calculated at aCO_2 of 0.6 and 1.0 and shown as broken lines. Gr 1990 and FS 1978 indicate P-T conditions calculated with the Chl-Grt-Qtz thermometer of Grambling (1990) and the Bt-Grt thermometer of Ferry and Spear (1978).

As for the P-T location of reactions 4 and 6 at Fiskenæsset and Madagascar, Ackermand et al. (1984; 1991) only presented upper limits defined by the kornerupine-bearing peak-metamorphic assemblages of respectively 730 °C and 700 °C at about 7 kbar. At Böylefossbru the breakdown reactions are displaced to very low temperatures as a result of the low mole fraction of H_2O in the fluid phase. Ackermand et al. (1984) reported CO_2-rich fluid inclusions in kornerupine and corundum, and tentatively suggested

these to represent the composition of the peak-metamorphic fluid. Re-examination of the Fiskenæsset locality by Grew et al. (1987b), however, indicated that primary amphibole-bearing assemblages were not compatible with high X_{CO_2}. Alternatively they proposed a possible late entrapment for the CO_2-rich fluids. If so, this may suggest similar low-temperature conditions at Fiskenæsset during the breakdown of kornerupine.

Fluid source

The development of discordant quartz-cordierite ± garnet segregations (Visser and Senior, 1990) indicates a low aH_2O environment at high temperatures during the early stages of a period of isobaric cooling, which succeeded the peak-metamorphic M_{3b}-phase. This may suggest H_2O buffering by neighbouring melt-pockets. The maintenance of such low aH_2O conditions also will have prevented significant HT-regression of the peak-metamorphic assemblages at the Böylefossbru locality. Progressing with time, the melt pockets expel dominantly H_2O-rich fluids during *in situ* crystallisation of the melt. As long as crystallising or crystallised leucosomes remain unaffected by deformation the coexisting fluid will cause rehydration only within the leucosomes, as shown in a fluid inclusion study by Touret & Dietvorst (1983) of metapelites and metabasites in other parts of the Bamble Sector, and possibly in the neighbouring neosomes. In the MIG 1 and MIG 2 leucosomes part of the exsolved H_2O will be incorporated in muscovite (back reaction of muscovite dehydration reactions). A large amount of H_2O may have been consumed through the development of notable amounts of fine-grained muscovite in neighbouring neosomes. As a result the remaining fluid phase will progressively be impoverished in H_2O, leaving a CO_2-enriched residual fluid, that may become trapped in fluid inclusions in early crystallising minerals. Subsequent folding and mobilisation of this CO_2-rich residual fluid along layer-parallel shear zones during D6 (Starmer, 1985) probably triggered the retrogradation at the Böylefossbru locality.

The CO_2-component of the fluid may have been generated according to the prograde interaction with hydrous minerals and graphite to produce melt and CO_2 (Hollister, 1988; Whitney, 1992). Trace amounts of graphite are still present in the gneisses. Alternatively CO_2 could have been produced by decarbonation reactions in marbles and carbonate-bearing lithologies. A magmatic derivation for CO_2 in the Bamble area was suggested by Touret (1985), who described abundant CO_2-rich inclusions in basic intrusives and in enderbitic gneisses within the granulite facies area of Tromöy, near Arendal. Both alternatives, however, are considered unlikely as marbles and calc-silicate rocks are not interlayered at the locality or along the strike, while only one small meter-sized meta-gabbro lens is discovered about 200 meters NE from the outcrop (not indicated in Fig. 3.1).

CONCLUSIONS

Field relations, the major-, trace- and rare-earth element geochemistry of the Böylefossbru kornerupine-biotite-spinel-garnet schist and gedrite-cordierite-biotite ± garnet rocks suggest that the possible precursors are composed of chlorite-quartz-illite mixtures, which may have been formed by low-grade hydrothermal alteration of mafic volcanic rocks by heated seawater at high water/rock ratios.

Textural evidence is given for the prograde formation of an Al-rich kornerupine corona between Zn-rich spinel, corundum, ilmenite and rutile and biotite at the Böylefossbru locality during or shortly after M_{3a} decompression (Visser & Senior, 1990) at estimated P-T conditions of about 6-8 kbar and 630-720 °C (Fig. 3.12). Boron is considered to not have been present in the sample and other samples from the lens prior to kornerupine formation. Kornerupine apparently formed by the interaction of the relatively permeable spinel-biotite schist with an externally derived boron-bearing fluid. The sequence of deformation and migmatisation in adjacent biotite-sillimanite-K-feldspar-plagioclase-(muscovite) ± garnet, graphite gneisses, which is similar to the sequence of events recorded by Nijland & Senior (1991), suggests that this fluid is likely to have been generated by dehydration of boron-bearing muscovite. Dehydration melting of biotite is considered to have been of limited importance at the Böylefossbru locality.

P-T conditions of garnet porphyroblast overgrowths are estimated at 7 kbar and 698-753 °C in agreement with previous reported peak metamorphic M_{3b} conditions (Visser & Senior, 1990).

Kornerupine breakdown proceeded at 3-4 kbar and 411-500 °C producing the assemblages tourmaline-andalusite-chlorite, tourmaline-chlorite-corundum ± hematite and dumortierite-chlorite. The breakdown textures and mineral compositions suggest that chloritisation of adjacent F-bearing biotite partially governed the silica activity and F-content of the fluid phase. The retrograde fluid is calculated to be CO_2-rich with X_{CO_2} of 0.7-0.8. Residual fluids mobilised from solidified leucosomes during D6 deformation may have had the appropriate CO_2-rich composition because much of the H_2O in the leucosomes was consumed during the crystallization of muscovite.

ACKNOWLEDGEMENTS

R. Poorter and T. Bouten are thanked for assistance with the microprobe analyses, T. Zalm with cathodoluminescence observations. X-Ray Diffractograms were made by V. Govers. E. Grew, C. Maijer, T.G. Nijland, R.D. Schuiling and D.J. Waters are thanked for critically reviewing the manuscript. Financial support for fieldwork from the Dr. Schürmann Foundation (grant 91-05) is gratefully acknowledged.

CHAPTER 4

MG-RICH DUMORTIERITE IN CORDIERITE-ORTHOAMPHIBOLE-BEARING ROCKS FROM THE HIGH-GRADE BAMBLE SECTOR, SOUTH NORWAY

ABSTRACT

Dumortierite is described from several occurrences of cordierite-orthoamphibole-bearing rocks in the upper-amphibolite facies area of the Bamble Sector, south Norway. Dumortierite occurs with chlorite, muscovite and quartz in late M_4 alteration zones or aggregates after M_3, peak-metamorphic, cordierite and garnet and early M_4 vein-cordierite, and intergrown with or replacing orthoamphibole. Late M_4 P-T conditions, which are interpreted as conditions of dumortierite formation, are estimated from the associated late M_4 kyanite-andalusite-chlorite-quartz assemblage and Mg-Fe exchange geothermometry to be 500 $\pm$ 50 °C and 3-4 kbar. Retrogression of M_3 mineral assemblages is initiated by influx of fluids with X_{CO_2} of 0.3-0.4 during early M_4 followed by more water-rich fluids during late M_4. Late M_4 fluids may show local variations in alkalies and boron. The dumortierites are the most Mg-rich (2.23-3.42 wt.% MgO) ever reported, and contain 0.00-2.05 wt.% TiO_2, 0.00-1.08 wt.% Fe_2O_3, 29.62-32.42 wt.% SiO_2 and 55.20-59.71 wt.% Al_2O_3. Al is the most likely substituent for Si, which shows a minor deficiency at the tetrahedral sites in most dumortierites. The major variations in the mineral chemistry can be described by the coupled substitutions $Mg + Ti = 2\ Al^{VI}$, $3\ Mg = 2\ Al^{VI}$ and possibly $Mg + H = Al^{VI}$. Favoured by low fO_2 prevailing conditions a significant part of total iron in dumortierites at one locality is present as Fe^{2+}, giving evidence for the $Fe^{2+} + Si^{IV} = Al^{IV} + Al^{VI}$ tschermakite substitution. $FeMg_{-1}$ substitution is considered to be limited. Ti-rich dumortierites coexist with rutile, ilmenite or titaniferous magnetite. The development of dumortierite from orthoamphibole correlates with an observed decrease of Al, Mg and Na and increase of Si and Fe in orthoamphibole towards dumortierite.

INTRODUCTION

Recent microscopic investigations of cordierite-orthoamphibole- bearing rocks from the Bamble Sector, south Norway, revealed several new occurrences of the relatively uncommon borosilicate dumortierite (Fig. 4.1). This rare mineral has already been reported from the same area by Bugge (1943) and Touret (1979). The first discovery, however, was questioned by Lamb (1981), who identified the blue mineral of Bugge as sapphirine.

Dumortierite is generally reported as a minor constituent in pegmatitic, aplitic, and

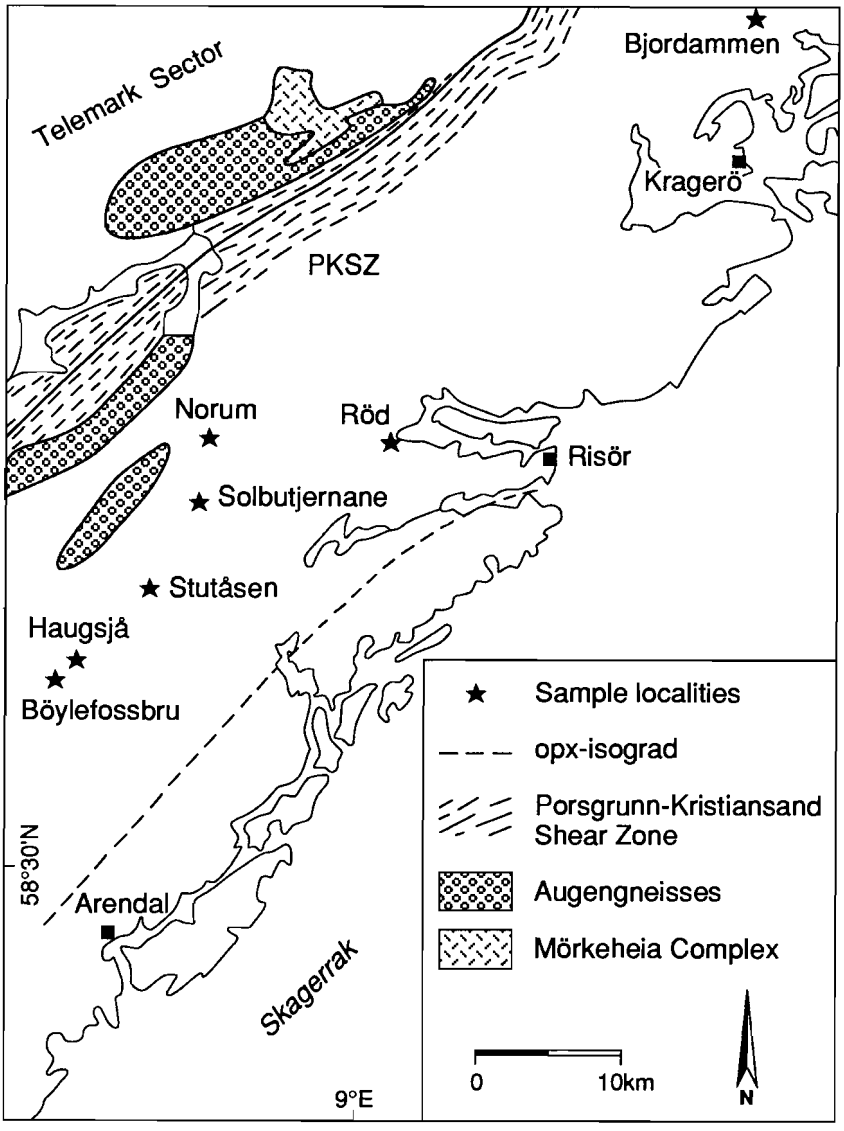

Figure 4.1. Locality and simplified geological map of the central part of the Bamble Sector, south Norway. Opx-isograd after Field & Clough (1976).

granitic rocks (e.g. Finlay, 1907; Graham & Robertson, 1951; Huijsmans et al., 1982), associated pneumatolytic-hydrothermal deposits (Kerr & Jenney, 1935; Sabzehei, 1971; Black, 1973), and regional metamorphic quartzites, argillaceous gneisses and granulites (e.g. Christophe-Michel-Lévy et al., 1959; Schreyer et al., 1975; Vrána, 1979; Takahata &

Uchiyama, 1985; Beukes et al., 1987). More than 75 years after its discovery by Gonnard (1881), the space group (Pmcn), unit-cell parameters and preliminary general formula for the orthorhombic dumortierite, $(Al,Fe^{3+})_7BSi_3O_{18}$, were deduced by Claringbull & Hey (1958). Its crystal structure was solved by Golovastikov (1965), confirming the space group Pmcn assigned by Claringbull & Hey (1958), and further refined by Moore & Araki (1978). The presence of water has undoubtedly been demonstrated by several studies (e.g. Moore & Araki, 1978; Alexander et al., 1986; Werding & Schreyer, 1988; 1990) giving the rearranged general formula of dumortierite, $Al_{6.75}\square_{0.25}BSi_3[O_{17.25}(OH)_{0.75}]$ (after Moore & Araki, 1978). Recently Werding & Schreyer (1988; 1990) were able to synthesize dumortierite in the system Al_2O_3-B_2O_3-SiO_2-H_2O. Their experimental data show a decreasing Al/Si ratio with increasing pressure and a large variation of H_2O-contents.

In this paper, the occurrence in cordierite-orthoamphibole-bearing rocks and the Mg-rich mineral chemistry of the Bamble dumortierites will be presented and discussed. Some considerations on the P-T conditions of formation will be given.

GEOLOGICAL SETTING

The dumortierite-bearing cordierite-orthoamphibole rocks occur as thin layers and lenses in the upper-amphibolite facies area of the central part of the Bamble Sector (Fig. 4.1). The high-grade Bamble Sector was subject to two major periods of metamorphism and deformation (Starmer, 1985). Aluminous reaction textures in orthoamphibole-bearing rocks record a "near-clockwise" prograde P-T trajectory (M_1-M_3) for the Kongsbergian Orogeny (1600-1500 Ma) (Chapter 2; Visser & Senior, 1990). This prograde P-T path is explained as a collision scenario with magmatic addition which produced N.E.-S.W. elongated structures. Peak-metamorphic conditions (M_3) reached upper-amphibolite to granulite facies conditions of about 800 $\pm$ 60 °C and 7.3 $\pm$ 0.5 kbar (Lamb et al., 1986). A long period (300 Ma) of near isobaric cooling occurred between the Kongsbergian Orogeny and the second major period of metamorphism and deformation, the Sveconorwegian (ca. 1200-900 Ma) Orogeny. The tectonic effects of the Sveconorwegian Orogeny (M_4 according to Visser & Senior, 1990) in the Bamble Sector are more pronounced towards its margin with the Telemark Sector. "Near"-isothermal uplift of the Bamble Sector, representing emplacement in the upper crust, is indicated by M_4 assemblages in cordierite-orthoamphibole-bearing rocks which include talc-kyanite-quartz (early M_4) and kyanite-andalusite-chlorite-quartz (late M_4) (Visser et al., 1990;). Domains with "Kongsbergian" structures and ages as e.g. the Arendal granulite facies terrain largely seem to have survived the effects of the Sveconorwegian Orogeny (Starmer, 1985; 1990). The Sveconorwegian Orogeny, an event of extensive but channelled fluid activity associated with the formation of pegmatites, granites, albitites and

quartz-veins, regionally reached greenschist to mid-amphibolite facies conditions. Locally upper-amphibolite to low-granulite facies contact-metamorphic conditions were recorded around augengneiss bodies (Nijland & Senior, 1991).

PETROGRAPHY

Dumortierite was found as a minor constituent at seven localities of cordierite-orthoamphibole-bearing rock types and associated quartz-cordierite veins in the upper-amphibolite facies area. At each locality, the dumortierite grains are so scarce and small that they were found in only about one out of five to ten thin sections. In Table 4.1, the location and metamorphic assemblages of the dumortierite-bearing samples are listed. Dumortierites in all samples have a secondary origin. Three types can be distinguished (see Table 4.1):

Table 4.1.
The location and mineral assemblage in selected samples. Map references are from maps prepared by Norges Geografiske Oppmåling, Series M711, sheets 1612 II-III and 1712 IV.

	Locality		Sample	Minerals
1	Böylefossbru	4831-64956	DV030	Qtz, Grt, Oam, Bt, Crd (M_3), Ap, Rt, St, (Chl, Ms, Dum II)
			DV034	Qtz, Crd (M_4), Ap, (Chl, Ky, And, Ms, Tur, Dum I)
			DV249	Qtz, Oam, Crd (M_3), Bt, Rt, Ap, (Chl, Ms, Ky, Dum I)
2	Haugsjå	4844-64968	TN087	Qtz, Oam, Grt, Crd (M_3), Bt, Rt, Opq, (Ky, Ms. Chl, Dum I, Cc)
3	Stutåsen	4886-65009	DV183	Qtz, Oam, Bt, Crd (M_3), Rt, Grt, (Ms, Chl, Dum III)
4	Solbutjernane	4915-65059	RV070	Qtz, Crd (M_4), Bt, Rt, Opq, (Tlc, Chl, Tur, Dum I, Cc, Preh)
5	Norum	4921-65098	AK034	Qtz, Grt, Tur, Bt, Rt, Opq, Crd (M_3), (Rt, Ms, Chl, Tur, Ky, And, Dum I)
			AK036	Qtz, Oam, Grt, Crd (M_4), Bt, Tur, Opq, Rt, (Ky, And, Ms, Chl, Cc, Tlc, Dum II)
6	Rød	5030-65096	MA780	Grt, Bt, Crd (M_3), Oam, Qtz, Ap, Tur, Krn, Gr, Opq, Rt, Ilm, (Dum II, Dum III, Chl, Ms)
7	Bjordammen	5245-65342	MA822	Qtz, Bt, Crd (M_4), Ap, Tur, Mag, (Chl, Ky, And, Ms, Tur, Dum I)

Mineral abbrevations after Kretz (1983)
Dumortierite type I, II or III (Dum I, Dum II and Dum III) (see text), Muscovite/pinite (Ms), Opaque (Opq). Brackets indicate secondary minerals. (M_3, M_4) - Primary M_3-cordierite and early-M_4 vein-cordierite.

I Dumortierite intergrown with retrograde alteration products of cordierite (samples AK034, DV034, DV249, MA822, RV070, TN087),

II Dumortierite intergrown with retrograde alteration products along cracks in garnet (samples AK036, DV030, MA780),

III Dumortierite intergrown with orthoamphibole or replacing orthoamphibole (samples DV183, MA780),

The first type of dumortierite occurs in two generations of cordierite, namely a primary cordierite of the peak metamorphic M_3-assemblage and a secondary cordierite in probably early-M_4 quartz-cordierite veins which cut across M_3-assemblages. Both generations of cordierite locally show severe pinitisation and in some grains the typical coarse-grained late-M_4 assemblage consisting of kyanite-($\pm$ andalusite)-chlorite-quartz developed.

The euhedral to subhedral dumortierite grains occur at the margin of the alteration aggregates constituted by chlorite + quartz + pinite $\pm$ kyanite $\pm$ andalusite (Figs. 4.2 and 4.3). Intergrowth of dumortierite with kyanite or andalusite has not been observed. Type I dumortierite occasionally is in contact with titaniferous magnetite (C. Maijer, unpublished data). The dumortierite grains normally are very small (50-175 μm in length) but dumortierite in sample AK034 measures up to 350 μm in length (Fig. 4.3). Besides the red

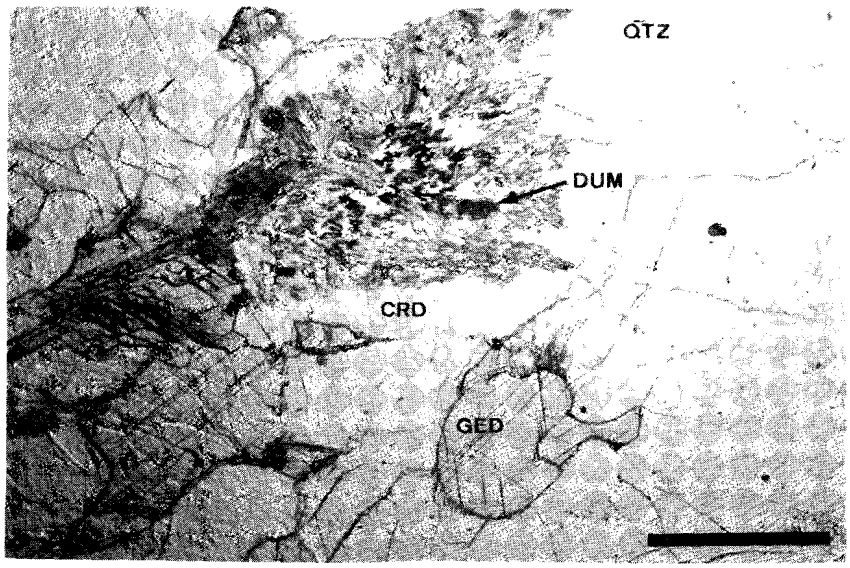

Figure 4.2. Photomicrograph of an alteration aggregate in cordierite (CRD) from sample DV249. Type I dumortierite (DUM) is intergrown with chlorite and muscovite. Scale bar = 450 μm.

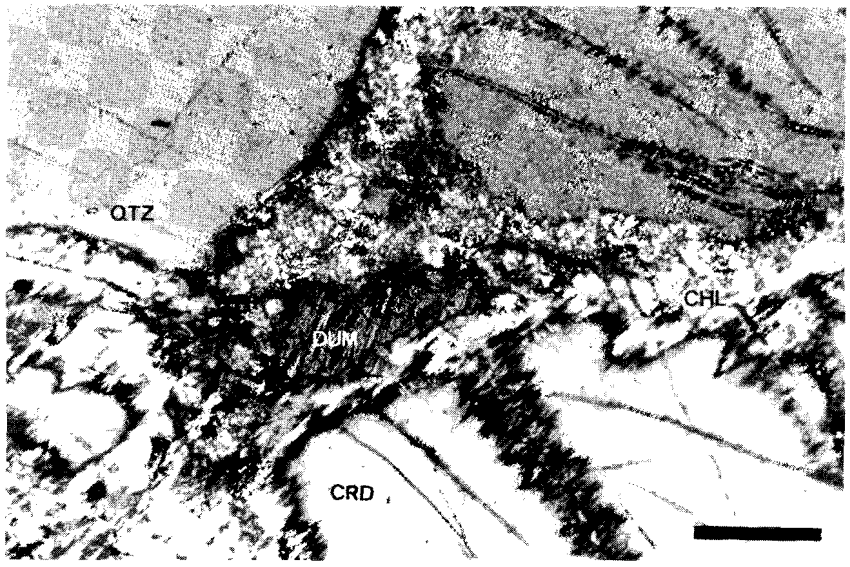

Figure 4.3. Photomicrograph with crossed nicols of an alteration aggregate in cordierite (CRD) from sample AK034. Type I dumortierite (DUM) is intergrown with chlorite, muscovite and pinite. Scale bar = 250 μm.

pleochroism (X = red, Y = Z = colourless), the type I dumortierites sometimes display a faint purple-blue pleochroism in the centre of the grains. Large euhedral, optically unzoned, pale yellow to light brown-green tourmaline grains up to 700-900 μm accompany quartz and cordierite in samples MA822, AK034 and AK036; smaller euhedral yellow-green tourmaline grains (up to 400 μm) occur with chlorite, quartz and Al-silicate in the centre and at the margin of the alteration aggregates of cordierite in samples DV034, RV070, AK034 and MA822. The smaller tourmalines and dumortierites never occur intergrown within the same alteration aggregate.

Type II dumortierite occurs along narrow retrograde zones or cracks in garnet blasts (Fig. 4.4), which may measure up to several centimeters in diameter in sample DV030. Dumortierite commonly forms single acicular euhedral crystals (X = red, Y = Z = colourless to very pale yellow) but subparallel bundles may be present. The dumortierites in DV030 are accompanied by euhedral large chlorites (up to 600 μm), quartz and fine grained white mica. Type II dumortierite grains may be up to 400 μm in length and 80 μm in width. Although rutile is an important minor phase no contacts with dumortierite are observed.

Type III dumortierite is situated in narrow (up to 4 mm wide) retrograde zones or cracks, along which severe pinitisation of cordierite, chloritisation of garnet, biotite and orthoamphibole occurs. Dumortierites in these zones predominantly are intergrown as irregular shaped crystals (X = red-rosa, Y = Z = colourless to pale yellow) and fibrous

masses (Fig. 4.5) with or developed at the expense of subhedral to euhedral orthoamphibole. Rarely type III dumortierites occur as subparallel and sheave-like aggregates of euhedral crystals (X = red, Y = Z = colourless to pale yellow) intergrown with orthoamphibole along the cleavages. Individual crystals measure up to 200 μm in length. Minor quartz, ilmenite and rutile accompany the dumortierite grains. Euhedral type II dumortierite may be present in sample MA780 (Table 4.1).

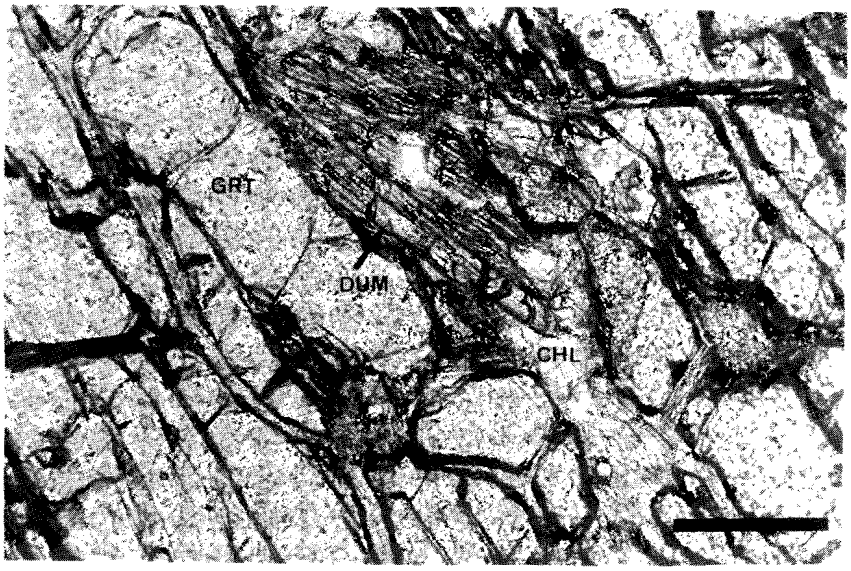

Figure 4.4. Photomicrograph of type II dumortierite fibers (DUM) intergrown with chlorite (CHL) and muscovite along cracks in garnet (GRT) blasts of sample DV030. Scale bar = 200 μm.

Colourless kornerupine and yellow-brown tourmaline occur together with dumortierite in sample MA780. Kornerupine is present as euhedral to subhedral grains intergrown with garnet, quartz and graphite and with orthoamphibole along the cleavage-planes. Although intergrowth-textures with orthoamphibole are very similar no overgrowths or intergrowths of type III dumortierite and kornerupine are observed. Retrogradation of kornerupine from kornerupine-orthoamphibole intergrowths dissected by alteration zones only produces chlorite and fine-grained white mica.

Subhedral to euhedral yellow-brown tourmaline occurs in minor amounts overgrowing biotite and as inclusion or intergrowth with M_3-cordierite, garnet and quartz. No textural relation with kornerupine or dumortierite is observed.

Common alteration products of dumortierite such as muscovite/sericite and kaolinite (Schaller, 1905; Sabzehei, 1971; Beukes et al., 1987) were not observed in the investigated samples.

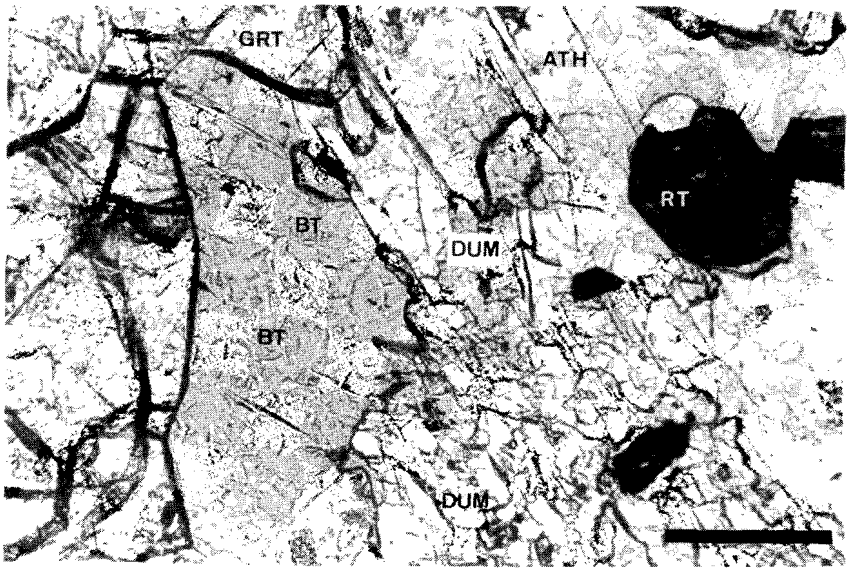

Figure 4.5. Photomicrograph of irregular shaped type III dumortierite (DUM) patches replacing anthophyllite (ATH) in sample MA780. Scale bar = 150 μm.

MINERAL CHEMISTRY

Mineral analyses have been obtained using a Jeol JXA-8600 Superprobe at the University of Utrecht which operated at an acceleration potential of 15 kV, and a sample current of 10 nA. Raw data were corrected with a Tracor Northern PROZA computer program. Natural minerals and synthetic compounds were used as standards. Due to the small size of the dumortierite grains no boron or water analyses could be obtained.

Dumortierite compositions were calculated on the basis of 18 oxygens assuming 1 B and 0.75 OH per formula unit (after Moore & Araki, 1978). The crystal structure of dumortierite can be visualized to consist of three distinct types of chains built of AlO_6 octahedra and running parallel to the [001] direction (see Moore & Araki (1978), for graphic representation of the structure and site-notation). The first, $Al(1)O_3$ chain, is a disordered central infinite face-sharing chain linked in a pseudohexagonal fashion to six external, $3Al(2)_2$-$Al(3)_2O_{12}$ and $3Al(4)_4O_{12}$, octahedral chains by six isolated $2Si(1)O_4$ + $4Si(2)O_4$ tetrahedra. The second, $Al(2)_2$-$Al(3)_2O_{12}$ chain, is an inversion doubled pyroxene-like edge-sharing chain. The third type is a pyroxene-like edge-shared chain doubled to a $Al(4)_4O_{12}$ chain by face-sharing. The external chains are interconnected by BO_3 triangles. X-ray site refinements of Moore & Araki (1978) and Alexander at al. (1986) indicate that site-occupancies of the B, Al(2), Al(3) and

Si(1,2) sites converge to full occupancy ($\approx$ 0.95). The Al(1) central site is only partially occupied (75 and 80 percent according to Moore & Araki (1978) and Alexander et al. (1986) respectively). Charge-balance requirements for this site involve the $3H^+ + \square^{VI} = Al^{3+VI}$ substitutional mechanism and give the general formula $(Al_{6.75}\square_{0.25})BSi_3[O_{17.25}(OH)_{0.75}]$. As postulated by Alexander et al. (1986) the total amount of (OH) will not only vary with the number of octahedral vacancies but also with the di- (Mg, Ca, Fe^{2+}) and tetravalent (Ti) substituents for octahedral Al and trivalent substituents (Al) for tetrahedral Si (see also Werding & Schreyer, 1990). The assumption of 0.75 OH per formula unit in our calculations, although the average oxide total including boron and water is 100.24 % (n = 36, σ_n = 1.30), will, therefore, only be a rough estimate. Recent analytical data on the boron content of natural (Kayupova & Tilepov, 1977) and synthetic dumortierite (Werding & Schreyer, 1988; 1990) are generally supportive for full occupation of B-site by boron.

Dumortierite grains were analysed from samples MA822 (Type I, 3 grains, 5 analyses), DV030 (Type II dumortierite, 3 grains, 8 analyses) and MA780 (Type III, 5 grains, 23 analyses). Representative compositions of the dumortierites and associated minerals are presented in Table 4.2.1-4.2.3.

All three types of **dumortierite** are magnesium-rich (2.23-3.42 wt.% MgO) with variable but sometimes high iron (0.00-1.08 wt.% Fe_2O_3) and low to intermediate TiO_2 contents (0.00-2.05 wt.%). The Bamble dumortierites record the highest MgO content to date for this mineral (1.36 wt.% MgO has been reported by Vrána (1979)). Individual dumortierite grains from the three localities show no zoning but notably TiO_2, Al_2O_3 and MgO vary from grain to grain in the same sample and between the different textural types. Titanium is low in type II dumortierite (0.00-0.46 wt.% TiO_2) and type I and III dumortierite grains not associated with respectively titaniferous magnetite and ilmenite/rutile. Moderate values (1.11-2.05 wt.% TiO_2) are obtained in type I and III dumortierites associated with the Ti-bearing phases.

Our analyses show most of the tetrahedral sites (Si(1,2)) to be slightly deficient in silicon. Al is the most likely substituent for Si at the tetrahedral sites (Fig. 4.6a). More important substitutions are implied by the very low Al-values (6.259-6.601) of the dumortierites. A high correlation between Al^{VI} and Ti, Al^{VI} and Mg (r = -0.91; r = -0.86 respectively) and a strong correlation between Ti and Mg (r = 0.72) indicate the predominant Mg + Ti = 2 Al^{VI} coupled substitution (see Fig. 4.6b-6c). Subtracting the effects of this substitution, that is, adding the total amount of Ti and an equal amount of the coupled Mg to Al^{VI} (labeled Al^{VI}*) and subtracting the total amount of Ti from Mg (labeled Mg*), reveals a strong negative correlation (r = -0.71) between Al^{VI}* and Mg* (Fig. 4.6d) and no significant correlation of Mg* with other elements. This indicates the introduction of Mg at the octahedral sites by the possible substitutions 3 Mg = 2 Al^{VI} and Mg + H = Al^{VI}.

Table 4.2.1.
Representative analyses of dumortierite, tourmaline, cordierite, chlorite and kyanite from sample MA822.

Mineral	Dumortierite		Tur	Crd	Chl	Ky
Spot	45	48	Ma 1	51	50	53
SiO_2	30.90	30.31	36.92	49.73	28.05	36.83
TiO_2	1.11	0.46	0.59	0.00	0.00	0.00
Al_2O_3	57.24	58.42	30.88	33.42	23.72	62.54
Fe_2O_3(T)	0.44	0.00	-	-	-	1.00
FeO(T)	-	-	5.64	1.18	4.99	-
MgO	2.92	2.55	9.58	12.86	29.35	0.00
CaO	0.00	0.00	0.77	0.00	0.00	0.00
Na_2O	0.00	0.00	2.65	0.26	0.00	0.00
K_2O	0.00	0.00	0.08	0.00	0.00	0.00
B_2O_3	6.09*	6.05*	10.77*	-	-	-
H_2O	1.18*	1.17*	3.71*	(1.96)	-	-
CO_2	-	-	-	(0.17)	-	-
Cl	0.00	0.00	0.00	0.00	0.02	0.00
Total	99.88	98.96	101.59	99.58	86.16	100.37
O-Basis	18	18	31	18	28	5
Si	2.939	2.902	5.960	5.002	5.381	0.993
Ti	0.079	0.033	0.072	0.000	0.000	0.000
Al^{IV}	0.061	0.098	0.040	3.962	2.619	0.000
Al^{VI}	6.357	6.496	5.836		2.744	1.988
Fe^{3+}	0.031	0.000	-	-	-	0.020
Fe^{2+}	-	-	0.761	0.099	0.801	-
Mg	0.414	0.364	2.305	1.928	8.393	0.000
Ca	0.000	0.000	0.133	0.000	0.000	0.000
Na	0.000	0.000	0.829	0.025	0.000	0.000
K	0.000	0.000	0.016	0.000	0.000	0.000
B	1.000	1.000	3.000	-	-	-
H	0.750	0.750	4.000	-	-	-
Cl	0.000	0.000	0.000	0.000	0.013	0.000
Total	11.632	11.643	22.952	11.016	19.951	3.001
X_{Mg}	-	-	0.752	0.951	0.913	-

Mn, F, Cr, Sc, Ba and Zn not detected
* - H_2O and B_2O_3 in dumortierite and tourmaline calculated assuming one B and 0.75 (OH) per formula unit for dumortierite, after Moore & Araki (1978), and 3 B and 4 (OH) per formula unit for tourmaline.
H_2O and CO_2 in cordierite determined by wet chemical methods on mineral separates.

Table 4.2.2.
Representative analyses of dumortierite, chlorite and garnet from sample DV030.

Mineral	Dumortierite		Chl	Core Grt	Rim Grt
Spot	186	187	198	196	GF
SiO_2	31.62	30.79	26.70	39.92	38.63
TiO_2	0.46	0.37	0.00	0.00	0.00
Al_2O_3	58.13	58.28	24.18	22.44	21.99
Fe_2O_3(T)	0.49	0.77	-	-	-
FeO(T)	-	-	10.23	24.14	31.42
MnO	0.00	0.00	0.00	0.58	0.82
MgO	2.37	3.42	25.72	11.32	6.57
CaO	0.00	0.00	0.00	2.46	1.90
B_2O_3	6.13*	6.15*	-	-	-
H_2O	1.19*	1.19*	-	-	-
Total	100.39	100.95	86.82	100.86	100.33
O-Basis	18	18	28	12	12
Si	2.985	2.901	5.226	3.000	2.991
Ti	0.033	0.025	0.000	0.000	0.000
Al^{IV}	0.015	0.099	2.774	0.000	0.000
Al^{VI}	6.454	6.375	2.805	1.987	1.998
Fe^{3+}	0.035	0.055	-	-	-
Fe^{2+}	-	-	1.675	1.517	2.035
Mn	0.000	0.000	0.000	0.037	0.054
Mg	0.334	0.480	7.505	1.268	0.759
Ca	0.000	0.000	0.000	0.198	0.157
B	1.000	1.000	-	-	-
H	0.750	0.750	-	-	-
Total	11.606	11.685	19.985	8.007	8.003
X_{Mg}	-	-	0.818	0.456	0.272

Na, K, Cl, F, Cr, Sc, Ba and Zn not detected

Table 4.2.3.
Representative analyses of dumortierite, kornerupine, tourmaline and anthophyllite from sample MA780.

Mineral	Dumortierite		Krn	Tur	Ath#
Spot	157	151	176	TBA	KAA
SiO_2	31.42	31.30	30.87	34.84	51.61
TiO_2	1.78	1.58	0.00	1.68	0.13
Al_2O_3	57.43	56.95	41.27	30.41	4.68
Fe_2O_3(T)	0.48	0.00	-	-	-
FeO(T)	-	-	7.16	3.66	16.27
MnO	0.00	0.00	0.00	0.00	0.04
MgO	3.23	2.99	16.52	9.52	21.38
CaO	0.00	0.00	0.00	2.60	0.53
Na_2O	0.00	0.00	0.00	1.30	0.42
K_2O	0.00	0.00	0.00	0.01	0.00
B_2O_3	6.19*	6.11*	-	10.45*	-
H_2O	1.20*	1.19*	-	3.60*	-
Total	101.73	100.12	95.87	98.07	95.06
O-Basis	18	18	21.5	31	23
Si	2.939	2.967	4.015	5.795	7.494
Ti	0.125	0.113	0.000	0.210	0.014
Al^{IV}	0.061	0.033	-	0.205	0.506
Al^{VI}	6.270	6.330	6.326	5.758	0.295
Fe^{3+}	0.033	0.000	-	-	-
Fe^{2+}	-	-	0.779	0.509	1.911
Mn	0.000	0.000	0.000	0.000	0.005
Mg	0.450	0.422	3.203	2.361	4.628
Ca	0.000	0.000	0.000	0.464	0.082
Na	0.000	0.000	0.000	0.420	0.118
K	0.000	0.000	0.000	0.002	0.000
B	1.000	1.000	-	3.000	-
H	0.750	0.750	-	4.000	-
Total	11.629	11.615	14.323	22.724	15.118
X_{Mg}	-	-	0.804	0.823	0.718

Cl, F, Cr, Sc, Ba and Zn not detected
- Fe^{3+} calculated from stoichiometry (Robinson et al., 1982)

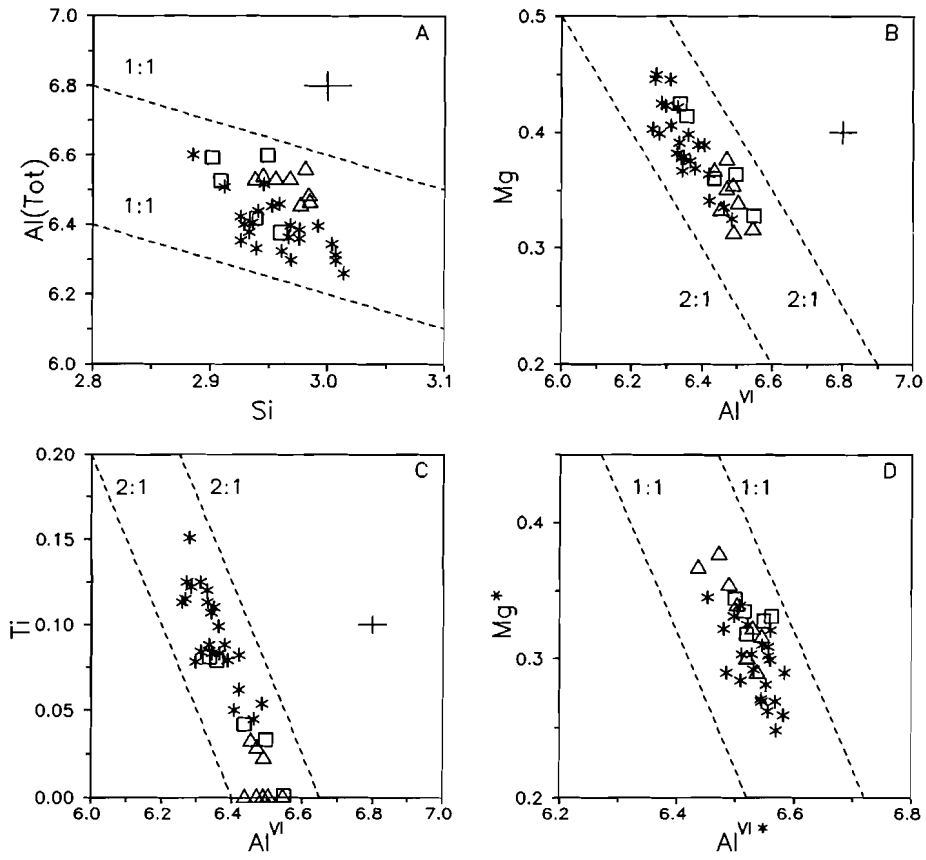

Figure 4.6a-d. Plots of Si versus Al(Tot) (a), Al^{VI} versus Mg (b), Al^{VI} versus Ti (c) and Al^{VI*} versus Mg^* (d) in type I (sample MA822, triangles), type II (DV030, squares) and type III (MA780, asterics) dumortierites. Broken lines show 1:1 or 2:1 ratios. Error bars are typical 1σ counting-statistics errors.

Data on the oxidation state of Fe in dumortierite are scarce. The only two wet chemical analyses which include FeO and Fe_2O_3 (Claringbull & Hey, 1958) show that both trivalent and divalent Fe may be present. The weak inverse relation of Fe with Al^{VI} in type I and II dumortierites may suggest a low $Fe^{2+}/(Fe^{2+}+Fe^{3+})$ ratio due to substitution of most Fe as Fe^{3+} for Al^{3+} at the octahedral sites but the substitution $Fe^{2+} + H^+ = Al^{3+}$ would also be possible. Type III dumortierites (excluding one iron-free grain), however, show a high positive correlation of Fe with Si (r = 0.88, Fig. 4.7a) and Mg (r = 0.60), strong negative with Al^{IV} (r = -0.87) and Al^{VI} (r = -0.69, Fig. 4.7b) and a weak correlation of Mg with Si (r = 0.40) and Al^{IV} (r = -0.39). This essentially involves Fe as Fe^{2+} in the, Fe^{2+},(Mg) + Si = Al^{IV} + Al^{VI}, tschermakite substitution, suggesting relatively high $Fe^{2+}/(Fe^{2+}+Fe^{3+})$

ratios.

The **cordierite** from sample MA822, associated with type I dumortierites, is chemically unzoned and Mg-rich (X_{Mg} = Mg/(Mg+Fe^{2+}) = 0.95) with trace amounts of Na. Cordierite is able to incorporate important gas species such as H_2O and CO_2 in its channels. The wet chemical analyses show relatively high H_2O contents of 1.96 wt.% ($n(H_2O)$ = 0.67 moles H_2O per formula unit) and very low CO_2 contents of 0.17 wt.% ($n(CO_2)$ = 0.025). The optically unzoned cordierites have optic angles ($2V_X$) between 79° and 92° with an average of 84°, γ-α ranges 0.0075-0.009. Application of the triangular diagram constructed by Armbruster et al. (1982, p. 265) to explain the influence of H_2O and CO_2 on optical properties like birefringence and optic angle of cordierite, likewise shows that cordierite is systematically CO_2-poor with an average $n(CO_2)$ of about 0.065. The H_2O content differs from the wet chemical determination in that much lower values are recorded ($n(H_2O)$ = 0.33-0.38). The H_2O content is overestimated by the wet chemical methods, most likely due to intergrowth of chlorite/muscovite in the analysed cordierite fraction. The optically determined H_2O and CO_2 contents correspond to a molar ratio Xco_2 $CO_2/(CO_2+ H_2O)$, of 0.155. The molar ratio Xco_2, $CO_2/(H_2O+CO_2)$, in cordierites is, according to Johannes & Schreyer (1981), indicative for the ratio of these species in the coexisting fluidsystem. Utilizing their experimental data in the system Mg-cordierite-H_2O-CO_2 at P_{fluid} = 5 kbar and T = 600 °C, Xco_2 of 0.155 in the analysed Mg-rich early M_4 vein-cordierite of sample MA822 implies a Xco_2 of the fluidphase of 30-40 percent.

The large **garnet** blasts in sample DV030 show homogeneous pyrope-rich cores with an average X_{Mg} of 0.470. Towards the retrograde cracks garnet shows a sharp but continuous decrease of Mg and an increase of Fe and Mn. X_{Mg} varies from 0.470 to 0.293; the spessartine component ranges from 1 mol. % in the core to 2 mol. % along the cracks. The grossular component ranges 5-7 mol. %, showing no relation to the zoning in Mg, Fe and Mn.

The structural formula of the **orthoamphiboles** in sample MA780, which are partly consumed by type III dumortierite, have been normalized to 15 cations. K and Na are excluded and assigned to the A-site. Negligible amounts of Fe^{3+} are suggested by calculations from stoichiometry (Robinson et al., 1982). The anthophyllites are slightly zoned with Al^{IV} (0.18 to 0.60), Al^{VI} (0.25-0.47), Mg (4.43-4.69) and Na (A) (0.06-0.15) decreasing and Si and Fe (1.90-2.22) increasing towards the orthoamphibole-dumortierite contact.

Typically the compositional variation of orthoamphiboles shows three main types of substitution: $FeMg_{-1}$, $Na(A) + Al^{IV} = \square + Si^{IV}$, and $Mg + Si^{IV} = Al^{VI} + Al^{IV}$. The anthophyllites of sample MA780 deviate from this scheme, to the effect that Fe^{2+} is showing a moderate strong negative correlation with Al^{IV}, Al^{VI} and Na(A). This suggests that the tschermakite coupled substitution essentially involves Fe^{2+} instead of Mg. The orthoamphiboles further contain low to negligible amounts of TiO_2, MnO, CaO and K_2O.

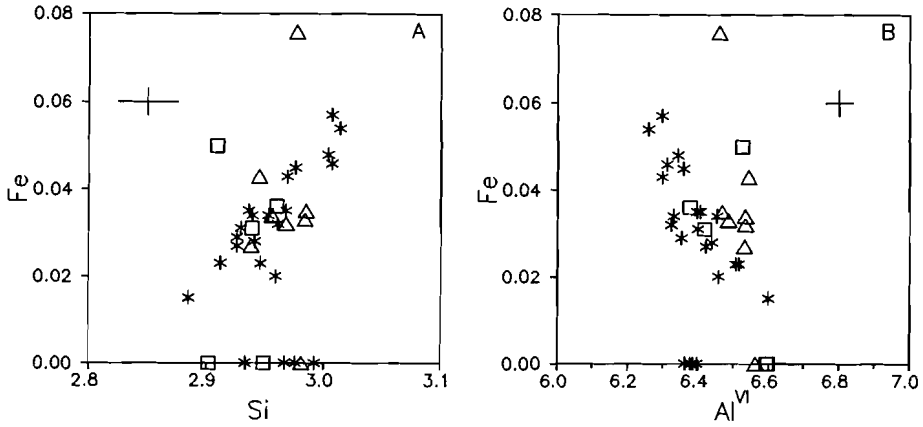

Figure 4.7a-b. Plots of Si versus Fe (a) and Al^{VI} versus Fe. Symbols as in Fig. 4.6a-d.

The **kornerupine** formula was calculated on the basis of 21.5 oxygens or 21 O + (OH, F, Cl) after Moore & Araki (1979). The unzoned kornerupines with X_{Mg} ranging from 0.75 to 0.82 are relatively Al-poor with compositions close to 4(Mg,Fe)O : $3Al_2O_3$: $4SiO_2$ (4:3:4) and slightly more siliceous than the join between the 1:1:1 and 4:3:4 compositions. The low electron probe totals of 95.2 to 97.6 wt.% indicate high water and boron contents. Na, Ca, Mn and Ti occur in trace amounts with together total of less than 0.3 wt.%.

The small yellow-green **tourmalines** intergrown with chlorite, kyanite and quartz and the large brown-green tourmaline intergrown with vein-quartz in sample MA822 show very similar compositional ranges. Both types of tourmaline and the large yellow tourmalines from sample MA780 are unzoned dravites with X_{Mg} of 0.75-0.76 and 0.80-0.85 respectively. The Na/(Ca+Na) ratios are variable from grain to grain and within a grain in both samples and range 0.77-0.89 in MA822 and 0.33-0.63 in MA780. The high TiO_2-contents (0.50-1.68 wt.% in MA780 and 0.49- 0.69 wt.% in MA822) are comparable to those reported from rock types containing a Ti-saturating phase (Abraham et al., 1972; Henry & Guidotti, 1985).

The **chlorites** associated with type I (MA822) and type II (DV030) dumortierites are Al-rich clinochlores with X_{Mg} of 0.91 and 0.81 respectively.

Analyses of **kyanite**, which accompanies chlorite and quartz in cordierite replacement aggregates, show moderate to high amounts of Fe_2O_3 (0.59-1.20 wt.%).

DISCUSSION

The textures in the investigated samples indicate that the Bamble dumortierites exclusively occur as and together with retrograde alteration products of M_3 and early M_4 assemblages in orthoamphibole-cordierite-bearing rocks.

Type I dumortierites occur intergrown with alteration products of cordierite such as chlorite, quartz and pinite. In these textures dumortierite occurs instead of kyanite and/or andalusite suggesting:

$$\text{cordierite} + \text{vapour } (B_2O_3 + H_2O) \longrightarrow$$
$$\text{chlorite} + \text{dumortierite} + \text{quartz.} \quad (1)$$

Reaction 1 and the development of the late M_4 mineral phases andalusite and kyanite both may occur within the same decomposed Mg-rich cordierite grains in most samples indicating similar P-T conditions for both reactions. P-T conditions are estimated at pressures of 3-4 kbar and temperatures of about 500-550 °C, when based on the Al-silicate polymorph transition of Holdaway (1971) and the low-temperature stability field of Mg-cordierite (Seifert & Schreyer, 1970). The absence of clear major optical heterogeneities or zoning towards alteration aggregates and grain boundaries in unaltered parts of the early M_4 vein-cordierite in sample MA822 suggests that the exchange of cordierite with late M_4 fluids was limited to these alteration aggregates. From this it may be concluded that the X_{CO_2} of 30-40 percent deduced from the optical data represents the X_{CO_2} of the fluidphase during the early M_4 event. Late M_4 fluids probably have lower X_{CO_2} as indicated by the hydrous signature of the replacement zones and channels in cordierite. Type II dumortierites occur together with chlorite and quartz along retrograde cracks within garnet. The development of these dumortierites probably took place through the reaction of the form:

$$\text{garnet (core)} + \text{vapour } (B_2O_3 + H_2O) \longrightarrow$$
$$\text{garnet (rim)} + \text{chlorite} + \text{dumortierite} + \text{quartz.} \quad (2)$$

Temperature estimates for the rim of the garnet and coexisting cordierite and biotite in sample DV030 are 420-510 °C and 460- 530 °C respectively at a pressure of 4 kbar (Visser & Senior, 1990). Temperature estimates based upon the Fe-Mg exchange reaction between garnet-rim and chlorite (Grambling, 1990) are somewhat lower and range 400-470 °C at 4 kbar.

Type III dumortierites developed only by intergrowth with or decomposition of orthoamphibole. The compositional zoned orthoamphiboles essentially show a decrease of the

ferro-tschermakite substitution, ($Al_2Fe_{-1}Si_{-1}$) towards the newly formed dumortierite grains, implying:

orthoamphibole + Fe-tschermakite (Oam) + vapour ($B_2O_3 \pm H_2O$) ⟶ dumortierite. (3)

The P-T conditions during the development of type III dumortierite can not be estimated accurately, but the associated pinitisation of cordierite, chloritisation of biotite and growth of muscovite in garnet-cracks in the same alteration zones may suggest that hydrothermal conditions are comparable with those during the formation of type I and II dumortierites. Titanium concentration in type I and III dumortierites depends on the presence of phases like rutile, ilmenite and titaniferous magnetite. These minerals, therefore, must have acted as the major source of TiO_2 for dumortierite in reactions 1 and 3. Minor TiO_2 could have been supplied by orthoamphibole. Ti-rich dumortierites reported from literature generally occur likewise associated with Ti-bearing phases (e.g. Beukes et al., 1987; Vrána, 1979), while dumortierites intergrown with Ti-poor phases as e.g. corundum (Schreyer et al., 1975) or plagioclase and quartz (Takahata & Uchiyama, 1985) show low titanium concentrations.

Oxygen fugacity levels must have been low in sample MA780 during the dumortierite formation as suggested by the presence of Fe^{2+} in type III dumortierites. This is consistent with a very high $Fe^{2+}/(Fe^{2+}+Fe^{3+})$-ratio of the whole rock and the persistence of primary graphite in the alteration zones. Relatively higher oxygen fugacity levels are suggested during the formation of type I dumortierites from sample MA822 on the basis of the moderately high Fe_2O_3 contents (0.69-1.20 wt.%) of kyanite grains not associated with titaniferous magnetite. According to Grew (1980) and Feenstra (1985), these values are characteristic of moderately to highly oxidized rock types. Dumortierite-producing reactions (1-3) and associated formation of M_4 assemblages require the addition of fluid components. In 60% of the investigated samples dumortierite is accompanied by tourmaline or kornerupine, which might have acted as a source of boron for the dumortierite formation. However, textural relationships between the three minerals are lacking. Kornerupine breakdown only produces chlorite and fine-grained micas, while tourmaline grains are not observed to decompose. In fact, tourmalines from some tourmaline-bearing samples are likewise associated with the breakdown products of M_3 and early M_4 assemblages. It is, therefore, considered very likely that the boron oxide component in the fluid was generated outside the immediate rock volume rather than from inside. Only in sample MA780, the breakdown of boron-bearing precursors like kornerupine might have supplied the boron for the dumortierite formation. Possible sources of boron are the late-stage K-feldspar-quartz veins and often tourmaline-bearing granitic pegmatites, which are present and sometimes abundant at most localities. The ubiquitous presence of pinite replacements in cordierite and fine grained muscovite in cracks

of the garnet suggests that K, and probably other alkalies, were also available in the fluid phase.

Higher B_2O_3/H_2O-ratios in the alteration fluid stabilize dumortierite relative to kyanite/andalusite together with chlorite and quartz. The presence of both dumortierite and the aluminosilicates in alteration aggregates of the same cordierite grain indicate, however, that B_2O_3/H_2O-ratios in the fluid are not uniform and vary on thin section scale. As the chemical environment for the components (FeO,MgO), SiO_2 and Al_2O_3 is very similar for both dumortierite and late M_4 tourmaline, the development of late M_4 tourmaline instead of dumortierite will mainly depend on the local availability of alkalies, notably higher Na^+ and Ca^{2+} (see mineral chemistry), higher B_2O_3 and higher H_2O in the host rock and the fluid phase.

It should be realized that late M_4 overprint mainly is restricted to rock types which re-equilibrated under local rather than pervasive hydrothermal conditions. Pressure-temperature conditions for the formation of type I, II and possibly type III dumortierites in most and probably all localities are thought, nevertheless, to be very similar (500 $\pm$ 50 °C, 3-4 kbar, see above), showing no large deviation on regional scale. This implies that metamorphic conditions during retrogradation of M_3 and early M_4 assemblages and development of late M_4 assemblages in cordierite-orthoamphibole-bearing rocks, despite the local signature of the dumortierite development, are of regional importance in the Bamble Sector. The development of dumortierite in late M_4 assemblages seems to be restricted to the upper-amphibolite facies area (Fig. 4.1). This probably is the result of the limited metamorphic overprint during the Sveconorwegian Orogeny (M_4) in the Arendal granulite facies area.

ACKNOWLEDGEMENTS

We are indebted to René Poorter for assistance with the microprobe analyses. Critical comments on earlier drafts of this manuscript were provided by Cees Maijer, Timo Nijland and Theo Kloprogge. Gunnar Raade and an anonymous referee are thanked for review of the manuscript. Financial support for field-work from the Dr. Schürmann and the Molengraaff Foundations (to D.V.) is gratefully acknowledged.

CHAPTER 5

GEDRITE BREAKDOWN IN A GEDRITE-OLIGOCLASE ROCK, BLENGSVATN, BAMBLE SECTOR, SOUTH NORWAY*.

** dedicated to Dr. C. Maijer, University of Utrecht, on the occasion of his retirement*

ABSTRACT

A gedrite-oligoclase rock at Blengsvatn, Bamble Sector, south Norway, shows textural evidence of partial breakdown of gedrite along narrow (100-300 μm), parallel zones. The gedrite is replaced by medium-grained magnetite, cordierite and anthophyllite. Plagioclase is zoned to more Na-rich compositions near the breakdown aggregates. The textures suggest the reaction: gedrite + quartz + plagioclase (An_{30-34}) + O_2 + CO_2 $\longrightarrow$ cordierite + anthophyllite + magnetite + plagioclase (An_{27-28}) + H_2O, which can be balanced to a high degree, using microprobe analyses. The system is considered closed, except for O_2, CO_2 and H_2O. Gedrite breakdown is inferred to have proceeded at T = 527-560 °C, P = 3-6 kbar and $\log fO_2$ between -18.7 and -21.2 and to be the result of an increase in oxygen fugacity and a high $CO_2/(H_2O+CO_2)$ ratio of the infiltrating fluid.

INTRODUCTION

Orthoamphibole-cordierite-bearing rocks are a well-known, widespread rock type of minor volumetric occurrence in the upper-amphibolite- and granulite facies areas of the Proterozoic Bamble Sector, south Norway (e.g. Brøgger, 1934; Bugge, 1943; Beeson, 1976, 1978; Grant, 1981). Recently, Visser (1987) and Visser & Senior (1990) reported several new occurrences of orthoamphibole-$\pm$ cordierite-bearing rocks from the upper-amphibolite facies area of the Froland commune, northwest of the Arendal granulite-facies terrain. In one of these occurrences, a gedrite-oligoclase rock briefly described by Visser (1987), textural evidence is preserved of an unreported gedrite-breakdown reaction. It is the purpose of this paper to present the detailed mineralogical, petrographical and textural features of this reaction, together with the P-T conditions calculated from this and other assemblages present at the same outcrop.

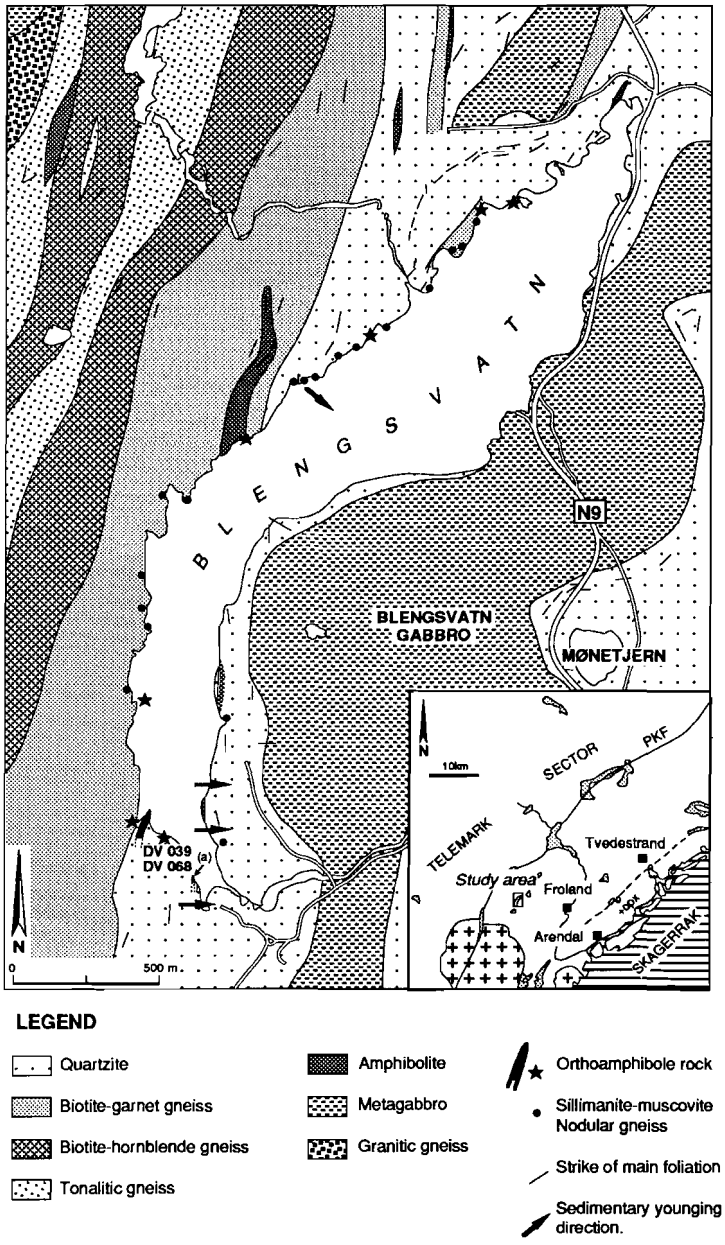

Figure 5.1. Geological map of rocks around Blengsvatn, Bamble Sector, south Norway, showing the locality of samples DV039 and DV068. Opx-isograd is after Field & Clough (1976)

GEOLOGICAL SETTING

A comprehensive compilation of the geology and tectonic evolution of the Proterozoic of the Bamble Sector during the Kongsbergian (1600-1500 Ma) and Sveconorwegian (ca. 1200-900 Ma) orogenies can be found in Starmer (1985, 1991). Relevant isotopic data are reviewed by Verschure (1985). A compilation of the mapping activities of our team, together with a detailed description of the geology of the Froland area is in preparation. A brief account on the geology of the Froland area and its P-T evolution, as deduced from orthoamphibole-bearing rock-types in the area, is given by Visser & Senior (1990).

The samples studied (DV039, DV068) were taken from a small (0.8x2 m), internally layered elliptical body, located on the southern shore of Blengsvatn (4686-64886, map reference from Series M711 maps, sheet 1512 II Mykland; Fig. 5.1). This body consists of foliated and non-foliated plagioclase-quartz-biotite-gedrite-magnetite-ilmenite-apatite (± garnet, cordierite, cummingtonite, hornblende, graphite) assemblages. The small body is one of several small lenses or concordant layers of orthoamphibole-cummingtonite-bearing rocks (Visser, in prep.) that occur interlayered with massive muscovite-biotite-bearing quartzites (with preserved sedimentary cross-stratification), muscovite-sillimanite-bearing nodular gneisses, migmatic biotite-(muscovite) gneisses, biotite-garnet schists, actinolite-hedenbergite-bearing calc-silicates and thin garnet amphibolites. The metasedimentary sequence is intruded by the Blengsvatn coronitic gabbro (2x3 km) and several small pegmatites and quartz-veins.

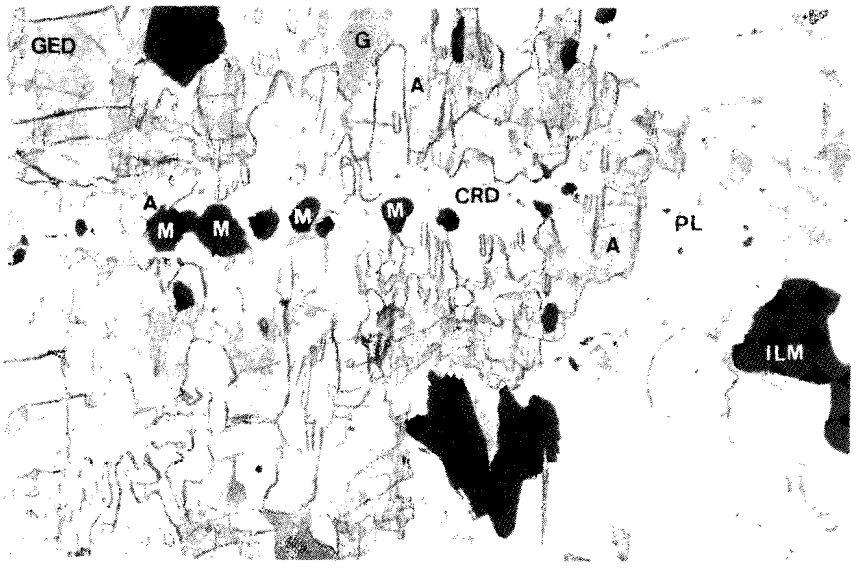

Figure 5.2. Photomicrograph of linearly arranged magnetite (M) with cordierite (CRD) and anthophyllite (A, light grey), replacing gedrite (GED and G, medium-grey). Horizontal width of field is 1500 μm.

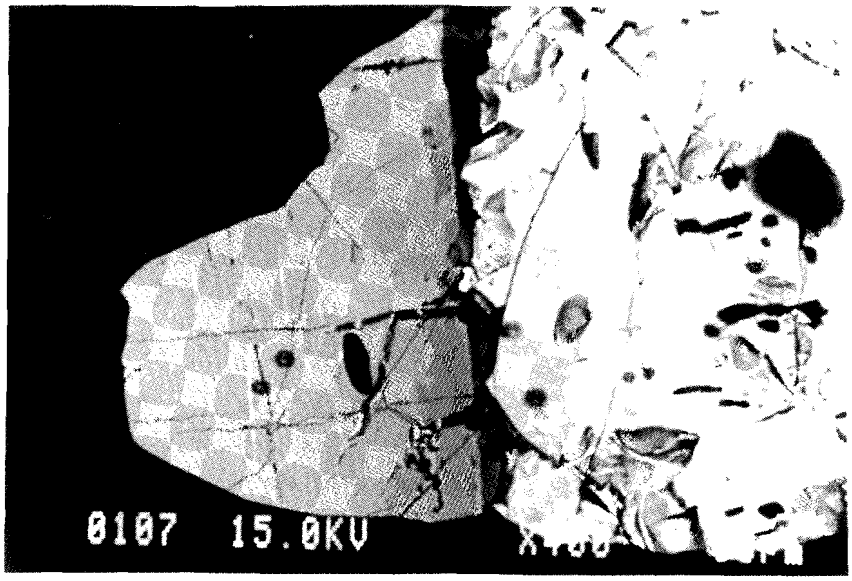

Figure 5.3. Backscattered electron image of magnetite and ilmenite within the gedrite breakdown textures showing a contact zone of homogeneous exsolution-free ilmenite between magnetite and ilmenite with exsolved hematite lenses.

PETROGRAPHY

In sample DV039 gedrite occurs as coarse-grained (up to 5 cm long) greyish-green (Z,Y) to pale yellow (X), highly elongated blades in a matrix of subhedral plagioclase, quartz and euhedral to subhedral ilmenite, euhedral brown-green biotite and rounded apatite. The minor constituents ilmenite and apatite occur in layers which are parallel to the macroscopic layering in the outcrop. A second generation of brown-green biotite occurs as a late secondary replacement of the gedrite. All ilmenite grains, checked with aid of backscattered-electron images in the electron microprobe, are found to contain exsolution lamellae and lenses of hematite along 0001. Except for plagioclase, all matrix minerals also occur as inclusions in gedrite.

Along narrow (100-300 μm), parallel zones or cracks an irregularly developed and limited breakdown of gedrite is observed (Fig. 5.2). The center of the replacement zone consists of a string of euhedral magnetite grains enveloped by irregularly shaped outer rims of cordierite (100-300 μm). Small green tourmaline very rarely rims magnetite. Orthoamphibole itself exhibits a discontinuous colour zoning towards the replacement zone with colourless anthophyllite rimming the grey-green gedrite core. Contacts between primary

ilmenite and magnetite are regular and straight. In large ilmenite grains (> 100 μm) exsolution lamellae and lenses are absent within a 40-100 μm wide zone adjacent to optical homogeneous magnetite (Fig. 5.3). Smaller ilmenite grains within the replacement aggregates are completely devoid of lamellar and lensoid hematite exsolution. Biotite inclusions do not appear to be affected by the breakdown of gedrite. Cordierite contains numerous inclusions of rounded quartz in the quartz-richer parts of the sample, while in the more plagioclase-rich parts quartz inclusions are rare or even absent. Occasionally, cordierite-quartz intergrowths have developed adjacent to plagioclase grains (Fig. 5.4). Fine microscopic exsolution lamellae, parallel to 010, are observed in the gedrite cores but not in the anthophyllite rims.

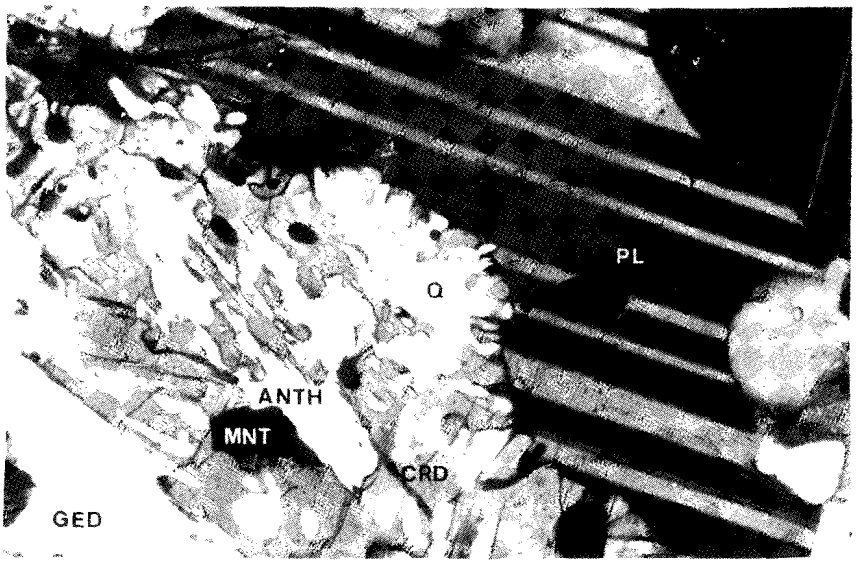

Figure 5.4. Photomicrograph of cordierite (CRD)-quartz (Q) intergrowths next to plagioclase (PL). Horizontal width of field is 100 μm.

Cathodoluminiscence (CL) observations failed to detect any carbonate in the thin sections. CL images of both plagioclase and apatite showed no apparent zoning. Late, patchily developed, retrogression produced chlorite after biotite and cordierite and sericite after plagioclase.

DV068 was sampled from the layer containing DV039, and not surprisingly has a similar mineralogy and comparable textural and optical features. It differs from DV039 in higher orthoamphibole and plagioclase and lower modal amounts of quartz. Cordierite in this sample developed as large (Ø 1 cm) poikiloblastic grains with rounded or smooth inclusions of quartz, biotite, plagioclase and anthophyllite. Euhedral magnetite occurs in the center of the cordierite poikiloblasts. Orthoamphiboles rimming the cordierites show similar discontinuous

colour zoning similar to that in sample DV039. Traces of small (10-150 μm) subhedral garnet (only two or four grains were detected per thin section) exclusively occur included in cordierite or between two cordierite-blasts. The numerous small ilmenite and quartz inclusions in some of the grains may suggest these subhedral garnets to represent a relic phase, however, formation together with magnetite and cordierite can not be excluded. Despite the absence of clear textural evidence for the role of these garnets during gedrite breakdown, their presence in DV068 is very useful in that they, as new or re-equilibrated phases, provide one with an extra check on the P-T conditions at the locality.

Table 5.1
Major (wt.%) and trace element (ppm) analysis of samples DV039 and DV068, Blengsvatn, Bamble Sector, south Norway.

	DV039	DV068		DV039	DV068
SiO_2	54.19	49.16	Ba	106	129
TiO_2	2.22	2.74	Co	43	57
Al_2O_3	13.68	15.43	Cs	<6	<6
Fe_2O_3	3.70	2.23	Cu	<8	9
FeO	10.50	13.44	Ga	24	27
MnO	0.33	0.24	La	20	42
MgO	8.57	9.61	Nb	7	7
CaO	2.48	3.66	Ni	7	27
Na_2O	2.84	2.21	Pb	6	7
K_2O	0.49	0.59	Rb	17	20
P_2O_5	0.50	0.56	Sc	50	55
			Sr	77	115
Total	99.50	99.87	Th	<5	<5
			U	<5	<5
L.O.I.	0.59	0.80	Y	44	45
			V	281	450
			Zn	88	100
			Zr	205	185
			Cr	11	18
			B	23	17
			S	<25	<25
			Li	130	105
			F	412	598
			Cl	488	252

Analyses obtained at the University of Utrecht by gravimetry (LOI), colorimetric titration (FeO), ion selective electrodes (F and Cl), standard X-ray fluorescence techniques using an automated Philips PW1400 Spectrometer (see Bol, 1990, for analytical procedures and accuracies) and Inductively Coupled Plasma Emission Spectroscopy (ICPES) on an ARL 34000 spectrometer (for the elements B, S, Li and Cr.)

Table 5.2. Selected mineral analyses in sample DV039.

		Orthoamphibole			Crd	Plagioclase		Mag	Ilm	Chl	Bt	Ap
Spot	85	114	87	9	121	92	90	76	5/8	80	4/173	4/171
SiO_2	43.80	44.60	53.46	54.81	49.34	60.20	60.86	0.00	0.00	27.59	37.15	0.15
TiO_2	0.00	0.00	0.00	0.03	0.00	0.00	0.00	0.00	48.44	0.00	1.18	0.00
Al_2O_3	16.09	14.73	2.77	0.63	33.34	25.40	24.85	0.43	0.00	23.21	17.31	0.00
Cr_2O_3	0.03	0.00	0.00	0.00	0.00	0.00	0.00	0.09	0.00	0.02	-	-
Fe_2O_3	-	-	-	-	-	-	-	68.56	8.19	-	-	-
FeO	21.52	20.92	20.33	19.77	4.54	0.00	0.00	31.03	42.18	15.14	13.07	0.00
MnO	0.34	0.81	0.38	0.45	0.00	0.00	0.00	0.00	1.27	0.00	0.07	0.12
MgO	14.41	15.56	19.73	20.71	10.50	0.00	0.00	0.00	0.00	22.05	16.66	0.00
CaO	0.31	0.31	0.00	0.17	0.00	6.86	5.83	0.00	0.00	0.00	0.00	54.50
Na_2O	1.61	1.56	0.24	0.04	0.35	8.03	8.50	0.03	0.03	0.04	0.30	0.00
K_2O	0.00	0.00	0.00	0.00	0.00	0.05	0.06	0.00	0.00	0.00	8.16	0.10
P_2O_5	-	-	-	-	-	-	-	0.00	0.00	-	0.00	42.00
SO_3	-	-	-	-	-	-	-	0.00	0.00	-	0.18	0.27
Cl	0.05	0.02	0.00	0.02	0.00	0.00	0.00	0.00	0.00	0.00	0.09	1.02
F	0.10	0.00	0.00	0.06	0.00	0.00	0.00	0.00	0.00	0.00	0.00	2.14
Total	98.21	98.51	96.91	96.64	98.07	99.99	100.10	100.14	100.11	88.15	94.16	99.17
O-basis			23		18		8	4	3	28	22	25
Si	6.378	6.473	7.744	7.905	5.006	2.669	2.703	0.000	0.000	5.441	5.704	0.025
Ti	0.000	0.000	0.000	0.000	0.000	0.000	0.000	0.000	0.926	0.000	0.136	0.000
Al^{IV}	1.622	1.527	0.256	0.095	3.987	1.327	1.301	0.000	0.000	2.559	2.296	0.000
Al^{VI}	1.140	0.993	0.217	0.044	-	0.000	0.000	0.019	0.000	2.859	0.837	0.000
Cr	0.003	0.000	0.000	0.000	0.000	0.000	0.000	0.003	0.000	0.003	-	-
Fe^{3+}	-	-	-	-	-	-	-	1.980	0.150	-	-	-
Fe^{2+}	2.621	2.539	2.463	2.393	0.385	0.000	0.000	0.996	0.896	2.497	1.678	0.000
Mn	0.042	0.100	0.047	0.055	0.000	0.000	0.000	0.000	0.027	0.000	0.009	0.016
Mg	3.128	3.366	4.260	4.469	1.588	0.000	0.000	0.000	0.000	6.482	3.813	0.000
Ca	0.048	0.048	0.000	0.026	0.000	0.326	0.277	0.000	0.000	0.000	0.000	9.843
Na	0.455	0.439	0.067	0.011	0.069	0.690	0.732	0.002	0.000	0.015	0.089	0.000
K	0.000	0.000	0.000	0.000	0.000	0.003	0.003	0.000	0.000	0.000	1.598	0.019
P	-	-	-	-	-	-	-	0.000	0.000	-	0.000	5.995
S	-	-	-	-	-	-	-	0.000	0.000	-	0.021	0.034
Cl	0.012	0.005	0.000	0.005	0.000	0.000	0.000	0.000	0.000	0.000	0.023	0.291
F	0.046	0.000	0.000	0.027	0.000	0.000	0.000	0.000	0.000	0.000	0.000	1.141
Total	15.437	15.485	15.054	14.999	11.035	5.013	5.013	3.000	1.999	19.857	16.204	17.364
X_{Mg}	0.539	0.570	0.634	0.651	0.805	-	-	-	-	0.722	0.694	-

Fe^{3+} in magnetite and ilmenite calculated from stoichiometry. Totals corrected for O≡Cl,F

Samples DV039 and DV068 are characterised by moderately low SiO_2, low alkalies, especially K_2O, and high $FeO+Fe_2O_3+MgO$ (Table 5.1). High TiO_2 and P_2O_5 contents correlate well with the observed ilmenite and apatite abundances. Among the trace elements, the high Sc and Li and low S, Cr and Ni are noticeable. Major-element chemistry is very similar to some of the orthoamphibole gneisses and pelitic rocks from the Limpopo belt, South Africa (van Reenen, 1986).

Table 5.3.
Selected mineral analyses in sample DV068.

	Orthoamphibole		Garnet		Crd	Bt	Pl
Spot	1/18	1/14	Core	Rim	1/11	1/26	1/19
SiO_2	45.19	52.91	37.76	37.65	48.61	37.16	57.25
TiO_2	0.00	0.00	0.00	0.03	0.00	1.30	0.00
Al_2O_3	14.30	2.19	21.35	21.43	33.20	17.21	27.28
FeO	22.99	23.18	32.29	33.41	5.47	16.03	0.00
MnO	0.48	0.43	1.94	2.35	0.12	0.06	0.00
MgO	13.60	18.31	4.81	3.91	10.06	13.78	0.00
CaO	0.49	0.18	2.56	2.52	0.00	0.00	9.05
Na_2O	1.31	0.15	0.00	0.00	0.30	0.23	6.79
K_2O	0.00	0.00	0.00	0.00	0.00	8.69	0.10
SO_3	0.00	0.12	0.00	0.00	0.00	0.00	0.00
Cl	0.03	0.02	0.00	0.00	0.00	0.11	0.00
F	0.00	0.14	0.00	0.00	0.00	0.13	0.00
Total	98.39	97.63	100.71	101.30	97.76	94.70	100.47
O-basis	23		12		18	22	8
Si	6.604	7.722	2.984	2.978	4.975	5.789	2.558
Ti	0.000	0.000	0.000	0.002	0.000	0.152	0.000
Al^{IV}	1.396	0.278	-	-	4.005	2.211	1.437
Al^{VI}	1.067	0.099	1.989	1.998	-	0.949	-
Fe^{2+}	2.810	2.829	2.134	2.210	0.468	2.088	0.000
Mn	0.059	0.053	0.130	0.157	0.010	0.008	0.000
Mg	2.963	3.984	0.567	0.461	1.535	3.200	0.000
Ca	0.077	0.028	0.217	0.214	0.000	0.000	0.433
Na	0.371	0.042	0.000	0.000	0.060	0.069	0.588
K	0.000	0.000	0.000	0.000	0.000	1.727	0.006
S	0.000	0.013	0.000	0.000	0.000	0.000	0.000
Cl	0.007	0.005	0.000	0.000	0.000	0.029	0.000
F	0.000	0.065	0.000	0.000	0.000	0.064	0.000
Total	15.347	15.049	8.021	8.021	11.053	14.467	5.017
X_{Mg}	0.513	0.585	0.210	0.173	0.766	0.605	-

Cr and P below detection limit.

MINERAL CHEMISTRY

Mineral analyses were carried out on a JEOL JXA-8600 Superprobe at the University of Utrecht, which operated at an acceleration potential of 15 kV and a sample current of 10 nA. Raw data were corrected with a Tracor Northern PROZA computer program. Natural minerals and synthetic compounds were used as standards. Optical properties of cordierite were determined on a Zeiss-GFL Universal Stage, using hemispheres with refractive index 1.555. Selected analyses of DV039 are listed in Table 5.2. Analyses of minerals from sample DV068 (Table 5.3) are mainly used for comparative P-T calculations and not discussed in this chapter.

Gedrites outside and within the replacement zones are unzoned and show compositional overlap. Al^{IV}, Na(A) and X_{Mg} range 1.367-1.637, 0.396-0.498 and 0.53-0.57 respectively. Colourless orthoamphibole rims are unzoned anthophyllites with Al^{IV}, Na(A) and X_{Mg} of respectively 0.063-0.308, 0.000-0.034 and 0.62-0.65 (Fig. 5.5). $Fe^{3+}/(Fe^{3+}+Fe^{2+})$ ratios calculated on the basis of 15 cations, excluding Na + K as suggested by Robinson et al. (1982), range 0-0.07 for both gedrite and anthophyllite. F and Cl contents in both gedrite and anthophyllite are low ranging 0.00-0.22 wt.% F and 0.00-0.05 wt.% Cl.

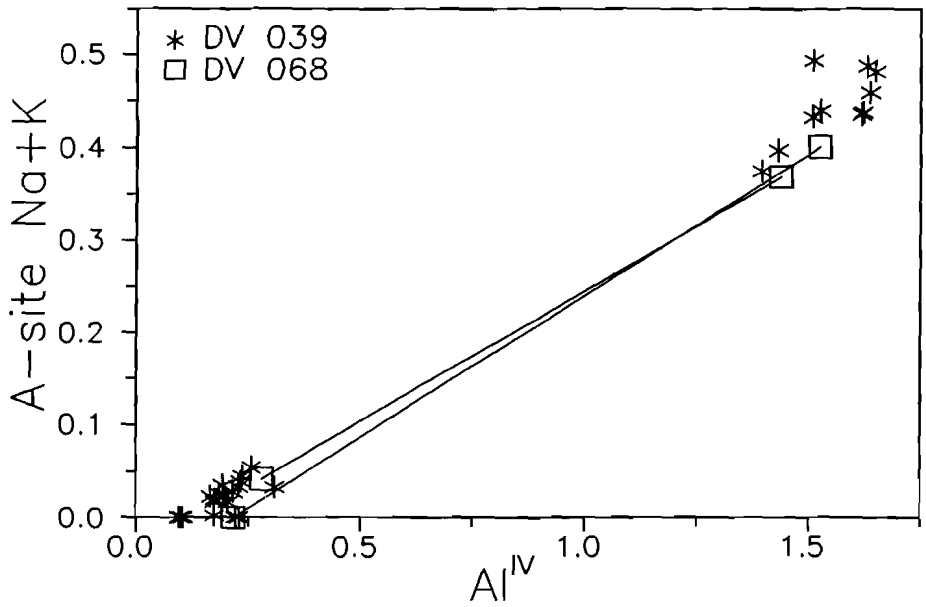

Figure 5.5. Plot of tetrahedral Al versus Na + K in A-site for gedrites and anthophyllites of samples DV039 and DV068.

Plagioclase (An_{30-34}, $Or_{0-0.3}$) is zoned to more Na-rich compositions near the breakdown aggregates (An_{27-28}).

Cordierite is homogeneous and the most Mg-rich phase, with X_{Mg} of 0.79-0.81. The optical properties ($2V_X$ 82-84°, delta 0.009-0.010) indicate about 0.1 moles CO_2 and 0.4-0.5 moles H_2O as channel filling species (cf. Armbruster et al., 1982). The molar ratio Xco_2 $[CO_2/(H_2O+CO_2)]$ of 0.17-0.20 in cordierite suggests an Xco_2 of the coexisting fluid phase of about 0.45-0.50, when using the experimental data of Johannes & Schreyer (1981) for Mg-cordierite at P_{fluid} = 5 kbar and T = 600 °C. The relatively high amount of the channel cation Na present in the cordierites, 0.35-0.52 wt.% Na_2O, may have hindered the incorporation of H_2O and especially CO_2 in cordierite, due to the ability of Na to act as an obstruction. The deduced molar ratio Xco_2 of the fluid may, therefore, be too low.

Magnetite is nearly pure Fe_3O_4 with only trace amounts of Al_2O_3 and Na_2O. Titanium (0.20-0.23 wt.% TiO_2) is only detected in magnetites which are in contact with ilmenite.

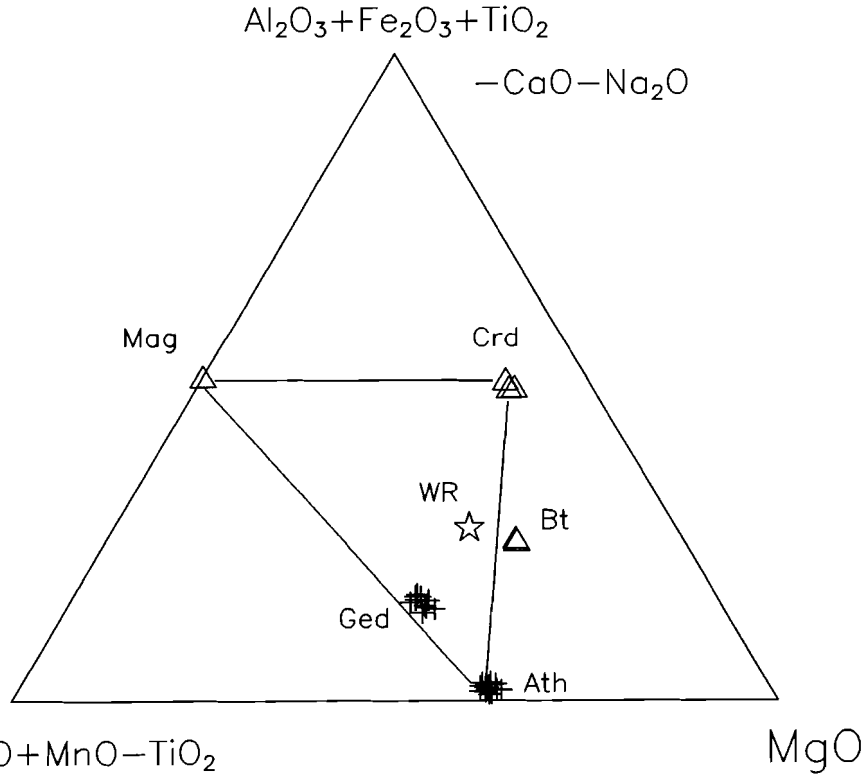

Figure 5.6. ($Al_2O_3+Fe_2O_3+TiO_2$-CaO-Na_2O)-MgO-(FeO+MnO-TiO_2) triangular plot illustrating the whole rock composition (DV039, open star) and the chemical range of relevant phases (+) in DV039 as a projection from SiO_2, H_2O and plagioclase after Robinson & Tracy (1979) and J.C. Schumacher (pers. comm., 1992).

Ilmenite grains with exsolved hematite lamellae contain 20-22 mol % Fe_2O_3 component (exsolved hematite lamellae not reintegrated) and small amounts of MnO, MgO and Na_2O. Compared with these ilmenites, lamellae-free ilmenites are lower in hematite-component (12-15 mol % Fe_2O_3) and higher in MnO (0.74-1.32 wt.%). No zoning has been detected in the lamellae-free ilmenites. Vanadium, a common component in ilmenite and present in moderate amounts in both samples (Table 5.1), has not been analysed.

Apatite is unzoned with Cl and F ranging respectively 0.80-1.05 and 2.06-2.40 wt.%. Its Ca-content approaches the theoretical value of 10 cations per formula (9.833-9.945). Together phosphorus + sulphur (0.20-0.42 wt.% SO_3) totals are close to or over six cations. No compositional difference could be detected between apatites outside and within the gedrite breakdown textures.

Biotite occurs as a minor, homogeneous phase with X_{Mg} and Al^{VI} of respectively 0.69-0.70 and 0.53-0.54. F was not detected, while Cl and S contents are low (0-0.09 wt.% Cl, 0-0.18 wt.% SO_3). Tourmaline was not analysed.

Mn/Fe atom ratios of the minerals in DV039 show the following trend: Crd-Chl-Mag (0.00)< Bt (0.005)< primary ilmenite (0.00-0.015)< Ath-Ged (0.016-0.042) ≈ reequilibrated ilmenite (0.029-0.031).

DISCUSSION

Textural and chemical evidence demonstrates the breakdown of gedrite to anthophyllite, cordierite and magnetite in the investigated gedrite-oligoclase rock (Fig. 5.6). The linear arrangement of the breakdown aggregates suggests that the introduction of fluids along cracks triggered the breakdown of gedrite. The optical data of cordierite provide a lower estimate of 0.45-0.50 for X_{CO_2} of this infiltrating fluid. The breakdown reaction can be balanced to a high degree by using the compositions listed in Table 5.2 of the minerals involved (excluding minor amounts of Ti, Cr, Mn and K, and excluding the trace amounts of tourmaline):

$$\underset{\text{gedrite}}{Na_{0.46}Ca_{0.05}Mg_{3.13}Fe_{2.62}Al_{2.76}Si_{6.38}O_{22}(OH)_2} + 1.64\ \underset{\text{quartz}}{SiO_2} +$$
$$1.92\ \underset{\text{plagioclase } (An_{30\text{-}34})}{Na_{0.69}Ca_{0.33}Si_{2.67}Al_{1.33}O_8} + 0.05\ CO_2 \pm 0.18\ O_2 \longrightarrow$$

$$0.51\ \underset{\text{anthophyllite}}{Na_{0.01}Ca_{0.03}Mg_{4.47}Fe_{2.39}Al_{0.14}Si_{7.91}O_{22}(OH)_2} +$$
$$0.53\ \underset{\text{cordierite}}{Na_{0.07}Mg_{1.59}Fe_{0.39}Al_{3.99}Si_{5.01}O_{18}.(0.5\ H_2O,\ 0.1\ CO_2)} +$$
$$0.40\ \underset{\text{magnetite}}{FeFe_{1.98}Al_{0.02}O_4} + 2.39\ \underset{\text{plagioclase } (An_{27\text{-}28})}{Na_{0.73}Ca_{0.28}Al_{1.30}Si_{2.70}O_8} + 0.23\ H_2O. \quad (1)$$

The calculated amount of participating phases in equation 1 are in reasonable agreement with the observed modal amounts.

The possible participation of the trace amounts of garnet in the gedrite breakdown reaction in sample DV068 can be balanced only approximately and may be of the following generalised form:

$$\text{gedrite} + \text{quartz} \longrightarrow$$
$$\text{anthophyllite} + \text{cordierite} + \text{garnet} \pm \text{magnetite} \quad (2)$$

suggesting garnet to be a newly formed phase due to a local variation in fO_2. There is, however, no unequivocal textural evidence supporting this reaction.

The linear arrangement of magnetite grains in the center of the aggregates suggests that the reaction 1 may have been initiated by oxidation of gedrite resulting in exsolution of magnetite. The high amount of magnetite formed and the similar low $Fe^{3+}/(Fe^{3+}+Fe^{2+})$ ranges calculated for both gedrite and anthophyllite likewise indicate that oxidation is one of the driving forces of reaction 1.

Table 5.4.
Molar volumes (cm^3) and stoichiometric coefficients of minerals participating in the breakdown reaction.

Reactants:	cm^3		
Gedrite	266.4	x	1.0
Quartz	22.69	x	1.64
Plagioclase (An_{32})	100.30	x	1.92
Total volume reactants	496.19		
Products:			
Anthophyllite	265.4	x	0.51
Cordierite	237.98	x	0.53
Magnetite	44.52	x	0.40
Plagioclase (An_{27})	100.26	x	2.39
Total volume products	518.91		

Volume in cm^3 of the minerals at 1 bar and 298 K are from the thermodynamic dataset of Holland & Powell (1990) except for gedrite and the volume effect of H_2O in cordierite which are from Helgeson et al. (1978). Molar volumes of cordierite and plagioclase are estimated by linear extrapolation of end-member data.

Sodium released by the breakdown of gedrite is partially incorporated in cordierite, which exhibits relatively high Na-contents, and partially in adjacent plagioclase, which is zoned to more Na-rich compositions near the breakdown aggregates. Mn is distributed between the reequilibrated ilmenites within the replacement aggregates, anthophyllite and garnet (in DV068). Quartz grains present in or adjacent to gedrite most likely participated in the reaction. The cordierite-quartz intergrowths next to plagioclase and the numerous small rounded quartz inclusions in cordierite-aggregates in the quartz-richer parts of the sample can be explained by the nucleation of cordierite around and growth at the expense of the quartz grains already present.

The gedrite breakdown reaction is considered to be a closed system for all major elements except for the addition of CO_2, O_2 and trace amounts of boron (tourmaline) and removal of H_2O. The breakdown reaction involves a volume increase of the solid phases (Table 5.4), indicating a decrease in P. The volume change is too large to be due to uncertainties of the selected molar volumes and the compositional ranges of the minerals involved and is, therefore, thought to be realistic.

The only direct estimate of the metamorphic conditions for the breakdown of gedrite in sample DV039 can be extracted from coexisting magnetite and reequilibrated, homogeneous, exsolution-free ilmenite in the breakdown aggregates. Temperatures and log fO_2 data calculated on basis of the magnetite-ilmenite geothermometer and oxygen barometer of Spencer & Lindsley (1981), using the recalculation scheme of Stormer (1983), range 527-547 °C with logfO_2 between -18.7 and -21.2. A similar temperature range was calculated on basis of coexisting garnet-biotite and garnet-cordierite pairs in sample DV068. DV068 garnets show homogeneous cores and slightly Fe-Mn enriched rims and yield rim-temperatures of 500-517 °C, and cores of 547-559 °C using the Ferry & Spear (1978) garnet-biotite thermometer. The garnet-cordierite temperature estimates (Thompson, 1976; Holdaway & Lee, 1977; Perchuk & Lavrent'eva, 1983) fall into the same range with rim- and core-temperatures of respectively 498-517 °C and 536-557 °C. The estimated temperatures in DV039 and DV068 meet the requirement set by the absence of any core-rim zoning in gedrite and the large miscibility gap between the gedrite and anthophyllite analyses (Fig. 5.5), which indicates that the reaction proceeded at temperatures below the crest of the orthoamphibole solvus (Spear, 1980). It is suggested, therefore, that the temperature during the breakdown of gedrite was about 527-560 °C. Both the temperature estimates and the volume change of the breakdown reaction are consistent with the P-T conditions (500 $\pm$ 50 °C at 3-6 kbar) experienced during or short after the uplift of the Bamble Sector (M_4 phase according to Visser & Senior, 1990; 1991). As pressure conditions of the breakdown reaction can not be estimated from the mineral data the 3-6 kbar pressure range provides the only reasonable estimate. The M_4 metamorphic phase is characterised by extensive retrogradation of the peak-metamorphic (M_3) assemblages after a period of prolonged isobaric cooling between M_3 and M_4 (Visser & Senior, 1990). The extensive exsolution of hematite in the matrix-ilmenites in sample DV039 preceding the breakdown of gedrite and re-equilibration of ilmenites in the breakdown aggregates is most likely the result of this cooling phase.

The abundant granitic pegmatites are considered a possible fluid source at the M_4-phase (Visser & Senior, 1990). At the estimated temperature of the gedrite-breakdown reaction, the fluids released by consolidating granitic pegmatites are dominantely H_2O-rich (Thomas & Spooner, 1988; Černý, 1991). The generation of the high CO_2-component of the fluid probably involves the interaction of the oxidizing hydrous pegmatite-derived fluid with

graphite-bearing biotite-rich cordierite-gedrite layers which are present at the locality. Alternatively the infiltrating CO_2-bearing retrograde fluid may have been derived from the contact zone of the Blengsvatn coronitic gabbro and the surrounding rocks of the metasedimentary sequence (quartzites and calc-silicate rocks). In this contact zone the residual liquid of the solidified Blengsvatn gabbro interacted with the quartzites and calc-silicates probably as a result of the tectonic unloading during M_4 and formed an extensive network of apatite, scapolite, actinolite $\pm$ albite, quartz and carbonate-bearing breccia and veins (Verdonk et al., 1986).

ACKNOWLEDGEMENTS

I thank R. Poorter and T. Bouten for their assistance with the electron microprobe analyses and T.G. Nijland, M.T. Otten, J.C. Schumacher and two anonymous reviewers for their constructive comments on the manuscript. W.J.H. Eussen and A.I. Lesquillier performed the XRF- and wet-chemical analyses of DV039 and DV068. Financial support for fieldwork from the Dr. Schürmann Foundation (grant 91-05) is greatfully acknowledged.

CHAPTER 6

HÖGBOMITE IN SAPPHIRINE-BEARING ROCKS FROM THE BAMBLE SECTOR, SOUTH NORWAY.

ABSTRACT

Högbomite is reported from two upper-amphibolite and granulite-facies, sapphirine-bearing, Al-Mg-Fe-rich and silica-poor lens-shaped layers within the Bamble Sector, south Norway. Primary assemblages, indicating peak metamorphic conditions of 773-844 °C at 7 kbar (Mg-Fe exchange thermometry), are spinel-sapphirine-biotite-gedrite, spinel-corundum-sapphirine-cordierite and orthopyroxene-biotite-cordierite-plagioclase. Högbomite formed by hydrous alteration and oxidation of primary spinel and rutile and/or ilmenite according to the generalized reaction:

$$\text{spinel} + \text{ilmenite/rutile} \pm \text{sapphirine} \pm \text{gedrite} + H_2O + O_2 \longrightarrow$$
$$\text{högbomite} \pm \text{corundum} \pm \text{magnetite} \pm \text{chlorite.}$$

Suggested conditions of högbomite formation are 550-620 °C and 6-7 kbar. The högbomites contain 10.2-14.7 wt.% MgO, 0-0.3 wt.% ZnO, 58.9-62.1 wt.% Al_2O_3 and 15.6-17.6 wt.% Fe as FeO. The two högbomites may belong to different polytypes as suggested by their differing TiO_2 (9.9-10.1 versus 5.7-5.8 wt.%) and calculated Fe^{3+}- and H_2O-contents. The partitioning of Zn between spinel and högbomite is not uniform and is considered to depend upon prevailing fO_2 and aH_2O.

INTRODUCTION

Högbomite, a complex Fe-Mg-(Co-Zn)-Al-Ti oxide, occurs as a minor constituent of sapphirine-bearing rocks at Snaresund and in the vicinity of Rangleåsen, Bamble Sector, south Norway (Fig. 6.1). The Snaresund sampling site is situated in the granulite-facies zone of the Arendal-Tvedestrand area, whereas the Rangleåsen sampling site is located in the adjacent upper-amphibolite facies zone. Peak metamorphic conditions for this Kongsbergian (Gothian) (1600-1500 Ma) granulite facies event are estimated to be 800 ± 60 °C and 7.3 ± 0.5 kbar (Lamb et al., 1986). P-T conditions for the associated upper-amphibolite facies metamorphism are 740 ± 60 °C and 7 kbar (Visser & Senior, 1990). Uplift of the area occurred during the Sveconorwegian Orogeny (ca. 1200-900 Ma), which manifested itself

as a retrograde greenschist- to amphibolite-facies event with extensive fluid activity. P-T conditions for the onset and completion of this uplift and rehydration event are constrained at 625-700 °C and 6-7 kbar and 420-530 °C at 3-4 kbar respectively (Nijland et al., 1993; Visser & Senior, 1990).

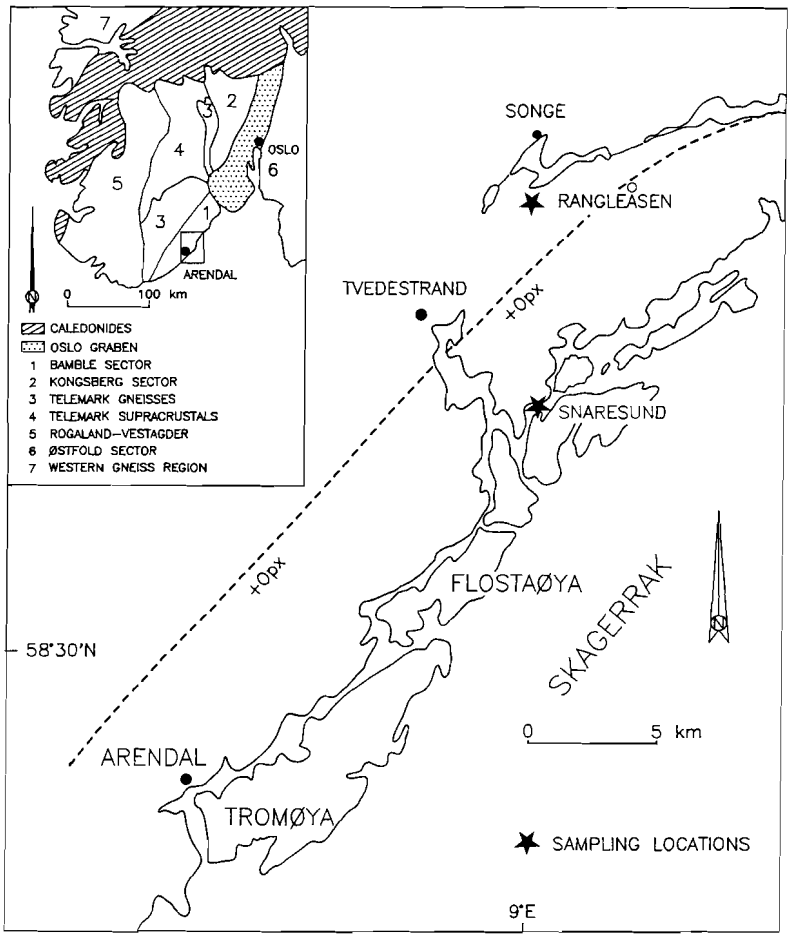

Figure. 6.1. Location map of the Arendal-Tvedestrand area, Bamble Sector, south Norway. Opx-isograd is after Field and Clough (1976). Geological division of southern Norway (inset) has been adapted from Verschure (1985).

The sapphirine-bearing rocks of the Snaresund locality were first described by Touret & de la Roche (1971). Subsequently Lamb (1981) presented a detailed study of several sapphirine-bearing occurrences from the Bamble Sector including the Snaresund and Rangleåsen localities. Högbomite was not reported in either study. The occurrence of högbomite in such high-grade aluminous and silica-poor rock types would not be surprising,

since it has been reported from similar aluminous high-grade, regional metamorphic rocks from Australia (Woodford & Wilson, 1976), W. Greenland (Ackermand et al., 1983), India (Grew et al., 1987) and Antarctica (Grew et al., 1990).

Högbomite was first reported from Norway by Schetelig (1917) in iron-ores from the Fe-Ti-V Rödsand deposit, near Kristiansund. Kolderup (1928) described högbomite associated with ilmenite-ores from the Sogn district and from the Bergen district associated with iron-ores in anorthositic rocks (Kolderup, 1936).

The present paper, which was largely motivated by the extensive review on högbomite occurrences by Petersen et al. (1989) and the numerous reports by Grew and coworkers (1987, 1989, 1990), describes the detailed petrography and mineral chemistry of the Bamble högbomites and associated minerals and discusses the conditions of their formation. As far as we are aware this is only the fourth report of högbomite from Norway, and the first in which compositional data are given.

PETROGRAPHY

At Snaresund the only högbomite-bearing sample (MA818) was collected from the core of a 0.4 m thick sapphirine-bearing lens-shaped outcrop within a layered sequence of acid to intermediate gneisses, quartzites and metabasites. The outer zone of the lens is dominantly phlogopite (60-80 vol.%) with minor amounts of orthopyroxene, gedrite, cordierite, sapphirine, spinel, corundum, rutile and garnet. An intermediate zone between the core and outer zone consists of orthopyroxene + gedrite + plagioclase (An% 50) with minor phlogopite, cordierite and rutile. The core consists of alternating layers of orthopyroxene poikiloblasts + phlogopite ± cordierite + plagioclase (An% 31-33) + quartz and cordierite + sapphirine + spinel + corundum. Minor rutile and trace amounts of ilmenite are present in the sample. Ilmenite shows variable amounts of hematite exsolution (Lamb, 1981). Embayed sapphirine aggregates and grains that are in optical continuity separate anhedral spinel and/or corundum from a polygonal fabric of cordierite. Spinel is locally found in direct contact with corundum, but, generally, these minerals are separated by sapphirine. The green to black anhedral spinels show a moderate degree of magnetite exsolution. Some spinel grains are replaced by aggregates of magnetite, corundum and rarely chlorite. Högbomite is restricted to the alteration aggregates after spinel containing rutile and/or ilmenite inclusions or intergrowths. Högbomite forms euhedral to subhedral grains up to 100 μm partially rimming rutile and/or ilmenite (Fig. 6.2). Högbomite also occurs adjacent to spinel and sapphirine.

Sample PT160 was collected west of Rangleåsen from a 0.5-2 m thick horizon in a layered sequence of cordierite-orthoamphibole gneisses and garnet-amphibolites. The layer

consists of a decussate texture of euhedral orthoamphibole grains (75-90 vol.%) intergrown or interfingered with green to black spinel (1-15 vol.%). Sapphirine (1-3 vol.%) commonly forms a discontinuous rim between orthoamphibole and spinel but may also occur as solitary grains intergrown with orthoamphibole. Pale brown phlogopite, orthopyroxene, rutile, and ilmenite are present in minor amounts. Euhedral monazite is present in trace amounts in sample PT160 but occurs as an important accessory mineral (up to 5 vol.%) in many other samples from this locality. Sample PT160 is cut by linear retrograde zones or fractures along which orthoamphibole, sapphirine and biotite are altered to chlorite. Spinel grains cut by these zones show more extensive magnetite exsolution and, locally, are pseudomorphosed by magnetite, corundum and chlorite. Spinel grains outside these zones exhibit only minor magnetite $\pm$ corundum exsolution. Högbomite occurs exclusively within the alteration zones. Small euhedral to subhedral grains, often in the absence of another Ti-bearing phase, are located on or in the margins of spinel and pseudomorphs of spinel. Larger euhedral grains occur in fractures within the decomposed spinels and along spinel-rutile and spinel-ilmenite contacts. Additionally, högbomite can be found in grain contact with orthoamphibole and sapphirine, but has not been found with biotite. Breakdown of högbomite was not observed in either sample MA818 or sample PT160.

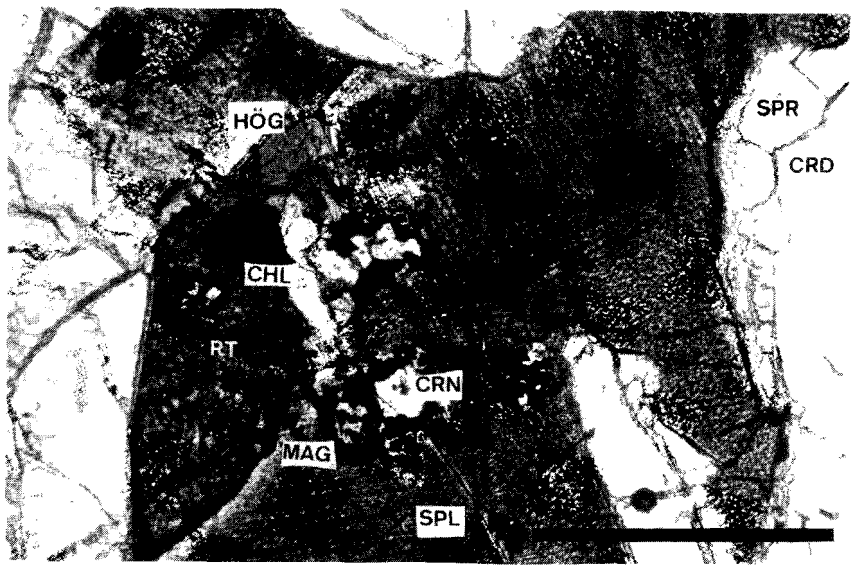

Figure 6.2. Photomicrograph of sample MA818 showing the replacement of spinel (Spl) adjacent to rutile (Rt) by högbomite (Hög), corundum (Cor), magnetite (Mag) and chlorite (Chl). Spinel grains are dusted due to exsolved magnetite. Scale bar = 200 μm.

MINERAL CHEMISTRY

Minerals in sample MA818 were analysed with a JEOL JXA-8600 superprobe at 15 kV and 10 nA at the University of Utrecht; mineral and synthetic compounds were used as standards. Raw count data were corrected with a Tracor Northern PROZA correction program. Analyses of minerals in sample PT160 were performed using the Cameca electron microprobe (Camebax Micro), at 15 kV, 10 nA with PAP (Pouchou & Pichoir, 1984) correction at the University of Kiel, Germany. Representative analyses of högbomite and associated minerals are listed in Tables 6.1 and 6.2.

The **högbomites** from both samples are unzoned and display no major compositional differences within the sample. Compared to those from sample PT160 the högbomites from sample MA818 are distinctly richer in TiO_2, lower in Al_2O_3 and MgO and slightly higher in Fe as FeO (see Tables 6.1 and 6.2 for specific ranges). ZnO (below detection limit in MA818), MnO and Cr_2O_3 values are low. SiO_2, NiO, CaO, K_2O, Na_2O, Cl and F are below detection limit. $Mg/(Mg+Fe_{Tot})$ range 0.51 (MA818) and 0.60-0.63 (PT160).

Oxide totals of the högbomite analyses with Fe_{tot} = FeO are well below 100 %, 96.71-97.91 % for MA818 and 98.36-98.8 % for PT160. The deficit could be made up by Fe^{3+}, H_2O and/or unanalysed light elements such as BeO and Li_2O. Calculation of Fe^{3+} on basis of the anhydrous general formula for högbomite ($R^{2+}{}_{2-2x}Ti_xR^{3+}{}_4O_8$, with R^{2+} = Mg, Fe^{2+}, Mn, Zn, Co,... Ni and R^{3+} = Al, Fe^{3+}, Cr and V) as proposed by Zakrzewski (1977) yields appreciable Fe^{3+}, $Fe^{3+}/(Fe^{3+}+Fe^{2+})$ = 0.46-0.47 and 0.35-0.38 respectively for MA818 and PT160, with recalculated oxide totals close to 100 % for PT160 but still far below 100 % for sample MA818 (see Tables 6.1 and 6.2). The correlation of the total cation content with Ti used by Zakrzewski (1977) to calculate Fe^{3+} is probably invalid (c.f. Grew et al., 1987; Petersen et al., 1989) or perhaps only applicable to anhydrous polytypes. Schmetzer & Berger (1990) observed the general replacement scheme $(2a-b)Mg^{2+} + (2b)Al^{3+} \longrightarrow (a+b)Ti^{4+}$ in iron-free högbomite-24R from Tanzania (högbomite can be described as various stacking sequences or polytypes of spinel-like ($R^{2+}Al_2O_4$) and nolanite-like ($TiAl_4O_8$) layers; terminology is taken from Peacor, 1967), and on basis of structure refinements, Gatehouse & Grey (1982) found one Ti per 22 cations and 32 anions of a 8H polytype högbomite instead of two Ti predicted by Zakrzewski's formula.

The refinements of Gatehouse & Grey (1982) further suggest the presence of 2 hydroxyl-groups, on basis of undersaturated oxygen-positions, giving an anion composition of 30 O + 2 OH instead of 32 O. However, the formula of Gatehouse & Grey (1982) gives more than 22 cations for complete analyses of 36R and 10H polytypes (see Rammlmair et al., 1988) and appears, therefore, only applicable to 8H polytypes. Evidence for the presence of water in the högbomite structure is still very inconclusive. While Nel (1949) reported H_2O-values of 1.10 and 1.29 wt.% H_2O^+ in iron-rich högbomites, infrared spectra of Fe-Ti-

Table 6.1.
Chemical compositions of minerals in sample MA818, Snaresund, Bamble Sector, south Norway.

	Högbomite#		range	Spl	Ilm	Mag	Crn	Spr	Crd
SiO_2	0.00	0.00	0.00	0.00	0.38	0.00	0.00	12.70	48.91
TiO_2	9.95	9.95	9.95 - 10.14	0.02	51.51	0.15	0.03	0.04	0.03
Al_2O_3	60.06	60.06	58.90 - 60.06	63.55	0.00	0.36	99.82	62.29	33.26
Cr_2O_3	0.00	0.00	0.00 - 0.12	0.24	0.00	0.00	0.11	0.00	0.00
Fe_2O_3	3.80	8.51	-	2.08	3.55	67.37	0.79	2.17	-
FeO	14.15	9.91	17.37 - 17.57	19.12	42.30	30.67	-	6.96	3.16
ZnO	0.00	0.00	0.00	0.83	0.00	0.00	0.00	0.00	0.00
MnO	0.12	0.12	0.00 - 0.12	0.00	0.28	0.00	0.00	0.11	0.00
MgO	10.22	10.22	10.18 - 10.22	14.58	2.34	0.00	0.00	15.81	11.63
CaO	0.00	0.00	0.00	0.00	0.00	0.12	0.00	0.00	0.00
Na_2O	0.00	0.00	0.00	0.00	0.00	0.00	0.00	0.00	0.16
H_2O(calc)	1.48	0.00	-	-	-	-	-	-	-
Total	99.78	98.77		100.42	100.36	98.67	100.74	99.86	97.15
O-basis	31	32		4	3	4	3	20	18
Si	0.000	0.000		0.000	0.009	0.000	0.000	1.516	4.978
Ti	1.520	1.551		0.000	0.958	0.004	0.000	0.004	0.002
Al	14.380	14.673		1.954	0.000	0.017	1.991	8.766	3.991
Cr	0.000	0.000		0.005	0.000	0.000	0.001	0.000	0.000
Fe^{3+}	0.580	1.327		0.041	0.066	1.975	0.010	0.195	-
Fe^{2+}	2.405	1.718		0.418	0.875	0.999	-	0.695	0.269
Zn	0.000	0.000		0.016	0.000	0.000	0.000	0.000	0.000
Mn	0.021	0.022		0.000	0.006	0.000	0.000	0.011	0.000
Mg	3.095	3.158		0.567	0.086	0.000	0.000	2.814	1.765
Ca	0.000	0.000		0.000	0.000	0.005	0.000	0.000	0.000
Na	0.000	0.000		0.000	0.000	0.000	0.000	0.000	0.032
Sum	22.000	22.449		3.001	2.000	3.000	2.002	14.000	11.030
X_{Mg}	0.563	0.648		0.576	0.089	-	-	0.802	0.868
$X_{Fe^{3+}}$	0.194	0.436		0.089	0.070	0.664	-	0.219	-

K, F and Cl below detection limit. Mineral abbreviations after Kretz (1983). Fe^{3+} in spinel, ilmenite, magnetite and sapphirine were calculated assuming perfect stochiometry.
- H_2O and Fe^{3+} in högbomite calculated respectively on basis of 32 O + 2 OH, 22 cations (Gatehouse and Grey, 1982) and 32 O (Zakrzewski, 1977). $X_{Mg} = Mg/(Mg+Fe^{2+})$ and $X_{Fe^{3+}} = Fe^{3+}/(Fe^{2+}+Fe^{3+})$.

rich högbomites obtained by Zakrzewski (1977) and a wet-chemical analysis of a zincian högbomite (Wilson, 1977) did not yield any meaningful H_2O or hydroxyl content.
Nonetheless low oxide totals have been reported from an increasing number of (frequently 8H) högbomite occurrences (Čech et al., 1976; Coolen, 1981; Mancktelow, 1981; Ackermand et al., 1983; Beukes et al., 1986, sample 217-6; Gieré, 1986; Grew et al., 1987; Grew et al., 1990). This deficit appears not to be due to BeO or Li_2O, at least in cases where these constituents have been sought (Wilson, 1977; Coolen, 1981; Grew et al., 1987).

Table 6.2. Chemical compositions of minerals in sample PT160, Rangleåsen, Bamble Sector, south Norway.

	Högbomite#		range	Spl	Ilm	Mag	Chl	Crn	Rt	Ged	Spr
SiO_2	0.00	0.00	0.00	0.00	0.00	0.00	26.36	0.00	0.00	44.69	13.29
TiO_2	5.66	5.66	5.66 - 5.75	0.00	53.11	0.00	0.00	0.13	98.50	0.29	0.10
Al_2O_3	62.11	62.11	61.21 - 62.11	64.71	0.00	0.00	25.21	99.04	0.04	17.87	61.81
Cr_2O_3	0.00	0.00	0.00 - 0.05	0.02	0.00	0.00	0.00	0.00	0.02	0.00	0.03
Fe_2O_3	13.93	6.33	-	2.81	0.00	68.02	-	0.98	-	-	3.27
FeO	3.85	10.70	15.61 - 16.98	15.01	45.83	29.93	5.23	-	0.23	10.23	3.79
ZnO	0.32	0.32	0.25 - 0.32	0.55	0.00	0.07	0.00	0.00	0.02	0.00	0.04
MnO	0.04	0.04	0.02 - 0.10	0.07	0.00	0.00	0.00	0.00	0.04	0.16	0.08
MgO	14.26	14.26	14.09 - 14.75	17.55	0.04	0.34	27.82	0.00	0.00	21.60	18.16
CaO	0.00	0.00	0.00	0.00	0.00	0.00	0.00	0.00	0.00	0.56	0.00
Na_2O	0.00	0.00	0.00	0.00	0.00	0.00	0.00	0.00	0.00	1.60	0.00
H_2O(calc)	1.54	0.00	-	-	-	-	-	-	-	-	-
Total	101.71	99.41		100.77	98.98	98.36	84.62	100.15	98.85	97.00	100.57
O-basis	31	32		4	3	4	28	3	2	23	20
Si	0.000	0.000		0.000	0.000	0.000	5.156	0.000	0.000	6.250	1.563
Ti	0.831	0.873		0.000	1.013	0.000	0.000	0.002	0.998	0.031	0.009
Al	14.291	15.023		1.946	0.000	0.000	5.813	1.990	0.001	2.946	8.568
Cr	0.000	0.000		0.000	0.000	0.000	0.000	0.000	0.000	0.000	0.003
Fe^{3+}	2.047	0.977		0.054	0.000	2.000	-	0.013	-	-	0.289
Fe^{2+}	0.629	1.836		0.321	0.973	0.978	0.856	-	0.003	1.197	0.372
Zn	0.046	0.048		0.010	0.000	0.002	0.000	0.000	0.000	0.000	0.003
Mn	0.007	0.007		0.002	0.000	0.000	0.000	0.000	0.000	0.019	0.008
Mg	4.149	4.363		0.667	0.002	0.020	8.112	0.000	0.000	4.503	3.184
Ca	0.000	0.000		0.000	0.000	0.000	0.000	0.000	0.000	0.084	0.000
Na	0.000	0.000		0.000	0.000	0.000	0.000	0.000	0.000	0.434	0.000
Sum	22.000	23.127		3.000	1.988	3.000	19.937	2.004	1.002	15.464	14.000
X_{Mg}	0.868	0.817		0.675	-	0.020	0.905	-	-	0.790	0.895
$X_{Fe^{3+}}$	0.765	0.347		0.144	0.000	0.672	-	-	-	-	0.437

K, Ni, F and Cl below detection limit. See Table 1 for other notes.

Assuming that the deficit is due to OH and possibly Fe^{3+} counted as Fe^{2+} and that the högbomites are 8H polytypes, we also calculated our högbomite analyses on basis of 30 O + 2 OH. With recalculated oxide totals close to 100 % these assumptions could be valid for sample MA818, but are not supported by the higher oxide totals in PT160. Clearly, the assumption of Zakrzewski (1977) gives the preferable formula (10H-polytype ?) for PT160, while the formula for the 8H-polytype is favoured for MA818, suggesting that the two högbomites belong to different polytypes. This is supported by the large difference in Ti content between the two samples, that is the proportion of spinel-like and nolanite-like layers differs for the two högbomites.

Spinels are principally hercynite-spinel solid solutions with low gahnite (MA818: 1.4-3.7 mol. %; PT160: 0.8-1 mol. %) and magnetite contents (MA818: 1.5-2.0 mol. %; PT160: 2.0-2.8 mol. %). All analysed spinels from sample MA818 show weak compositional zoning with X_{Mg} (0.58-0.61) and ZnO (0.75-1.95 wt.%) increasing from rim to core. The unzoned spinels from sample PT160 are more magnesian with X_{Mg} = 0.67-0.70.

Sapphirine grains of sample PT160 lie on the join between the 2:2:1 and 7:9:3 compositions in terms of $(Mg,Fe^{2+})O$:(Al, Fe^{3+}, $Cr)_2O_3$:SiO_2. The compositions of MA818 sapphirines are slightly more aluminous than the 7:9:3 composition and are, therefore, termed peraluminous (Schreyer & Abraham, 1975). X_{Mg} values are 0.80-0.83 (MA818) and 0.89-0.90 (PT160). The calculated $Fe^{3+}/(Fe^{2+}+Fe^{3+})$ ratios are 0.21-0.28 (MA818) and 0.39-0.44 (PT160).

The **orthoamphibole** in sample PT160 is a gedrite with Al^{IV}, Na (A) and X_{Mg} of respectively 1.75-1.87, 0.40-0.43 and 0.79-0.81. Stoichiometry on basis of 15 cations (excluding Na+K, which are assigned to the A-site) suggests 0.09-0.24 Fe^{3+} per formula unit and $Fe^{3+}/(Fe^{3+}+Fe^{2+})$ of 0.08-0.21. TiO_2 values range 0.29-0.44 wt.%.

Chlorite was only analysed in sample PT160 and is an Al-rich clinochlore with X_{Mg} and Al^{IV} ranging respectively 0.90-0.91 and 2.45-2.84. Magnetite contains traces of Ti, Al, Cr, Mn, Mg, Ca Zn (in PT160, but below detection limit in MA818).

Corundum contains 0-0.13 wt.% TiO_2, 0-0.11 wt.% Cr_2O_3 and 0.48-0.88 wt.% Fe_2O_3. **Rutile** is nearly pure TiO_2 with minor FeO (0.23 wt.%) and traces (< 0.15 wt.%) of ZnO (PT160), MnO, Cr_2O_3 and Al_2O_3. **Ilmenite** from sample MA818 contains 2.34-3.00 wt.% MgO and minor MnO (<0.50 wt.%). Ilmenite from sample PT160 is nearly pure $FeTiO_3$ with less than 0.15 wt.% MgO and Al_2O_3.

HÖGBOMITE GENESIS

The primary assemblages orthopyroxene-phlogopite-cordierite-spinel-corundum (MA818), gedrite-spinel (PT160) and the sapphirine coronas formed by the generalized reactions based on textural relations: spinel + corundum + cordierite ⟶ sapphirine + vapour (MA818) and gedrite + spinel + corundum ⟶ sapphirine + vapour (PT160), developed coevally with the upper-amphibolite to granulite facies regional metamorphic event (M3b according to Visser & Senior, 1990) in the Arendal-Tvedestrand area of the Bamble Sector. The second reaction is more Al-rich on the product than on the reactant side suggesting, although primary corundum is not observed in the sample, that corundum must have participated in the reaction. Temperature estimates on the basis of sapphirine-spinel (Owen & Greenough, 1991; with estimated precision of ± 100 °C) and orthopyroxene-phlogopite (Sengupta et al., 1990; with estimated precision of ± 50 °C) Mg-Fe exchange reactions for this event yield 773-815 °C (MA818) and 811-844 °C (PT160) for sapphirine-spinel(rim) pairs and 775-823 °C at 7 kbar for coexisting orthopyroxene-phlogopite pairs (MA818).

The spatial relationship with spinel in the alteration zones in PT160 and with the alteration aggregates after spinel in MA818 suggests a secondary formation of högbomite from the primary high-grade spinel-bearing assemblages. The breakdown of spinel in the absence of Ti-bearing phases took place according to the generalised reaction:

$$\text{spinel} \pm \text{sapphirine} \pm \text{gedrite} + H_2O + O_2 \longrightarrow \text{corundum} + \text{magnetite} \pm \text{chlorite.} \quad (1)$$

A prerequisite for the development of large högbomite grains in PT160 and högbomite in MA818 is the presence of ilmenite and/or rutile intergrowths with or inclusions in spinel suggesting the generalised reaction:

$$\text{spinel} + \text{ilmenite/rutile} \pm \text{sapphirine} \pm \text{gedrite} + H_2O + O_2 \longrightarrow \text{högbomite} \pm \text{corundum} \pm \text{magnetite} \pm \text{chlorite.} \quad (2)$$

The continued stability of spinel and ilmenite and/or rutile outside of the alteration zones in PT160 implies that the introduction of a hydrous fluid was essential for the production of högbomite (reaction 2). The increased exsolution of magnetite within spinel that are cut by the alteration zones and the high $Fe^{3+}/(Fe^{2+}+Fe^{3+})$ ratio that is calculated for högbomite suggests increased oxygen fugacity levels associated with the hydrous fluids. Oxygen fugacity levels in sample MA818 are inferred from the similar $Fe^{3+}/(Fe^{2+}+Fe^{3+})$ ratios of primary and secondary minerals and suggest very little change accompanied högbomite formation.

Temperature conditions of högbomite-forming reaction 2 can not be determined from the mineralogy of the two samples. Biotite-garnet thermometry in other samples from the Snaresund lens (Thijssen, 1990; unpublished data) in which cordierite is pinitised and sapphirine is chloritised have, therefore, been used to estimate the temperature of reaction 2. Adjacent biotite and garnet grains, which are believed to have reequilibrated during this rehydration event, yield 550-620 °C at 6-7 kbar. These P-T conditions are similar to those of the first stages of rehydration during the Sveconorwegian orogeny (M III according to Nijland et al., 1993; early M_4 according to Visser & Senior, 1990) before uplift occurred. Garnet-core and matrix biotite pairs in the samples analysed by Thijssen (1990) yield 760-825 °C at 6-7 kbar, consistent with T-estimates of primary assemblages in MA818 and PT160.

Gedrite could have been a source of Ti for small högbomite grains located on or in the margins of spinel and spinel pseudomorphs and not associated with ilmenite or rutile in sample PT160 (TiO_2 in spinel is below detection limit). However, Ackermand et al. (1983) concluded that a comparable TiO_2 content (up to 0.43 wt.%) of gedrites associated with högbomites in the Fiskenaesset rocks was insufficient to enable högbomite to form in the absence of rutile. Alternatively Ti could have been mobilised along grain boundaries from nearby (5 to 20 mm distance) alteration aggregates which involve ilmenite and/or rutile. Introduction of Ti from outside the local rock system by Cl^-, F^- and/or PO_4^{3-}-complexes analogous to those described by Gieré (1986) is considered unlikely since apatite and monazite are not associated with högbomite and Cl and F in högbomite and coexisting hydrous phases are below or close to detection limit. The partitioning of elements between högbomite and spinel appears to be close to unity for Fe-Mg in both samples, with högbomite showing minor enrichment in iron relative to spinel. The Fe-Mg partitioning is consistent with the partitioning data of Coolen (1981), Gieré (1986) and Rammlmair et al. (1988) and supports reaction 2 deduced from petrography. The partitioning data of Zn between högbomite and spinel, expressed in terms of the partitioning coefficient K_D Zn-Fe(Hög-Spl) [$K_D = (Zn/Fe)^{Hög}/ (Zn/Fe)^{Spl.}$ with Fe as total Fe], show a moderate depletion in högbomite relative to spinel in sample PT160 (K_D = 0.56-0.63), while Zn was not detected in högbomite from sample MA818 although coexisting spinel contains 0.75-1.95 wt.% ZnO (K_D = 0.00). The distribution of zinc between högbomite and spinel pairs from other localities is not uniform. The majority of the occurrences show K_D in the range of 0.40-0.75 (e.g. Beukes et al., 1986; Gieré, 1986; Spry & Petersen, 1989; Grew et al., 1990). A very low K_D (0.017) was recorded by Rammlmair et al. (1988) and $K_D \geq 1$ was found in the studies by Beukes et al. (1986; sample 023 WDB), Grew et al. (1989) and Spry & Petersen (1989; sample PS84-132).

In case of the Bamble högbomite, the difference in Zn distribution for the two samples could be due to their possible difference in polytype. Data available in the literature

concerning this point are still scarce and inconclusive, but the data seem to suggest that Zn-partitioning is independent of the polytype. $K_D < 1$ is recorded for 18R, 8H and most 10H högbomite-spinel pairs (Rammlmair et al., 1988; Petersen et al., 1989; Grew et al., 1990). Some 10H (e.g. Beukes et al., 1986; Grew et al., 1987) and mixed 8H/10H (Petersen et al., 1989) högbomite-spinel pairs are shown to have a $K_D \geq 1$.

The irregular distribution of Zn may depend on the geochemical behaviour of the gahnite component ($ZnAl_2O_4$) in spinel in assemblages without other Zn-bearing phases such as staurolite.

Increase of the gahnite component will stabilize hercynite-spinel solid solutions with decreasing temperatures and increasing fO_2 (Spry & Scott, 1986). Increased aH_2O will involve decomposition of the gahnite component according to:

$$ZnAl_2O_4 + H_2O \longrightarrow Al_2O_3 + Zn^{2+} + 2OH^- \quad (3),$$

liberating zinc which then becomes available for incorporation in högbomite. In many localities, högbomite formation is reported to have formed during the cooling or uplift stages following peak metamorphic conditions in amphibolite- and granulite-facies terrains (e.g. Grew et al., 1987; Rammlmair et al., 1988; Grew et al., 1990). The increase of fO_2 and/or decrease in temperature associated with this högbomite formation will tend to concentrate the gahnite component in the decomposing spinel at contacts with högbomite. This may explain the observed Zn-depletion in högbomite relative to spinel in many of the occurrences. A good example of this is reported by Rammlmair et al. (1988) who observed a discontinuously zoned spinel with extreme Zn-enrichment in a very thin rim adjacent to högbomite. Variations in aH_2O and fO_2 may account for the observed variation in Zn-partitioning. The difference in Zn-partitioning between samples PT160 and MA818 is believed to be caused by higher aH_2O in sample PT160. This is supported by more extensive retrogression in PT160.

ACKNOWLEDGEMENTS

We are indebted to R. Poorter, T. Bouten (Utrecht), B. Mader and D. Ackermand (Kiel) for their assistance with electron microprobe analysis and to E.S. Grew, C. Maijer, T.G. Nijland, W. Schreyer, P.G. Spry and M. Zakrzewski for their critical reviews of the manuscript. C. Maijer kindly provided sample MA818. Financial support for fieldwork and research by the Dr. Schürmann (to D.V.), the Rens-Holle (to P.H.M.T.) and the Molengraaff Foundations (to P.H.M.T.) is gratefully acknowledged.

CHAPTER 7

ON AMMONIUM IN UPPER-AMPHIBOLITE FACIES CORDIERITE-ORTHOAMPHIBOLE-BEARING ROCKS FROM RØD, BAMBLE SECTOR, SOUTH NORWAY.

ABSTRACT

NH_4^+ values of 1100-3000 ppm and 250-458 ppm have been measured in biotites and whole rock samples respectively, from cordierite-orthoamphibole-bearing rocks at Rød, Bamble Sector, south Norway. The results indicate that given:

- suitable, (Mg,Fe,Al)-rich and (Ca,Na)-poor, bulk compositions,
- no high-grade (breakdown-)reactions involving biotite,
- reducing conditions defined by graphite-bearing assemblages, and
- an ammonium-rich protolith,

significant amounts of ammonium in biotite can survive high-grade metamorphism. The high ammonium contents are considered supplementary evidence for a sedimentary origin of the cordierite-orthoamphibole-bearing rocks. The significant quantities of N_2 previously reported in quartz from this locality are thought to be genetically related to the retrogression of the ammonium-bearing biotites.

INTRODUCTION

The presence of substantial amounts of ammonium in sedimentary, metamorphic and igneous rocks has been shown by the studies of e.g. Urano (1971), Honma & Itihara (1981) and Duit et al. (1986). The ammonium levels in igneous systems commonly range 10-100 ppm for granitic rocks and much lower, 1-12 ppm, for basic and ultrabasic rocks (Hall 1988a, b). Sedimentary rock types show variable ammonium levels due to the inheritance of nitrogen from organic matter. Shales (Urano 1971; Haendel et al., 1986) show high ammonium levels of several hundred ppm and occasionally over one thousand ppm, while levels in sandstones and cherts are in the 1-150 ppm range.

Ammonium concentrations in metamorphic rock types, in which ammonium may substitute isomorphously for potassium in minerals such as biotite, K-feldspar, plagioclase and muscovite, mainly depend on the sedimentary or igneous signature of the pre-metamorphic precursor. In principle, high ammonium levels may be used to indicate the sedimentary signature of the rock (Itihara & Honma 1979), while low levels alone are not

enough to distinguish between a possible igneous or sedimentary origin of the rock. The primary ammonium content, however, can be modified due to the breakdown or formation of ammonium-bearing minerals during both prograde and retrograde regional or contact metamorphism (Duit et al. 1986; Cooper & Bradley 1990) and hydrothermal alteration processes (Cooper & Bradley 1990).

The occurrence of nitrogen in metamorphic fluids is reported by an increasing number of fluid inclusion studies. Breakdown or formation of ammonium-bearing minerals may involve N_2 (and NH_3?) as trace, minor or even dominant fluid species. In other words, the presence of these fluid species may serve as an exploration tool for ammonium-bearing minerals and rock-types, as demonstrated by Duit et al. (1986) who investigated the nitrogen content of rock types in which nitrogen-rich fluid inclusions were described (Kreulen & Schuiling 1982).

Nitrogen-bearing fluids have been described by fluid inclusion studies in the high-grade metamorphic Bamble Sector, south Norway (Touret & Dietvorst 1983; Touret 1985; Touret 1987; Ploegsma 1989). Touret (1987) presented preliminary fluid inclusion data obtained from a cordierite-orthoamphibole-bearing sample indicating "abundant CO_2 inclusions mixed with significant quantities of N_2 and some other unknown species (not CH_4), giving strange and yet unexplained microthermometric results" at excursion stop 2.3 of the NATO south Norway geological excursion in July 1984, near Rød in the central part of the Bamble Sector. The cordierite-orthoamphibole rocks occur within a unit consisting of metasediments (nodular gneisses, sillimanite-garnet-biotite schists and quartzites) and garnet-bearing amphibolites of undetermined origin. Various explanations have been presented concerning the origin of cordierite-orthoamphibole-bearing rocks in the Bamble and genetically related Kongsberg Sectors. Jøsang (1966), Touret (1979) and Beeson (1988) suggested an evaporitic/ metasedimentary origin, while metasomatic or hydrothermal alteration associated with metagabbros was suggested as the origin of these rocks by e.g. Bugge (1943), Starmer (1976) and Munz (1990). Morton et al. (1970) proposed a formation from hydrothermally altered basic volcanics. The nitrogen-rich fluid inclusions thus not only provide a good opportunity to test the presence of ammonium-rich rock types in high grade metamorphic terrains but may also be used to evaluate the possible origin of the cordierite-orthoamphibole-bearing rocks at this locality. For this purpose, ammonium contents of both biotite and whole rock of two cordierite-orthoamphibole-bearing samples from the Rød locality were investigated.

SAMPLES

The locality investigated (5030-65096, map references are taken from the 1:50.000 map Tvedestrand, 1612 II) in this study is situated in the Søndeled-Sandnesfjord area, Bamble Sector, south Norway. The major structures and petrology of the rocks in this area have been described by Starmer (1976). The main geologic characteristics of the Proterozoic of the Bamble Sector have been summarized by Starmer (1985). Modal amounts and mineral associations in the selected samples are given in Table 7.1.

Table. 7.1.
Mineralogy and modal composition (%) of specimens studied, Rød locality, Bamble Sector, south Norway.

Sample	DV 122	MA 780
Quartz	27.8	8.2
Biotite	26.2	12.3
Garnet	32.6	42.6
Cordierite	8.0	14.0
Orthoamphibole	1.2	15.4
Tourmaline	-	0.2
Kornerupine	-	0.4
Graphite	0.2	0.5
Ilmenite	0.4	0.2
Rutile	1.2	2.0
Apatite	1.0	1.8
Dumortierite*	-	0.1
Chlorite*	0.8	0.7
Muscovite*/pinite*	0.6	1.6

* - secondary phases

The samples studied are a quartz-biotite-garnet-cordierite ± orthoamphibole schist (DV122) and a melanocratic quartz-garnet-orthoamphibole-biotite-cordierite-kornerupine-rock (MA780). Euhedral to subhedral brown biotite (Table 7.2) is the only major potassium-bearing phase in both samples; plagioclase and K-feldspar are absent. Together with euhedral orthoamphibole and cordierite (wet chemical analysis: 0.17 wt.% CO_2, 2.36 wt.% H_2O and 0.04 wt.% K_2O; IR analysis: 0.30 wt.% type-I H_2O, 0.17 wt.% type-II H_2O and 1.05 wt.% CO_2), biotite defines a very weak foliation in MA780. An early generation of biotite is included in both orthoamphibole and cordierite. Garnet developed as large (max. 3 cm) anhedral to subhedral poikiloblasts overgrowing and consuming biotite, cordierite and orthoamphibole. Cordierite-quartz symplectites developed very

irregularly between garnet and orthoamphibole. In MA780 colourless kornerupine occurs as subparallel to irregular shaped aggregates intergrown with orthoamphibole. Accessory phases in both samples are rutile, apatite, ilmenite and graphite. Tourmaline occurs only in MA780. Graphite usually occurs intimately intergrown with biotite and occasionally with garnet. Along narrow (up to 4 mm) retrograde zones or cracks pinite, muscovite, chlorite and rarely pink dumortierite (Visser & Senior 1991) form after cordierite, garnet, biotite and orthoamphibole.

Garnet-biotite (Ferry & Spear 1978) and garnet-cordierite (Holdaway & Lee 1977) Fe-Mg exchange reactions indicate temperature ranges at 7 kbar of 770-805 °C (MA780, von Scheibler 1988) and 730-760 °C (DV122) for garnet cores and matrix biotites and 690-725 °C (MA780) and 655-700 °C (DV122) for garnet cores and matrix cordierites. Temperature estimates calculated from garnet-biotite rims and garnet-cordierite rims, assuming pressures of 4-5 kbar (Visser & Senior 1990), are 540-620 °C, 530-590 °C (MA780) and 500-540 °C, 520-550 °C (DV122) respectively.

Table 7.2.
Average biotite composition in samples DV 122 and MA 780

	DV 122 (n=15)	MA 780 (n=26)
SiO_2	38.56	37.44
TiO_2	1.99	2.63
Al_2O_3	17.38	17.01
FeO	11.72	11.83
MnO	0.15	0.01
MgO	17.08	16.21
CaO	0.03	0.00
Na_2O	0.47	0.31
K_2O	7.04	7.80
BaO	n.a.	0.10
Cl	0.38	n.a.
Total	94.80	93.34

n.a. = not analysed

ANALYTICAL PROCEDURES

Mica fractions of 125-250 μm were separated and purified by means of a Frantz magnetic separator, heavy liquids and handpicking. For wet chemical analysis the whole rock samples and mica fractions were dissolved in a concentrated HF/H_2SO_4 solution for 24 hours at 80 °C. The decomposed samples were subsequently neutralized with a saturated solution of boric acid. The ammonium was distilled with a Kjeldahl apparatus into a weak (0.05 N) H_2SO_4 solution. The ammonium was measured colorimetrically with a Perkin-Elmer type 550S spectro-photometer applying the Berthelot coloring reaction (Verdouw et al. 1978) at λ = 660 nm.

The characteristic absorption bands of the ammonium molecule occur at about 3250, 3060 and 2850 cm^{-1} for N-H stretching and at 1430 cm^{-1} for N-H-N bending. The peak intensity of the 1430 cm^{-1} bending vibration is proportional to the NH_4^+ concentration. Duit et al. (1986) calibrated the absorbances at 1430 cm^{-1} of micas against the concentrations of nitrogen liberated by heating under vacuum. Their calibration curve and KBr-disk preparation techniques were used in this study. Possible disturbance of the 1430 cm^{-1} vibration by carbonate vibrations was prevented by a weak acid treatment of the powdered samples before preparation. The infrared absorption spectra of the mica fractions were measured with a Perkin Elmer 580 infrared spectrophotometer. The total ammonium contents of whole rock and separated biotites are given in Table 7.3.

Table 7.3.
Ammonium concentration (ppm) in biotite and whole-rock

Sample No.	Kjeldahl analysis	Infrared absorption
DV 122 Biotite	1120 (n=2)	1080 (n=1)
MA 780 Biotite	3000 (n=4)	3200 (n=3)
DV 122 WR	250 (n=2)	-
MA 780 WR	458 (n=5)	-

n - number of analyses

RESULTS AND DISCUSSION

The Kjeldahl results are reproducible within 5-8 % for whole rock and 7-10 % for biotite. Correlation of the ammonium contents in biotite determined by Kjeldahl and infrared techniques is very good. The ammonium content of the biotites, 1080 in sample DV122 and 3000 ppm in sample MA780 are among the highest ever recorded. Itihara & Suwa (1985) recorded 1558 ppm NH_4^+ (n=1) for biotite in tourmaline-muscovite-biotite schist from the Svecofennian Basement in Finland, and 1060-1940 ppm (n=16) were reported in biotites from low to medium grade schists and quartzveins from Dôme de l'Agout, France (Duit et al. 1986). The ammonium concentration of biotite from sample MA780 is comparable to the richest NH_4^+-bearing biotite found thus far (2000-5000 ppm by IR or 3000 ppm by wet chemical analysis; Darimont et al. 1988). The whole rock contents are 250 and 458 ppm NH_4^+ and are compatible with biotite as the only major ammonium-bearing phase. These high values and the presence of primary graphite, thought to have been derived from decomposed organic material, are compatible with a sedimentary rock precursor. A hydrothermal or metasomatic origin related to metagabbros can be precluded on basis of the absence of metagabbros and the absence of any evidence of extensive metasomatic or hydrothermal activity at or near the outcrop. The sedimentary origin of the rocks is also supported by the REE geochemistry of MA780. The REE pattern of MA780 (Visser et al., in preparation) closely resembles that of North American and European Shale Composites (NASC and ES), with LREE enrichment ($(La/Yb)_N$ = 5.3), flat HREE pattern and a distinct negative Eu-anomaly (Eu/Eu* = 0.57). The presence of primary borosilicates indicates that the possible precursor shales, which may have consisted of a mixture of kaolinite/gibbsite, Fe oxides, Mg-rich chlorite, quartz and illite, originally contained a significant amount of boron.

As shown by the geothermometric and geobarometric results ammonium-rich biotite is able to survive P-T conditions of high-grade upper-amphibolite facies. This is in accordance with the experimental data of Bos (1990), who observed the decomposition of the ammonium-phlogopite endmember at conditions of 750 °C and 850 °C at 2 kbar, while intermediate compositions remained stable. The main factors explaining these high ammonium values in biotite are, apart from high initial amounts of ammonium, the Mg,-Fe-, Al-rich and Ca-, Na-poor bulk chemistry of the cordierite-orthoamphibole rocks, which produced biotite-bearing assemblages instead of other possible NH_4^+-(K^+)-bearing phases, and the absence of textural evidence for prograde breakdown reactions involving biotite that might have liberated NH_4^+ to the fluid system or other mineral phases. The presence of graphite in the samples, indicating a relatively low oxygen fugacity, fixes the fNH_3/fN_2 ratio of the coexisting fluid at a relatively elevated level. This will stabilize the

ammonium component of the micas at higher grade conditions (Eugster & Munoz 1966).

Low grade oxidation and retrogradation of the ammonium-bearing biotite along the narrow alteration zones may account for the abundant N_2 in the fluid inclusions. Low grade release of ammonium is in agreement with the N_2 isochores presented by Touret & Dietvorst (1983) and the low densities encountered in all other N_2 fluid inclusions observed so far in the Bamble Sector (Touret 1985; Ploegsma 1989).

ACKNOWLEDGEMENTS

I thank K. Bucher, C. Maijer, J. Munoz, T.G. Nijland, J. Touret and R.G. Trønnes for constructive reviews of the manuscript, C. Maijer for provision of sample MA780, A. van der Eerden for assistance with the Kjeldahl analyses and R. Poorter for assistance with the microprobe analyses. Financial support for fieldwork and research was provided by the Dr. Schürmann Foundation.

CHAPTER 8

CONCLUDING REMARKS

The prograde P-T evolution

From the textural, mineralogical and mineral-chemical data of orthoamphibole-bearing rocks in the Froland area and their interpretation (Chapter 1) it is concluded that, during the early stages of the Kongsbergian orogeny (1.6-1.5 Ga), the prograde metamorphic evolution of the Bamble Sector involves features of both compressional tectonics with crustal thickening- and magmatic thickening (and/or lithospheric thinning) models. The first three successive metamorphic stages (M_1-M_{3a}) of this prograde evolution document a clock-wise P-T path which is compatible with the P-T path experienced by an orogen that has undergone crustal thickening during a continental collision (Schuiling, 1963; Thompson & England, 1984).

The clockwise P-T path is perturbed at high temperatures (600-700 °C) just when slow uplift of the area had started. This perturbation (M_{3b}) essentially involves an additional isobaric temperature increase of ca. 50-100 °C or more at 7 kbar. The anomalously high heat flow may be explained by extensional lithospheric thinning and/or asthenospheric upwelling. These are likely to result in basaltic to andesitic intrusion into, and underplating beneath the crust (Furlong & Fountain, 1986; Harley, 1989). Significant evidence for this intrusive activity is provided by the coastal enderbites and metabasites occurring in the core of the granulite facies area at Arendal and Tromøy (Smalley et al., 1983; Field et al., 1985) and the smaller charnockite-granite bodies east of Gjerstad and at Levang (Starmer, 1991). Starmer (1991) claims several stages of pre- and syn-peak metamorphic magmatic activity during the Kongsbergian orogeny. This may suggest that extensional lithospheric thinning already started *during* the process of crustal thickening (c.f. Loosveld & Etheridge, 1990). De Haas (1992) proposed a mafic underplate at the base of the crust to account for the heat for amphibolite-granulite facies metamorphism. More recently, Nijland & Maijer (1993) developed the concept of a thermal dome in the Arendal area, as the result of elevation of the asthenosphere. Although both De Haas (1992) and Nijland & Maijer (1993) tentatively suggested the underplating respectively the thermal dome to have started during the early Sveconorwegian, they did not exclude an earlier onset.

Isobaric cooling

The first significant retrograde changes of peak metamorphic assemblages in the cordierite-bearing rocks are constrained to have started at relatively high P and T (Chapters 1 and 6). Based on the appearance of one of these assemblages, which consists of talc-kyanite-quartz after cordierite and gedrite (Visser et al., 1990), a near isobaric cooling path following peak metamorphic conditions is established for the Bamble Sector. The time scale of isobaric cooling is tentatively constrained at about 300-400 Ma as no evidence has been found for uplift or retrogression between the Kongsbergian and Sveconorwegian events (e.g. Starmer, 1991).

P-T paths succeeding a clockwise P-T path with contemporaneous extensional lithospheric thinning, and underplating of basaltic or andesitic magmas may initially show isobaric cooling if thinning produced a crust that is in isostatic equilibrium (e.g. Sandiford & Powell, 1986; Bohlen, 1987). Hence, the Bamble Sector must have resided at about 21-25 km depth within a continental crust of *normal* thickness until uplift occurred. The prolonged crustal residence time of the area at the base of such a crust is consistent with this tectonic model.

Dehydration versus CO_2 influx

Observed variations in H_2O, CO_2, Na and Li content of cordierites from the Arendal amphibolite- to granulite facies transition (Chapter 2) are best explained by progressive dehydration and decarbonation with increasing metamorphic grade. This is consistent with the increased heat flow and related temperature gradient (Nijland & Maijer, 1993), which must have promoted dehydration reactions and partial melting in this transition area. The cordierite data rule out infiltration of a large amounts of homogeneous CO_2-rich fluid during high-grade metamorphism (Touret, 1971b).

Retrogradation and late CO_2-rich fluids

The isobaric cooling phase (early M_4) is succeeded by a near-isothermal decompression phase (late M_4), resulting in the emplacement of the Bamble Sector into the upper crust during the later stages of the Sveconorwegian orogeny. Late M_4 assemblages, consisting of kyanite-(andalusite-dumortierite)-chlorite-quartz after cordierite, are widespread in the cordierite-bearing rocks of the upper-amphibolite facies area. Late M_4 retrogradation appears to be nearly absent in cordierite-bearing rocks of the granulite facies area (Chapter 4),

suggesting that the intensity of late M_4 retrogradation decreases towards the Skagerrak coast. P-T conditions during late M_4 are calculated at 3-4 kbar and 420-530 °C (Chapters 1, 3 and 4).

Volatile data of cordierites from late M_4 retrograded localities (Chapter 2), and late M_4 reactions (Chapters 3 and 5) show the retrograde fluid to be CO_2-rich at many of the localities. The recognition of CO_2-rich retrograde fluids is significant for the discussion on the origin of CO_2 in the Bamble area. In combination with the shape of the established cooling path it would be possible that some or many of previously documented high density "peak metamorphic" CO_2 fluid inclusions are in fact entrapped at much lower temperatures (cf. Lamb et al., 1987; Morrison & Valley, 1991).

Boron

The behaviour of boron with increasing grade is illustrated by an occurrence of the borosilicate kornerupine in a permeable biotite-spinel schist near Böylefossbru. The boron required for the prograde formation of kornerupine most likely was generated outside the outcrop by dehydration of possible boron-bearing muscovite in adjacent polyphase migmatitic metapelites (Chapter 3). This proces of boron-depletion in metapelites is similar to that proposed by Leeman et al. (1992) to account for the low B contents in the 100 granulite samples they used to investigate the boron geochemistry of the lower crust. Their estimated lower crustal average for B of 2.5 ppm is, however, in contradiction with the many high-grade borosilicate-bearing lithologies such as tourmalinites (Krijgsman, 1991; Nijland et al., 1992), tourmaline-bearing quartzites and cordierite-orthoamphibole rocks (Touret, 1979; Visser, 1987, unpublished data) found in the Bamble Sector. The use of such averages for the lower crust in general must, therefore, be questioned.

Significant retrograde introduction of boron is suggested by the development of M_4 dumortierite at several localities (Chapter 4). This is consistent with studies of Truscott et al. (1986) and Shaw et al. (1988), which showed that boron frequently is introduced by the fluid during later hydrous alteration.

REFERENCES

Abraham, K., Mielke, H. & Povondra, P., 1972. On the enrichment of tourmaline in metamorphic sediments of the Arzberg Series, W.Germany (NE-Bavaria). *Neues Jahrbuch für Mineralogie, Monatshefte,* 209-219.

Ackermand, D., Herd, R.K. & Windley, B.F., 1984. Kornerupine replacement reactions involving tourmaline, Fiskenæsset region, W. Greenland. *Neues Jahrbuch für Mineralogie, Monatshefte,* Heft **11,** 490-500.

Ackermand, D., Windley, B.F. & Herd, R.K., 1983. Magnesian högbomite in a sapphirine-bearing rock from the Fiskenaesset region, W. Greenland. *Mineralogical Magazine,* **47,** 555-561.

Ackermand, D., Windley, B.F. & Razafiniparany, A.H., 1991. Kornerupine breakdown reactions in paragneisses from southern Madagascar. *Mineralogical Magazine,* **55,** 71-80.

Aines, R.D. & Rossman, G.R., 1984. The high temperature behavior of water and carbon dioxide in cordierite and beryl. *American Mineralogist,* **69,** 319-327.

Alexander, V.D., Griffen, D.T. & Martin, T.J., 1986. Crystal chemistry of some Fe- and Ti-poor dumortierites. *American Mineralogist,* **71,** 786-794.

Armbruster, Th. & Irouschek, A., 1983. Cordierites from the Lepontine Alps: Na+Be→Al substitution, gas content, cell parameters, and optics. *Contributions to Mineralogy and Petrology,* **82,** 389-396.

Armbruster, Th., Schreyer, W. & Hoefs, J., 1982. Very high CO_2 cordierite from Norwegian Lapland: Mineralogy, petrology, and carbon isotopes. *Contributions to Mineralogy and Petrology,* **81,** 262-267.

Baker, J.H. & Groot, P.A. de, 1983. Proterozoic seawater - felsic volcanics interaction W. Bergslagen, Sweden. Evidence for high REE mobility and implications for 1.8 Ga seawater compositions. *Contributions to Mineralogy and Petrology,* **82,** 119-130.

Baker, J., Powell, R., Sandiford, M. & Muhling, J., 1987. Corona textures between kyanite, garnet and gedrite in gneisses from Errabiddy, western Australia. *Journal of Metamorphic Geology,* **5,** 357-370.

Bebout, G.E., Ryan, J.G. & Leeman, W.P., 1990. B and Be systematics in high P/T metamorphic rocks of the Catalina Schist, California: implications for subduction recycling. *EOS,* **71,** 1663.

Beeson, R., 1976. The orthoamphibole-bearing rocks of the Søndeled-Tvedestrand area, Aust-Agder, south Norway. *Norsk Geologisk Tidsskrift,* **56,** 125-139.

Beeson, R., 1978. The geochemistry of orthoamphiboles and coexisting cordierites and phlogopites from south Norway. *Contributions to Mineralogy and Petrology,* **66,** 5-14.

Beeson, R., 1988. Identification of cordierite-orthoamphibole rock types associated with sulphide deposits of copper, lead and zinc. *Transactions of the Institution of Mining and Metallurgy,* **97B,** 108-115.

Berman, R.G., 1988. Internally-consistent thermodynamic data for minerals in the system Na_2O-K_2O-CaO-MgO-FeO-Fe_2O_3-Al_2O_3-SiO_2-TiO_2-H_2O-CO_2. *Journal of Petrology,* **29,** 445-522.

Beukes, G.J., Slabbert, M.J., Bruiyn, H. de, Botha, B.J.V., Schoch, A.E. & Westhuizen, W.A. van der, 1987. Ti-dumortierite from the Keimoes area, Namaqua mobile belt, South Africa. *Neues Jahrbuch für Mineralogie, Abhandlungen,* **157,** 303-318.

Beukes, G.J., Zyl, V.C. van, Schoch, A.E., Bruiyn, H. De, Aswegen, G. van & Strydom,

D., 1986. A högbomite-spinel-gedrite paragenesis from northern Bushmanland, Namaqua mobile belt, South Africa. *Neues Jahrbuch für Mineralogie, Abhandlungen,* **155,** 53-66.

Bhattacharja, A. & Sen, S.K., 1985. Energetics of hydration of cordierite and water barometry in cordierite-granulites. *Contributions to Mineralogy and Petrology,* **89,** 370-378.

Black, P.M., 1973. Dumortierite from Karikari peninsula: a first record in New Zealand. *Mineralogical Magazine,* **39,** 245.

Bohlen, S.R., 1987. Pressure-Temperature-Time paths and a tectonic model for the evolution of granulites. *Journal of Geology,* **95,** 617-632.

Bol, L.C.G.M., 1990. Geochemistry of high-temperature granulitic supracrustals from Rogaland, SW Norway. Ph.D. thesis, University of Utrecht, *Geologica Ultraiectina,* **66,** 137 pp.

Bos, A., 1990. Hydrothermal element distributions at high temperatures. An experimental study on the partitioning of major and trace elements between phlogopite, haplogranitic melt and vapour. Ph.D. thesis, University of Utrecht, The Netherlands. *Geologica Ultraiectina,* **69,** 99 pp.

Broch, O.A., 1926. Ein suprakrustaler gneiss-complex auf der halbinsel Nesodden bei Oslo. *Norsk Geologisk Tidsskrift,* **9,** 81-224.

Brøgger, W.C., 1934. On several Archäan rocks from the south coast of Norway. II. The south Norwegian hyperites and their metamorphism. *Det norske vitenskapsakademi i Oslo, Skrifter I, Mat. Naturv. klasse,* No. **1,** 421 pp.

Bruin, M. de, 1983. Instrumental neutron activation analysis - a routine method. Ph.D. thesis, *Delft University Press,* Delft, pp 270.

Bugge, J.A.W., 1943. Geological and petrographical investigations in the Kongsberg-Bamble Formation. *Norges Geologiske Undersøkelse,* **160,** 150 pp.

Bugge, J.A.W., 1978. Kongsberg-Bamble complex. In: Bowie, S.H.O., Kvalheim, A. & Haslam, M.W. (eds) Mineral deposits of Europe. Northwest Europe, Vol. **1,** 213-217.

Čech, F., Rieder, M. & Vrána, S., 1976. Cobaltoan högbomite from Zambia. *Neues Jahrbuch für Mineralogie, Monatshefte,* Heft **12,** 525-531.

Černý, P., 1991. Rare-element granitic pegmatites. Part I: anatomy and internal evolution of pegmatite deposits. *Geoscience Canada,* **18,** 49-67.

Christophe-Michel-Lévy, M., Enberger, A. & Sandréa, A., 1959. Matériaux pour la minéralogie de Madgascar. II. - La Dumortiérite de Riampotsy. *Bulletin de la Société française de minéralogie et de cristallographie,* **82,** 77-79.

Claringbull, G.F. & Hey, M.H., 1958. New data for dumortierite. *Mineralogical Magazine,* **31,** 901-907.

Coolen, J.J.M.M.M., 1981. Högbomite and aluminum spinel from some metamorphic rocks and Fe-Ti ores. *Neues Jahrbuch für Mineralogie, Monatshefte,* Heft **8,** 374-384.

Cooper, D.C. & Bradley, A.D., 1990. The ammonium content of granites in the English Lake District. *Geological Magazine,* **127,** 579-586.

Cooper, D.C. & Field, D., 1977. The chemistry of Proterozoic low-potash, high-iron, charnockitic gneisses from Tromoy, south Norway. *Earth and Planetary Science Letters,* **35,** 105-115.

Crowley, P.D. & Spear, F.S., 1981. The orthoamphibole solvus: P, T, X(Fe-Mg) relations. *Geological Society of America, Abstracts with programs,* **13,** 436.

Darimont, A., Burke, E. & Touret, J., 1988. Nitrogen-rich metamorphic fluids in Devonian metasediments from Bastogne, Belgium. *Bulletin de Minéralogie,* **111,** 321-330.

Duit, W., Jansen, J.B.H., Breemen, A. van & Bos, A., 1986. Ammonium micas in metamorphic rocks as exemplified by Dôme de l'Agout (France). *American Journal of Science,* **286,** 702-732.

Dutrow, B.L., Holdaway, M.J. & Hinton, R.W., 1986. Lithium in staurolite and its petrologic significance. *Contributions to Mineralogy and Petrology,* **94,** 496-506.

Dymek, R.F. & Smith, M.S., 1990. Geochemistry and origin of Archean quartz-cordierite gneisses from the Godthåbsfjord region, West Greenland. *Contributions to Mineralogy and Petrology,* **105,** 715-730.

Ellis, D.J., 1987. Origin and evolution of granulites in normal and thickened crusts. *Geology,* **15,** 167-170.

Enami, E. & Zang, Q., 1988. Magnesian staurolite in garnet-corundum rocks and eclogite from the Donghai district, Jiangsu province, east China. *American Mineralogist,* **73,** 48-56.

England, P.C. & Richardson, S.W., 1977. The influence of erosion upon mineral facies of rocks from different metamorphic environments. *Journal of the Geological Society of London,* **134,** 201-213.

England, P.C. & Thompson, A.B., 1984. Pressure-Temperature-Time paths of regional metamorphism I. Heat transfer during the evolution of regions of thickened continental crust. *Journal of Petrology,* **25,** 894-928.

Eugster, H.P. & Munoz, J., 1966. Ammonium micas: Possible sources of atmospheric ammonia and nitrogen. *Science,* **151,** 683-686.

Feenstra, A., 1985. Metamorphism of bauxites on Naxos, Greece. *Geologica Ultraiectina,* **39,** 206 pp.

Ferry, J.M. & Spear, F.S., 1978. Experimental calibration of the partitioning of Fe and Mg between biotite and garnet. *Contributions to Mineralogy and Petrology,* **66,** 113-117.

Field, D. & Clough, P.W.L., 1976. K/Rb ratios and metasomatism in metabasites from a Precambrian amphibolite-granulite transition zone. *Journal of the Geological Society of London,* **132,** 277-288.

Field, D., Drury, S.A. & Cooper, D.C., 1980. Rare-earth and LILE element fractionation in high grade charnockitic gneisses, south Norway. *Lithos,* **13,** 281-289.

Field, D. & Råheim, A., 1979. Rb-Sr total rock isotope studies on Precambrian charnockitic gneisses from south Norway: evidence for isochron resetting during a low-grade metamorphic deformational event. *Earth and Planetary Science Letters,* **45,** 32-44.

Field, D. & Råheim, A., 1981. Age relationships in the Proterozoic high grade gneiss regions of southern Norway. *Precambrian Research,* **14,** 261-275.

Field, D., Smalley, P.C., Lamb, R.C. & Råheim, A., 1985. Geochemical evolution of the 1.6-1.5 Ga-old amphibolite-granulite facies terrain, Bamble sector, Norway: dispelling the myth of Grenvillian high-grade reworking. In: Tobi, A.C. & Touret, J. (eds.). The Deep Proterozoic Crust in the North Atlantic Provinces, *NATO ASI Series C,* **158,** Reidel, Dordrecht, 567-578.

Finlay, G.I., 1907. On an occurrence of corundum and dumortierite in pegmatite in Colorado. *Journal of Geology,* **15,** 479-484.

Foit, Jr. F.F. & Rosenberg, P.E., 1977. Coupled substitutions in the tourmaline group. *Contributions to Mineralogy and Petrology,* **62,** 109-127.

Furlong, K.P. & Fountain, D.M., 1986. Continental crustal underplating: thermal considerations and seismic-petrologic consequences. *Journal of Geophysical Research,* **91,** B8, 8285-8294.

Gammon, J.B., 1966. Fahlbands in the Precambrian of southern Norway. *Economic Geology,* **61,** 174-188.

Gatehouse, B.M. & Grey, I.E., 1982. The crystal structure of högbomite-8H. *American Mineralogist,* **67,** 373-380.

Gieré, R., 1986. Zirconolite, allanite and högbomite in a marble skarn from the Bergell contact aureole: Implications for mobility of Ti, Zr and REE. *Contributions to Mineralogy and Petrology,* **93,** 459-470.

Ginzburg, A.I. & Stravrov, O.D., 1961. Content of rare elements in cordierite. *Geokhimiya,* **2,** 183-185.

Girault, J.P., 1952. Kornerupine from Lac Ste-Marie, Quebec, Canada. *American Mineralogist,* **37,** 531-541.

Goldman, D.S., Rossman, G.R. & Dollase, W.A., 1977. Channel constituents in cordierite. *American Mineralogist,* **62,** 1144-1157.

Golovastikov, N.I., 1965. The crystal structure of dumortierite. *Soviet Physics-Doklady,* **10,** 493-495.

Gonnard, M.F., 1881. Note sur l'existence d'une espèce minérale nouvelle, la dumortiérite dans le gneiss de Beaunan, au-dessus des anciens aqueducs gallo-romains de la vallée de l'Izeron (Rhone). *Bulletin de la Société française de Minéralogie,* **4,** 2-8.

Graham, C.E. & Robertson, F., 1951. A new dumortierite locality from Montana. *American Mineralogist,* **36,** 916-917.

Grambling, J.A., 1990. Internally-consistent geothermometry and H_2O barometry in metamorphic rocks: the example garnet- chlorite-quartz. *Contributions to Mineralogy and Petrology,* **105,** 617-628.

Grant, J.A., 1981. Orthoamphibole and orthopyroxene relations in high-grade metamorphism of pelitic rocks. *American Journal of Science,* **281,** 1127-1143.

Graversen, O., 1984. Geology and structural evolution of the Precambrian rocks of the Oslofjord-Øyeren area, southeast Norway. *Norges Geologiske Undersøkelse Bulletin,* **398,** 1-50.

Green, T.L. & Vernon, R.H., 1974. Cordierite breakdown under high-pressure, hydrous conditions. *Contributions to Mineralogy and Petrology,* **46,** 215-226.

Grew, E.S., 1980. Sillimanite and ilmenite from high-grade metamorphic rocks of Antarctica and other areas. *Journal of Petrology,* **21,** 39-68.

Grew, E.S., 1988. Kornerupine at the Sar-e-Sang, Afghanistan, whiteschist locality: Implications for tourmaline-kornerupine distribution in metamorphic rocks. *American Mineralogist,* **73,** 345-357.

Grew, E.S., Abraham, K. & Medenbach, O., 1987a. Ti-poor hoegbomite in kornerupine-cordierite-sillimanite rocks from Ellammankovilpatti, Tamil Nadu, India. *Contributions to Mineralogy and Petrology,* **95,** 21-31.

Grew, E.S., Chernosky, J.V., Werding, G., Abraham, K., Marquez, N. & Hinthorne, J.R., 1990. Chemistry of kornerupine and associated minerals, a wet chemical, ion microprobe, and X-Ray study emphasizing Li, Be, B and F contents. *Journal of Petrology,* **31,** 1025-1070.

Grew, E.S., Drugova, G.M. & Leskova, N.V., 1989. Högbomite from the Aldan shield, Eastern Siberia, USSR. *Mineralogical Magazine,* 53, 376-379.

Grew, E.S., Herd, R.K. & Marquez, N., 1987b. Boron-bearing kornerupine from Fiskenæsset, West Greenland: a re-examination of specimens from the type locality. *Mineralogical Magazine,* **51,** 695-708.

Grew, E.S., Hiroi, Y. & Shiraishi, K., 1990. Högbomite from the Prince Olav Coast, East Antarctica: An example of oxidation-exsolution of a complex magnetite solid solution. *American Mineralogist,* **75,** 589-600.

Grew, E.S. & Sandiford, M., 1984. A staurolite-talc assemblage in tourmaline-phlogopite-chlorite schist from northern Victoria Land, Antarctica, and its petrogenitic significance. *Contributions to Mineralogy and Petrology,* **87,** 337-350.

Grieve, R.A.F. & Fawcett, J.J., 1974. The stability of chloritoid below 10 kb PH_2O. *Journal of Petrology,* **15,** 113-139.

Griffen, D.T. & Ribbe, P.H., 1973. The crystal chemistry of staurolite. *American Journal of Science,* **273-A,** 479-495.

Griffen, D.T., Gosney, T.C. & Phillips, W.R., 1982. The chemical formula of natural staurolite. *American Mineralogist,* **67,** 292-297.

Gupta, L.N. & Johannes, W., 1982. Petrogenesis of a stromatic migmatite (Nelaug, southern Norway). *Journal of Petrology,* **23,** 548-567.

Haas, G.J.L.M. de, 1992. Source, evolution, and age of coronitic gabbros from the Arendal-Nelaug area, Bamble, southeast Norway. Ph.D. thesis, *Geologica Ultraiectina,* **86,** 129 pp.

Haas, G.J.L.M. de, Verschure, R.H., Maijer, C. & Valbracht, P.J., 1992. Isotopic age determinations in South Norway III: Rb-Sr isotope systematics of the coronitic Vestre Dale Gabbro and its country rocks, Bamble Sector. *Geologiska Föreningens i Stockholm Förhandlingar,* **114,** 417-422.

Haendel, D., Mühle, K., Nitzsche, H.-M., Stiehl, G. & Wand, U., 1986. Isotopic variations of the fixed nitrogen in metamorphic rocks. *Geochimica et Cosmochimica Acta,* **50,** 749-758.

Hall, A., 1988a. Crustal contamination of minette magmas: evidence from their ammonium contents. *Neues Jahrbuch für Mineralogie, Monatshefte,* 137-143.

Hall, A., 1988b. The distribution of ammonium in granites from South-West England. *Journal of the Geological Society of London,* **145,** 37-41.

Harder, H., 1959. Beitrag zur Geochemie des Bors. I. Bor in Mineralen und magmatischen Gesteinen. Akademie der Wissenschaften in Göttingen, *Mathematisch-physikalische Klasse, Nachrichten,* **5,** 67-122.

Harley, S.L., 1985. Paragenetic and mineral-chemical relationships in orthoamphibole-bearing gneisses from Enderby Land, east Antarctica: a record of Proterozoic uplift. *Journal of Metamorphic Geology,* **3,** 179-200.

Harley, S.L., 1989. The origins of granulites: a metamorphic perspective. *Geological Magazine,* **126,** 215-331.

Helgeson, H.C., Delany, J.M., Nesbitt, H.W. & Bird, D.K., 1978. Summary and critique of the thermodynamic properties of rock-forming minerals. *American Journal of Science,* **278-A,** 1-221.

Henry, D.J. & Guidotti, C.V., 1985. Tourmaline as a petrogenetic indicator mineral: an example from the staurolite-grade metapelites of NW Maine. *American Mineralogist,* **70,** 1-15.

Hoinkes, G., 1986. Effect of grossular-content in garnet on the partitioning of Fe and Mg between garnet and biotite. An empirical investigation on staurolite-zone samples from the Austroalpine Schneeberg complex. *Contributions to Mineralogy and Petrology,* **92,** 393-399.

Holdaway, M.J., 1971. Stability of andalusite and the aluminum silicate phase diagram.

American Journal of Science, **271,** 97-131.

Holdaway, M.J. & Lee, S.M., 1977. Fe-Mg cordierite stability in high-grade pelitic rocks based on experimental, theoretical, and natural observations. *Contributions to Mineralogy and Petrology,* **63,** 175-198.

Holland, T.J.B. & Powell, R., 1990. An enlarged and updated internally consistent thermodynamic dataset with uncertainties and correlations: the system K_2O-Na_2O-CaO-MgO-MnO-FeO-Fe_2O_3-Al_2O_3-TiO_2-SiO_2-C-H_2-O_2. *Journal of Metamorphic Geology,* **8,** 89-124.

Hollister, L.S., 1988. On the origin of CO_2-rich fluid inclusions in migmatites. *Journal of Metamorphic Geology,* **6,** 467-474.

Honma, H. & Itihara, Y., 1981. Distribution of ammonium in the minerals of metamorphic and granitic rocks. *Geochimica et Cosmochimica Acta,* **45,** 983-988.

Hörmann, P.K., Raith, M., Raase, P., Ackermand, D. & Seifert, F., 1980. The granulite complex of Finnish Lapland: petrology and metamorphic conditions in the Ivalojoki-Inarijärvi area. *Geological Survey of Finland,* Bulletin **308,** 95 pp.

Hudson, N.F.C. & Harte, B., 1985. K_2O-poor, aluminous assemblages from the Buchan Daldarian, and the variety of orthoamphibole assemblages in aluminous bulk compositions in the amphibolite facies. *American Journal of Science,* **285,** 224-266.

Hulzebos-Sijen, N.M.P.E., Visser, D., Maarschalkerweerd, M.H. & Maijer, C., 1990. Two new kornerupine-localities in the Bamble Sector, south Norway. *Abstract 19th Nordic Geological Winter Meeting, Geonytt,* **17,** 58.

Huijsmans, J.P.P., Barton, M. & Bergen, M.J. van, 1982. A pegmatite containing Fe-rich grandidierite, Ti-rich dumortierite and tourmaline from the Precambrian, high-grade metamorphic complex of Rogaland, S.W. Norway. *Neues Jahrbuch für Mineralogie, Abhandlungen,* **143,** 249-261.

Indares, A. & Martignole, J., 1985. Biotite-garnet geothermometry in the granulite facies: the influence of Ti and Al in biotite. *American Mineralogist,* **70,** 272-278.

Itihara, Y. & Honma, H., 1979. Ammonium in biotite from metamorphic and granitic rocks of Japan. *Geochimica et Cosmochimica Acta,* **43,** 503-509.

Itihara, Y. & Suwa, K., 1985. Ammonium contents of biotites from Precambrian rocks in Finland: The significance of NH_4^+ as a possible chemical fossil. *Geochimica et Cosmochimica Acta,* **49,** 145-151.

Johannes, W., 1988. What controls partial melting in migmatites? *Journal of Metamorphic Geology,* **6,** 451-465.

Johannes, W. & Schreyer, W., 1981. Experimental introduction of CO_2 and H_2O into Mg-cordierite. *American Journal of Science,* **281,** 299-317.

Jøsang, O., 1966. Geologiske og petrografiske undersøkelse i Modumfeltet. *Norges Geologiske Undersøkelse,* **235,** 148 pp.

Kayupova, M.M. & Tilepov, Z.T., 1977. First find of dumortierite concretions. *Doklady Akademii Nauk SSSR,* **235,** 121-124.

Kerr, P.F. & Jenney, P., 1935. The dumortierite-andalusite mineralization at Oreana, Nevada. *Economic Geology,* **30,** 287-300.

Kihle, J., 1990. CO_2-CO-H_2O distribution within the polymetamorphic cordierite-bearing metapelites of the Bamble Sector, southern Norway. *Geonytt,* **17,** 65.

Kihle, J. & Bucher-Nurminen, K., 1992. Orthopyroxene-sillimanite-sapphirine granulites from the Bamble granulite terrane, southern Norway. *Journal of Metamorphic Geology,* **10,** 671-683.

Kirchener, D., Mirwald, P.W. & Schreyer, W., 1984. Experimenteller Li-Einbau in Mg-Cordierit. *Fortschritte der Mineralogie,* **62,** Beiheft 1, 119-120.

Kolderup, N.H., 1928. Fjellbygningen i kyststrøket mellem Nordfjord og Sognefjord (with English Summary). *Bergens Museums Årbok,* **1,** 1-222.

Kolderup, N.H., 1936. Korund, Høgbomit, Staurolith und Skapolith in den Anorthositgabbros des Bergengebietes. *Bergens Museums Årbok,* **8,** 1-11.

Kosse, S., Daniels, P., Medenbach, O. & Schreyer, W., 1992. Hohe Druckstabilität von borhaltigem Kornerupin und ein neues Hochdruck-Mg-Al-Borat. *European Journal of Mineralogy 4,* Beiheft **1,** 166.

Kretz, R., 1983. Symbols for rock-forming minerals. *American Mineralogist,* **68,** 277-279.

Kreulen, R. & Schuiling, R.D., 1982. N_2-CH_4-CO_2 fluids during formation of the Dôme de l'Agout, France. *Geochimica et Cosmochimica Acta,* **46,** 193- 203.

Krijgsman, A., 1991. Geology and ore-genesis of the Ettedalgrube, a Proterozoic Pb-Zn-Ag deposit in SE-Norway. Unpublished M.Sc. thesis, University of Utrecht, 34 pp.

Lamb, R.C., 1981. Geochemical studies in Proterozoic high-grade gneiss terrain, Bamble sector, south Norway. Unpublished Ph.D. thesis, University of Nottingham.

Lamb, R.C., Smalley, P.C. & Field, D., 1986. P-T conditions for the Arendal granulites, southern Norway: implications for the roles of P,T and CO_2 in deep crustal LILE-depletion. *Journal of Metamorphic Geology,* **4,** 143-160.

Lamb, W.M., Valley, J.W. & Brown, P.E., 1987. Post-metamorphic CO_2-rich fluid inclusions in granulites. *Contributions to Mineralogy and Petrology,* **96,** 485-495.

Langer, K. & Schreyer, W., 1969. Infrared and powder X-ray diffraction studies on the polymorphism of cordierite, $Mg_2(Al_4Si_5O_{18})$. *American Mineralogist,* **54,** 1442-1459.

Leake, B.E., 1978. Nomenclature of amphiboles. *American Mineralogist,* **63,** 1023-1053.

Le Breton, N., 1989. Infrared investigation of CO_2-bearing cordierites. Some implications for the study of metapelitic granulites. *Contributions to Mineralogy and Petrology,* **103,** 387-396.

Le Breton, N. & Thompson, A.B., 1988. Fluid-absent (dehydration) melting of biotite in metapelites in the early stages of crustal anatexis. *Contributions to Mineralogy and Petrology,* **99,** 226-237.

Lee, S.M. & Holdaway, M.J., 1976. Cordierite breakdown under high-pressure hydrous conditions: A Comment. *Contributions to Mineralogy and Petrology,* **56,** 289-295.

Leeman, W.P., Sisson, V.B. & Reid, M.R., 1992. Boron geochemistry of the lower crust: evidence from granulite terranes and deep crustal xenoliths. *Geochimica et Cosmochimica Acta,* **56,** 775-788.

Lieftink, D.J., Nijland, T.G. & Maijer, C., 1993. Cl-rich scapolite from the ancient Ødegården Verk. *Norsk Geologisk Tidsskrift,* **73,** 55-57.

Lonker, S.W., 1981. The P-T-X relations of the cordierite-garnet-sillimanite-quartz equilibrium. *American Journal of Science,* **281,** 1056-1090.

Lonker, S.W., 1988. An occurrence of grandidierite, kornerupine, and tourmaline in southeastern Ontario, Canada. *Contributions to Mineralogy and Petrology,* **98,** 502-516.

Loosveld, R.J.H. & Etheridge, M.A., 1990. A model for low-pressure facies metamorphism during crustal thickening. *Journal of metamorphic Geology,* **8,** 257-267.

Mancktelow, N.S., 1981. Högbomite of unusual composition from Reedy Creek, South Australia. *Mineralogical Magazine,* **44,** 91-94.

Martignole, J. & Sisi, J.-C., 1981. Cordierite-garnet-H_2O equilibrium: A geological thermometer, barometer and water fugacity indicator. *Contributions to Mineralogy and*

Petrology, **77,** 38-46.

Maijer, C. & Padget, P. (Eds.), 1987. The geology of southernmost Norway: An excursion guide. *Norges Geologiske Undersøkelse,* Special Publication, **1,** 109 pp.

Milne, K.P. & Starmer, I.C., 1982. Extreme differentiation in the Proterozoic Gjerstad-Morkeheia complex of south Norway. *Contributions to Mineralogy and Petrology,* **79,** 381-393.

Mirwald, P.W., 1986. Ist Cordierite ein geothermometer? *Fortschritte der Mineralogie,* **64,** Beiheft 1, 113.

Mirwald, P.W., Maresch, W.V. & Schreyer, W., 1979. Der Wassergehalt von Mg-Cordierit zwischen 500 °C und 800 °C sowie 0,5 und 11 kbar. *Fortschritte der Mineralogie,* **57,** Beiheft 1, 101-102.

Miyashiro, A., 1957. Cordierite-indialite relations. *American Journal of Science,* **255,** 43-62.

Moine, B., Sauvan, P. & Jarousse, J., 1981. Geochemistry of evaporite-bearing series: A tentative guide for the identification of metaevaporites. *Contributions to Mineralogy and Petrology,* **76,** 401-412.

Moore, P.B. & Araki, T., 1978. Dumortierite, $Si_3B[Al_{6.75}\square_{0.25}O_{17.25}(OH)_{0.75}]$: a detailed structure analysis. *Neues Jahrbuch für Mineralogie, Abhandlungen,* **132,** 231-241.

Moore, P.B., 1979. Kornerupine: a detailed crystal-chemical study. *Neues Jahrbuch für Mineralogie, Abhandlungen,* **134,** 317-336.

Morrison, J. & Valley, J.W., 1991. Retrograde fluids in granulite: stable isotope evidence of fluid migration. *Journal of Geology,* **99,** 559-570.

Morton, R.D., Batey, R. & O'Nions, R.K., 1970. Geological investigations in the Bamble Sector of the Fennoscandian Shield, south Norway. 1. The geology of Eastern Bamble. *Norges Geologiske Undersøkelse,* **263,** 72 pp.

Munz, I.A., 1990. Whiteschists and orthoamphibole-cordierite rocks and the P-T-t path of the Modum Complex, south Norway. *Lithos,* **24,** 181-200.

Nel, H.J., 1949. Högbomite from the corundum fields of the eastern Transvaal. *Memoir of the Geological Survey of South Africa,* **43,** 1-17.

Newton, R.C., 1972. An experimental determination of the high pressure stability limits of magnesian cordierite under wet and dry conditions. *Journal of Geology,* **80,** 398-420.

Newton, R.C., 1992. Charnockitic alteration: evidence for CO_2 infiltration in granulite facies metamorphism. *Journal of Metamorphic Geology,* **10,** 383-400.

Newton, R.C. & Wood, B.J., 1979. Thermodynamics of water in cordierite and some petrologic consequences of cordierite as a hydrous phase. *Contributions to Mineralogy and Petrology,* **68,** 391-405.

Nicollet, C., 1986. Saphirine et staurotide riche en magnésium et chrome dans les amphibolites et anorthosites à corindon du Vohibory Sud, Madagascar. *Bulletin de Minéralogie,* **109,** 599- 612.

Nijland, T.G., 1993. The Bamble amphibolite te granulite facies transition zone, Norway. Ph.D. thesis, *Geologica Ultraiectina,* **101,** 166 pp.

Nijland, T.G., Liauw, F., Visser, D., Maijer, C. & Senior, A., 1993. Metamorphic petrology of the Froland corundum-bearing rocks: the cooling and uplift history of the Bamble Sector, south Norway. *Norges Geologiske Undersøkelse* (in press).

Nijland, T.G. & Maijer, C., 1992. Lower crustal transitions I. Changing mineral assemblages and thermobarometric estimates over a classical amphibolite to granulite transition zone, Bamble, Norway. *Abstract 1th Netherlands Earth Scientific Congress,* 139.

Nijland, T.G. & Maijer, C., 1993. The regional amphibolite to granulite facies transition at Arendal, Norway: evidence for a thermal dome. *Neues Jahrbuch für Mineralogie* (in press).

Nijland, T.G., Maijer, C., Senior, A. & Verschure, R.H., 1992. Primary sedimentary structures and composition of the high-grade metamorphic Nidelva Quartzite Complex [Bamble, Norway], and the origin of nodular gneisses. *Proceedings of the Koninklijke Nederlandse Akademie van Wetenschappen,* **96** (1), in press.

Nijland, T.G. & Senior, A., 1991. Sveconorwegian granulite facies metamorphism of polyphase migmatites and basic dykes, south Norway. *Journal of Geology,* **99,** 515-525.

Owen, J.V. & Greenough, J.D., 1991. An empirical sapphirine-spinel Mg-Fe exchange thermometer and its application to high grade xenoliths in the Popes Harbour dyke, Nova Scotia, Canada. *Lithos,* **26,** 317-332.

Peacor, D.R., 1967. New data on nigerite. *American Mineralogist,* **52,** 864-866.

Perchuk, L.L., 1981. Correction of the biotite-garnet thermometer in case of the Mn = Mg + Fe isomorphism in garnet. *Doklady USSR AS,* **256,** 38-41.

Perchuk, L.L. & Lavrent'eva, I.V., 1983. Experimental investigation of exchange equilibria in the system cordierite-garnet-biotite. In: Saxena, S.K. (Ed.), Kinetics and equilibrium in mineral reactions. *Advances in physical Geochemistry,* **3,** Springer Verlag, New York, 199-240.

Petersen, E.U., Essene, E.J., Peacor, D.R. & Marcotty, L.A., 1989. The occurrence of högbomite in high-grade metamorphic rocks. *Contributions to Mineralogy and Petrology,* **101,** 350-360.

Ploegsma, M., 1989. Shear zones in the west Uusimaa area, SW Finland. Unpublished Ph.D. thesis, Free University, Amsterdam, The Netherlands, 134 pp.

Pouchou, J.L. & Pichoir, F., 1984. A new model for quantitative X-ray microanalysis. Part I: Application to the analysis of homogeneous samples. *La Récherche Aérospatiale,* **3,** 13-36.

Putnis, A., 1980. The distortion index in anhydrous Mg-cordierite. *Contributions to Mineralogy and Petrology,* **74,** 135-141.

Rammlmair, D., Mogessie, A., Purtscheller, F. & Tessadri, R., 1988. Högbomite from the Vumba schist Belt, Botswana. *American Mineralogist,* **73,** 651-656.

Ramsay, C.R. & Morton, R.D., 1971. Hydrothermal retrogression of cordierite in the Bamble sector, south Norway. *Neues Jahrbuch für Mineralogie, Monatshefte,* 398-403.

Reenen, D.D. van, 1986. Hydration of cordierite and hypersthene and a description of the retrograde orthoamphibole isograd in the Limpopo Belt, South Africa. *American Mineralogist,* **71,** 900-915.

Reinhardt, J., 1987. Cordierite-anthophyllite rocks from north-west Queensland, Australia: metamorphosed magnesian pelites. *Journal of Metamorphic Geology,* **5,** 451-472.

Robinson, P. & Jaffe, H.W., 1969. Aluminous enclaves in gedrite-cordierite gneiss from southwestern New Hampshire. *American Journal of Science,* **267,** 389-421.

Robinson, P., Ross, M. & Jaffe, H.W., 1971. Composition of the anthophyllite-gedrite series, comparisons of gedrite and hornblende, and the anthophyllite-gedrite solvus. *American Mineralogist,* **56,** 1005-1041.

Robinson, P., Spear, F.S., Schumacher, J.C., Laird, J., Klein, C., Evans, B.W. & Doolan, B.L., 1982. Phase relations of metamorphic amphiboles: Natural occurrence and theory. In: Velben, D.R. & Ribbe, P.H. (eds.), Amphiboles: Petrology and experimental phase relations, *Reviews in mineralogy,* **9B,** 1-227.

Robinson, P. & Tracy, R.J., 1979. Gedrite-cordierite, gedrite-orthopyroxene and cummingtonite-orthopyroxene assemblages from ferromagnesian gneisses, sillimanite-K-feldspar zone, central Massachusetts. *Geological Society of America, Abstracts with programs,* **11,** 504.

Sabzehei, M., 1971. Dumortierite from Iran: a first record. *Mineralogical Magazine,* **38,** 526-527.

Sandiford, M. & Powell, R., 1986. Deep crustal metamorphism during continental extension: modern and ancient examples. *Earth and Planetary Science Letters,* **79,** 151-158.

Sauerer, A. & Troll, G., 1990. Abundance and distribution of boron in the Hauzenberg (Bavaria) granite complex. *Geochimica et Cosmochimica Acta,* **54,** 49-55.

Schaller, W.T., 1905. Dumortierite. *American Journal of Science,* **19,** 211-224.

Scheibler von, W.H.Th.M., 1988. Geothermometrie en geobarometrie toegepast op anthophylliet-cordieriet gesteenten uit de Bamble Sector, zuid Noorwegen. Unpublished M.Sc. thesis, University of Utrecht, The Netherlands, 40 pp.

Schenk, V., Herms, P., Le Breton, N., Craven, J. & Harley, S., 1992. Cordierit als Fluidindikator in metamorphen Gesteinen. *European Journal of Mineralogy* **4,** Beiheft 1, 238.

Schetelig, J., 1917. Høgbomite i norsk jernmalm. *Norsk Geologisk Tidsskrift,* **4,** 249-253.

Scheurs, J., 1985. The West Uusimaa low pressure thermal dome SW Finland. Unpublished Ph.D thesis, Free University of Amsterdam, 179 pp.

Schmetzer, K. & Berger, A., 1990. Lamellar iron-free högbomite-24R from Tanzania. *Neues Jahrbuch für Mineralogie, Monatshefte,* Heft **9,** 401-412.

Schreyer, W., 1985. Experimental studies on cation substitutions and fluid incorporation in cordierite. *Bulletin de la Société françcaise de Minéralogie,* **108,** 273-291.

Schreyer, W. & Abraham, K., 1975. Peraluminous sapphirine as a metastable reaction product in kyanite-gedrite-talc schist from Sar e Sang, Afghanistan. *Mineralogical Magazine,* **40,** 171-180.

Schreyer, W., Abraham, K. & Behr, H.J., 1975. Sapphirine and associated minerals from the kornerupine rock of Waldheim, Saxony. *Neues Jahrbuch für Mineralogie, Abhandlungen,* **126,** 1-27.

Schreyer, W., Gordillo, C.E. & Werding, G., 1979. A new sodian-beryllian cordierite from Soto, Argentina, and the relationship between distortion index, Be content and state of hydration. *Contributions to Mineralogy and Petrology,* **70,** 412-428.

Schreyer, W. & Schrairer, J.F., 1961. Compositions and structural states of anhydrous Mg-cordierites: A reinvestigation of the central part of the system MgO-Al_2O_3-SiO_2. *Journal of Petrology,* **2,** 324-406.

Schreyer, W. & Seifert, F., 1969. Compatibility relations of the aluminum silicates in the systems MgO-Al_2O_3-SiO_2-H_2O and K_2O-Al_2O_3-SiO_2-H_2O at high pressures. *American Journal of Science,* **267,** 371-388.

Schuiling, R.D., 1963. Some remarks concerning the scarcity of retrograde vs. progressive metamorphism. *Geologie en Mijnbouw,* **42,** 177-179.

Schumacher, J.C., 1980. Gedrite of extreme Al and Na content in the metamorphosed Ammonoosuc volcanics, sillimanite-staurolite zone, central Massachusetts. *Geological Society of America, Abstracts with programs,* **12,** 518.

Schumacher, J.C. & Robinson, P., 1987. Mineral chemistry and metasomatic growth of aluminous enclaves in gedrite-cordierite-gneiss from southwestern New Hampshire, USA. *Journal of Petrology,* **28,** 1033-1073.

Seifert, F., 1975. Boron-free kornerupine: a high-pressure phase. *American Journal of Science,* **275,** 57-87.

Seifert, F. & Schreyer, W., 1970. Lower temperature stability field of Mg-cordierite in the range 1-7 kb water pressure: A redetermination. *Contributions to Mineralogy and Petrology,* **27,** 225-238.

Selkregg, K.R. & Bloss, F.D., 1980. Cordierites: compositional controls of Δ, cell parameters, and optical properties. *American Mineralogist,* **65,** 522-533.

Sengupta, P., Dasgupta, S., Bhattacharya, P.K. & Mukherjee, M., 1990. An orthopyroxene-biotite geothermometer and its application in crustal granulites and mantle derived rocks. *Journal of Metamorphic Geology,* **8,** 191-197.

Sharma, R.S. & MacRae, N.D., 1981. Paragenetic relations in gedrite-cordierite-staurolite-biotite- sillimanite-kyanite gneisses at Ajitpura, Rajasthan, India. *Contributions to Mineralogy and Petrology,* **78,** 48-60.

Shaw, D.M., Truscott, M.G., Gray, E.A. & Middleton, T.A., 1988. Boron and lithium in high-grade rocks and minerals from the Wawa-Kapuskasing region, Ontario. *Canadian Journal of Earth Sciences,* **25,** 1485-1502.

Sisson, V.B. & Xu, P., 1991. Boron depletion and enrichment trends associated with contact metamorphism caused by the Ponder pluton, Coast Plutonic Complex, British Colombia, Canada. *Geological Society of America, Abstracts with programs,* **23,** 174.

Smalley, P.C. & Field, D., 1985. Geochemical constraints on the evolution of the Proterozoic continental crust in southern Norway (Telemark sector). In: Tobi, A.C. & Touret, J. (eds.). The Deep Proterozoic Crust in the North Atlantic Provinces, *NATO ASI Series C,* **158,** Reidel, Dordrecht, 551-566.

Smalley, P.C., Field, D., Lamb, R.C. & Clough, P.W.L., 1983. Rare earth, Th-Hf-Ta and large-ion lithophile element variations in metabasites from the Proterozoic amphibolite-granulite transition zone at Arendal, south Norway. *Earth and Planetary Science Letters,* **63,** 446-458.

Smalley, P.C., Field, D. & Råheim, A., 1988. Rb-Sr systematics of a Gardar-age layered alkaline monzonite suite in southern Norway. *Journal of Geology,* **96,** 17-29.

Spear, F.S., 1980. The gedrite-anthophyllite solvus and the composition limits of orthoamphibole from the Post Pond volcanics, Vermont. *American Mineralogist,* **65,** 1103-1118.

Spear, F.S. & Rumble III, D., 1986. Pressure, temperature, and structural evolution of the Orfordville belt, West-Central New Hampshire. *Journal of Petrology,* **27,** 1071-1093.

Spencer, K.J. & Lindsley, D.H., 1981. A solution model for coexisting iron-titanium oxides. *American Mineralogist,* **66,** 1189-1201.

Spry, P.G. & Petersen, E.U., 1989. Zincian högbomite as an exploration guide to metamorphosed massive sulphide deposits. *Mineralogical Magazine,* **53,** 263-269.

Spry, P.G. & Scott, S.D., 1986. The stability of zincian spinels in sulfide systems and their potential as exploration guides for metamorphosed massive sulfide deposits. *Economic Geology,* **81,** 1446-1463.

Starmer, I.C., 1969. The migmatite complex of the Risör area. *Norges Geologisk Tidsskrift,* **49,** 33-56.

Starmer, I.C., 1972. The Sveconorwegian regeneration and earlier events in the Bamble series, south Norway. *Norges Geologiske Undersøkelse,* **277,** 37-52.

Starmer, I.C., 1976. The early major structure and petrology of rocks in the Bamble Series, Søndeled-Sandnesfjord, Aust-Agder. *Norges Geologiske Undersøkelse,* **327,** 77-97.

Starmer, I.C., 1985. The evolution of the south Norwegian Proterozoic as revealed by the major and Mega-tectonics of the Kongsberg and Bamble sectors. In: Tobi, A.C. & Touret, J. (ed.). The Deep Proterozoic crust in the North Atlantic Provinces, *NATO ASI Series C,* **158,** Reidel, Dordrecht, 259-290.

Starmer, I.C., 1986. Geological map of the Bamble sector, south Norway: (1:100.000), 3 sheets. In: Maijer C. & Padget, P., (Eds.) 1987. The geology of southernmost Norway: An excursion guide. *Norges Geologiske Undersøkelse, Special Publication* **1.**

Starmer, I.C., 1990. Rb-Sr systematics of a Gardar-age layered alkaline monzonite suite in southern Norway: a discussion. *Journal of Geology,* **98,** 119-123.

Starmer, I.C., 1991. The Proterozoic evolution of the Bamble Sector shear Belt, southern Norway: correlations across southern Scandinavia and the Grenvillian controversy. *Precambrian Research,* **49,** 107-139.

Stormer, J.C., Jr., 1983. The effects of recalculation on estimates of temperature and oxygen fugacity from analyses of multicomponent iron-titanium oxides. *American Mineralogist,* **68,** 586-594.

Strom, C. 1976. UNITCELLC, an interactive APL program for computing cell constants. Geological and Mineralogical Institute of the State University of Leiden, The Netherlands.

Swamy, V., Godhavari, K.S., Menon, A.G. & Anatha Iyer, G.V., 1992. Channel volatiles of south Indian cordierites as indicators of metamorphic fluid composition. *Neues Jahrbuch für Mineralogie, Monatshefte,* Heft **8,** 359-375.

Takahata, H. & Uchiyama, K., 1985. Dumortierite-bearing argillaceous gneisses from the Abukuma metamorphic terrain, northeast Japan. *Journal of the Faculty of Science, Hokkaido University, Series IV,* **21,** 465-481.

Taylor, S.R. & McLennan, S.M., 1985. The continental crust: its composition and evolution. Blackwell, Oxford, 312 pp.

Theulings, W.T., Ditshuizen, G.P. van & Huijsmans, J.P.P., 1986. Petrology, mineralogy and geochemistry of a coronitic gabbro from Vestre Dale, Bamble, south Norway. *EOS,* **67,** No. 44, 1252.

Thomas, A.V. & Spooner, E.T.C., 1988. Fluid inclusions in the system H_2O-CH_4-NaCl-CO_2 from metasomatic tourmaline within the border unit of the Tanco zoned granitic pegmatite, S.E. Manitoba. *Geochimica et Cosmochimica Acta,* **52,** 1065-1075.

Thompson, A.B., 1976. Mineral reactions in pelitic rocks: II. Calculation of some P-T-X(Fe-Mg) phase relations. *American Journal of Science,* **276,** 425-454.

Thompson, A.B., 1982. Dehydration melting of pelitic rocks and the generation of H_2O-undersaturated granitic liquids. *American Journal of Science,* **282,** 1567-1595.

Thompson, A.B. & England, P.C., 1984. Pressure-Temperature-Time paths of regional metamorphism II. Their inference and interpretation using mineral assemblages in metamorphic rocks. *Journal of Petrology,* **25,** 929-955.

Thompson, A.B. & Ridley, J.R., 1987. Pressure-temperature-time (P-T-t) histories of orogenic belts. *Philosophical Transactions of the Royal Society of London,* **A321,** 27-45.

Thijssen, P.H.M., 1990. Sapphirine bearing rocks from Snaresund, Bamble, Norway: A petrological and geochemical study. Unpublished M.Sc. thesis, University of Utrecht.

Touret, J., 1971a. Le faciès granulite en Norvège Méridional, I: les associations minerales. *Lithos,* **4,** 239-249.

Touret, J., 1971b. Le faciès granulite en Norvège Méridional, II: les inclusions fluides. *Lithos,* **4,** 423-436.

Touret, J., 1974. Faciès granulite et fluides carboniques. *Centenaire de la Société Géologique de Belgique* (vol. P. Michot, Liège), 267-287.

Touret, J., 1979. Les roches à tourmaline-cordiérite-disthène de Bjordammen (Norvège méridionale) sont-elles liées a d'anciennes évaporites? *Science de la Terre XXIII* **(2),** 95-97.

Touret, J., 1985. Fluid regime in southern Norway: The record of fluid inclusions. In Tobi A.C. & Touret J.L.R. (eds.): The deep Proterozoic crust in the North Atlantic Provinces. *NATO ASI Series C,* **158,** 517-549.

Touret, J., 1986. Fluid inclusions in rocks from the lower continental crust. In: Dawson, J.B., Carswell, D.A., Hall, J. & Wedepohl, K.H. (eds.), 'The Nature of the Lower Continental Crust'. *Geological Society, Special Publication,* **24,** 161-172.

Touret, J., 1987. The high-grade metamorphic Bamble Sector. In Maijer C. & Padget P. (eds.): The geology of southernmost Norway: an excursion guide. *Norges Geologiske Undersøkelse, Special Publication* **1,** 25-30.

Touret, J., 1988. Synmetamorphic fluid inclusions in granulites. *Terra cognita,* **8,** D7, 255.

Touret, J. & Dietvorst, P., 1983. Fluid inclusions in high-grade anatectic metamorphites. *Journal of the Geological Society of London,* **140,** 635-649.

Touret, J. & Olsen, S.N., 1985. Fluid inclusions in migmatites. In: Ashworth, J.R. (ed.). Migmatites, Blakie Publications, 265-286.

Touret, J. & Roche, H. de la, 1971. Saphirine à Snaresund, près de Tvedestrand (Norvège méridionale). *Norsk Geologisk Tidsskrift,* **51,** 169-175.

Truscott, M.G., Shaw, D.M. & Cramer, J.J., 1986. Boron abundance and localization in granulites and the lower continental crust. *Geological Society of Finland Bulletin,* **58** (part 1), 169-177.

Urano, H., 1971. Geochemical and petrological study of the origins of metamorphic rocks and granitic rocks by determination of fixed ammoniacal nitrogen. *Journal of Earth Sciences, Nagoya University,* **19,** 1-24.

Verdonk, E.M., Dam, B.P. & Huijsmans, J.P.P., 1986. Coronitic gabbros ("hyperites") intruding the lower Proterozoic crust of Bamble, south Norway. *EOS,* **67,** No. 44, 1252.

Verdouw, H., Echteld, C.J.A. van & Dekkers, E.M.J., 1978. Ammonia determination based on indophenol formation with sodium salicylate. *Water Research,* **12,** 399-402.

Verschure, R.H., 1985. Geochronological framework for the late-Proterozoic evolution of the Baltic Shield in south Scandinavia. In: Tobi, A.C. & Touret, J. (eds.): The deep Proterozoic crust in the north Atlantic provinces. *NATO ASI Series C,* **158,** Reidel, Dordrecht, 381-410.

Visser, D., 1987. Orthoamphibole-bearing rocks in the Nidelva area, south Norway. Unpublished M.Sc. thesis, University of Utrecht, 45 pp.

Visser, D., Maijer, C. & Senior, A., 1990. Retrograde talc-kyanite-quartz assemblage from Bjordammen, Bamble Sector, south Norway. *Abstract 19th Nordic Geological Winter Meeting, Geonytt,* **17,** 119.

Visser, D., Nijland, T.G. & Maijer, C., 1991. Orthopyroxene-cordierite-garnet-kornerupine-albite-bearing metaevaporites intercalated with enderbitic gneisses at Færvik School, Tromøya. Excursion log of the 2nd SNF Workshop, Bamble 1991: 60-64.

Visser, D. & Senior, A., 1990. Aluminous reaction textures in orthoamphibole-bearing rocks: the pressure-temperature evolution of the high-grade Proterozoic of the Bamble Sector, south Norway. *Journal of Metamorphic Geology,* **8,** 231-246.

Visser, D. & Senior, A., 1991. Mg-rich dumortierite in cordierite-orthoamphibole-bearing

rocks from the high-grade Bamble Sector, south Norway. *Mineralogical Magazine,* **55,** 563-577.

Voncken, J.H.L., Vriend, S.P., Kocken, J.W.M. & Jansen, J.B.H., 1986. Determination of beryllium and its distribution in rocks of the Sn-W granite of Regoufe, Northern Portugal. *Chemical Geology,* **56,** 93-103.

Vrána, S., 1979. A polymetamorphic assemblage of grandidierite, kornerupine, Ti-rich dumortierite, tourmaline, sillimanite and garnet. *Neues Jahrbuch für Mineralogie, Monatshefte,* Heft **1,** 22-33.

Vry, J.K., Brown, P.E. & Valley, J.W., 1990. Cordierite volatile content and the role of CO_2 in high-grade metamorphism. *American Mineralogist,* **75,** 71-88.

Ward, C.M., 1984a. Magnesium staurolite and green chromium staurolite from Fiordland, New Zealand. *American Mineralogist,* **69,** 531-540.

Ward, C.M., 1984b. Titanium and the color of staurolite. *American Mineralogist,* **69,** 541-545.

Waters, D.J., 1986. Metamorphic history of sapphirine-bearing and related magnesian gneisses from Namaqualand, South Africa. *Journal of Petrology,* **27,** 541-565.

Waters, D.J. & Moore, J.M., 1985. Kornerupine in Mg-Al-rich gneisses from Namaqualand, South Africa: mineralogy and evidence for late-metamorphic fluid activity. *Contributions to Mineralogy and Petrology,* **91,** 369-382.

Wel, D. van der, 1973. Kornerupine: a mineral new to Norway. *Norsk Geologisk Tidsskrift,* **53,** 349-357.

Werding, G. & Mirwald, P.W., 1982. Infrarotspektren CO_2-haltiger Mg-Cordierite. *Abstract Bunsentagung Ulm und Neu-Ulm* **C25**

Werding, G. & Schreyer, W., 1978. Synthesis and crystal chemistry of kornerupine in the system MgO-Al_2O_3-SiO_2-B_2O_3-H_2O. *Contributions to Mineralogy and Petrology,* **67,** 247-259.

Werding, G. & Schreyer, W., 1984. Alkali-free tourmaline in the system MgO-Al_2O_3-B_2O_3-SiO_2-H_2O. *Geochimica et Cosmochimica Acta,* **48,** 1331-1344.

Werding, G. & Schreyer, W., 1988. Synthetic dumortierites: Their PTX-dependent compositional variations in the system Al_2O_3-SiO_2-B_2O_3-H_2O. *Fortschritte der Mineralogie,* **66,** Beiheft, 1, 168.

Werding, G. & Schreyer, W., 1990. Synthetic dumortierite: its PTX-dependent compositional variations in the system Al_2O_3-B_2O_3-SiO_2-H_2O. *Contributions to Mineralogy and Petrology,* **105,** 11-24.

Westra, L. & Scheurs, J., 1985. The West Uusimaa Complex, Finland: An early Proterozoic thermal dome. In: Tobi, A.C. & Touret, J.L.R. (eds.), 'The Deep Proterozoic Crust in the North Atlantic Provinces'. *NATO ASI Series C,* **158,** 369-380.

Whitney, D.L., 1992. Origin of CO_2-rich fluid inclusions in leucosomes from the Skagit migmatites, North Cascades, Washington, USA. *Journal of Metamorphic Geology,* **10,** 715-725.

Wilson, A.F., 1977. A zincian högbomite and some other högbomites from the Strangways Range, Central Australia. *Mineralogical Magazine,* **41,** 337-344.

Windley, B.F., Ackermand, D. & Herd, R.K., 1984. Sapphirine/Kornerupine-bearing rocks and crustal uplift history of the Limpopo belt, southern Africa. *Contributions to Mineralogy and Petrology,* **86,** 342-358.

Windrim, D.P., McCulloch, M.T., Chappell, B.W. & Cameron, W.E., 1984. Nd isotopic systematics and chemistry of Central Australian sapphirine granulites: an example of rare

earth element mobility. *Earth and Planetary Science Letters,* **70,** 27-39.
Woodford, P.J., Wilson, A.F., 1976. Sapphirine, högbomite, kornerupine, and surinamite from aluminous granulites, north-eastern Strangways Range, central Australia. *Neues Jahrbuch für Mineralogie, Monatshefte,* Heft **1,** 15-35.
Zakrzewski, M.A., 1977. Högbomite from the Fe-Ti deposit of Liganga (Tanzania). *Neues Jahrbuch für Mineralogie, Monatshefte,* Heft **8,** 373-380.
Zimmermann, J-L., 1981. La libération de l'eau, du gaz carbonique et des hydrocarbures des cordiérites. Cinétique des mécanismes. Détermination des sites. Intérêt pétrogénétique. *Bulletin de la Société française de Minéralogie et de Crystallographie,* **104,** 325-338.

SUMMARY

In this thesis the results of a mineral chemical and paragenetic study of cordierite-orthoamphibole-bearing rocks from the Mid-Proterozoic Bamble Sector, south Norway are presented. The scope of this study was 1) to deepen the knowledge of the metamorphic evolution of the amphibolite to granulite facies grade Bamble Sector, 2) to study the regional metamorphic fluid variation in cordierite-bearing rocks, and 3) to provide some insights on the behaviour of boron in the lower continental crust by studying borosilicate-bearing mineral assemblages.

In Chapter 1 a detailed outline of the prograde and part of the retrograde metamorphic evolution of the Bamble Sector is given. Mineral assemblages from three key localities in the Froland area describe a three stage (M_1-M_{3a}) prograde reaction sequence during the Kongsbergian orogeny (1.6-1.5 Ga). The deduced clockwise P-T path, compatible with a model of crustal thickening during continental collision, is perturbed at higher grade (600-700 °C and 6-7 kbar) by an isobaric heating event (M_{3b}) involving a temperature increase of about 50-100 °C. The M_{3b} event is explained by a proces of extensional lithospheric thinning (and some magmatic thickening) which is thought to have started already *during* the crustal thickening stage. A prolonged isobaric cooling path (early M_4) is suggested for the area before uplift and significant greenschist- to low-amphibolite facies retrogression occurred during the late Sveconorwegian (1.2-0.9 Ga; late M_4). Late M_4 P-T conditions are estimated at 420-530 °C and 3-4 kbar.

The variation of volatiles (H_2O, CO_2) and the light elements Na, Li and Be in cordierites from the classical Arendal-Tvedestrand amphibolite to granulite facies transition is considered in Chapter 2. It is shown that the H_2O-, CO_2-, Na- and Li-content decreases with increasing metamorphic grade. This behaviour suggests a model of progressive dehydration and decarbonation for this transition area. Cordierites which re-equilibrated with externally derived fluids during a retrograde greenschist- to low-amphibolite facies event (M_4) show significant volatile gains, especially in CO_2.

A detailed petrological and mineralogical account on the prograde growth (M_{3a}) and retrograde breakdown of the rare borosilicate kornerupine in a biotite-spinel-garnet schist near Böylefossbru, is given in Chapter 3. The data indicate that kornerupine developed at P-T conditions of about 630-720 °C and 6-8 kbar in response to fluids derived from the dehydration of possibly boron-bearing muscovite in adjacent or near-by migmatites. Partial breakdown of kornerupine at lower grade (T = 411-500 °C, P = 3-4 kbar) was triggered by CO_2-rich fluids, and produced the assemblages tourmaline-andalusite-chlorite, tourmaline-corundum-chlorite ± hematite and dumortierite-chlorite.

The borosilicate dumortierite occurs as a widespread trace constituent in many of the cordierite-bearing rocks from the Bamble Sector. The mineral chemistry and petrology of

several of these occurrences are described in Chapter 4. Dumortierite is shown to occur exclusively as a retrograde late-M_4 replacement of peak metamorphic minerals cordierite, garnet and orthoamphibole. Estimated P-T conditions are 500 $\pm$ 50 °C and 3-4 kbar. Two new coupled substitutions, $Mg+Ti \longrightarrow 2\ Al^{VI}$ and $3\ Mg \longrightarrow 2\ Al^{VI}$ are reported to account for the bulk of the observed compositional variations in these Mg-rich dumortierites.

Chapter 5 gives a detailed description of a new gedrite breakdown reaction in a gedrite-oligoclase rocks at Blengsvatn. The breakdown assemblage anthophyllite-cordierite-magnetite formed at 527-560 °C and 3-6 kbar in response to infiltrating CO_2-rich aqueous and oxidizing retrograde fluids.

Chapter 6 deals with the formation of the complex Fe-Mg-(Co-Zn)-Al-Ti oxide högbomite in spinel-sapphirine rocks at Snaresund and Rangleåsen. Two different polytypes of högbomite are reported which both developed due to hydrous alteration and oxidation of primary spinel and rutile/ilmenite. The observed heterogeneous Zn-partitioning between spinel and högbomite is presumably caused by differences in fO_2 and aH_2O.

In Chapter 7, it is shown that amphibolite facies grade metamorphic biotites in Mg,Fe,Al-rich and Ca,Na-poor, reduced rock types may contain very high amounts of ammonium (up to 3000 ppm NH_4^+). The high ammonium values concur with a pre-metamorphic sedimentary origin of the investigated rocks.

Finally, some concluding remarks and implications concerning the metamorphic evolution of the Bamble Sector, the importance of retrograde CO_2-rich fluids, and the behaviour of boron in the lower continental crust are presented in Chapter 8.

SAMENVATTING

In dit proefschrift worden de resultaten gepresenteerd van een mineraal-chemisch en paragenetisch onderzoek van cordieriet-orthoamfibool houdende gesteenten uit de midden-Proterozoïsche Bamble Sector, zuid-Noorwegen. Het doel van dit onderzoek was 1) het uitdiepen van de kennis over de metamorfe evolutie van de Bamble Sector, 2) het bestuderen van de regionale variatie in de metamorfe vloeistofsamenstelling in cordieriet-houdende gesteenten en 3) het verkrijgen van inzicht in het gedrag van boor in de continentale onderkorst, door het bestuderen van boorsilicaat-houdende mineraal-assemblages.

Hoofdstuk 1 geeft een gedetailleerd overzicht van de prograde en een deel van de retrograde metamorfe evolutie van de Bamble Sector. Mineraal-assemblages van drie sleutel-vindplaatsen in het Froland-gebied beschrijven een driedelige prograde reactie-sequentie (M_1-M_{3a}) gedurende de Kongsbergse orogenese (1.6-1.5 Ga). Het afgeleide kloksgewijze P-T pad, compatibel met een model van korstverdikking tijdens continent-continent-botsing, wordt verstoord bij hogere druk en temperatuur (600-700 °C en 6-7 kbar) door een gebeurtenis (M_{3b}) welke een isobare opwarming van 50-100 °C inhoudt. De M_{3b}-fase wordt verklaard door een proces van extensionele lithosferische verdunning, welke waarschijnlijk al begon *gedurende* de fase van korstverdikking. Een langdurig isobaar afkoelingspad (vroeg M_4) wordt gesuggereerd voor het gebied voordat opheffing en belangrijke groenschist- tot laag-amfiboliet-facies retrogradatie tijdens het laat-Sveconorwegicum (1.2-0.9 Ga; laat M_4) inzette. Late M_4 P-T omstandigheden worden geschat op 420-530 °C en 3-4 kbar.

De variatie in gassen (H_2O, CO_2) en de lichte elementen Na, Li en Be in cordierieten van de klassiek Arendal-Tvedestrand amfiboliet naar granuliet-facies overgang wordt bestudeerd in hoofdstuk 2. Aangetoond wordt dat het H_2O-, CO_2-, Na-, en Li-gehalte afneemt met toenemende metamorfosegraad. Deze relatie suggereert een model van progressieve ontgassingsreacties (dehydratie en decarbonatie) voor dit overgangsgebied. Cordierieten die re-equilibreerden met extern gevormde fluïde oplossingen tijdens een retrograad groenschist tot laag-amfiboliet facies gebeurtenis (M_4) laten een toename zien in het gas-gehalte van cordieriet, met name in CO_2.

Een gedetailleerde petrologische en mineralogische beschrijving betreffende de prograde vorming (M_{3a}) en retrograde omzetting van het zeldzame boorsilicaat kornerupien in een biotiet-spinel-granaat schist nabij Böylefossbru wordt gegeven in hoofdstuk 3. De data laten zien dat de vorming van kornerupien plaatsvond bij druk-temperatuur-condities van 630-720 °C en 6-8 kbar als gevolg van fluïde oplossingen, vrijgekomen bij de dehydratie van mogelijke boorhoudende muscoviet in naast of dichtbij

gelegen migmatieten. Gedeeltelijke laaggradige (T = 411-500 °C, P = 3-4 kbar) omzetting van kornerupien, geïnitieerd door CO_2-rijke vloeistoffen, vormde de mineraal-assemblages toermalijn-andalusiet-chloriet, toermalijn-korund-chloriet ± hematiet en dumortieriet-chloriet.

Het boorsilicaat dumortieriet komt voor in de meeste van de cordieriet-houdende gesteentes van de Bamble Sector. De mineraalchemie en petrologie van verscheidene van deze voorkomens worden beschreven in hoofdstuk 4. Dumortieriet komt exclusief voor als een laat-M_4 retrograde omzetting van de piekmetamorfe mineralen cordieriet, granaat en orthoamfibool. De vormingscondities worden geschat op 500 ± 50 °C en 3-4 kbar. Twee nieuwe gekoppelde substituties, $Mg+Ti \longrightarrow 2Al^{VI}$ en $3Mg \longrightarrow 2Al^{VI}$ beschrijven de bulk van de geobserveerde samenstellingsvariaties in deze Mg-rijke dumortierieten.

Hoofdstuk 5 geeft een gedetailleerde beschrijving van een nieuwe omzettingsreactie van gedriet in een gedriet-oligoklaas-gesteente bij Blengsvatn. De omzettingsassemblage bestaande uit anthophylliet, cordieriet en magnetiet ontstond bij temperaturen van 527-560 °C en een lithostatische druk van 3-6 kbar als gevolg van geïnfiltreerde CO_2-rijke, waterige, oxiderende en retrograde oplossingen.

Hoofdstuk 6 behandelt de vorming van het complexe Fe-Mg-(Co-Zn)-Al-Ti-oxide högbomiet in spinel-sapphirien-gesteentes bij Snaresund en Rangleåsen. Twee verschillende högbomiet-polytypes worden beschreven die beiden ontstonden als gevolg van waterige omzetting en oxidatie van de primair aanwezige spinel en rutiel/ilmeniet. De geobserveerde heterogene zinkdistributie tussen spinel en högbomiet wordt waarschijnlijk veroorzaakt door verschillen in fO_2 en aH_2O.

Hoofdstuk 7 laat zien dat amfiboliet-facies metamorfe biotieten uit Mg,Fe,Al-rijke, Ca,Na-arme en gereduceerde gesteentes zeer hoge ammoniumgehaltes kunnen bevatten (tot aan 3000 ppm NH_4^+). De hoge ammoniumwaarden bevestigen de pre-metamorfe sedimentaire oorsprong van de onderzochte gesteentes.

Tenslotte worden in hoofdstuk 8 enkele laatste algemene opmerkingen en implicaties gegeven betreffende de metamorfe evolutie van de Bamble Sector, de importantie van retrograde CO_2-rijke fluïde fasen en het gedrag van het element boor in de continentale onderkorst.

CURRICULUM VITAE

Diederik Visser werd op 10 maart 1963 geboren te 's-Gravenhage. Na het behalen van de diploma's HAVO (1981) aan de Rommert Casimir HAVO en Atheneum-B (1983) aan het Lorentz Lyceum te Eindhoven, begon hij in 1983 met de studie Geologie aan de Rijksuniversiteit Utrecht. In augustus 1984 werd het propadeutisch examen afgelegd en in augustus 1988 het doctoraal examen (cum laude) met als hoofdvak Petrologie en als bijvak Geochronologie. In de periode september 1988 tot en met oktober 1989 was hij werkzaam als assistent in opleiding bij de vakgroep Geochemie. Na een onderbrekking van bijna een jaar werd van september 1990 tot heden dit proefschrift op eigen gelegenheid afgerond. Gedurende deze periode was hij als part-time administratief medewerker in dienst bij Rijkswaterstaat, directie Utrecht, dienstkring Huis ter Heide, om in zijn levensonderhoud te voorzien.